Title

Mechanisms Behind the Causal Role of Dietary Oxylipins of the Lipoxygenase Pathway in the Development of Pulmonary Arterial Hypertension

Author

O'Connor, Ellen Ines

Publication Date

2021

Peer reviewed|Thesis/dissertation

UNIVERSITY OF CALIFORNIA

Los Angeles

Mechanisms Behind the Causal Role of Dietary Oxylipins of the Lipoxygenase Pathway in the Development of Pulmonary Arterial Hypertension

A dissertation submitted in partial satisfaction of the

requirements for the degree Doctor of Philosophy

in Molecular Toxicology

by

Ellen Ines O'Connor

2021

ABSTRACT OF THE DISSERTATION

Mechanisms Behind the Causal Role of Dietary Oxylipins of the Lipoxygenase Pathway in the Development of Pulmonary Arterial Hypertension

by

Ellen Ines O'Connor

Doctor of Philosophy in Molecular Toxicology

University of California, Los Angeles, 2021

Professor Srinivasa T. Reddy, Chair

Hypertension, high blood pressure, is a common condition with more than three million cases in the United States per year. Pulmonary hypertension (PH), a chronic condition targeting the lungs, leading to vascular remodeling, right ventricle hypertrophy, and death in 50% of cases 5 years after diagnosis, is multi-factorial, not fully understood, and is without a permanent cure to this day. Utilizing multiple animal models involving xenobiotic injections, hypoxic conditions, growth factor receptor antagonists, and the combinations thereof have provided valuable insights into pathways and abnormalities associated with PH, however, the precise mechanisms remain unknown. In the last decade, it was discovered that a common feature of PH is the increase of oxidized lipids (especially the oxylipins of the lipoxygenase [LOX] pathway) in the plasma and lung tissues in not only human PAH patients but also in multiple animal models of PH. Animal studies demonstrated that apolipoprotein A-I (apoA-I) mimetic peptides ameliorated PH while lowering levels of oxylipins of the lipoxygenase pathway, including hydroxyeicosatetraenoic acids (HETEs) and hydroxyoctadecadienoic acids (HODEs).

Taking this one step further, myself and our collaborators have developed a new animal model of PH in which feeding wild type C57BL6/J mice 5µg per mouse per day of 15-HETE resulted in increases in right ventricle systolic pressure (RVSP), Fulton index, vascular remodeling, lung weight, and plasma levels of HETEs and HODEs. In this thesis, I set out to utilize our new animal model to explore the mechanisms by which oxylipins of the lipoxygenase pathway (focusing on 15-HETE) cause PH and apoA-I mimetic peptides (specifically Tg6F) prevent the development of PH. My hypothesis is that 15-HETE initiates, and Tg6F mitigates, intestinal inflammation by modulating pro-inflammatory lipids and immune responses, which result in PH. I utilized cell culture (rat intestinal epithelial cells; IEC-6 cells, mouse T-cells; TK-1 cells, and mouse pulmonary arterial endothelial cells, PAECs), and animal models (C57BL6/J and 12/15 lipoxygenase KO mice) to test my hypothesis. I determined that 15-HETE diet (i) induces the accumulation of oxylipins in the intestine and plasma, (ii) activates pulmonary arterial endothelial cells (PAEC), and (iii) increases CD8 cell mediated PAEC apoptosis. I demonstrated that Tg6F treatment prevented all the above changes and prevented PH. Further, analyses of RNA-seq data from lung samples of PAH patients, lung samples of 15-HETE fed mice, and intestinal samples of 15-HETE fed mice, identified interferon induced protein 44 (IFI44) as the only gene that was significantly increased between all three groups. IFI44 increases in the intestine as early as one week into the 3 week 15-HETE PH protocol, preceding the increase in IFI44 observed in the lungs, and when IFI44 is blocked via intratracheal instillation of siRNA, it prevented the onset of PH in mice on the 15-HETE diet when compared with those administered scrambled siRNA, establishing IFI44 as a novel target for preventing PH. Finally, I determined that anti-inflammatory short chain

fatty acids (SCFAs) play a role in the development of PH and identified oral butyrate as a potential therapy for PH. Luminal microbiota analysis from mice fed a 15-HETE diet revealed that bacterial species that participate in SCFA production were significantly reduced. Tg6F fed mice, interestingly, had increased SCFA producing bacterial species and fecal pellet levels of the SCFAs butyrate, propionate, and acetate compared to 15-HETE fed mice. Furthermore, supplementing 15-HETE fed mice with sodium butyrate in their drinking water increased the abundance of SCFA producing bacteria, decreased intestine and lung expression of IFI44, prevented the onset of PH, and reduced RVSP of mice fed 15-HETE diet for 2 weeks before adding sodium butyrate to their diet in the third, suggesting that oral butyrate is a potential therapy for both prevention and progression of PH. Combined, these experiments not only establish the role of oxylipins of the LOX pathway in the onset of PH, but also reveal mechanisms by which it causes it and multiple targets for future therapeutic applications.

The dissertation of Ellen Ines O'Connor is approved.

Robert H. Schiestl

Jesus A. Araujo

Mansoureh Eghbali

Srinivasa T. Reddy, Committee Chair

University of California, Los Angeles

2021

Table of Contents

List of Figures

List of Tables

ACKNOWLEDGEMENTS

Chapter 2 was previously published as: Ruffenach, G., O'Connor E., et al. Oral 15-Hydroxyeicosatetraenoic Acid Induces Pulmonary Hypertension in Mice by Triggering T Cell-Dependent Endothelial Cell Apoptosis. Hypertension 985–996 (2020). doi:10.1161/HYPERTENSIONAHA.120.14697

I would like to thank Gregoire Ruffenach, PhD for doing all the echocardiography and direct catheterization on top of being a great mentor and collaborator, Jason Hong, MD PhD, for re-analyzing the intestine RNA-seq, Dr. Eghbali for being a supportive advisor all these years, and the entire Eghbali lab for helping me become a hypertension pro when I came from a lab that focuses on the small intestine and systemic inflammation.

Thanks to Dr. Hankinson and the entire Molecular Toxicology IDP. I would also like to thank my funding sources, Competitive Edge, the Eugene V. Cota Robles Fellowship, and R01HL129051-01A1.

Obviously, none of this would be possible without the support of the Reddy lab, especially Victor (aka "golden hands"), Dawoud, Arnab, David, Rita, Sam, Prisca, Nasrin, Pallavi, and other lab members who have come and gone over the years including Hannah, Anna, Jeremy, and Xingying.

Thank you to my parents, Tim and Juana, and my brother Peter, for trying to memorize phrases like "molecular toxicology," "pulmonary hypertension," and "mass spectrometer" and for supporting not only my research but all aspects of my life during these past 6 years. Thank you to my friends for all the memes, videos, dinners, brunches, and outings that did NOT interfere with my lab work but put a smile on my

face when the data looked bleak and helped get some fresh air to my brain to better tackle the challenges of research.

Of course thank you to my committee members, Dr. Eghbali, Dr. Araujo, Dr. Schiestl, and especially the chair of my committee, Dr. Reddy for the day-in-day-out support when things went well, when things went wrong, and for responding to an email that said “check this out” with overflowing encouragement to go after a new story so late into my PhD and after the Covid shutdown, ultimately leading to Chapter 5, the pride and joy of my research.

I’d also like to say thank you to my mice, or “chonks” as I have affectionately referred to them over the years. I know the butyrate water smelled awful but hey it helped you not get hypertension and contributes to further understanding of PH so you’re the real MVPs.

Vita

EDUCATION

University of California, Berkeley BS 2012 Molecular Toxicology

Positions/Employment, Memberships and Honors

2013-2014	Product Safety Technician, Nutrilite™
2015	Eugene V. Cota-Robles Fellowship Award
July 2015-Aug 2015	UCLA Competitive Edge: NSF Summer Transition Program
2016-2021	Graduate Student Researcher
2018-2019	Molecular Toxicology Student Representative, UCLA

PUBLICATIONS

Kelesidis Theodoros, Madhav Sharma, Petcherski Anton, Christelle Hugo, **O'Connor Ellen**, Eleni Ritou, Shirihai Orian S, Reddy Srinivasa T. The ApoA-I mimetic peptide 4F attenuates in vitro replication of SARS-CoV-2, associated apoptosis, oxidative stress and inflammation in epithelial cells. Virulence (2021) Accepted as of July 30, 2021.

Gregoire Ruffenach, **Ellen O'Connor**, Mylene Vaillancourt, Jason Hong, Nancy Cao, Shervin Sarji, Shayan Moazeni, Jeremy Papesh, Victor Grijalva, Christine Cunningham, Le Shu, Arnab Chattopadhyay, Shuchita Tiwari, Olaf Mercier, Frederic Perros, Soban Umar, Xia Yang, Aldrin Gomes, Alan Fogelman, Srinivasa Reddy, Mansoureh Eghbali. Oral 15-HETE Induces Pulmonary Hypertension in Mice by Triggering T-cell Dependent Endothelial Cell Apoptosis. Hypertension 985–996 (2020). doi:10.1161/HYPERTENSIONAHA.120.14697
PMCID: PMC8008496

David Meriwether, Dawoud Sulaiman, Carmen Volpe, Anna Dorfman, Victor Grijalva, Nasrin Dorreh, R. Sergio Solorzano-Vargas, Jifang Wang, **Ellen O'Connor**, Jeremy Papesh, Muriel Larauche, Hannah Trost, Mayakonda N. Palgunachari, G.M. Anantharamaiah, Harvey R. Herschman, Martin G. Martin, Alan M. Fogelman, and Srinivasa T. Reddy. Apolipoprotein A-I mimetics mitigate intestinal inflammation in a COX2-dependent inflammatory disease model. The Journal of Clinical Investigation. 2019 Sep 3; 129(9): 3670–3685. doi: 10.1172/JCI123700
PMCID: PMC6715371

Pallavi Mukherjee, Greg Hough, Arnab Chattopadhyay, Victor Grijalva, **Ellen Ines O'Connor**, David Meriwether, Alan Wagner, James M. Ntambi, Mohamad Navab, Srinivasa T. Reddy, and Alan M. Fogelman. Role of enterocyte stearoyl-Co-A desaturase-1 in LDLR-null mice. Journal of Lipid Research. Oct 2018:59, 1818-1840. doi: 10.1194/jlr.M083527 PMCID: PMC6168294

ABSTRACTS

Nancy Merino, Meng Wang, Rocio Ambrocio, Kimberly Mak, **Ellen O'Connor**, An Gao, Elisabeth L. Hawley, Rula A. Deeb, Linda Y. Tseng, Shaily Mahendra. Fungal biotransformation of 6:2 fluorotelomer alcohol. *Remediation*. 2018;28:59–70. https://doi.org/10.1002/rem.21550

Gregoire Ruffenach, **Ellen I O'Connor**, Mylène vaillancourt, Victor Grijalva, Shervin Sarji, Christine Cunningham, Abbas Ardehali, Aman Mahajan, Soban Umar, Srinivasa T Reddy and Mansoureh Eghbali. Dietary Oxydized Lipids Induce Pulmonary Hypertension Circulation 136:A18029 (2017)

Pallavi Mukherjee, Greg Hough, Arnab Chattopadhyay, Victor Grijalva, **Ellen I O'Connor**, Alan Wagner, Susan S Smyth, Wouter H Moolenaar, Mohamad Navab, Srinivasa T Reddy and Alan

M Fogelman. Role of the Enterocyte Enpp2 Gene in Western Diet-induced Systemic Inflammation. Circulation 136:A14930 (2017)

Pallavi Mukherjee, Greg Hough, Arnab Chattopadhyay, Victor Grijalva, **Ellen I O'Connor**, Xinying Yang, Alan Wagner, James M Ntambi, Mohamad Navab, Srinivasa T Reddy and Alan M Fogelman. Role of Lysophosphatidylcholine 18:1 in Enterocytes of LDLR Null Mice on Western Diet. Circulation 136:A14968 (2017)

CHAPTER 1: Introduction

Abbreviations

PAH	Pulmonary Arterial Hypertension
PH	Pulmonary Hypertension
BMPR2	Bone Morphogenic Protein Receptor Type 2
CHP	Chronic Hypoxia
MCT	Monocrotaline
HETE	Hydroxyeicosatetraenoic Acid
HODE	Hydroxyoctadecadienoic Acid
PUFA	Polyunsaturated Fatty Acid
LA	Linoleic Acid
AA	Arachidonic Acid
COX	Cyclooxygenase
LOX	Lipoxygenase
CYP	Cytochrome P450
LDL	Low Density Lipoprotein
PPARs	Peroxisome Proliferator-Activated Receptors
GPCRs	G Protein-Coupled Receptors
PASMC	Pulmonary Arterial Smooth Muscle Cells
HDL	High Density Lipoprotein
ApoA-I	Apolipoprotein A-I
RVSP	Right Ventricle Systolic Pressure
RV	Right Ventricle
mir193	MicroRNA 193
Alox	Lipoxygenase, interchangeable with LOX
BLT2	Leukotriene B4
MAPK	Mitogen-Activated Protein Kinase
GI	Gastrointestinal
TMA	Trimethylamine
FMO3	Flavin-Containing Monooxygenase 3
TMAO	Trimethylamine N-Oxide
BMI	Body Mass Index
SCFA	Short Chain Fatty Acid
SHR	Spontaneously Hypertensive Rats
IEC	Intestinal Epithelial Cell
PAEC	Pulmonary Arterial Endothelial Cell
CD8+	Cluster of Differentiation 8
IFI44	Interferon Induced Protein 44
PAAT	Pulmonary Arterial Acceleration Time

1.1 Pulmonary Arterial Hypertension (PAH)

Pulmonary hypertension (PH) has an overall definition of resting mean pulmonary artery pressure greater than 25 mmHg that is classified into five categories by The World Health Organization.[1] These categories are (I) Pulmonary Arterial Hypertension (PAH), (II) Pulmonary hypertension owing to left heart disease, (III) Chronic obstructive pulmonary disease, (IV) Chronic thromboembolic pulmonary hypertension, and (V) Pulmonary Hypertension with unclear multifactorial mechanisms.[2] Common symptoms of PH include dyspnea, fatigue, weakness, angina, presyncope and syncope. Clinicians often examine resting electrocardiography and resting echocardiography to estimate the probability of PH and a right-sided heart catheterization is key to diagnose and characterize the different forms of PH effectively.[3]

Group I PH, PAH, is an incurable and fatal disease that affects men and women alike of any age with a median survival of 2.8 years from diagnosis.[4] PAH is characterized by the remodeling of the pulmonary arteries leading to increased pulmonary arterial pressure, which ultimately leads to right ventricle hypertrophy and failure.[5] There are many abnormalities and altered pathways associated with PAH including pulmonary arterial smooth muscle cell proliferation, inflammation, vasoconstriction, angiogenesis, endothelial dysfunction, plexiform lesions, fibrosis, vascular remodeling, and mitochondrial dysfunction.[6] Within group I PH there are subgroups of PAH including (i) idiopathic, or sporadic onset, of disease with no familial context, (ii) familial or heritable PAH which includes germline mutation in bone morphogenic protein receptor type 2 (BMPR2) [which accounts for 70% of cases], (iii) drug-and-toxin induced PAH, (iv) PAH

associated with conditions such as connective tissue disease, HIV infection, portal hypertension, congenital heart diseases, Schistosomiasis, and chronic hemolytic anemia, and (v) persistent pulmonary hypertension of the newborn.[2]

Treatments for PAH include endothelin 1 receptor antagonists, phosphodiesterase type 5 inhibitors, soluble guanylate cyclase stimulators, prostacyclin analogues, prostacyclin receptor agonists.[7] Balloon atrial septostomy, a percutaneous procedure that creates atrial communication via balloon dilation of the atrial septum, is also used in PAH therapies to improve symptoms and hemodynamics and also as a bridge to lung transplantation when medical therapies fail.[8]

Unfortunately, there is no cure for PAH and there is an unmet need for new approaches for not only understanding the pathology of PAH but for also identifying novel therapeutic strategies for PAH. There are multiple models of PH being used in efforts to understand the mechanisms of disease development and pathology. A few key ones include chronic hypoxia (CHP), in which rats or mice are placed in a hypobaric chamber of 10% fraction of inspired oxygen for 3-4 weeks, CHP combined with SU-5416 injections at 20mg/kg for 1-3 weeks, and monocrotaline (MCT) injury, in which a single subcutaneous or intraperitoneal injection of MCT, result in the progressive development of PH.[5,9] Shortcomings of animal models of PH include poor correlation to the severity observed in human PH, variability in response across species, and ability to cure PH in animal models.[5,9,10]

Plasma levels of pro-inflammatory lipids are significantly elevated in two established models of PAH; rats subjected to MCT injury and mice in CHP have increased plasma levels of hydroxyeicosatetraenoic acids (HETEs) and hydroxyoctadecadienoic acids

(HODEs), oxylipins from the arachidonic acid pathway.[11] Interestingly, these are also significantly increased in the plasma and lung tissue of PAH patients.[12,13] This common increase in HETEs and HODEs observed in human patients and animal models provided a clue to one *unexplored* potential cause of PAH.

1.2 Oxylipins and 15-HETE

The HETEs and HODEs increasing in both patients and animal models of PH are metabolites of omega-6 polyunsaturated fatty acids (PUFA), arachidonic acid (AA) and linoleic acid (LA), respectively.[14] LA, and its byproduct AA, cannot be synthesized by humans and are therefore essential fatty acids that must be consumed in the diet. LA is the most highly consumed PUFA in the human diet, with its sources including vegetable oils, nuts, seeds, meats, and eggs, as well as processed foods containing soybean oil as a commercial additive.[15,16] After consumption, LA may be metabolized or incorporated into cell membrane phospholipids.[15] Similarly, AA is present in all human cells, usually esterified to membrane phospholipids.[17] LA and AA serve as precursors of pro-inflammatory and anti-inflammatory signaling lipids called eicosanoids via metabolism by cyclooxygenases (COX-I and COX-2), lipoxygenases (12-LOX, 15-LOX, and 5-LOX), and epoxygenases (cytochrome P450 or CYP).[14,16] LOX enzymes in particular are what give rise to HETEs and HODEs, HETEs coming from metabolism of AA and HODEs coming from LA.[6,14,16]

HETEs and HODEs are pro-inflammatory lipids, with HODEs regulating macrophage differentiation, decreasing platelet adhesion to endothelial cells, and is highly abundant in the low density lipoprotein (LDL) of patients with atherosclerosis, while HETEs can activate peroxisome proliferator-activated receptors (PPARs) and G

protein-coupled receptors (GPCRs) and have been implicated in promoting tumor cell proliferation and metastasis, mediating proinflammation in diabetes, and are also elevated in altherosclerosis.[16,18,19] 15-LOX overexpression in *Ldlr-/-* mice in the vessel wall as associated with significantly larger atherosclerotic lesions at the aortic sinus.[20] In relation to PAH, it has been reported that HETEs and HODEs contribute to vascular remodeling, pulmonary arterial smooth muscle cells (PASMC) proliferation and resistance to apoptosis, inflammation, vasoconstriction, angiogenesis, and fibrosis.[6,21–24] Given the potential of HETEs and HODEs to alter multiple pathways involved in PAH, one must wonder whether decreasing levels of HETEs and HODEs can prevent or even rescue animals and humans from PH and what kind of compounds would be effective in reducing the amount of circulating HETEs and HODEs in the body.

1.3 ApoA-I Mimetic Peptides

It has been well-established since the 1970s that there is an inverse correlation between high-density lipoprotein (HDL) cholesterol levels and cardiovascular disease (CVD).[25–27] HDL plays a role in mediating cholesterol efflux out of cells while providing anti-oxidative, anti-inflammatory, anti-apoptotic, and vasoprotective effects.[28] While HDL treatment has shown to have beneficial effects *in vitro*, clinical trials attempting to raise HDL levels have not shown consistent reduction of endpoints such as death, myocardial infarction, and stroke.[26,29,30] Therefore, approaches aiming to increase components of HDL have been investigated as potential therapeutics, apolipoprotein A-I (ApoA-I), the major protein component of HDL, being one of particular interest. ApoA-I in involved in cholesterol traffic as well as inflammatory and immune response.[31] ApoA-I also binds to oxylipins, including HETEs and HODEs, that would account for its anti-inflammatory properties.[32]

Our laboratory pioneered the development of apoA-I mimetic peptides that are anti-inflammatory and therapeutic for many inflammatory diseases including atherosclerosis, cancer, and lung disease.[28,30,33] Compared with human apoA-I, apoA-I mimetic peptides bind oxylipins with an affinity that is ~4-6 orders of magnitude higher.[32,34,35] Work from a recent collaboration showed that 4F has antiviral activity against SARS-CoV-2, attenuated apoptosis, and attenuated proinflammatory cytokines related to Covid-19 in monkey kidney and human lung epithelial cells.[36]

A collaboration between our lab and Dr. Mansoureh Eghabli's lab investigated the effectiveness of the apoA-I mimetic peptide 4F in two models of PH: MCT and CHP. In the MCT rats, 4F treatment (50 mg/kg day) from days 21-30 post injection improved right ventricle systolic pressure (RVSP), decreased right ventricle (RV) hypertrophy measured by Fulton Index, increased survival compared with rats that did not receive 4F, and improved vascular remodeling.[11] Hypertensive rats also had increased plasma levels of HETEs and HODEs that were decreased with 4F treatment. Similarly, in CHP mice 4F treatment on days 14-21 of hypoxia decreased RVSP and right ventricle hypertrophy.[11] Interestingly, both the MCT rats and the CHP mice had decreased levels of microRNA 193 (mir193), a finding also seen in the lungs of human PAH patients, that was increased by 4F treatment. Overexpression of mir193 rescued PH in both MCT rats and CHP mice, and decreased expression of Alox5, Alox12, and Alox15, the enzymes responsible for producing HETEs and HODEs. The ability of the apoA-I mimetic peptide 4F to treat PH in two different animal models in part by modulating levels of HETEs and HODEs suggests that oxylipins of the LOX pathway may play a critical role in the induction and progression of PAH.[6,11]

1.4 15-HETE is sufficient in causing PH

The major question based on the observed correlation between hypertensive animals and patients with PH and HETEs and HODEs levels is whether oxylipins of the LOX pathway are causal agents of PH or byproducts of another pathway? Exogenous 15-HETE at 5 µg per mouse per day for three weeks was found sufficient to increase RVSP, lung weight, and downregulate mir193 expression in wild-type male mice.[11] While it is exciting that dietary administration of one oxylipin is capable of causing PH in wild-type mice, the mechanisms behind how PH occurs have not been fully investigated.

As mentioned previously in sections 1.1 Pulmonary Arterial Hypertension, increased HETEs and HODEs levels have been observed in PAH and PH patients as well as two animal models of PH.[11,12,37] The dietary 15-HETE model of PH was designed to recreate this observation, making it highly relevant and representative of human patient PH. As exogenous 15-HETE leads to increases in RVSP and not left ventricle systolic pressure, and downregulates mir193, this would translate most closely to Group 1 PH, PAH, in the clinic.[3,11,38] Dietary 15-HETE has no effect on the left side of the heart in the time-frame described in the protocol, is too short to be considered representative of a chronic lung disease, does not result in blood clots that lead to PH, nor does it fit the description of “unclear or multifactorial mechanisms” as one lipid is added to the diet, making it unsuitable to fit into the other four categories of PH classification.[3]

As previously mentioned, HETEs and HODEs contribute to the alteration of many pathways implicated in PH.[6] Liquid chromatography of plasma samples from PAH patients and healthy controls found that PAH treatment naïve, or patients that have not received treatment for PAH, had increased plasma concentrations of 5-, 8-, 12-, and 15-

HETE.[12] In the same study, it was noted that survival was significantly worse in patients with high 12- and 15-HETE plasma levels. 15-HETE itself is a PPAR β/δ agonist and an activator of the low affinity leukotriene B_4 receptor, BLT2, which is expressed in human granulocytes, eosinophils, and mononuclear cells.[39,40] 15-LOX and 15-HETE have been associated with hypoxic PH with regards to vascular remodeling, vascular angiogenesis, and vascular adventitia fibrosis via the Rho-kinase and the 15-LOX-12/15-HETE-mitogen-activated protein kinases (MAPKs) pathways, providing strong evidence to potential ways the 15-HETE diet could cause the onset of PH.[6,22–24] As PH is caused by an addition of 15-HETE to the diet, the intestine is of peak interest to investigate as the potential starting point of the cascade of events leading to the onset of PH.

1.5 Microbiota

Dietary 15-HETE must pass through the gastrointestinal (GI) tract long before it reaches the lungs, therefore, investigating changes in the intestine is of interest when investigating this model of PH. The GI tract serves as an interface between the host, environmental factors and antigens in the human body, serving as home to 10^{14} microorganisms including bacteria, archaea, and eukarya in what is called the 'gut microbiota'.[41] It is believed that the microbiota begins development at birth and shifts in response to illness, antibiotic treatment and changes in diet.[41] Four phyla dominate the adult microbiota, *Firmicutes*, *Bacteroidetes*, *Actinobacteria*, and *Proteobacteria* and the composition of them is key to maintaining intestinal immunity and whole body homeostasis, with disruptions to the microbiota, also known as dysbiosis, having potentially devastating pathophysiological consequences.[42] Dietary lipids are also capable influencing the gut microbiota profile. They can serve as substrates for lipid metabolism, exerting toxic

effects on residential bacteria, affecting the microbial metabolites produced, and exerting effects on the host phenotype.[43] Advances in next generation high throughput sequencing and mass spectrometry have helped expand our understanding of the impact of the microbiome on the human body by assessing the diversity and composition of human microbes, their functional gene capacity, and the biochemicals they generate.[44] The gut microbiota has been implicated in many immune dysfunctions and chronic diseases including inflammatory bowel disease, behavioral disorders, obesity, type 2 diabetes, cardiovascular disease, and autoimmune diseases such as rheumatoid arthritis.[44,45]

One example of the microbiota producing a chemical that leads to an overall host phenotype is seen with regards to the gut microbiota-initiated trimethylamine (TMA))/flavin-containing monooxygenase 3 (FMO3)/trimethylamine N-oxide (TMAO) pathway.[45] Elevated TMAO levels are associated with Type 2 diabetes in humans and in obese mice, expression of FMO3, which produces TMAO, is positively correlated with body mass index (BMI) and negatively correlated with insulin sensitivity and negatively correlated with genetic markers of brown and beige adipocytes.[45] Knockdown of FMO3 in wild-type female mice and in *Ldlr*$^{-/-}$ mice protected them from high fat diet by decreasing TMAO and TMA plasma levels, stimulating beiging of white adipose tissue.[45]

The microbiota also produces chemicals that are beneficial to the human host. An example of such compounds includes short chain fatty acids (SCFAs). The three predominant SCFAs are propionate, butyrate, and acetate, which are found in a proportion of 1:1:3 in the GI tract.[41] SCFAs are known to be anti-inflammatory, regulate hepatic lipid and glucose homeostasis, regulate the immune and inflammatory response,

and modulation appetite regulation.[41,46–48] Butyrate and propionate are histone deacetylase inhibitors and can epigenetically regulate gene expression.[41,49] Due to their beneficial effects, some SCFAs are available to take as supplements and clinical trials have been conducted using supplemental butyrate to improve lipid metabolism, inflammatory, and in combination with whey, according to Clinical Trials.gov.

Modulations in the SCFA producing microbiota and SCFA levels have been observed in the context of hypertension.[42,50,51] SCFAs can activate GPCRs to influence blood pressure, changes in the balance of the *Firmicutes* and *Bacteroidetes* ratio are a biomarker for pathological conditions and inflammation, and milk fermented with *Lactobacilli* lowered blood pressure in hypertensive humans.[52] Spontaneously hypertensive rats (SHR) are reported to have an increased Firmicutes/Bacteroidetes ratio and decreased acetate- and butyrate-producing bacteria.[42] With regards to PAH, shotgun metagenomic analysis was done on the fecal microbiome of 18 PAH patients and 13 reference patients and it was seen that among the observed changes in the microbiota, it was seen that the reference group had a larger abundance of bacteria that produced SCFAs, namely butyrate and propionate, both of which, as mentioned before, have anti-inflammatory effects.[50] Rats that underwent Sugen/hypoxia treatment had decreases in butyrate and acetate producing bacteria along with decreased acetate serum levels.[53] Not only do these findings indicate that an unbalanced microbiota could contribute to conditions such as PH, but also proposes that targeting the microbiota and supplementing patients with beneficial compounds such as SCFAs could be potential therapeutic approaches to diseases such as PAH.

1.6 Hypothesis

Based on the above findings, we set out to determine whether HETEs and HODEs play a causal role in PAH. We demonstrated that feeding male mice chow diet containing 5 µg 15-HETE (Cayman)/mouse/day for 21 days is sufficient to induce PAH mice as evident by increases in RVSP, Fulton Index, vascular remodeling, lung weight, and plasma levels of HETEs and HODEs. Using this novel diet-induced (15-HETE) model of PAH, I not only investigated the mechanisms by which dietary oxylipins are causal in PAH but also explored the mechanisms by which apoA-I mimetic peptides mitigate PAH. ***I hypothesize that 15-HETE initiates (and Tg6F mitigates) intestinal inflammation by modulating pro-inflammatory lipids, immune response, microbiota composition, and short chain fatty acid levels, which collectively result in the development of PH.***

Recently, in a joint effort with our collaborators, we have reported that dietary 15-HETE induced pulmonary hypertension in mice by triggering T cell-dependent endothelial cell apoptosis, that is modulated by Tg6F both as a preventative and as a rescue, as I will discuss further in Chapter 2.[54] In brief, 15-HETE diet induces oxylipin production by the intestinal epithelial cells (IECs) increasing the concentration of plasma oxylipins that activates the pulmonary arterial endothelial cells (PAECs) which are recognized by cluster of differentiation 8 (CD8+) cells which trigger apoptosis of activated endothelial cells while the apoA-I mimetic peptide Tg6F prevents this cascade of events.[54]

In Chapter 3, I will look further into the scope of changes caused by the 15-HETE diet, specifically how in addition to leading to PH in wild type mice, it also modulates multiple lipid species, specifically triacylglycerol, cholesterol ester, hexosylceramides, and free fatty acids, increases AA and LA, the precursors of HETEs and HODEs, and

alters plasma cytokine levels. I look deeper into the importance of 12/15 and 5 LOX in two key experiments, in the first, we found that 5μg of 5-HETE and 5μg of 5, 12, and 15-HETE total per mouse per day were able to cause PH in wild type mice, and in the second, we found that in mice with the 12/15 LOX gene knocked out 5 LOX is inhibited, the onset of PH is prevented.

In Chapter 4, we combined results from RNA-seq analysis from the lungs of PAH patients as well as the lungs and intestine of 15-HETE fed hypertensive mice and identified interferon induced protein 44 (IFI44) as the only common gene increasing in all three datasets. Time course analysis of intestine and lung tissues note that IFI44 first increases in the intestine, as early as one week into feeding, while it does not increase in the lungs until week three. While much about its function is unknown, we tested its role in our model of PH by silencing it *in vivo* using IFI44 siRNA and determined that knocking down IFI44 prevented PH in 15-HETE fed mice when compared to mice administered scramble IFI44 siRNA, identifying it as an exciting novel target for future studies and therapies for PH.

Finally, in Chapter 5, I investigate modulation of the microbiota and SCFA production by the 15-HETE diet and determine whether the addition of butyrate, one SCFA produced by the microbiota, can protect mice from 15-HETE induced PH. Microbiota analysis showed that the abundances of *Lachnospiraceae*, *Ruminococcaceae*, and *Anaerostipes* were reduced in female mice fed after three weeks of consuming the 15-HETE diet. All three species of bacteria are noted to be producers of the SCFA butyrate, which is known to have anti-inflammatory properties.[50] Measuring SCFA levels in the fecal pellets showed mice that consumed Tg6F had increased levels

of acetate, propionate and butyrate in their fecal pellets compared 15-HETE fed mice, all of which also have anti-inflammatory properties.[47,50] I set out to determine whether adding supplementary butyrate would be able to prevent the onset of PH by feeding it to mice in their drinking water as they consumed the 15-HETE diet concurrently or if it could rescue mice from PH after two weeks of eating the 15-HETE diet, when pulmonary arterial acceleration time (PAAT) has significantly decreased. Interestingly, the addition of sodium butyrate to the drinking water decreased the RVSPs of mice when administered for all three weeks and for only the final week, showing its potential to be a novel therapeutic in PH.

In Chapter 6, I discuss the future directions of my research. To further implicate the role of intestinal production of HETEs and HODEs, I have, and am breeding, 12/15 LOX-floxed mice that can be crossed with villin-cre mice to generate mice that can have 12/15 LOX knocked out specifically in the intestine. The intestine only 12/15 LOX KO mice will be fed 15-HETE supplemented diet, PAAT will be assessed over three weeks, and direct catheterization of their RVSPs will determine whether intestinal knockout of 12/15 LOX prevents the onset of PH. More work to understand the pathway by which IFI44 acts to induce PH is underway by investigating which genes that are highly correlated with IFI44 in the RNA-seq datasets are also being increased in hypertensive mice and patients *in vivo*. The microbiota and SCFA story can be continued first by determining the mechanism by which butyrate is preventing PH and then by investigating whether other SCFAs such as acetate or propionate are effective in preventing PH in the 15-HETE diet as butyrate has done in my studies. The effectiveness of supplemental SCFA administration can also be investigated in other animal models of PH including the

rat MCT and the mouse CHP models. In addition to adding supplemental SCFAs to prevent PH, studies focusing supplementing the diet with fiber and probiotics to improve production of bacteria that produce SCFAs as a method to prevent PH in animal models can also be explored to assess their potential as therapeutics for PAH.

CHAPTER 2: Oral 15-Hydroxyeicosatetraenoic Acid Induces Pulmonary Hypertension in Mice by Triggering T Cell–Dependent Endothelial Cell Apoptosis

Abbreviations

PAH	Pulmonary Arterial Hypertension
15-HETE	15-Hydroxyeicosatetraenoic Acid
PH	Pulmonary Hypertension
PAEC	Pulmonary Arterial Endothelial Cells
ApoA-I	Apolipoprotein A1
Tg6F	Transgenic Tomatoes Expressing the ApoA-I Mimetic Peptide 6F
mPAP	Mean Pulmonary Arterial Pressure
EC	Endothelial Cells
SMC	Smooth Muscle Cells
RV	Right Ventricle
HODE	Hydroxyoctadecadienoic Acid
PASMC	Pulmonary Arterial Smooth Muscle Cells
WT	Wild Type
EV	Empty Vector Tomatoes
RVSP	Right Ventricle Systolic Pressure
LV	Left Ventricle
IVS	Interventricular Septum
B2M	β2 Microglobulin
CD8	Cluster of Differentiation 8
VCAM1	Vascular Cell Adhesion Protein 1
PSMB9	Proteasome Subunit Beta Type-9
MCT	Monocrotaline
HDL	High-Density Lipoprotein
PPARγ	Peroxisome Proliferator-Activated Receptor Gamma
MHC	Major Histocompatibility Complex
HLA-DP	Human Leukocyte Antigen-DP

Abstract

Pulmonary arterial hypertension (PAH) is a fatal disease characterized by increased mean pulmonary arterial pressure. Elevated plasma and lung concentrations of oxidized lipids, including 15-hydroxyeicosatetraenoic acid (15-HETE), have been demonstrated in PAH patients and animal models. We previously demonstrated that feeding mice with 15-HETE is sufficient to induce pulmonary hypertension (PH), but the mechanisms remain

unknown. RNA-Seq data from the mouse lungs on 15-HETE diet revealed significant activation of pathways involved in both antigen processing and presentation and T cell mediated cytotoxicity. Analysis of human microarray from PAH patients also identified activation of identical pathways compared to controls. We show that in both 15-HETE fed mice and PAH patients, expression of the immuno-proteasome subunit 5 is significantly increased, which was concomitant with an increase in the number of CD8/CD69 double positive cells as well as pulmonary arterial endothelial cell (PAEC) apoptosis in mice. Human PAEC cultured with 15-HETE were more prone to apoptosis when exposed to CD8 cells. Cultured intestinal epithelial cells secreted more oxidized lipids in response to 15-HETE which is consistent with accumulation of circulating oxidized lipids in 15-HETE fed mice. Administration of transgenic tomatoes expressing the apolipoprotein A1 (apoA-I) mimetic peptide 6F (Tg6F) that is known to prevent accumulation of circulating oxidized lipids, not only inhibited PAEC apoptosis but also prevented and rescued 15-HETE induced PH in mice. In conclusion, our results suggest that (i) 15-HETE diet induces PH by a mechanism that involves oxidized lipid-mediated T-cell dependent PAEC apoptosis and (ii) Tg6F administration may be a novel therapy for treating PAH.

Introduction

PAH is a life-threatening disease defined by an increased mean pulmonary arterial pressure (mPAP) above 25mmHg.[55] The increase in mPAP is due to multiple factors including inflammation and dysfunction of vascular endothelial cells (EC) and smooth muscle cells (SMC) leading to pulmonary vascular wall thickening.[55–57] Over time, sustained increase in mPAP results in right ventricle (RV) hypertrophy and subsequently to RV failure and death.[58]

The role of oxidized fatty acids and oxidized phospholipids in atherosclerosis and other

inflammatory diseases is well established.[20,59] Biological metabolites of arachidonic acid and linoleic acid, hydroxyeicosatetraenoic acids (HETEs) and hydroxyoctadecadienoic acids (HODEs), respectively, play a critical role in the pathogenesis of atherosclerosis. Recently, our group and others demonstrated increased concentrations of oxidized fatty acids 5-, 12-, and 15-HETE, and 9-, 13- HODE in the plasma and lung tissues of patients with PAH[12,13,60] and in several animal models of PH.[21,61] Increased 15-HETE levels in the context of PH has been shown to induce pulmonary arterial smooth muscle cells (PASMC) pro-proliferative/anti-apoptotic phenotype[21,22,61,62], inflammation[60], and fibrosis.[24] The causal role of oxidized fatty acids is now well established in atherosclerosis, however; it is not known whether oxidized lipids participate in PH development.

In the present study we demonstrate that dietary 15-HETE is sufficient to induce PH in wild type (WT) mice. Using unbiased large-scale transcriptomics, we identified key pathways that are dysregulated by dietary 15-HETE and further confirmed the dysregulation of similar pathways in PAH patients. We established that increased endothelial cell (EC) apoptosis by 15-HETE *via* a T cell-dependent mechanism is at least one of the mechanisms triggering PH in WT mice. Furthermore, we demonstrate that the apoA-I mimetic peptide Tg6F, which has previously been shown to reduce plasma oxidized lipids and atherosclerosis[63,64], can prevent and rescue PH development in WT mice.

Materials and Methods

Materials in the Data Supplement provide details on all methods. The RNA sequencing (RNA-Seq) data that support the findings of this study are available from the

corresponding author upon reasonable request.

Human Subjects

Patients studied were part of the French Network on Pulmonary Hypertension, a program approved by institutional Ethics Committee, and had given written informed consent (Protocol N8CO-08-003,IDRCB:2008-A00485-50, approved on June 18, 2008). Patient's characteristics are given in Table S1 of the Data Supplement.

Mice and treatments

Male and female C57BL6/J mice (wild type, 2-3 months old) were used. Experimental protocols are described in detail in Supplementary Materials.

To prepare the HETE diets, Teklad diet was prepared so that each mouse consumed 4 g chow per day. The HETE diets were supplemented with either 5 µg 15-HETE (34720, Cayman Chemical), 5 ug 5-HETE (34210, Cayman Chemical), or 5 ug total of 15-HETE, 5-HETE, and 12-HETE (34550, Cayman Chemical) per mouse per day. Tg6F or control empty vector tomatoes (EV) were freeze-dried, powdered, and added to the diet at 2.2% by weight as previously described.[63,65] The Tg6F prevention protocol consisted of 21 days of feeding mice 15-HETE+Tg diet whereas the rescue protocol involved feeding just the 15-HETE diet for 2 weeks before switching to the 15-HETE+Tg diet in the final week.

Pulmonary Hypertension assessment, Histology, Western Blot analysis, immunohistochemistry and imaging

Development of PH was monitored weekly by noninvasive two-dimensional Doppler echocardiography using Vevo 2100 (Visualsonics). At the end of the protocol, open chest

catheterization was performed to assess right and left ventricular systolic pressure. Right ventricular index was measured by dividing the weight of the right ventricle by the sum of the left ventricle and intra-ventricular septum. Mouse lungs were used for Histology, Western Blot analysis, immunohistochemistry and imaging as described Supplementary Materials.

Mass Spectrometry

Mouse Plasma and lung samples were used for measurements of oxidized lipids using liquid chromatography–tandem mass spectrometry analysis (SCIEX). A detailed protocol is provided in the Supplemental Methods and in the study by Meriwether et al.[66]

RNA sequencing and microarray Analysis and Real Time PCR

Total RNA from lungs was isolated with Trizol extraction method for Real-time PCR and miRvana Total RNA Isolation Kit for RNA-Seq. Details of the method for Real Time PCR, and RNA-Seq analysis are given in the Data Supplement.

Proteasome and Immunoproteasome activity

Mouse and human lungs were used for measurements of proteasome and immunoproteasome activity and expression as described in details in the Data Supplement.

Cell culture

Primary cultures of healthy human pulmonary arterial endothelial cells (PAEC) were purchased from ATCC and used for gene expression, and apoptosis as described in the Data Supplement.

Statistical analysis

Values were summarized between groups using mean±SEM. For comparing numerical measures between 2 groups, we used the unpaired t test. To compare >2 groups, we used a 1-way ANOVA test, when the overall ANOVA was significant, we performed a Sidak multiple comparisons test to compare a set of means. The normality assumption for these comparisons was assessed using the Shapiro- Wilk test. The Brown-Forsythe (Modified Levene) test was used to verify the homogeneity of variance assumption. When these assumptions were not fulfilled, values were log transformed to stabilize variances, and statistical analyses were performed on the log-transformed data. When statistics were performed on males and females, we applied a 2-way ANOVA test to assess the potential interaction between sex and 15-HETE diet. To assess the strength and magnitude of associations between continuous measures, we used Pearson correlation coefficient. A significance level of 5% ($P<0.05$) was considered statistically significant. All analyses were made with Graph Pad Prism v.6.

Results

15-HETE diet induces PH in wild type mice

To assess the causal role of 15-HETE in the development of PH, WT mice were fed either normal chow or chow supplemented with 15-HETE for 3 weeks. Doppler echocardiography of the pulmonary artery blood flow showed a significant decrease in pulmonary arterial acceleration time after 2 weeks in male mice fed the 15-HETE diet, which continued to further decrease toward the third week (**Figure 1A**). These results were confirmed by RV catheterization and RV index measurement showing significantly increased right ventricular systolic pressure (RVSP) and RV hypertrophy at the end of the

protocol (**Figure 1B and C**). Left ventricle (LV) systolic pressure was significantly increased (**Figure S1A**) while the LV hypertrophy index ((LV + interventricular septum [IVS)/body weight) was not altered (**Figure S1B**). The mice did not have any detectable atherosclerotic lesions in the aortas as assessed by oil-red-O staining (**Figure S1C**). Furthermore, pulmonary vascular wall thickness was significantly increased (**Figure 1D**) and vascular wall thickness correlated with RVSP (**Figure 1E**) which further confirmed the presence of PH in mice on 15-HETE diet. We next examined whether 15-HETE-induced PH is mediated by direct action of 15-HETE or by its metabolites. 15-HETE methyl ester, which cannot be readily metabolized, also induced PH in WT mice, suggesting that 15-HETE, and not its metabolites, is primarily responsible for PH induction (**Figure S1D**). We also found significant increases in plasma (**Figure S1E**) concentrations of 15-HETE and 12-HETE, concomitant with significant increases of 15-, 12-, and 5-HETE in the lungs (**Figure 1F**) of these mice. In addition, we examined whether 15-HETE diet could induce PH in female mice. Similar to the male mice, female mice also developed PH when fed 15-HETE diet. Interestingly, PH severity was worse in female mice than in male mice since RVSP was significantly higher (49.4±3.1 versus 38.8±1 mm Hg in male mice, $P<0.0001$; **Figure S1F**). Taken together, our results demonstrate a causal role for 15-HETE in the development of PH in both male and female mice.

RNA-Seq of Lung Tissues From Mice on 15-HETE Diet Reveals Dysregulation of Several Pathways, Which Were Similarly Dysregulated in Lungs of Patients With PAH

To decipher the impact of 15-HETE diet on lung biology, we performed RNA-Seq on the lungs of mice on 15-HETE diet. RNA-Seq data analysis revealed 132 genes were

upregulated and 106 were downregulated (**Figure 2A**). Using pathway enrichment analysis, we discovered significant enrichment of 18 gene sets **(Figure 2B and 2C; Figure S2A and S2B**), which are implicated in antigen presentation, T cell–mediated cytotoxicity, and cell killing. Furthermore, leading-edge analysis on these pathways revealed a strong overlap between gene sets (**Figure 2D**). Finally, to define the most relevant genes from the leading-edge analysis, we focused on genes significantly up/downregulated and overlapping between gene sets (**Figure 2E**). We confirmed a significant upregulation of B2m (β2 microglobulin), known to be responsible for antigen presentation, Psmb8, a subunit of the proteasome participating in antigen processing, as well as cluster of differentiation (CD) 8 (cluster of differentiation 8), CD4, and CD69 markers of T cells (**Figure 2F; Figure S2C**), in the lungs of male mice on15-HETE diet compared with chow diet. Interestingly, CD8 and CD69 were similarly upregulated in the lungs of female and male mice on 15-HETE diet compared with chow diet while CD4 was only significantly increased in male but not in female mice (**Figure S2D**).

To examine whether the same gene sets are also enriched in patients with PAH, we reanalyzed publicly available human microarray data (GSE5340818). This analysis revealed the differential expression of genes implicated in similar gene sets enriched both in human and mouse (**Figure 3A and 3B**). Furthermore, we confirmed the upregulation of CD69 and VCAM1 (vascular cell adhesion protein 1) mRNA, as well as the downregulation of PSMB9 (proteasome subunit beta type-9) (**Figure 3C and 3E**) by real-time quantitative polymerase chain reaction using an independent set of PAH patient's lung samples. Taken together, our results from mouse and human transcriptome analyses suggested that our dietary animal model is well suited for understanding the

pathways that were also dysregulated in human disease.

Proteasomal Activity Is Modified in the Lungs of Mice on 15-HETE Diet and in Human PAH Patients

Our comparison between the gene expression profiles of human PAH patients and 15-HETE diet–fed mice revealed activation of antigen processing and presentation pathways with altered expression of catalytic subunits of the proteasome and the immunoproteasome. In mice, we found the activity of the catalytic subunits β1/PSMB1, β2, and β5 (**Figure 4A**) was not significantly different between chow and 15-HETE diets. The immunoproteasome activity of β1i/PSMB9 **(Figure 4A**) was not significantly affected, whereas β5i/PSMB8 (**Figure 4A**) was increased significantly in the lungs of mice on 15-HETE diet compared with regular chow. Western blot analysis revealed a significant decrease in protein expression of the β5/PSMB5 subunit, but no changes in protein expression of β1i/PSMB9 and β5i/PSMB8 were noted (**Figure S3A through S3D**).

In humans, we found significantly decreased activity of the proteasome subunit β1/PSMB1 (**Figure 4B)** while the other catalytic subunits of the constitutive proteasome remained unchanged (**Figure 4B**). We also found significantly increased activity of the 2 catalytic subunits of the immunoproteasome measured (**Figure 4B**). The assessment of β5/PSMB5, β5i/PSMB8, and β1i/PSMB9 expression revealed a trend toward an upregulation of the mRNA and protein of β5/PSMB5 (**Figure S3E through S3G**) and a significant decreased expression of β5i/PSMB8 (**Figure S3F**) and β1i/PSMB9 mRNA (**Figure 3E**).

Increased Apoptosis of Pulmonary Arterial ECs by 15-HETE via Cytotoxic T-Cell

Induction

To understand the effect of the activation in antigen presentation and T cell–mediating cytotoxicity pathways in the lungs of 15-HETE diet–fed mice, we examined EC apoptosis—a known early event of PH development[67,68]—and the activation of CD8-positive cells into cytotoxic T cells. We found a significant increase in the number of apoptotic ECs (**Figure 4C**) concomitant with a significant increase in CD8 and CD69 double-positive cells (**Figure 4D**). In pulmonary arterial EC (PAEC) exposed to 15-HETE, we observed upregulation of B2m, PSMA4, and PSMB9, as well as a significant downregulation of PSMB8 and a trend toward decreased expression of PSMB5 (**Figure S4A through S4C**). These experiments demonstrated that 15-HETE treatment induces PAEC dysfunction. There was a significant increase in the number of apoptotic PAECs when exposed to 15-HETE and CD8+ cells compared with PAECs exposed to vehicle and CD8+ cells (**Figure 4E**). Since oral 15-HETE resulted in increased levels of not only circulating and tissue 15-HETE but also other oxidized fatty acids, it is possible that 15-HETE is acting on the intestinal epithelial cells. We found exposing intestinal epithelial cells to 15-HETE resulted in increased level of all oxidized lipids in the supernatant (**Figure 4F; Figure S5**). Altogether, these experiments suggest that 15-HETE alone is able to induce the production of oxidized lipids by the intestinal epithelial cells and can result in the activation of the antigen processing and presentation pathways in PAECs, making these cells prone to cytotoxic T cell–dependent induction of apoptosis.

ApoA-I Mimetic Peptide Tg6F Prevents and Rescues PH Induced by 15-HETE Diet

ApoA-I mimetic peptides are known to bind to oxidized fatty acids and to facilitate their clearance from the blood stream.[11,63,69,70] We examined whether Tg6F is able to prevent

or rescue PH in 15-HETE diet–fed mice (**Figure 5A**). In the prevention protocol, Tg6F abolished the decrease in pulmonary arterial acceleration time induced by 15-HETE (**Figure 5B**). Interestingly, in the rescue protocol, Tg6F was able to restore pulmonary arterial acceleration time to the level observed in mice on chow diet (**Figure 5B**). Mice in the prevention and rescue group also had significantly lower RVSP, vascular wall thickness, number of apoptotic ECs, and activated CD8-positive cells compared with 15-HETE plus empty vector–treated mice (**Figure 5C through 5F**). These results demonstrate the efficacy of Tg6F treatment to prevent and reverse PH induced by 15-HETE diet by inhibiting 15-HETE–mediated PAEC apoptosis.

Discussion

In the present study, we demonstrate that feeding WT mice with 15-HETE, the major metabolite of arachidonic acid in the lung,[71] with no other insults, is sufficient to induce PH both in male and female mice (**Figure 1; Figure S1F**). Although mice were exclusively fed with 15-HETE, the concentrations of other oxidized lipids (5-, 11-, and 12-HETE) were increased both in plasma (**Figure S1E**) and lung (**Figure 1F**). According to large-scale transcriptomic data, mice on 15-HETE diet and patients with PAH both exhibit activation of pathways involved in antigen processing (including proteasome activity) and presentation and T cell–mediated cytotoxicity in the lungs (**Figures 2 through 4**). Activation of these pathways in mice was concomitant with increased PAEC apoptosis (**Figure 4**) and in vitro exposure of human PAEC to 15-HETE together with CD8+ T cells resulted in increased apoptosis compared with cells only exposed to CD8+ T cells (**Figure 4**). Finally, we showed that Tg6F supplementation to the 15-HETE diet was able to prevent and rescue PH by reducing PAEC apoptosis (**Figure 5**).

The lipoxygenase pathway has emerged recently as an important player in the pathogenesis of PH. In the last decade, the implication of lipids, particularly oxidized lipids, in the pathogenesis of PH has been demonstrated by our group and others both in PH patients and in experimental models of PH.[11,12,60,72,73] Although oxidized lipids are known to play a role in PH, our work is the first to demonstrate that oxidized lipids can cause PH in WT mice in the absence of any other PH stimulus. Considering that mice have a single enzyme for generating 12-HETE and 15-HETE from 12/15-LOX (12/15 lipoxygenase and that 15-HETE is the major metabolite of this enzyme, we fed mice a diet rich in 15-HETE. After 3 weeks, the severity of PH in our new dietary model of PH is comparable with the well-established model of PH induced by hypoxia.[74] Our data also show a correlation between vascular wall thickness and RVSP. 15-HETE methyl ester—a stable form of 15-HETE that is not readily metabolized—was equally efficient in inducing PH suggesting that 15-HETE, and not its metabolites, drives PH development.

The 15-HETE diet affected both the pulmonary circulation and the systemic circulation, as the LV systolic pressure in 15-HETE–fed mice was also significantly higher than mice fed regular chow; however, we only observed hypertrophy of the RV. Because of the increased LV systolic pressures, it is plausible that LV hypertrophy could develop over a longer duration of the 15-HETE diet. Our model is not an atherosclerosis model, as no lipid deposition was observed in the aorta of these mice (**Figure S1**). Although the mice were only fed with 15-HETE diet, we observed an increase in the levels of 15-HETE, as well as 12-HETE, 11-HETE, 9-HODE, and 13-HODE, in the plasma following the 3-week diet (**Figure S1**). The induction of other oxidized lipid expression can be due to the activation of lipoxygenase that our group recently demonstrated.[11] We also observed

significantly increased levels of 5-, 11-, 12-, 15-HETE in the lungs of mice on 15-HETE diet (**Figure 1; Figure S1**). Since oral 15-HETE resulted in increased levels of not only circulating and tissue 15-HETE but also other oxidized fatty acids, it is possible that 15-HETE is acting on the intestine. We found exposing intestinal epithelial cells to 15-HETE resulted in increased level of all oxidized lipids in the supernatant (**Figure 4F**). These results provide evidence that 15-HETE diet is sufficient to induce PH in WT mice and leads to increased production of several HETEs and HODEs. In addition, our work suggests that intestinal epithelial cells could be the first cell type responding to dietary 15-HETE (**Figure S5; Figure 6**).

Despite the known implication of oxidized lipids in lung biology, the role of 15-HETE in PH pathology remains incompletely understood. Oxidized lipids have been implicated in pulmonary vasoconstriction,[75–77] vascular remodeling,[6,21,61] and to increase inflammation.[60] Furthermore, our group demonstrated that increased plasma oxidized lipids in PH were associated with downregulation of miR-193 in the lungs of PH rats and humans. In turn, miR-193 increases oxidized lipid production by targeting lipoxygenase enzymes, creating a positive feedback loop.[11] To further discover novel pathways that cause development of PH in mice on an oxidized lipid diet, we performed RNA-Seq on lungs of mice fed with 15-HETE. Our RNA-Seq analysis revealed antigen processing and presentation pathways and T cell–mediated cytotoxicity as top activated pathways. Our high-throughput sequencing analysis of the lungs of patients with PAH also confirmed activation of antigen processing and presentation pathways (VCAM1 and PSMB9) as well as T cell–mediated cytotoxicity (CD69) further strengthening our new mouse model of PH (**Figure 3**). In patients with PAH, the increased number of CD8+ T cells promotes disease

development by triggering pulmonary vascular remodeling.[78–80] We demonstrated that expression of CD8 and CD69 was similarly upregulated in the lungs of both male and female mice on the 15-HETE diet supporting the role of CD8 cell activation in 15-HETE–induced PH in both genders. Interestingly, we observed that the expression of anti-inflammatory regulatory T-cell CD4 was only upregulated in the lungs of male but not in female mice (**Figure S2C and S2D**), which could explain the development of more severe PH in female mice when compared with male mice on 15-HETE diet (**Figure S1E**). Our data are in agreement with the work of Dr Nicolls Laboratory demonstrating that regulatory T cell–deficient female rats developed more severe PH than males and immune reconstitution of regulatory T-cell CD4 abolished sex differences in athymic rats.[81] Our results support a potential role of CD4 cells in the differences observed between male and female mice on 15-HETE diet in addition to the role of CD8 cell activation.

Also, our in vivo data show that EC apoptosis is increased in the lungs of 15-HETE diet–fed mice, and our in vitro data demonstrate that CD8 cells are able to increase apoptosis in human PAEC exposed to 15-HETE (**Figure 4**). PAEC apoptosis has been described as an early event in monocrotaline (MCT) and Sugen/hypoxia rat models of PH,[82] and its inhibition blocks PH development in Sugen/hypoxia mice.[83] In agreement with our findings, an increased number of CD8+ T cells in patients with PAH has been shown to promote disease development by triggering pulmonary vascular remodeling.[78–80] Taken together, our data support the view that CD8+ cytotoxic T cell–induced PAEC apoptosis by 15-HETE is one of the major mechanisms triggering PH. The absence of PH and EC apoptosis in CD8-deficient mice on 15-HETE diet would further strengthen

the direct role of T cell–dependent EC apoptosis on 15-HETE–induced PH. In addition, oxidized lipids could act independently of CD8 cells as they are known to induce PASMC proliferation and thus could also participate in PH development by triggering pulmonary vascular hyperplasia.

Concomitant with increased CD8+ cells and PAEC apoptosis, we demonstrated a significant increase in the activity of immunoproteasome β5i/PSMB8 in the lungs of mice on 15-HETE diet compared with regular chow (**Figure 4**). This is especially significant because the immunoproteasome is important in producing antigenic peptides, which can be recognized by CD8+ cells leading to cell apoptosis.[84] While 15-HETE altered the mRNA and protein expression of the constitutive proteasome (β5 subunit; **Figure S3**), it did not affect the proteolytic activities of the proteasome (**Figure 4**). This suggests that a compensatory mechanism is likely occurring to maintain the constitutive proteasome activity close to control levels.

Using human lung samples, we found patients with PAH showed similar increases in immunoproteasome activity as observed in mice treated with 15-HETE diets (**Figure 4**). The β5i activity increased similarly in both human and mouse lungs, whereas the β1i immunoproteasome activity was exclusively increased in patients with PAH (**Figure 4**). While mouse lungs treated with 15-HETE showed a trend toward decreased β1 activity, human samples showed a significantly reduced activity in PAH lungs compared with control lungs (**Figure 4**). The significantly decreased expression of β5i/PSMB8 suggests that the immunoproteasome in PAH lungs was considerably more efficient that the immunoproteasome in control lungs and similar to mouse lungs is likely a result of altered posttranscriptional modifications on the immunoproteasome or associating partners

(**Figure S3**). Treatment of PAEC with 15-HETE for varying time periods resulted in decreased β5i mRNA expression similar to what was observed in lungs from patients with PAH (**Figure 4; Figure S3**). These results strongly suggest that 15-HETE either directly or indirectly affects immunoproteasome function.

A significant decrease in circulating levels of HDL (high-density lipoprotein) cholesterol was associated with worse clinical outcomes in patients with PAH.[85] ApoA-I is the major protein constituent of HDL, and apoA-I mimetic peptides have been developed, in part, to confer the anti-inflammatory functions of HDL and originally named as HDL-mimetic peptides.[63] Indeed, in animal models of dyslipidemia, apoA-I mimetic peptides improved HDL cholesterol levels modestly.[63] It must be noted that we did not see significant changes in HDL cholesterol in our animal model (data not shown). However, these results were not surprising since our model is on a nondyslipidemic C57BL/6 background and apoA-I mimetic peptides have not been reported to reduce lipoprotein cholesterol levels in WT mice.

A well-established functionality of HDL is the clearance of lipid oxidation products via reverse cholesterol transport.[86] ApoA-I mimetic peptides are known to bind to oxidized lipids, increasing their clearance from the circulation, thus promoting an anti-inflammatory response.[11,63,70,71] In line with mode of action and mechanism, previously, apoA-I–mimetic peptide 4F was shown to have therapeutic benefit in various disease models,[30] including endotoxemia,[87] atherosclerosis,[88] and cancer.[65] Furthermore, our group showed apoA-I mimetic peptides are effective in reducing PH severity in multiple animal models.[89] Tg6F has also been shown to mitigate a number of disease processes in animal models.[63,82,88,90] Oral administration of Tg6F has been associated with lowering levels of

5-HETE, 15-HETE in LDLR−/− mice on Western Diet.15 Here, we found that Tg6F is able to prevent and even rescue PH induced by the 15-HETE diet in WT mice (**Figure 5**). RVSP and vascular remodeling, as well as EC apoptosis and CD8+ T-cell activation, were all significantly reduced by Tg6F treatment. The efficacy of apoA-I mimetic peptides in treating PH in multiple animal models of PH,[11,22,73,74,91] as well as in ameliorating various diseases associated with secondary PH (autoimmune diseases,[92,93] atherosclerosis,[82] pulmonary fibrosis[28]), suggests a potential clinical benefit of apoA-I mimetic peptides for different forms primary or secondary PH.

Interestingly, in the last decade, numerous studies suggested that the small intestine accounts for ≈30% of the plasma HDL cholesterol pool and thus is a major site of regulation of inflammation.[94] Furthermore, Navab *et al*[69] demonstrated that apoA-I mimetic peptides were acting on the small intestine leading to decreased concentration of circulating oxidized lipids. These data suggest intestine plays a role in promoting PH in 15-HETE diet–induced mouse model and in patients with PAH. Nonetheless, the implication of intestine in PH pathology remains to be established, and to this end, our model of 15-HETE diet–induced PH could be a major investigating tool.

In this study, we showed 15-HETE diet is sufficient to cause PH in both male and female mice. Although high levels of plasma oxidized lipids are reported in diseases including connective tissue disease, left heart disease, and pulmonary fibrosis, only a subpopulation of patients with these diseases develops PH. In this context, high oxidized lipids are perhaps a “second hit” in patients with a genetic predisposition for PH. For example, the presence of a BMPR2 mutation could predispose patients with high plasma oxidized lipid concentration to develop PH. Indeed, the presence of a BMPR2 mutation is

known to decrease the expression of transcription factor PPARγ (peroxisome proliferator-activated receptor gamma), which is a major regulator of ApoE (apolipoprotein E) expression.[95–97] In addition, 15-HETE is known to bind to PPARγ and to increase PPARγ transcriptional activity.[98] Thus, we speculate that in subjects with no BMPR2 mutation, increased levels of plasma/lung 15-HETE result in activation of PPARγ in pulmonary vasculature leading to increased ApoE expression protecting them against PH development. However, in subjects with BMPR2 mutation, increased levels of 15-HETE are not able to induce ApoE expression through PPARγ, increasing the risk of developing PH. A similar speculation for increased vulnerability to develop PH with oxidized lipids as a second hit could also be made in subjects with the recently discovered single-nucleotide polymorphism in class II major histocompatibility complex (MHC) human leukocyte antigen-DP (HLA-DP).[99] Indeed, in the present study, we showed that antigen presentation pathways are dysregulated in patients with PAH and in mice on 15-HETE diet, thus patients carrying this single-nucleotide polymorphism could be more prone to develop PH. These speculations will need to be further investigated to understand the potential genetic implication of PAH susceptible patients with a high plasma concentration of oxidized lipids.

Conclusions

This study highlights the causal role of 15-HETE in PH by inducing PAEC apoptosis through a CD8+-dependent mechanism (**Figure 6**). Furthermore, we demonstrated that an apoA-I mimetic peptide, Tg6F, prevents and rescues PH induced by 15-HETE. Further investigation is needed to clarify the therapeutic potential of apoA-I mimetic peptides for patients with various forms of PH.

Perspectives

While oxidized lipids are known to cause numerous systemic cardiovascular diseases, this is the first study demonstrating that the major metabolite of arachidonic acid in the lung, 15-HETE, can cause PH. We show that a diet rich in 15-HETE is causal in PH through triggering PAEC death in a cytotoxic T cell–dependent mechanism. This finding further implicates CD8+ cells in PH and other diseases where 15-HETE is upregulated. In addition, we found 15-HETE–induced proteasome dysregulation in patients with PAH. This opens a new area of research, especially for PAH patients with an HLA-DPA1/DPB1 single-nucleotide polymorphism. Finally, we demonstrate that Tg6F—a safe compound known to reduce oxidized lipid burden—can prevent and rescue PH, making it a highly promising therapeutic compound for patients with PAH.

Sources of Funding:

This study is supported by the National Institutes of Health (R01HL129051, M. Eghbali and S.T. Reddy; R01HL148286 and P01HL030568, A. Fogelman and S.T. Reddy; R01HL147586, M. Eghbali), the American Heart Association (17POST33670424 and 20POST35210727, G. Ruffenach; 17PRE33420159, C.M. Cunningham), and the Foundation for Anesthesia Education and Research (S. Umar).

Disclosures:

A. Fogelman and S.T. Reddy are principals in Bruin Pharma, and A. Fogelman is an officer in Bruin Pharma. The other authors report no conflicts.

Figures

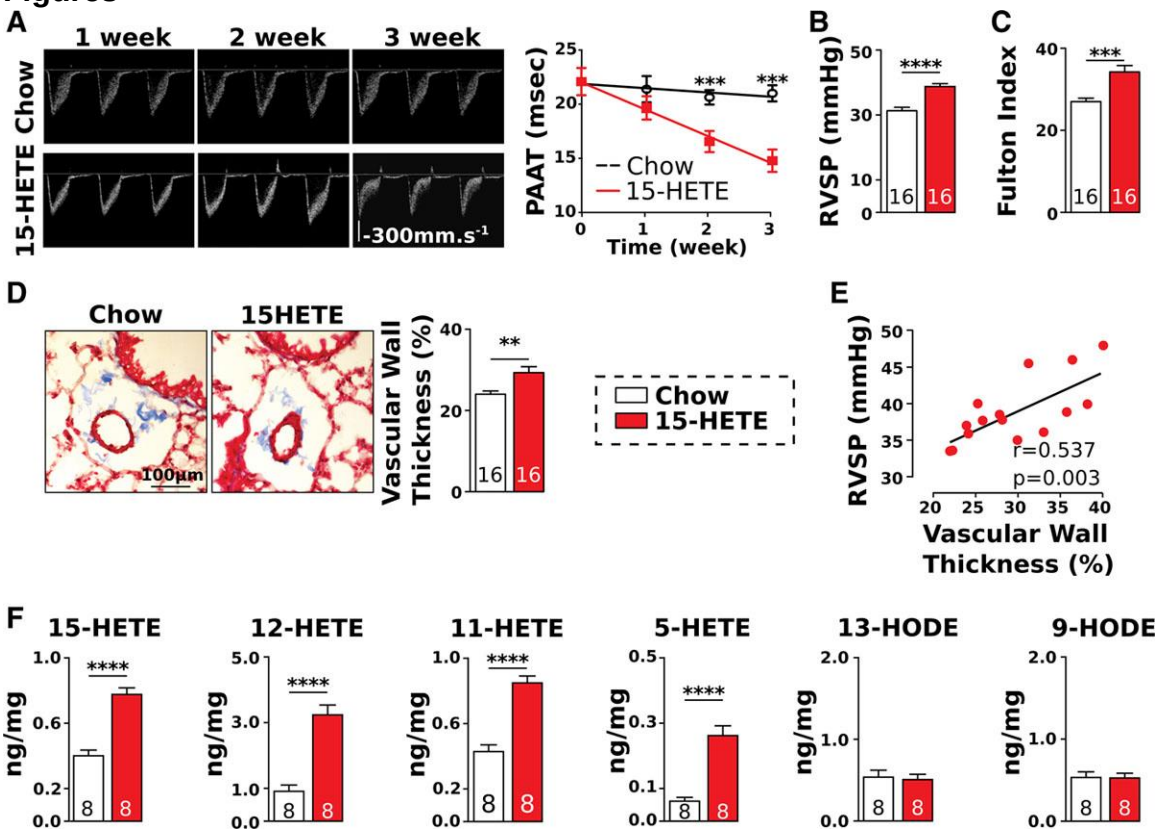

Figure 1: **15**-Hydroxyeicosatetraenoic acid (15-HETE) diet induces pulmonary hypertension. **A**, Representative images of weekly pulsed-wave Doppler and pulmonary arterial acceleration time (PAAT) quantification (n=16/group). **B**, Right ventricular systolic pressure (RVSP) at the end of 3 wk of chow or 15-HETE diet (n=16/group). **C**, Right ventricular hypertrophy in chow and 15-HETE diet mice (n=16/group). **D**, Representative images and quantification of pulmonary vascular wall thickness in chow and 15-HETE diet–fed mice (n=16/group). **E**, Correlation between vascular wall thickness and RVSP in mice fed 15-HETE diet (n=16). **F**, Lung concentration of oxidized lipids in chow and 15-HETE diet mice after 3 wk (n=8/group). HODE indicates hydroxyoctadecadienoic acid. **P*<0.05, ***P*<0.01, *** *P*<0.001, **** *P*<0.0001.

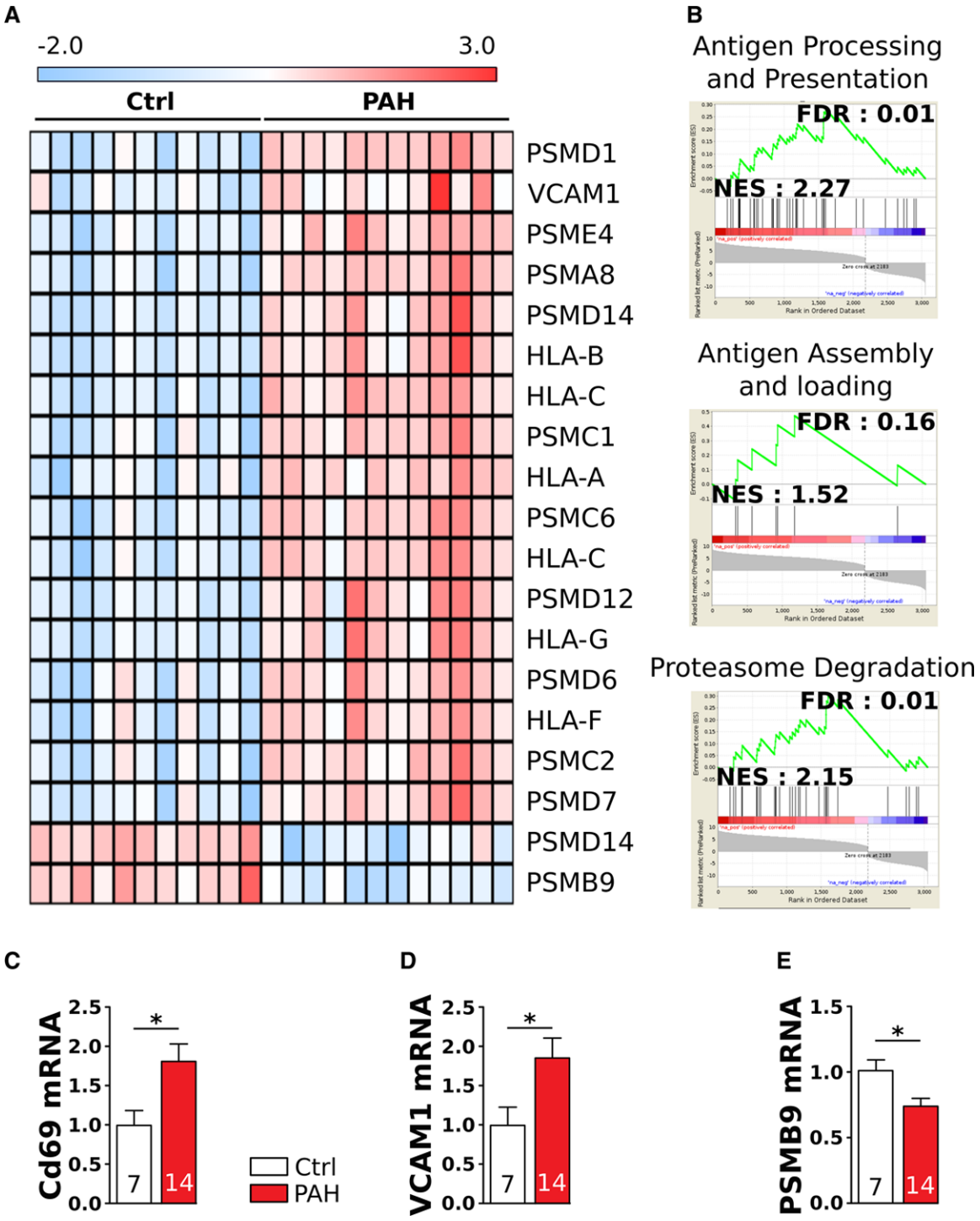

Figure 2: RNA sequencing reveals activation of antigen processing and presentation in the lung of mice fed with 15-hydroxyeicosatetraenoic acid (15-HETE) diet. **A**, Heat map of the 25 most upregulated genes in mice on 15-HETE diet compared with chow diet, and heat map of the 25 most downregulated genes in mice on 15-HETE diet compared with chow diet. **B**, STRING analysis showing the known connection between the upregulated genes. **C**, Gene set enrichment analysis showing the top 4 most upregulated gene sets in mice fed with 15-HETE diet compared with chow diet. **D**, Leading-edge analysis

showing the overlap between the enriched gene sets (darker green means more interaction between the 2 gene sets). **E**, Heat map of the upregulated genes overlapping between the 4 most enriched gene sets in **D**. **F**, Validation of RNA-Seq data using RT-qPCR for 3 genes that are significantly upregulated in the lung of mice fed 15-HETE diet compared with chow diet (n=8/group). *P<0.05, **P<0.01. n=6/group unless otherwise noted. FDR indicates false discovery rate; NES, nominal enrichement score; and RT-qPCR, real-time quantitative polymerase chain reaction.

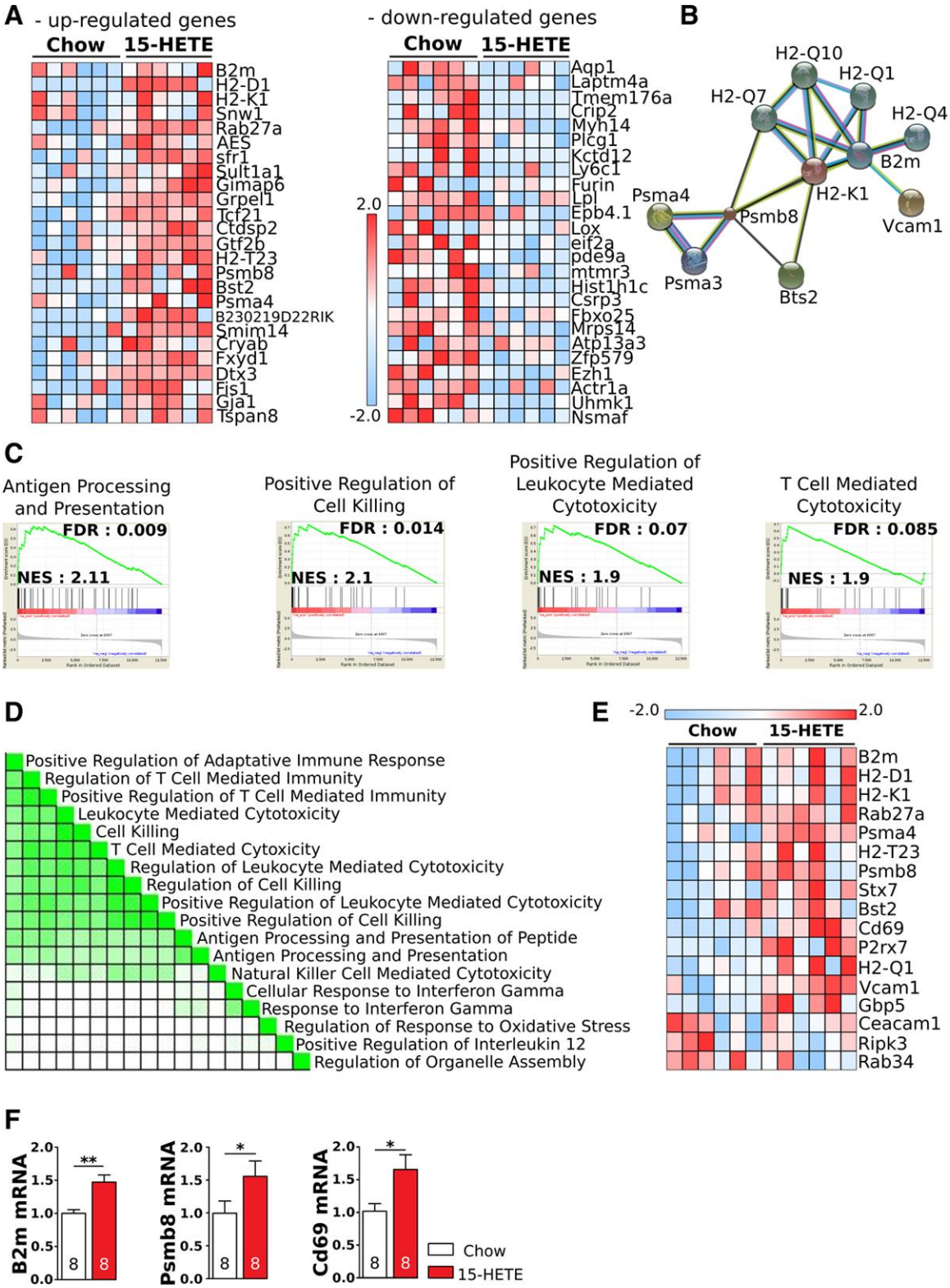

Figure 3: Analysis of online human microarray data shows activation of the same pathways in human pulmonary arterial hypertension (PAH) patients as in 15-hydroxyeicosatetraenoic acid (15-HETE). **A**, Heat map of significantly up/downregulated genes in human PAH patients (n=12) compared with control (Ctrl; n=11) using online

database (GSE53408). **B**, Gene set enrichment analysis shows the activation of the same pathways in human PAH patients (n=12) compared with Ctrl (n=11) as we found in 15-HETE diet mice. **C–F**, Validation of RNA-Seq data in PAH (n=12) compared with Ctrl (n=11) using RT-qPCR for 3 genes that are significantly up/downregulated in the lung of mice fed 15-HETE diet compared with chow diet. **P*<0.05. FDR indicates false discovery rate; HLA, human leukocyte antigen; NES, nominal enrichement score; PSMB9, proteasome subunit beta type-9; RT -qPCR, real-time quantitative polymerase chain reaction; and VCAM1, vascular celladhesion protein 1.

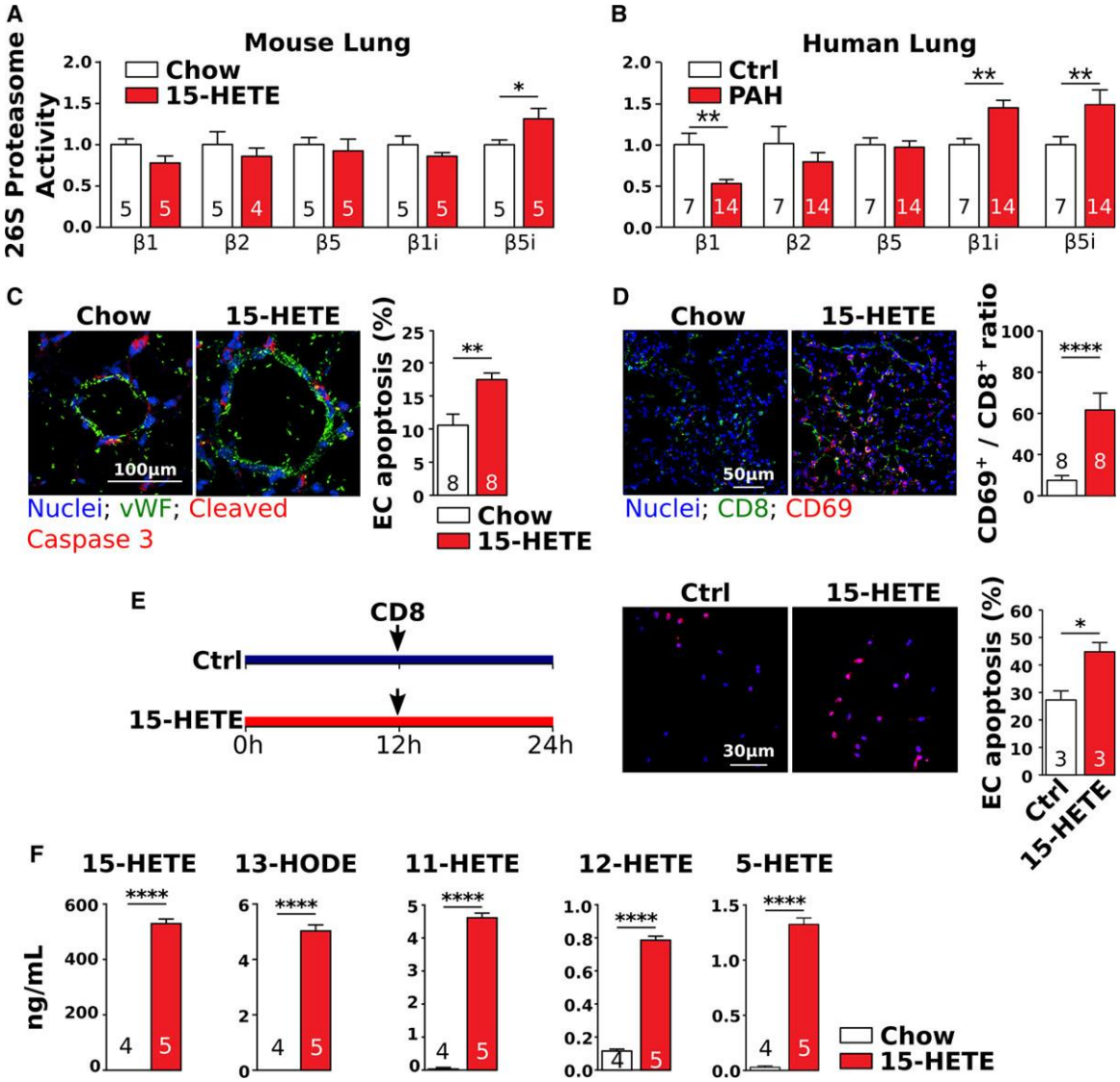

Figure 4: 15-Hydroxyeicosatetraenoic acid (15-HETE) diet induces oxidized lipid production and activates proteasome in pulmonary vascular endothelial cells (ECs). **A**, Mouse lung activity of the proteasome and immunoproteasome showing a significant increase activity of the β5i immunoproteasome subunit in mice fed a 15-HETE diet (n=4–5/group) compared with a chow diet. **B**, Human lung activity of the proteasome and the immunoproteasome in pulmonary arterial hypertension (PAH) patients (n=14) compared with control (Ctrl; n=7). **C**, Immunostaining and quantification of cleaved caspase 3–positive ECs (n=8/group). **D**, Immunostaining and quantification of the activation of CD8+

(cluster of differentiation 8+) cells into CD69+ showing a significant increase of the CD69+/CD8+ cell ratio (n=8/group). **E**, Schematic of the protocol (left) and (right) immunostaining and quantification of EC apoptosis showing 15-HETE does not induce pulmonary vascular endothelial apoptosis per se but leads to EC death through activation of CD8+ cells into cytotoxic T cells (CD69+; n=3/group). **F**, Measurements of oxidized lipid concentration in the media of intestinal epithelial cells exposed to 15-HETE (n=4–5/group). vWF indicates von Willebrand factor. *P<0.05, **P<0.01, ***P<0.001, ****P<0.0001.

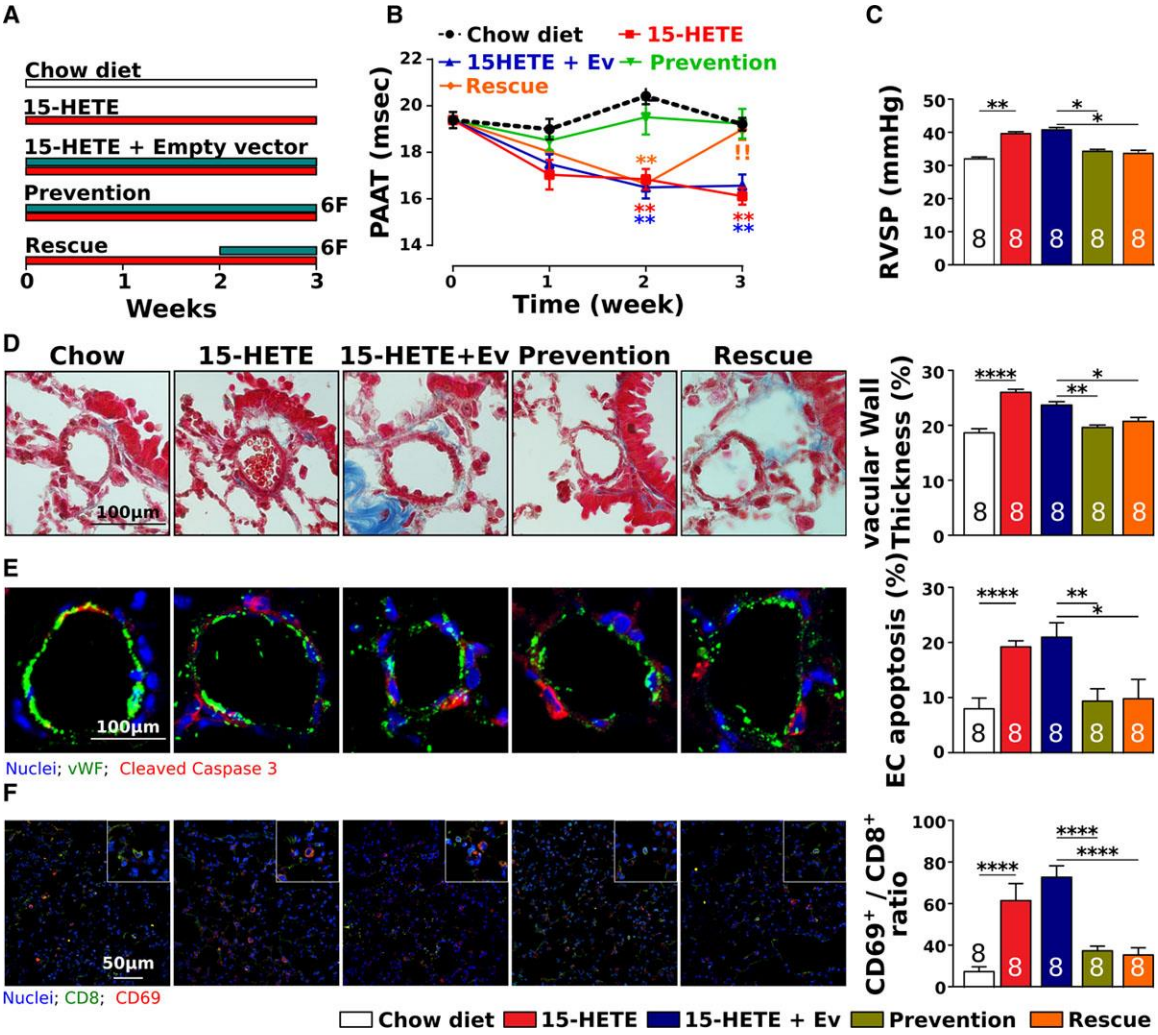

Figure 5: ApoA-I mimetic peptide Tg6F prevents and rescues 15-hydroxyeicosatetraenoic acid (15-HETE) diet–induced pulmonary hypertension. **A**, Schematic of the protocol. **B**, Pulmonary arterial acceleration time (PAAT) as a function of time for mice on chow diet, 15-HETE diet, 15-HETE diet treated with empty vector (Ev), Tg6F (transgenic 6F) for 3 wk (prevention) or the last week of 15-HETE diet (rescue). **C**, Right ventricular systolic pressure (RVSP). **D**, Representative images of small pulmonary arteries and quantification of wall thickness. **E**, Representative images and quantification of pulmonary arterial endothelial cell (EC) apoptosis. **F**, Representative images and quantification of the activation of CD8+ (cluster of differentiation 8+) cells into CD69+ cells. vWF indicates von Willebrand factor. *P<0.05, **P<0.01, ****P<0.0001. n=8/group.

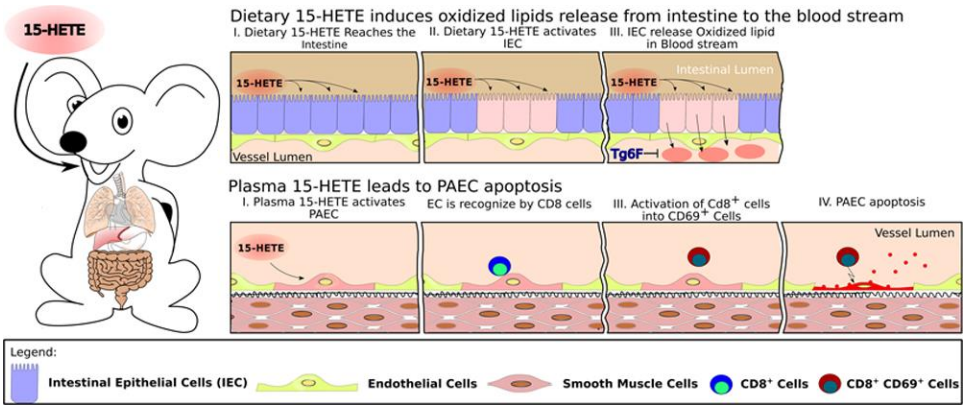

Figure 6: 15-Hydroxyeicosatetraenoic acid (15-HETE) diet induces oxidized lipid production by the intestinal epithelial cells (IECs) resulting in increased concentration of plasma oxidized lipids that activates the pulmonary arterial endothelial cells (PAECs). Activated endothelial cells (ECs) will be recognized by CD8 (cluster of differentiation 8) cells. CD8 cells will trigger apoptosis of activated endothelial cells. Tg6F indicates transgenic 6F.

Supplemental Methods

Pulmonary Hypertension assessment and gross histologic evaluation

Development of PH was monitored weekly by noninvasive two-dimensional Doppler echocardiography of the pulmonary artery blood flow using Vevo 2100 (Visualsonics). At the end of the protocol, open chest catheterization was performed to assess right and left ventricular systolic pressure. Right ventricular index was measured by dividing the weight of the right ventricle by the sum of the left ventricle and intra-ventricular septum.

Histology, Western Blot analysis, immunohistochemistry and imaging

Lungs were embedded in OCT and flash frozen for histological analysis. OCT embedded lungs were sectioned at 5μm. Vascular wall thickness was calculated from Masson's Trichrome staining by determining the mean distance between the lamina elastica externa and lumen in two perpendicular directions of transversally cut vessels

(<100μm) as already described [2,25]. At least 5 randomly selected arteries were measured per animal in a minimum of 8 mice per group. Standard Western Blot analysis and Immunofluorescence were conducted as previously described [2,26]. Images were taken using a confocal microscope (Nikon eclipse Ti confocal microscope). A list of the antibodies used for immunostaining and Western blots is provided in Table S1.

Mass Spectrometry

The plasma samples were prepared by adding 150 µl methanol, 1 µl of 20mM BHT, and 50 µl of internal standard mixture (15(S)-HETE-d8, 13(S)-HODE-d4, 12(S)-HETE-d8, 5(S)-HETE-d8, 10ng/ml each) in methanol to 100 µl plasma. The samples were left for 30 min in -80° before centrifuging them at 13,000 rpm for 10 minutes. The supernatant was then combined with 1.8 mL of acidified water (pH 3-4). The resulting sample was loaded onto a preconditioned 3cc Oasis HLB solid phase extraction (SPE) cartridge on a vacuum manifold (Waters). The SPE cartridge was equilibrated with 2ml methanol followed by 2ml water before the sample load. The sample was slowly loaded on

the cartridge, and the cartridge was washed with 2ml 5% methanol in water. HETEs/HODEs were subsequently eluted with 2 ml methanol. The eluate was then evaporated to dryness under a stream of argon. 100µl of methanol was added to the dried extract, vortexed for 30s, and the reconstituted extract was centrifuged at 13,200 rpm for 7 min to remove any precipitate that could clog the LC/MS/MS instrument. The

resulting supernatants were transferred to autosampler vials and processed for LC/MS/MS analysis.

The tissue sample was prepared by adding homogenizing 50 mg of tissue with 50 µl internal standard mix (15(S)-HETE-d8, 13(S)-HODE-d4, 12(S)-HETE-d8, 5(S)-HETE-d8, 10ng/ml each), 500 µl HPLC water, and 1 µl of 20 mM BHT. The samples were mixed with 1 ml methanol and left for 30 min in -80° before centrifuging them at 13,000 rpm for 10 minutes. The supernatant was then combined with 9 mL of acidified water (pH 3-4). The resulting sample was loaded onto a preconditioned 3cc Oasis HLB solid-phase extraction (SPE) cartridge on a vacuum manifold (Waters). The SPE cartridge was equilibrated with 3 ml methanol followed by 6 ml HPLC water before the sample load. The sample was slowly loaded on the cartridge, and the cartridge was washed with 3 ml 10% methanol in water. HETEs/HODEs were subsequently eluted with 3 ml methanol. The eluate was then evaporated to dryness under a stream of argon. 100µl of methanol was added to the dried extract, vortexed for 30s, and the reconstituted extract was centrifuged at 13,200 rpm for 7min to remove any precipitate that could clog the LC/MS/MS instrument. The resulting supernatants were transferred to autosampler vials and processed for LC/MS/MS analysis.

The cell supernatant samples were prepared by adding 480 µl methanol, 1 µl of 20mM BHT, and 20 µl of 5x internal standard mixture (15(S)-HETE-d8, 13(S)-HODE-d4, 12(S)-HETE-d8, 5(S)-HETE-d8, 10ng/ml each) in methanol to 1 ml supernatant that was spun down for 5 minutes at 13,000 RPM after collection to pellet out any cell or debris. After vortexing the samples and spinning them for 10 min at 13,000 RPM, the

supernatant was then combined with 5 mL of acidified water (pH 3-4). The resulting sample was loaded onto a preconditioned 3cc Oasis HLB solid-phase extraction (SPE) cartridge on a vacuum manifold (Waters). The SPE cartridge was equilibrated with 2ml methanol followed by 2ml water before the sample load. The sample was slowly loaded on the cartridge, and the cartridge was washed with 2ml 5% methanol in water. HETEs/HODEs were subsequently eluted with 2 ml methanol. The eluate was then evaporated to dryness under a stream of argon. 100µl of methanol was added to the dried extract, vortexed for 30s, and the reconstituted extract was centrifuged at 13,000 rpm for 7 min to remove any precipitate that could clog the LC/MS/MS instrument. The resulting supernatants were transferred to autosampler vials and processed for LC/MS/MS analysis.

Liquid chromatography–LC-MS/MS was performed with the use of a mass spectrometer (Triple Quad 5500 System; SCIEX) equipped with electrospray ionization (ESI) source. The HPLC system utilized an Agilent 1290 series LC pump equipped with a thermostatted autosampler (AgilentTechnologies, Santa Clara, CA). Chromatography was performed using a Kinetex C-18 column (2.6 µm particle, 150X3.0mm; Phenomenex, Torrance, CA) with a security guard cartridge (C-18; Phenomenex) at 50°C. Mobile phase A consisted of 0.1% formic acid in water, and mobile phase B consisted of 0.1% formic acid in acetonitrile. The auotosampler was set at 4°C. The injection volume was 5µl; the flow rate was controlled at 0.3mL/min. The gradient program was as follows: 0-1min, 100% A; 1-8.5min, linear gradient from 0% to 85% B; 8.5- 9.5min, linear gradient from 85-100% B; 9.5-10.5min, 100% B; 10.5-12min, linear gradient from 100-0% B; 12-14min 0% B. The data

acquisitions and instrument control were accomplished using Analyst 1.6.2 software (Applied Biosystems). Detection was accomplished by using the multiple reaction monitoring (MRM) mode with negative ion detection; the parameter settings used were: ion spray voltage=- 4500 V; curtain gas=25 (nitrogen); ion source gas 1=50; ion source gas 2 =50; ion source gas 2 temperature= 375°C. Collision energy, declustering potential and collision cell exit potential were optimized for each compound to obtain optimum sensitivity.

The transitions monitored were mass-to-charge ratio (m/z): m/z 295.09 for 13-HODE; 295.108-170.8 for 9-HODE; 319.063-219.1 for 15- HETE; 319.087-115.0 for 5-HETE; 319.039-178.8 for 12-HETE; 327.146-226 for 15(S)- HETE-d8; 327.139-115.9 for 5-HETE-d8; 299.066-198 for 13(S)-HODE-d4; 327.139-115.9 for 12-HETE-d8

RNA sequencing and microarray Analysis

Total RNA from mice on chow diet or 15-HETE diet (n=6/group) were extracted using miRvana Total RNA Isolation Kit (Applied Biosystems™). The purity and of extracted RNA were quantified using the Agilent 2100 Technology. RNA-sequencing was performed in the UCLA Technology Center for Genomics & Bioinformatics core. Briefly, the RNA-seq libraries were prepared following the standard Illumina protocol. Paired-end sequencing at 50bp length and 30 million coverage was performed on HiSeq 3000 (Illumina Inc, CA, USA). Data quality checks were performed on the Analysis Viewer and demultiplexing was performed with CASAVA 1.8.2 (Illumina Inc, CA, USA). Paired-end RNA sequencing reads were analyzed using open-source software tools (HISAT), StringTie, and Cuffmerge. The Ballgown package was used to

identify deferentially expressed genes with a p-value of 0.05. Genes with a fold change above 1.5 were considered up-regulated and genes with a fold change below -1.5 were considered down-regulated. Type II error was assessed with quantitative real time PCR to confirm the differential expression of these genes between the two diets. All up- or down-regulated genes were used for gene sets enrichment analysis using GSEA software on human and mouse gene sets (Hallmark gene sets).[100] Leading edge analysis was performed with GSEA software to define overlapping genes in multiple leading edge subset of genes between enriched gene sets. STRING online software was used to analyze known associations of genes up- or down-regulated by the 15-HETE diet.[101,102] Publicly available human microarray data from 8 PAH patients (40 ± 12 years of age, 5 females) and 8 controls (47 ± 15 years of age, 4 females) together with all available patient's information was taken from the original publication (GSE53408), and was reanalyzed using the Limma package [36]. A fold change above 1.5 with a false discovery rate of 0.05 was considered significant.

Real time PCR

Total RNA from lungs was isolated with Trizol extraction method and reverse transcribed with poly dT primers using the Omniscript reverse transcription kit (Qiagen, Cat#205113). Real-time PCR was performed on polyA+ cDNA with specific primers (Table S2) using iTaq Universal SYBR® (BioRad, Cat#1725121).

Proteasome activity

20 mg aliquots of pulverized lung samples (human & mice) were homogenized in 26S proteasome lysis buffer (50 mM Tris, 150 mM NaCl, 1mM EDTA, 5mM MgCl2, pH 7.5) with a glass dounce homogenizer. The homogenates were centrifuged at 12,000g for 15 min at 4°C and the supernatants were quantified with a Nanodrop 2000c (Thermo Scientific, Cat# ND-2000c). The samples were normalized to give equal protein concentrations of 2µg/µl using 26S proteasome lysis buffer. To measure the 26S proteasome catalytic activities 20 µg of protein was combined with homogenization buffer, bortezomib (a specific proteasome inhibitor, 10 µM for β5 activity and 100 µM for β1 and β2 activities) or an equal amount of DMSO (instead of bortezomib), and 100µM ATP to a total volume of 100µl per well in a black 96-well plate and incubated for 20 min at room temperature. The reaction was initiated by adding specific fluorogenic substrates for each catalytic proteasome subunit (Enzo Life Sciences, NY, USA): Z-LLEAMC for β1 (caspase-like) subunit, Boc-LSTR-AMC for β2 (trypsin-like) subunit and Suc-LLVY-AMC for β5 (chymotrypsin-like) subunit. The proteasomal activities were measured at excitation (390 nm) and emission (460 nm) wavelengths every 15 min up to 120 min.

Immunoproteasome activity

Protein samples (from human and mouse lungs) in immunoproteasome buffer 50 mM Tris, 5 mM MgCl2, 20 mM KCl, 1 mM DTT, pH 7.5 were incubated with specific inhibitor or an equal volume of DMSO for 20 min at room temperature. The reaction was initiated by adding 25 µM specific fluorogenic substrates ANW-R110 (AAT Bioquest, Inc, CA) for β5i and (Ac-Ala-Asn-Trp) 2-R110 (AAT Bioquest, Cat# 13455) for β1i

activities. 20 µM ONX-0914 (Ab mole Bioscience Inc., Houston, TX Cat# A4011) and 50 µM bortezomib were used as inhibitors for β5i and β1i immunoproteasome activities respectively. The fluorescence intensity was measured at an excitation of 498 nm and an emission of 520 nm every 5 mins for 60 min in a Tecan Infinite M1000.

Cell culture

Primary cultures of healthy human pulmonary arterial endothelial cells (PAEC) were purchased from ATCC. PAECs were used from passage 3 to 6 and each experiment was repeated at least 3 times. PAECs were exposed to 15-HETE (100ng/ml) as previously described [11] from 6 to 36 hours (Fig. S4). In some experiments, PAECs were incubated with or without 15-HETE and 12 hours later healthy CD8 cells (ALLCELLS, Lot# 3003028) were added. After 12 hours of contact between EC and CD8 cells, the cells were collected, fixed, and stained for cleaved caspase 3.

Healthy rat small intestine epithelial cells (IEC-6) were purchased from ATCC. IEC-6 were used from passage 5 to 7. IEC-6 were exposed to increased concentrations of 15-HETE (1, 5, and 10 µM, Figure S3), after 12 hours the supernatant was collected and oxidized lipids were measured via mass spectrometry.

Supplemental Figures and Tables

Table S1: Patient's clinical characteristics

Parameters	**Ctrl**	**PAH**
Age (years, n)	63.4 ± 4.5 (7)	29.1 ±2.5 (14)
mPAP (mmHg, n)	-	61.9±6 (14)
PVR (WU, n)	-	13.1±1.4 (11)
CO (L.min-1, n)	-	4.6±0.63 (8)
CI (L.min-1.m-2, n)	-	4.28±2 (9)
Medication	-	-

Prostacyclin	-	11 (78%)
ET1R inhibitor	-	11 (78%)
PDE5 inhibitor	-	9 (64%)

Definition of abbreviations: mPAP: mean pulmonary arterial pressure; PVR: pulmonary vascular resistance; CO: cardiac output; PAH: pulmonary arterial hypertension. Values are expressed as mean+/-SEM.

Table S2: Antibodies

Protein	Company	Reference
Beta 5	Enzo LifeSci	PW8895
Beta 5i	Enzo LifeSci	PW8200
Beta 1i	Enzo LifeSci	PW8205
Cleaved Caspase 3	Cell Signaling	9661
Von Willebrand Factor	Abcam	Ab6994

Table S3: Primer Sequences

Species	Genes	Sequences
Hs	GAPDH (NM_002046)	F: TGCCCTCAACGACCACTTTG R: ACTGTGAGGAGGGGAGATTCA
	B2M (NM_004048)	F: AGGGCTGGCAACTTAGAGGT R: GCTTTGAGTGCAAGAGATTGAAG
	VCAM1 (NM_001078)	F: TTCTCCTGAGCTTCTCGTGCT R: TCTGCCTCTCAGCTCATTGT
	PSMB8 (NM_148919)	F: CACTTATGCCTACGGGGTCA R: TCCTTGGACTTAACGTGGCT
	PSMB9 (NM_002800)	F: GCACATCTCATGGTAGCTGG R: TTGCCCAAGATGACTCGATGG
	PSMB5 (NM_002797)	F: CTATGATCTGGCCCGTCGAG R: TCTTTCAGGGGGTAGAGCCA
	Cd8a	F: AAGTGGTGAGCTTAACCCTGG R: GGGGTAGCCTGTCCTCTTTC
	Cd69 (NM_001781)	F: CCAACAGTGAGAGCCCTTCAT R: ACCATCGAAAAGGACCTGTCTAC
	PSMa4 (NM_001078)	F: ACTCTCTGCTGAAAAAGTGGAAA R: GTCCTATTTTCCCACTGCACC
Ms	Cd69 (NM_001033122)	F: AGTACAATTGCCCAGGCTTGT R: TCGCTTCAGAAACGTCATGTCC
	Psmb8 (NM_010724)	F: GGACAAGAAGGGACCAGGACT R: TGTCCATCACCCCATAGGCA
	Cd8 (NM_001081110)	F: CGTGGGACGAGAAGCTGAAT R: AGAGTTCACTTTCTGAAGGACTGG
	B2M (NM_009735)	F: CCCGCCTCACATTGAAATCC

		R: TCACATGTCTCGATCCCAGT
	GAPDH (NM_001289726)	F: CATGGCCTTCCGTGTTCCTA R: TACTTGGCAGGTTTCTCCAGG

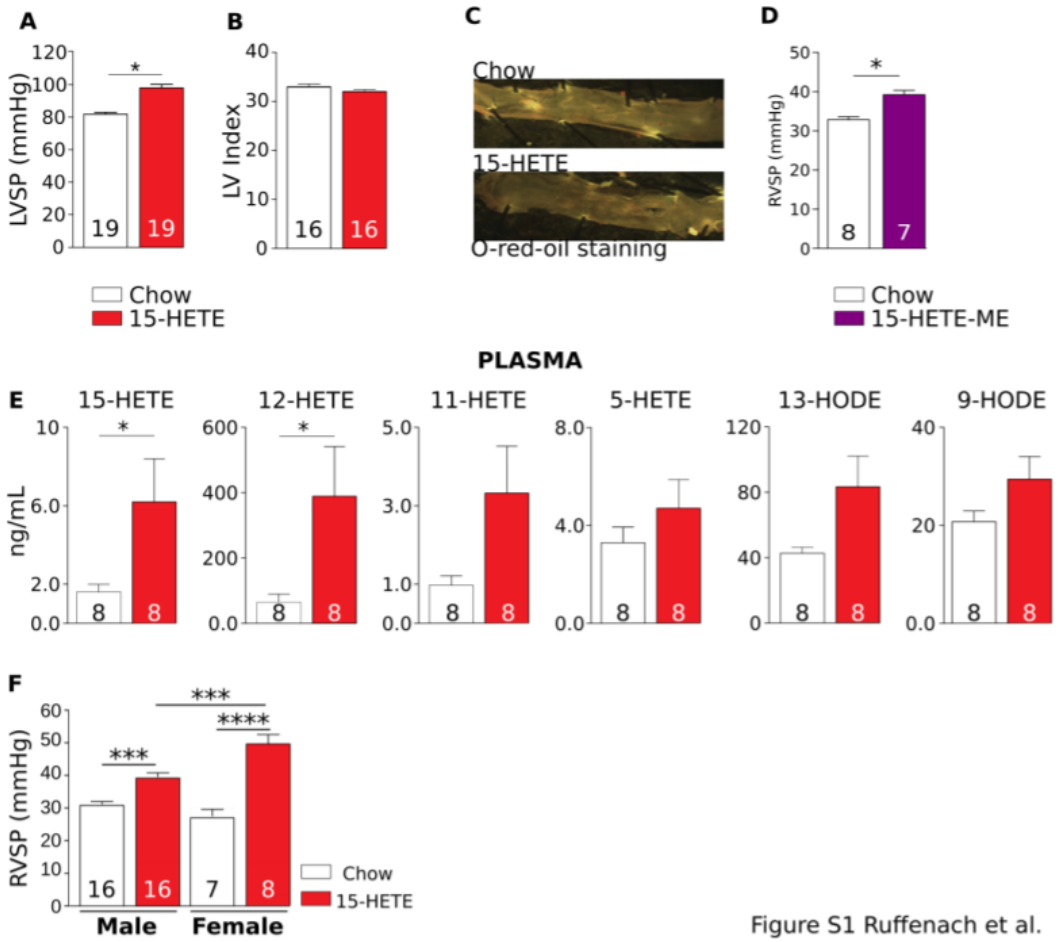

Figure S1 Ruffenach et al.

Suppl. Figure 1: (**A**) LVSP of 15-HETE diet and Chow diet fed mice (n=19/group). (**B**) LV index of 15- HETE diet and Chow diet fed mice (n=16/group). (**C**) Representative images of the absence of lipids deposition within the aorta of these mice. (**D**) RVSP in mice fed 15-HETE-methylester (15-HETE-ME, n=7) and Chow diet (n=8) for 3weeks. (**E**) Plasma concentration of oxidized lipids in Chow and 15- HETE diet mice after 3 weeks (n=8/group). (**F**) RVSP of female (n=7-8/group) and male (n=16/group) mice fed with 15-HETE diet compared to chow diet. Two-way ANOVA, with factors of treatment (15- HETE diet vs. Ctrl) and sex (male vs female), revealed a main effect of 15-HETE diet (p<0.0001).

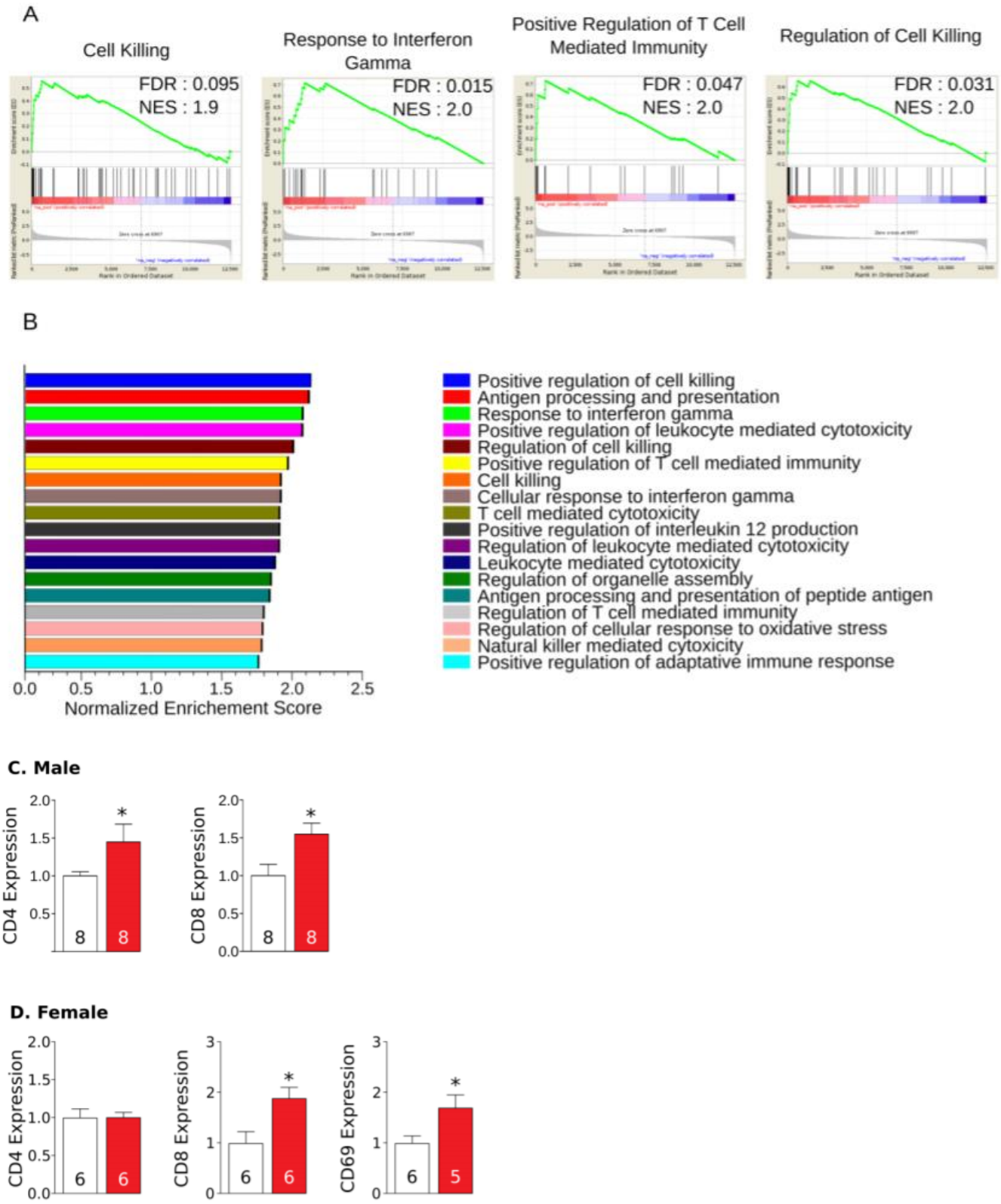

Suppl. Figure 2: (**A**) Schematic of the gene sets enrichment analysis of 4 of the most up-regulated gene sets in the lung of the 15-HETE diet fed mice (n=6/group). (**B**) Normalized enrichment score of all gene sets up-regulated in the lung of 15-HETE diet fed mice

(n=6/group). (**C**) CD4 and CD8 mRNA expression in 15-HETE diet fed male mice compared to chow diet fed male micel (n=8/group). (**D**) CD4, CD8 and CD69 mRNA expression in 15-HETE diet fed female mice compared to chow diet fed female mice (n=5-6/group)

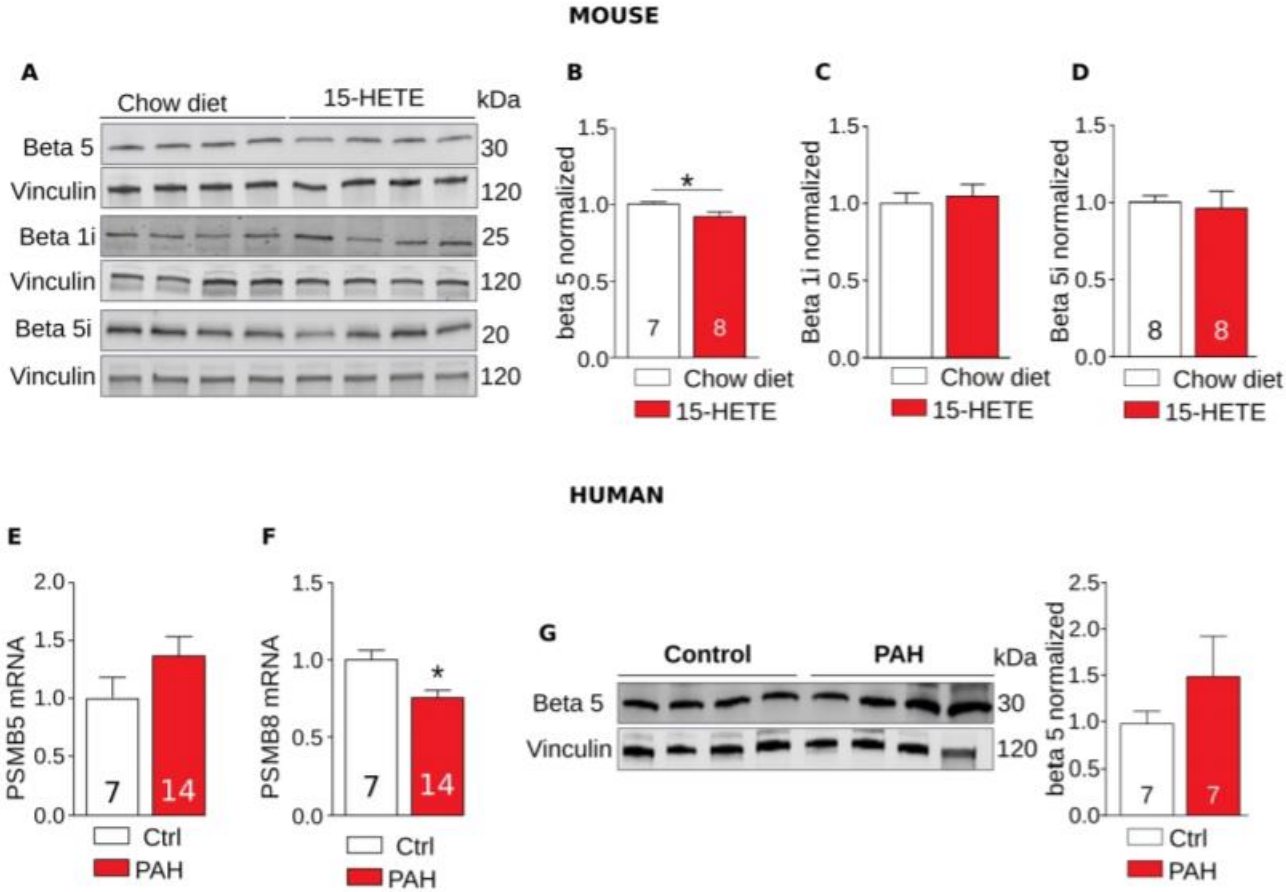

Suppl. Figure 3: (**A**) Representative Western Blot and quantification of beta 5, beta 1i and beta 5i subunit expression in chow diet fed mice and 15-HETE diet fed mice and quantification (n=7-8/group) (**B-D**). PSMB5 (**E**) and PSMB8 (**F**) mRNA quantification in healthy (n=7) and PAH patients (n=14). (**G**) Western blot and quantification of PSMB5 in human (n=7/group). *p<0.05

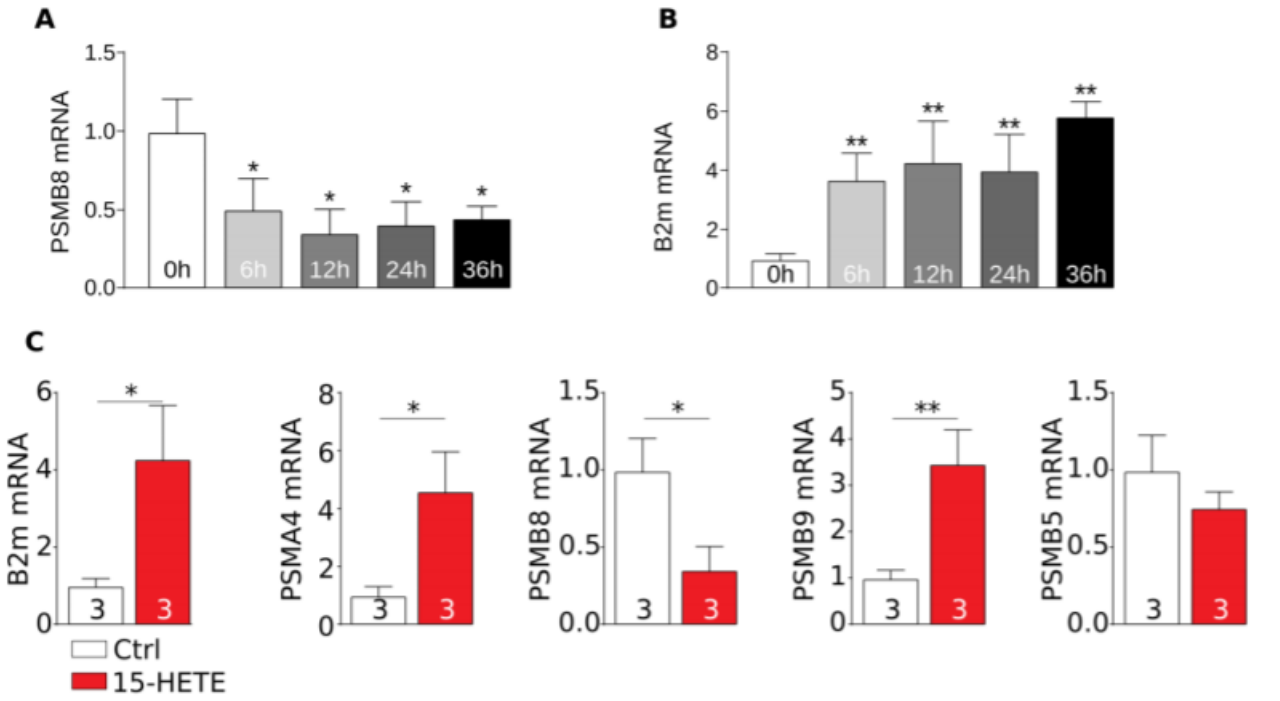

Suppl. Figure 4: Time course of mRNA expression of (**A**) PSMB8 and (**B**) B2m in pulmonary arterial endothelial cells exposed to 15-HETE (n=3/group). (**C**) Measurement of B2m, PSMA4, PSMB8, and PSMB5 in PAEC exposed to 15-HETE after 12 h (n=3/group). *p<0.05, **p<0.01; *** p<0.001, ****p<0.0001.

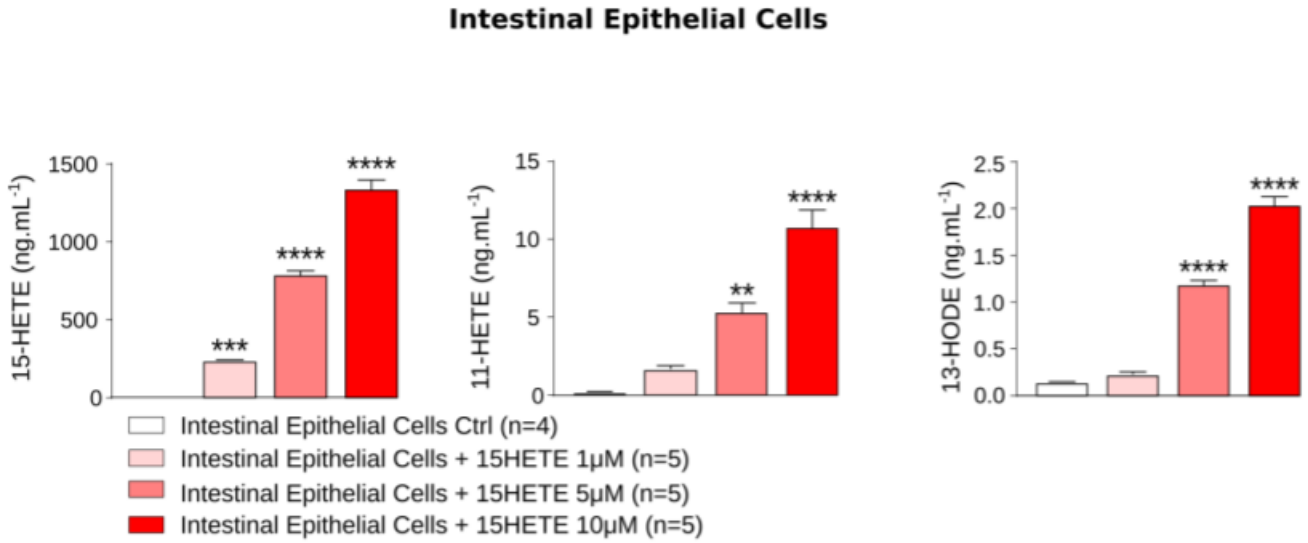

Suppl. Figure 5: Dose response of intestinal epithelial cells exposed to increased concentration of oxidized lipids (n=4-5/group). *p<0.05, **p<0.01; *** p<0.001, **** p<0.0001.

CHAPTER 3: 15-HETE, Lipoxygenase enzymes, Small Intestine, and PH

Abbreviations

PAH	Pulmonary Arterial Hypertension
PH	Pulmonary Hypertension
15-HETE	15-Hydroxyeicosatetraenoic Acid
WT	Wild Type
HODE	Hydroxyoctadecadienoic Acid
TAG	Triacylglycerol
CE	Cholesterol Ester
HCER	Hexosylceramides
FFA	Free Fatty Acids
LA	Linoleic Acid
AA	Arachidonic Acid
G-CSF	Granulocyte Colony-Stimulating Factor
Il-15/Il-15R	Interleukin-15/Interleukin-15 Receptor
MCP-1	Monocyte Chemoattractant Protein-1
BALF	Bronchiolar Lavage Fluid
KO	Knockout
LOX	Lipoxygenase
CHP	Chronic Hypoxia
MCT	Monocrotaline
MAPK	Mitogen-activated Protein Kinase
IEC-6	Rat Small Intestine Epithelial Cells
RV	Right Ventricle
ApoE	Apolipoprotein E
LPS	Lipopolysaccharide
LV	Left Ventricle
IVS	Interventricular Septum
PAAT	Pulmonary Arterial Acceleration Time
RVSP	Right Ventricle Systolic Pressure
HDL	High Density Lipoprotein
ROS	Reactive Oxygen Species
LTB_4	Leukotriene B4
PASMC	Pulmonary Artery Smooth Muscle Cell
COX	Cyclooxygenase

Abstract

Pulmonary arterial hypertension (PAH) is a chronic and incurable disease targeting the lungs, causing pulmonary vascular remodeling, leading to right ventricle hypertrophy and death. An elevation in plasma and tissue oxylipins has been noted in patient and animal model data. Previous work has shown that lowering oxylipins rescues mice and rats from pulmonary hypertension (PH) and that supplementation of mouse diet with 15-hydroxyeicosatetraenoic acid (15-HETE) at 5 μg per mouse per day was sufficient to cause PH in wild type (WT) mice while increasing levels of additional HETEs and hydroxyoctadecadienoic acids (HODEs) in the process. Here, we set out to further understand the processes underway in the dietary 15-HETE model of PH. First, we utilized the Lipidizer™ platform to examine the plasma of mice on chow and 15-HETE diets to see that of eleven lipid classes measured, there were significant increases in triacylglycerol (TAG), cholesterol ester (CE), hexosylceramides (HCER), and free fatty acids (FFA). Of particular interest, a significant increase in linoleic acid (LA), the precursor to arachidonic acid (AA), HETEs, and HODEs, was observed. As lipids can serve as modulators of immune processes, we investigated cytokine changes in the plasma and immune cell modulations in the intestine and lung. Examination of cytokines on a multiplex plate revealed that plasma levels of Eotaxin, (granulocyte conoly-stimulating factor) G-CSF/CSF/3, Interleukin-15/Interleukin-15 receptor (Il-15/Il-15R), and monocyte chemoattractant protein-1 (MCP-1) increased in mice on the 15-HETE diet and flow cytometry analysis of intestines and bronchiolar lavage fluid (BALF) showed a significant increase in type I macrophages and a significant decrease in neutrophils in the intestine, indicating resolution of inflammation by the end of the protocol. We then set out

to see whether the onset of PH induced by 15-HETE was specific to 15-HETE or could be reproduced by other HETEs as well by feeding mice 5 µg 15-HETE, 5 µg 5-HETE, and 5 µg total of 5, 12, and 15-HETE mixture, and found that all three diets induced PH. To investigate the role of the lipoxygenase (LOX) enzymes that produce HETEs and HODEs, we purchased 12/15 LOX knockout (KO) mice, added the 5-LOX inhibitor, Zileuton, to the diet, fed them the 15-HETE diet, and found that they did not develop PH. It was interesting to note that there were huge differences in HETEs and HODEs observed in the intestines of the KO mice, not only solidifying a causal role of oxylipins and LOX enzyme activity in the onset of PH, but also a potential role of the intestine.

Introduction

PAH is a rare but fatal disease characterized by abnormal vascular changes and structural remodeling that culminate in vasoconstriction and obstruction of pulmonary arteries, contributing to increased pulmonary vascular resistance, pulmonary hypertension, and right ventricular failure.[6] As discussed in Chapter 1.2, oxylipins, particularly HETEs and HODEs, are elevated in the plasma and lungs of PAH patients and in multiple animal models of PH. HETEs and HODEs are generated from LA and AA by the enzymes 5, 12, and 15-LOX. Previous work has shown that oxylipins can contribute to multiple hallmarks of PAH, including pulmonary artery smooth muscle cell proliferation and resistance to apoptosis, inflammation, vasoconstriction, angiogenesis, fibrosis, and vascular remodeling.[6] Previous work from our lab with collaborators has also shown that lowering them rescues PH in the chronic hypoxia (CHP) mouse and monocrotaline rat (MCT) models.[11]

While we have already shown that 15-HETE is causal to PH, leading to vascular remodeling T-cell endothelial cell apoptosis[11,54], however, the full spectrum of what

happens after three weeks of 15-HETE diet has yet to be explored. Studies have shown other lipid changes are noted in PAH patients including increased plasma TAG levels and FFA, as well as increased TAGs, diacylglycerol (DAG), and ceramides (CER) in the cytoplasm.[103–105] As we have noted, the addition of one oxylipin leads to changes in multiple oxylipins in the plasma and tissues, and here aim to implement the Lipidyzer™ platform to observe plasma changes in lipids across 11 major classes. Changes in immune responses are widely noted in PAH patients with respect to cytokines and modulations in nearly every immune cell type.[6,74,79,80,106–109] Here we set out to utilize a multiplex cytokine plate and flow cytometry to further elucidate modulations in immune response by the 15-HETE diet.

Focusing on HETEs, HODEs, and LOX enzymes, in Chapter 1.4, the known roles 15-HETE could play in the onset of PH was discussed, referencing its role in to vascular remodeling, vascular angiogenesis, and vascular adventitia fibrosis via the Rho-kinase and the 15-LOX-12/15-HETE- mitogen-activated protein kinase (MAPKs) pathways.[6,22–24] In Chapter 2, I showed that how 15-HETE induced rat intestinal epithelial cells (IEC-6) produced other oxylipins when exposed to 15-HETE[54], implicating not only 15-HETE, but additional HETEs and HODEs in the onset of PH in the dietary 15-HETE model. Studies have shown that LOX enzymes may play a role in the onset of PH as 5-LOX KO mice in CHP have less right ventricle (RV) hypertrophy than 5-LOX competent mice.[110] Sugen/hypoxic rats that were injected with diethylcarbamazine, a 5-LOX inhibitor, had decreased right ventricle systolic pressure (RVSP), blunted muscularization of pulmonary arterioles, fewer fully obliterated lung vessels, and decreased eicosanoid levels, including 12-HETE and 15-HETE, in the lungs.[73] Little research inhibiting 12/15 LOX in the context

of PH has been done, however, knocking out 12/15 LOX in apolipoprotein E deficient (*apoE-/-*) mice reduced atherosclerosis by diminishing and delaying fatty lesion development.[111] 12/15 LOX KO mice and wild type mice administered cyanocinnamate, a 12/15 LOX inhibitor, had decreased neutrophil recruitment following lipopolysaccharides (LPS) inhalation.[112] Based on these results, we hypothesized that 5, 12/15-LOX enzymes may play a role in the progression of PH in our dietary model and set out to determine whether knocking out or blocking all three will prevent onset of PH by 15-HETE.

Materials and Methods

Mice and treatments

Male C57BL6/J mice (wild type, 2-3 months old) were purchased from Jackson Laboratories and used. To prepare the HETE diets, Teklad diet was prepared so that each mouse consumed 4 gm chow per day. The HETE diets were supplemented with either 5µg 15-HETE (34720, Cayman Chemical), 5µg 5-HETE (34210, Cayman Chemical), or 5µg total of 15-HETE, 5-HETE, and 12-HETE (34550, Cayman Chemical) per mouse per day. Mice consumed the diets for 21 days before sacrifice and collection of tissues and plasma.

For the LOX KO study, male 12/15 LOX KO mice, B6.129S2-Alox15tm1Fun/J, were purchased from Jackson Labs, 002778) and were administered 15-HETE diet at 8-12 weeks old with Zileuton (10006967, Cayman Chemical), added at a dose of 50 mg/kg body weight for 21 days.

Pulmonary Hypertension assessment and gross histologic evaluation

Development of PH was monitored weekly by noninvasive two-dimensional Doppler

echocardiography of the pulmonary artery blood flow using Vevo 2100 (Visualsonics). At the end of the protocol, open chest catheterization was performed to assess right and left ventricular systolic pressure. RV index was measured by dividing the weight of the right ventricle by the sum of the left ventricle (LV) and intra-ventricular septum (IVS).

Preparation of Samples for FLOW Cytometry

Mice were euthanized using isoflurane immediately prior to preparing removing the small intestine and collecting the BALF fluid for FLOW cytometry. BALF fluid was prepared by inserting a 20-gauge needle filled with 1.5 mL of ice-cold PBS before injecting it into and gently aspirating the solution out of the lungs and collecting it in a 1.5 mL tube. Jejunum samples were prepared following the protocol coming with the Lamina Propria Dissociation Kit (Miltenyi Biotech, 130-098-463). Cell suspensions were incubated with 1 µl of each antibody listed in Table 1 for 45 minutes, washed with PBS, cells suspended in 300 µL of ice-cold PBS buffer and transferred to fresh tubes for FACS analysis. FACS was performed using a LSRII Analyzer by the Janis V. Giorgi Flow Cytometry Core Facility at UCLA. For analysis and computational compensation of the data, BD FACS Diva software was used. Events of live cells were gated. Only live and singlet cells were chosen for analysis and gating (i.e., dead cells and aggregates were excluded).

Cell Culture

Healthy IEC-6 cells were purchased from ATCC. IEC-6 were used from passage 5 to 7. IEC-6 were exposed to increased concentrations of 15-HETE (1, 5, and 10 µM, Figure S3), after 12 hours the supernatant was collected and oxylipins were measured via mass spectrometry.

Mass Spectrometry

The cell supernatant samples were prepared by adding 480 µl methanol, 1 µl of 20mM BHT, and 20 µl of 5x internal standard mixture (15(S)-HETE-d8, 13(S)-HODE-d4, 12(S)-HETE-d8, 5(S)-HETE-d8, 10ng/ml each) in methanol to 1 ml supernatant that was spun down for 5 minutes at 13,000 RPM after collection to pellet out any cell or debris. After vortexing the samples and spinning them for 10 min at 13,000 RPM, the supernatant was then combined with 5 mL of acidified water (pH 3-4).

The cell lysate samples were prepared by removing media from wells and washing cells twice with 1ml cold PBS before adding 300ul phosphate buffer (7.4pH) to wells, scrape cells, collecting the lysate in a 1.5ml Eppendorf, and adding 5ul of BHT (10mM) to the tube. 20ul of 5x internal standard mixture (final concentration 10ng/ml extract) was added and 180ul MeOH were added to each sample before vortexing and centrifuge them at 13,000rpm for 10 minutes. The supernatant was collected 2.5ml of acidified HPLC water (pH 3-4) was added to each tube before vortexing once more. Buffers present in supernatant were neutralized with formic acid until pH read 3-4.

The resulting samples were loaded onto a preconditioned 3cc Oasis HLB solid-phase extraction (SPE) cartridge on a vacuum manifold (Waters). The SPE cartridge was equilibrated with 2ml methanol followed by 2ml water before the sample load. The sample was slowly loaded on the cartridge, and the cartridge was washed with 2ml 5% methanol in water. HETEs/HODEs were subsequently eluted with 2 ml methanol. The eluate was then evaporated to dryness under a stream of argon. 100µl of methanol was added to the dried extract, vortexed for 30s, and the reconstituted extract was centrifuged at 13,000 rpm for 7 min to remove any precipitate that could clog the

LC/MS/MS instrument. The resulting supernatants were transferred to autosampler vials and processed for LC/MS/MS analysis.

Liquid chromatography–LC-MS/MS was performed with the use of a mass spectrometer (Triple Quad 5500 System; SCIEX) equipped with electrospray ionization (ESI) source. The HPLC system utilized an Agilent 1290 series LC pump equipped with a thermostatted autosampler (AgilentTechnologies, Santa Clara, CA). Chromatography was performed using a Kinetex C-18 column (2.6 µm particle, 150X3.0mm; Phenomenex, Torrance, CA) with a security guard cartridge (C-18; Phenomenex) at 50°C. Mobile phase A consisted of 0.1% formic acid in water, and mobile phase B consisted of 0.1% formic acid in acetonitrile. The auotosampler was set at 4°C. The injection volume was 5µl; the flow rate was controlled at 0.3mL/min. The gradient program was as follows: 0-1min, 100% A; 1-8.5min, linear gradient from 0% to 85% B; 8.5- 9.5min, linear gradient from 85-100% B; 9.5-10.5min, 100% B; 10.5-12min, linear gradient from 100-0% B; 12-14min 0% B. The data acquisitions and instrument control were accomplished using Analyst 1.6.2 software (Applied Biosystems). Detection was accomplished by using the multiple reaction monitoring (MRM) mode with negative ion detection; the parameter settings used were: ion spray voltage=- 4500 V; curtain gas=25 (nitrogen); ion source gas 1=50; ion source gas 2 =50; ion source gas 2 temperature= 375°C. Collision energy, declustering potential and collision cell exit potential were optimized for each compound to obtain optimum sensitivity.

The transitions monitored were mass-to-charge ratio (m/z): m/z 295.09 for 13-HODE; 295.108-170.8 for 9-HODE; 319.063-219.1 for 15- HETE; 319.087-115.0 for 5-

HETE; 319.039-178.8 for 12-HETE; 327.146-226 for 15(S)- HETE-d8; 327.139-115.9 for 5-HETE-d8; 299.066-198 for 13(S)-HODE-d4; 327.139-115.9 for 12-HETE-d8.

Results

15-HETE Diet causes Increases in Multiple Lipid Species and Precursors of HETEs and HODEs

Plasma analysis from mice fed chow and fed the 15-HETE diet revealed significant changes in four of eleven lipid classes analyzed on the Lipidyzer (Sciex) platform; TAG, CE, HCER, and FFA (**Figure 7**), showing that the addition of one lipid could alter the levels of numerous lipids across multiple classes. Interestingly, these increases included a significant increase in LA and a nonsignificant increase in AA, the precursors of HETEs and HODEs (**Figure 8**) which would in part explain why other HETEs and HODEs have been shown to increase after dietary administration of 15-HETE in our previous work.[54]

15-HETE diet leads to inflammatory changes in cytokine levels and immune cell populations in the intestine

Looking into potential pro-inflammatory effects of dietary 15-HETE, we measured multiple cytokine levels in the plasma of chow and 15-HETE fed mice and observed significant increases in eotaxin, G-CSF, Il-15/Il-15R, and MCP-1 (**Figure 9**). Flow cytometry analysis of immune cells revealed that after 3 weeks, Type 1 macrophages were significantly increased and neutrophils were significantly decreased in the intestines of 15-HETE fed mice, indicating resolving inflammation, while a nonsignificant increase in monocytes was observed in the bronchoalveolar lung fluid BALF (**Figure 10A and 10B**).

HETEs and HODEs aside from 15-HETE can induce PH alone or in combination

Previous data has shown that treating IEC-6 cells with 15-HETE for 12 hours increased supernatant levels of HETEs and HODEs (Chapter 2, Suppl. Figure 5).[54] To expand on these findings, I found that 1, 5, and 10 μM of 15-HETE treatment for 12 hours result in significant increases in HETEs and HODEs (in a dose-response fashion) in both the supernatant and lysates of cells **(Figure 11A and 11B)**. These finding implicate that the intestine generates more HETEs and HODEs that would then be shuttled to the circulatory system. Thus, we also set out to determine whether other oxylipins could lead to the development of PH or whether it was an effect specific to 15-HETE. To accomplish this, we fed mice either control diet or control diet fortified with 5μg of 15-HETE, 5-HETE, or a mixture of 12, 5, and 15-HETE adding up to 5μg of total lipid added. Decreasing Pulmonary arterial acceleration times (PAAT) and increasing right ventricle systolic pressures (RVSP) confirmed that mice fed either 5-HETE or 5, 12, and 15-HETE fortified diets developed PH (**Figure 12A-12D**).

12/15 LOX KO mice with 5-LOX inhibitor do not develop PH when fed 15-HETE diet

To further investigate the role of 12/15-LOX in PH, we acquired 12/15-LOX KO mice, B6.129S2-Alox15tm1Fun/J, (Jackson Labs, 002778), and fed them control Teklad diet with the 5-LOX inhibitor, Zileuton (Cayman Chemical), added at a dose of 50 mg/kg body weight, or 15-HETE diet with Zileuton added at the same concentration, for three weeks and found that compared with WT mice on the 15-HETE diet, the KO mice on 15-HETE diet did not have increased RVSP, showing that they did not develop PH (**Figure 13A and 13B**). Lipid panel analysis of the intestine revealed decreased levels of 5, 12, and 15-HETE compared with the intestines of WT mice fed 15-HETE (**Figure 13C**).

Discussion

PH is a multi-factorial disease that leads to right ventricle hypertrophy and death with no cure to date.[2,5] Although multiple animal models exist, there is still much unknown about this disease. Recently, work with our collaborators have shown that oxylipins, particularly HETEs and HODEs, produced by the LOX enzymes, play a role in PH and that the addition of one lipid, 15-HETE, at 5 µg/mouse/day is sufficient to cause PH in WT mice in 21 days.[6,11,54] Here, we sought to further elucidate further changes brought about by the addition of one lipid to the diet. First, we found that 15-HETE lead to the increase of plasma levels of TAGs, CEs, HCERs, and FFAs (**Figure 7**), consistent with findings of dyslipidemia in animal and patient models of PH. Increases in TAGs to high density lipoprotein cholesterol (HDL) ratio have been noted in PAH patients.[103] We have observed an increase or decrease in HDL in this model of PH[54], so this increase in TAGs is consistent with patient findings. FFAs have been found to be increased in the right ventricles (RVs) of animal models of PH, RVs of patients with PAH, and plasma levels of PAH.[104,105,113–115] Not much is known about CEs or HCERs in relation to PH, however, increased HCERs are promising biomarkers of disease progression in the cerebrospinal fluid of multiple sclerosis patients.[116] More research is required to investigate any roles of CEs and HCERs in PH or whether this is a secondary effect as opposed to a causal one. Many individual lipids were significantly increased as well, and the data could be mined to identify numerous potential lipid pathways that may contribute to the development of PH. Of note, I found that LA significantly increased in the plasma of 15-HETE fed mice while AA non-significantly increased (**Figure 8**). These would feed into the LOX pathway and in turn produce more HETEs and HODEs, leading us to pursue the importance of HETEs, HODEs, and the LOX enzymes in the development of PH.

Lipids are major players in immunity and immune response.[6,117] Following the observance of numerous lipids across multiple classes increasing, we followed up with investigating immune response via cytokine measurements and flow cytometry. Using a multiplex cytokine plate, we found that four cytokines, eotaxin, G-CSF-3, Il-15, and MCP-1 all significantly increased in the plasma of 15-HETE fed mice (**Figure 9**). Eotaxin is a potent chemoattractant for eosinophils during inflammation and allergic reactions as shown in the guinea pig model of allergic pathway inflammation and in mouse studies noting that eotaxin disruption partially reduces antigen-induced tissue eosinophilia after antigen challenge.[118] G-CSF has immunostimulatory effects on neutrophils as well as immunomodulatory effects such as reducing proinflammatory cytokines, associating it with both beneficial and detrimental roles in animal models of disease.[119] For example, in the MCT model of PH, rats have decreased endothelial progenitor cells and nitric oxide levels, but administration of recombinant human G-CSF elevated nitric oxide levels, increased the number of endothelial progenitor cells, and improved pulmonary hemodynamics and vascular reconstruction.[120] On the other hand, mice continuously infused with angiotensin II had elevated myocardial G-CSF expression and increased blood pressure, neutrophil accumulation, proinflammatory cytokine expression, reactive oxidative species production, and cardiac fibrosis that was attenuated by administration of anti-G-CSF neutralizing antibody.[121] Il-15 is a pro-inflammatory cytokine, has been upregulated in cardiovascular diseases, and promotes atherogenesis, however, Il-15 is also a mediator of inflammation and has protective effects such as protecting cardiomyocytes from oxidative stress, improved myocardial infarction in mice, regulates tissue-resident T cells and tissue destruction, and maintains natural killer cell integrity and

function.[122–124] MCP-1 is a proinflammatory chemokine with potent chemoattractant activity for monocytes and macrophages with elevated plasma levels in idiopathic PAH patients and chronic thromboembolic PH.[103,125,126] Anti-MCP-1 gene therapy inhibited progression of MCT-induced PH.[127] Given the dual nature of these cytokines as having pro-inflammatory and pro-resolving properties, further research will need to be done to determine whether these are driving PH or attempts to resolve the inflammation caused by 15-HETE. Here we also looked at immune cell changes on the 15-HETE diet, finding significant increases in type I macrophages in the intestine and a nonsignificant increase of monocytes in the BALF of 15-HETE fed mice (**Figure 10A and 10B**). Type 1 macrophages are known to be “pro-inflammatory” macrophages, and while they could contribute to PH, the fact that they are not similarly detected in the lungs is interesting and may implicate a role of intestinal inflammation in the onset of PH.[128–130] The increase of macrophages coupled with the significant decrease in neutrophils could also indicate resolution of inflammation as neutrophils undergo apoptosis and macrophages clear them out.[131–133] This implies that intestinal inflammation took place prior to the end of the three week protocol, possibly preceding the onset of PH. Investigation into immune cell composition at earlier time points in the 15-HETE/PH protocol would be needed to determine when intestinal inflammation that is being resolved by day 21 occurs. Monocytes have been known to infiltrate the lungs, specifically small pulmonary arteries, and promote vascular remodeling leading to PH.[134] They can also induce vascular inflammation as well as tissue remodeling, secrete chemokines and cytokines, produce reactive oxygen species (ROS), express coagulation factors and transforming into macrophages.[135] While nonsignificant, possibly due to low number yields in cell number

in our collection for flow cytometry, or simply needing a higher n for comparison between groups, it is interesting to observe a similar finding in mice with dietary induced PH.

We have previously established that it is indeed 15-HETE, and not a metabolite of it, that causes PH, as discussed in Chapter 2. We administered 15-HETE methyl ester, a stable and not readily metabolized form of 15-HETE, to mice at the same dose for three weeks, and found that they too developed PH, as expected.[54] However, we have not previously determined whether other HETEs and HODEs could also cause PH, or was this outcome specific to 15-HETE. It is well known that HETEs and HODEs contribute to hallmarks of PH as factors in oxidative stress, stimulators of proliferation in lung smooth muscle cells, vascular remodeling, endothelial cell migration, and angiogenesis, but determining whether dietary supplementation of HETEs and HODEs other than 15-HETE can cause PH in vivo has not been previously tested.[6,13,22,24,39] Dietary supplementation of 5-HETE on its own and in combination with 5, 12, and 15-HETE showed that 5 µg of HETEs is sufficient to induce PH in wild-type mice (**Figure 12A and 12B**). These findings implicated the role of 5 and 12/15 LOX in the onset of PH. As previously mentioned, mice with 5 LOX inhibited or knocked out in hypoxic mice and Sugen/hypoxic rats had decreased right ventricle hypertrophy and PH pathology compared to animals with normal functioning 5 LOX.[136,137] With regards to 12/15 LOX, it has been implicated in many diseases including atherosclerosis, hypertension, diabetes, obesity, and neurodegenerative disorders as well as many hallmarks of PH including inflammation, vessel wall remodeling, vasoconstriction, endothelial cell dysfunction, oxidation of low density lipoprotein, monocyte recruitment, and angiogenesis.[6,16,20,21,48,138] Furthermore, disruption, blockage, and knockdown of 12/15 LOX has proven beneficial in animal

models, where it diminished atherosclerosis in *apoE-/-*, reduced recruitment of neutrophils in a mouse model of acute lung injury, and provided resistance against both N^G-nitro-l-arginine-methyl ester- and deoxycorticosterone acetate/high-salt-induced hypertension to mice.[112,139] Here, we saw that knocking out 12/15 LOX and inhibiting 5 LOX prevented onset of PH by the 15-HETE diet (**Figure 13A and 13B**) interestingly, with decreased HETEs and HODEs specifically in the intestine tissue (**Figure 13C**). As we are interested in the role of the intestine on the development of PH in this dietary model, it would be worth administering this diet to mice with intestine specific 12/15 LOX KO to see whether intestinal LOX enzyme activity is the starting point of the progression of PH caused by 15-HETE.

It is also worth noting that while we are implicating HETEs and HODEs as the major causal oxylipins of the LOX pathway leading to PH, there are additional lipid products from LA and AA that could also play a role in dietary 15-HETE induced PH via additional inflammatory pathways, such as leukotrienes and thromboxanes.[6,12,13] Leukotrienes are particularly important to note as they are also products of the 5-LOX, the same enzyme responsible for the production of 5-HETE. Leukotrienes are implicated in pulmonary arterial smooth muscle cell (PASMC) proliferation and resistance to apoptosis and inflammation via recruitment and activation of leukocytes via the leukotriene receptor B4 receptor 2.[6,140] Rodent models of PH including MCT and Sugen rats have elevated plasma leukotriene B4 (LTB_4) which induces apoptosis of PAECs, proliferation of PASMCs and fibroblast activation.[6] Thromboxanes, while not produced from LOX enzymes, come from AA, which we have shown increases in the plasma of mice fed 15-HETE diet, are produced via cyclooxygenase (COX) enzymes.[12]

Thromboxane A_2 promotes vasoconstriction, platelet aggregation, and smooth muscle cell proliferation, and has been shown to increase in the lungs of PAH patients when compared to levels of prostacyclin, another AA metabolite, which is a vasodilator, antiproliferative, and anti-inflammatory.[12] Therefore, it is possible that dietary HETEs exert a broad pro-inflammatory effect on mice beyond those specific to HETEs and HODEs via activation of LOX enzymes which would produce additional pro-inflammatory lipids and by increasing plasma levels of LA and AA which would be broken down into pro-inflammatory metabolites by non-LOX enzymes such as COX.

The various analyses described here have shown the wide range by which dietary 15-HETE alters lipid levels and cytokine levels in wild type mice, of note, LA, the precursor of HETEs and HODEs, increased in mice on the 15-HETE diet. Coupling this finding with previous work showing that multiple HETEs and HODEs are increased in the plasma of mice on the 15-HETE diet, we showed that HETEs and HODEs other than 15-HETE could cause PH and that the LOX enzymes are essential to the onset of PH and potential targets for therapeutics for PAH.

Conclusions

- The 15-HETE model of PH causes changes in multiple lipid species and in precursors of HETEs and HODEs in the plasma
- 5-HETE and a combination of 5-12-and 15-HETE at a total dose of 5 μg/mouse/day can also cause PH in wild type mice
- 12/15 LOX KO mice administered 5 LOX inhibitor do not develop PH when fed 15-HETE diet
- Intestine levels of HETEs and HODEs are significantly lowered in 12/15 LOX KO mice

- Plasma cytokine levels and macrophage populations in the intestine increase in mice fed 15-HETE diet

Figures

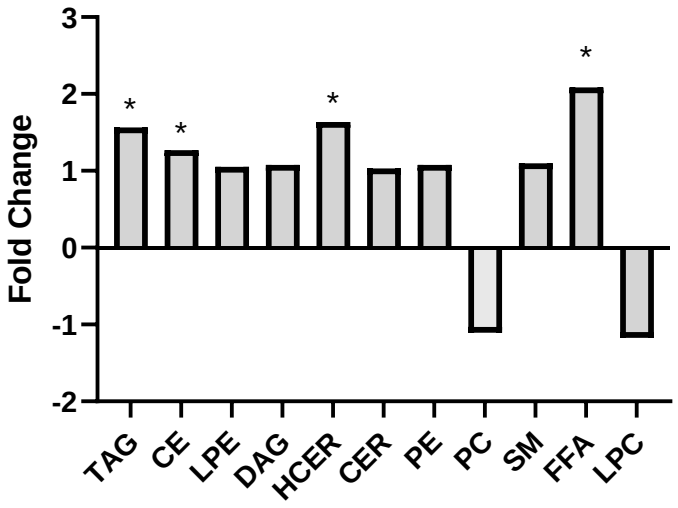

Figure 7: 15-Hydroxyeicosatetraenoic acid (15-HETE) diet moduclates plasma lipid levels across multiple classes Plasma samples from male wild-type mice fed chow diet and 15-HETE supplemented diets were analyzed on the Lipidyzer™ platform (n=4 per group). Lipids in the triacylglycerol (TAG), cholesterol ester (CE), lysophosphatidylethanolamines (LPE) diacylglycerols (DAG), hexosylceramides (HCER) ceramides (CER) phosphatidylethanolamines (PE) phosphatidylcholines (PC) sphingomyelins (SM), free fatty acids (FFA) lysophosphatidylcholines (LPC) classes were detected, with significant increases in TAG, CE, HCER, and FFA observed.

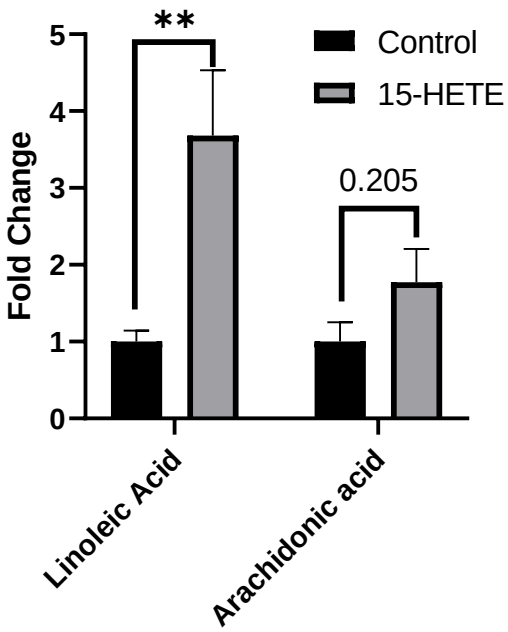

Figure 8: 15-Hydroxyeicosatetraenoic acid (15-HETE) Diet Increases Plasma Levels of Precursors of HETEs and HODEs. Lipidyzer™ analysis of the plasma of chow and 15-HETE fed mice detected a significant increase in Linoleic Acid and a nonsignificant increase in Arachidonic Acid.

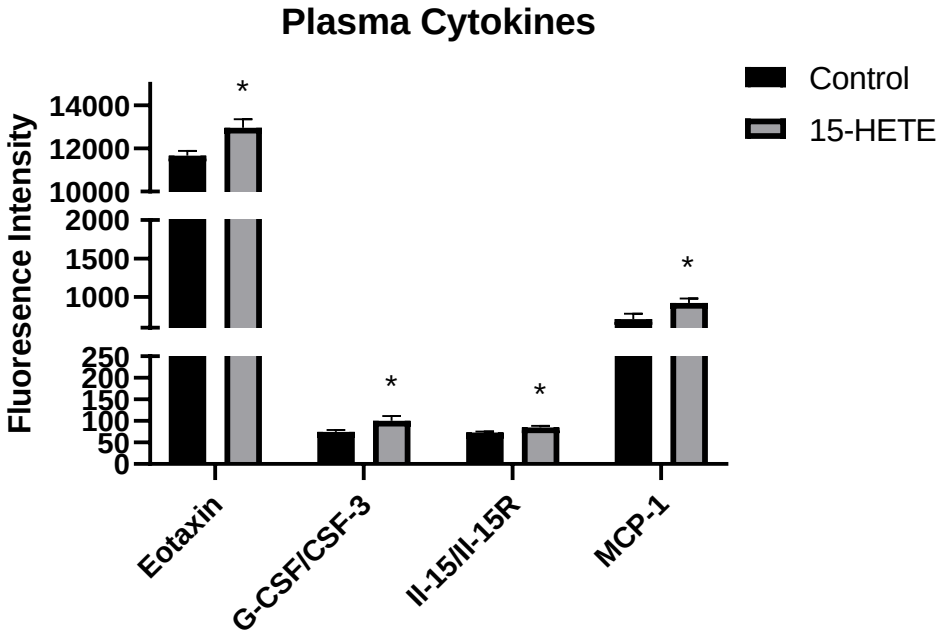

Figure 9: Plasma Cytokine Levels Increase in Mice on 15-Hydroxyeicosatetraenoic (15-HETE) Diet. Multiplex analysis of plasma levels of chow and 15-HETE fed mice (n=8 per group) of Eotaxin, G-CSF/CSF/3, Il-15/Il-15R, and MCP-1 increase in mice on the 15-HETE diet

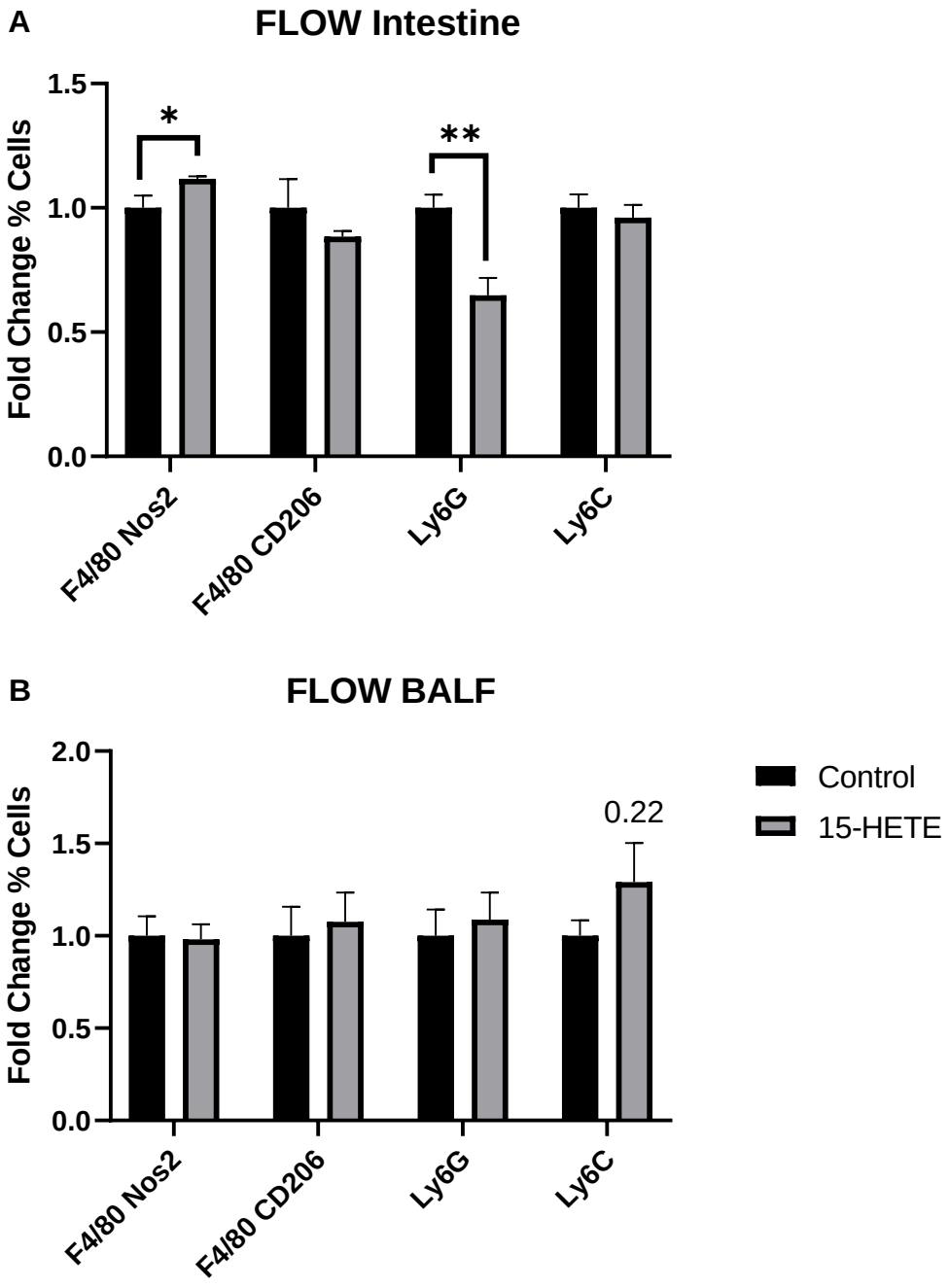

Figure 10: Flow Cytometry Analysis of Intestine and Lungs of 15-HETE Fed Mice Flow cytometry analysis of the A) Intestine shows increased levels of Type I macrophages (F4/80+Nos2) and decreased neutrophils (Ly6G) but no significant change in Type 2 Macrophages (F4/80+CD206) or Monocytes (Ly6C) while in the B) bronchiolar lavage fluid (BALF), there were no significant changes in Type 1 or Type

2 Macrophages or neutrophils, only a non-significant increase in monocytes was noted.

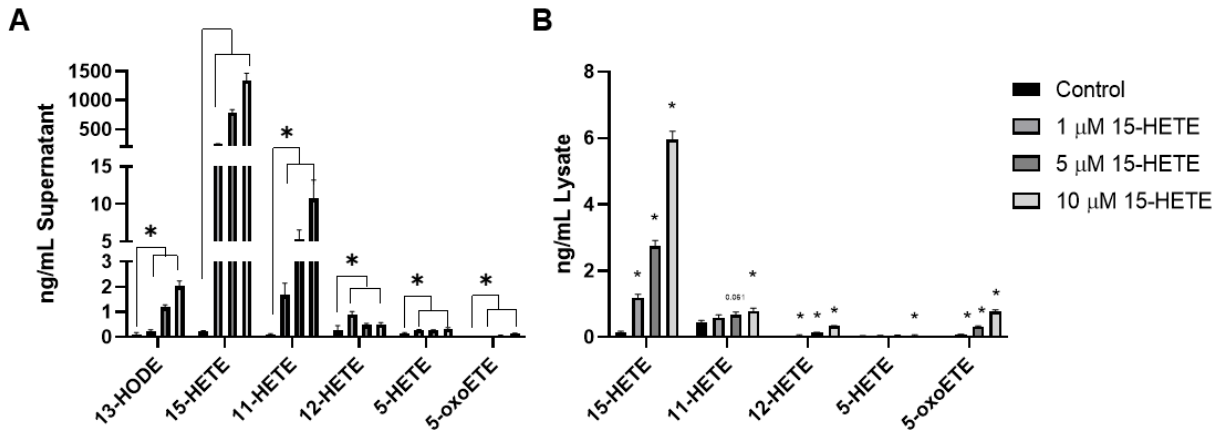

Figure 11: HETEs and HODEs from IEC-6 cells after 12 hours incubation with 15-HETE. A) Supernatant and B) lysate levels of HETEs and HODEs were measured via mass spectrometry after 12 hours incubation with 15-HETE.

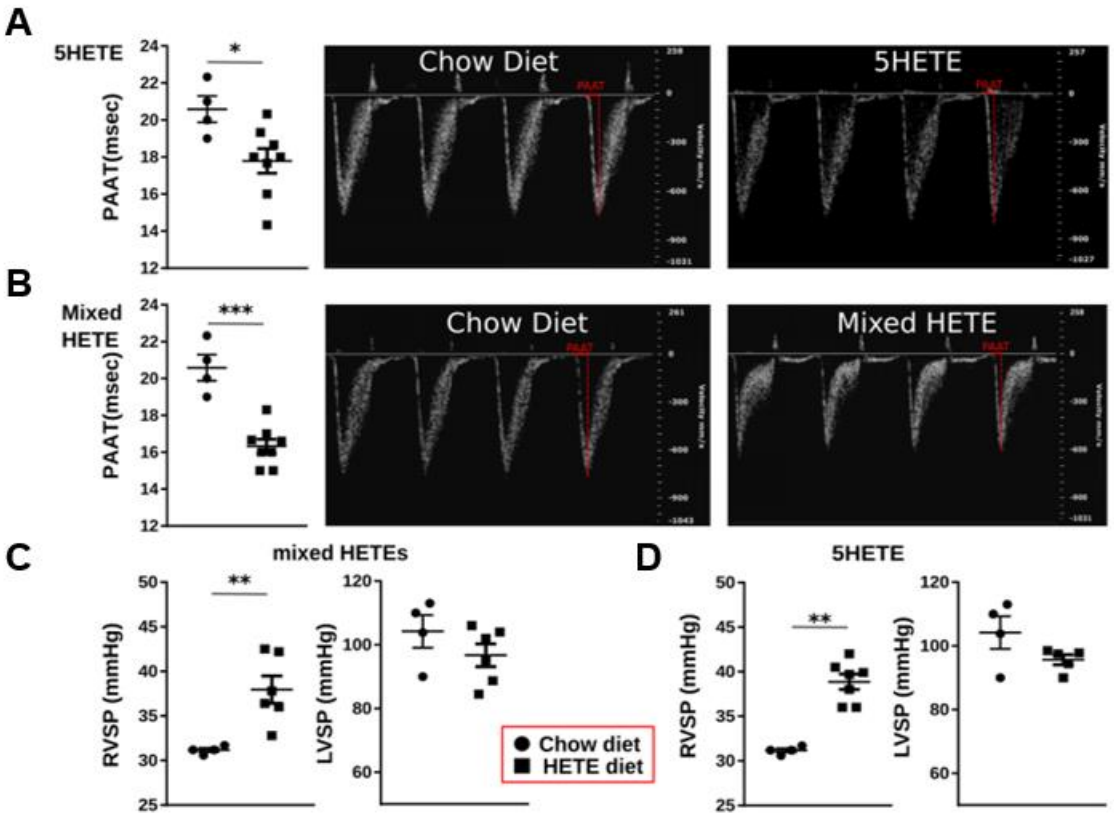

Figure 12: Chow Supplemented with 5-HETE and Mixed HETE Diets can Induce PH in Wild Type Mice A) Pulmonary arterial acceleration time (PAAT) decreases in mice fed 5 µg 5-HETE per day B) PAAT decreases in mice fed 5 µg total 5, 12, and 15-HETE mixture per day C) Right ventricle systolic pressure (RVSP) increases in mice fed 5 µg 5-HETE per day and D) in mice fed 5 µg total 5, 12, and 15-HETE mixture per day

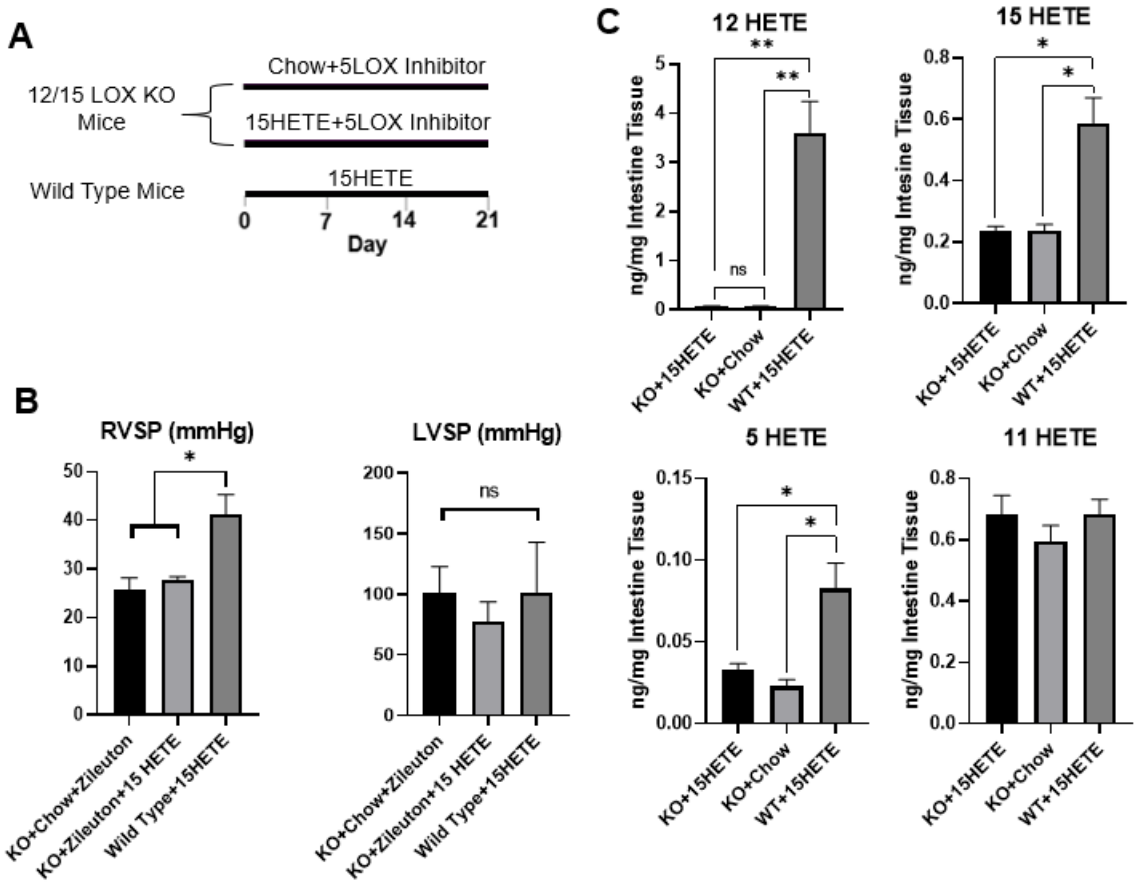

Figure 13: Inhibiting LOX activity blocks 15-HETE induced PH. A) Experimental schematic and timeline. Male mice (n=5 per group). B) Direct catheterization showed no increase in RVSP in KO mice with 15HETE. C) Intestine levels of 5-HETE, 12-HETE, and 15-HETE, were decreased whereas 11-HETE (a non-LOX HETE) levels were not.

Table 1: Antibodies for Flow Cytometry

Protein	Company	Reference
F480 Brilliant Violet 421	BioLegend	123131
Nos2 PE	eBiosciences	12-5920-82
MHCII APC	Invitrogen	17-5321-81
CD206 FITC	BioLegend	141703

Ly6G PE Cyanide 7	Miltenyi Biotech	130-123-712
Ly6C APC	eBiosciences	17-5932-82
Zombie Aqua	BioLegend	77143

Table 2: Antibody

Protein	Company	Reference
Cleaved Caspase 3	Cell Signaling	9661

CHAPTER 4: RNA-seq of the Intestines of 15-HETE fed Hypertensive Mice and the Discovery of IFI44 as a Key Player in PH

Abbreviations

PAH	Pulmonary Arterial Hypertension
HETE	Hydroxyeicosatetraenoic Acid
HODE	Hydroxyoctadecadienoic Acid
WT	Wild Type
PH	Pulmonary Hypertension
ApoA-I	Apolipoprotein A-I
Tg6F	Transgenic Tomatoes Expressing the ApoA-I Mimetic Peptide 6F
EV	Empty Vector Tomatoes
IFI44	Interferon Induced Protein 44
MCT	Monocrotaline
CHP	Chronic Hypoxia
RVSP	Right Ventricle Systolic Pressure
LV	Left Ventricle
IPA	Ingenuity Pathway Analysis
GO	Gene Ontology
STRING	Search Tool for the Retrieval of Interacting Genes/Proteins
GSEA	Gene Set Enrichment Analysis
PBMC	Peripheral Blood Mononuclear Cells
IFNα4	Interferon Alpha 4
IFNβ	Interferon Beta
IFNγ	Interferon Gamma
KD	Knockdown
PAAT	Pulmonary Arterial Acceleration Time
CD8	Cluster of Differentiation 8
PAEC	Pulmonary Arterial Endothelial Cells
Th17	T Helper 17
CXCL10	C-X-C Motif Chemokine Ligand 10
TRAIL	Tumor Necrosis Factor-Related Apoptosis-Inducing Ligand

Abstract

Pulmonary arterial hypertension (PAH) is a disease that targets the pulmonary vasculature causing increased mean arterial pressure and right ventricle hypertrophy leading to death in 50% of patients at 5 years. Studies have previously shown that

oxylipins, particularly hydroxyeicosatetraenoic acids (HETEs) and hydroxyoctadecadienoic acids (HODEs), increase in the lung tissue and plasma of patients with PAH and in mice and rat models of pulmonary hypertension (PH). We have demonstrated that the addition of one HETE, 15-HETE, to the diet is sufficient to cause PH in wild-type mice. As this is a dietary model of PH, we set out to look for a connection between the intestine and the lungs. We conducted RNA-seq analysis on the intestines of mice on the 15-HETE, 15-HETE and transgenic tomato expressing the apolipoprotein A1 (apoA-I) mimetic peptide 6F (Tg6F), and 15-HETE and empty vector tomato (EV) and found many pro-inflammatory genes, gene sets, and pathways increase in the 15-HETE and 15-HETE with empty vector groups, but not in the Tg6F groups. In a set of mechanistic studies, we analyzed gene expression data (RNA-seq) obtained from the lungs of PAH patients and the lungs and intestines of 15-HETE fed mice and discovered interferon-induced protein 44 (IFI44) is the only upregulated gene that is common to all three data sets. We demonstrated that in 15-HETE fed mice, IFI44 expression increases early (one week) in the small intestine before it increases in the lungs (two weeks) and PH is established. While the function of IFI44 is not well understood, several genes important to the immune response correlate with IFI44. We hypothesized that IFI44 plays an important role in 15-HETE mediated PH. We silenced IFI44 in the lungs of 15-HETE fed mice via intratracheal instillation and demonstrated that mice that received IFI44 siRNA do not develop PH while those administered a scramble siRNA did, showing that IFI44 expression is critical to the development of PH and a potential target for future therapeutics.

Introduction

PAH is a fatal disease targeting the lungs leading to right ventricle hypertrophy with no cure to date.[2,5,55,58] Evidence from studies involving many rodent models of PH have shown a close relationship between pro-inflammatory processes and the development of PAH.[6,109] This includes immune cell responses such as macrophage infiltration near lesion areas, an increase of dendritic cells in idiopathic PAH patients and in rats administered monocrotaline (MCT) to induce PH, and alterations in T cell subtypes, as well as cytokine production.[109,141] Pro-inflammatory oxylipins have been shown to increase in the plasma and lung tissues of patients with PAH and animal models of PH.[6,11] Previously, we have shown the causal effects of oxylipins in PH by showing that adding 5 µg of 15-HETE daily to the diets of wild type mice is sufficient to cause PH in 21 days.[11,54] Expanding on this exciting finding, we utilized RNA-seq analysis to show the role of the immunoproteasome in the lungs of 15-HETE fed mice and saw that 15-HETE played a role in leading to endothelial cell apoptosis in the lungs and that the apoA-I mimetic peptide, Tg6F, prevented this.[54] As this is a dietary induction of PH, we have been interested in whether the intestine has a role in initiating the cascade of events that lead to PH.

ApoA-I mimetic peptides have been utilized in animal models of multiple diseases as preventative and therapeutic tools including inflammatory bowel disease, atherosclerosis, cancer, the MCT model of PH in rats, and chronic hypoxia (CHP) in mice.[11,35,65,66,82,142] Previous work has shown that apoA-I mimetic peptides work, in part, my modulating the immune response in the intestine, which contains the largest number of immune cells of any tissue in the body.[65,142,143] Dietary treatment with apoA-I mimetics have also been shown to decrease systemic inflammation via modulation of

intestine oxylipin metabolism.[89] Therefore, changes in the intestine are of interest to investigate in our dietary 15-HETE model of PH.

Attempts to identify similar changes in genes exactly mirroring those of the lung have not been successful, therefore, we decided to conduct RNA-seq on the intestines of four groups of mice; (I) those on the chow diet (Chow), (II) mice on the Chow+15-HETE diet (15-HETE), (III) chow+15-HETE+Tg6F for 3 weeks (Prev), and (IV) Chow+15-HETE+EV. Mice on chow and Tg6F supplemented diets did not develop PH while those on the 15-HETE diet alone or supplemented with empty vector tomato did, as previously reported.[54] With this massive and thorough insight into the changes in the intestine, we will be able to narrow down what genes and pathways are increased by the 15-HETE diet and decreased by Tg6F, while using the EV group as a control for any beneficial effects caused by the tomato extract that ultimately did not contribute to prevention of PH, focusing particularly on inflammation pathways.

When combining and analyzing the data from three sets together the RNA-seq analysis in the intestines of 15-HETE fed mice with the analysis of lungs of 15-HETE fed mice and human PAH patients, IFI44 was found to be the common gene increasing in all three data sets. IFI44 was identified in the cytoplasm of chimpanzees infected with hepatis C and found to be induced by interferons alpha and beta (IFNα and IFNβ), not gamma (IFNγ).[144] IFI44 has been implicated in the immune responses and diseases including hepatitis C virus and head and neck squamous cell carcinoma, and respiratory syncytial virus.[144–147] IFI44 is positively correlated with antigen-presentation and nuclear factor (NF)-kappa B signaling pathways as well as the infiltration of CD4+ cells, macrophages, and neutrophils in neck squamous cell carcinoma.[146] With regards to

viruses, IFI44 restricts replication of respiratory syncytial virus and facilitates HIV-1 latency by inhibiting promoter activity, but also supports virus replication by negatively modulating immune responses.[147–149] In the context of PH, the role of IFI44 is unknown and therefore there is little to build from with regards to what role it may play, therefore, we are the first to set out to determine whether it is imperative to the onset of PH.

Materials and Methods

Mice and treatments

Male C57BL6/J mice (wild type, 2-3 months old) were purchased from Jackson Laboratories and used. To prepare the HETE diets, Teklad diet was prepared so that each mouse consumed 4 g chow per day. The HETE diets were supplemented with 5 μg 15-HETE (34720, Cayman) per mouse per day. Tg6F or control empty vector tomatoes (EV) were freeze-dried, powdered, and added to the diet at 2.2% by weight as previously described.[63,65] Mice were fed the diets for 21 days before sacrifice, collection of plasma, and collection of tissues.

siRNA knock down of IFI44 was achieved by administering siRNA against mouse IFI44 (Accell, A-051791-13-0050) or non-targeting control siRNA (Accell, D-001910-01-50) for control mice by instillation (1nmol) 2 times a week for a total of 6 instillations. Mice administered siRNA against IFI44 and scramble siRNA both consumed 15-HETE diet for 21 days.

Human Subjects

Patients studied were part of the French Network on Pulmonary Hypertension, a program approved by institutional Ethics Committee, and had given written informed

consent (Protocol N8CO-08-003,IDRCB:2008-A00485-50, approved on June 18, 2008). Patient's characteristics are given in Table S1, Chapter 2.

RNA Extraction for RNA-seq Analysis

Total RNA from the lungs of mice on chow diet or 15-HETE diet (n=6/group) and jejunum of mice on chow diet, 15-HETE diet, Tg6F diet, and EV diet (n=4/group) were extracted using miRvana Total RNA Isolation Kit (Applied Biosystems™). The purity and concentration of extracted RNA were quantified using the Agilent 2100 Technology and NanoDrop 2000 Spectrophotometer (Thermo Scientific).

RNA-seq Analysis

Libraries for RNA-Seq were prepared by the Technology Center for Genomics & Bioinformatics at UCLA with Kapa Hyper Kit. The workflow consisted of rRNA depletion, cDNA generation, and end repair to generate blunt ends, A-tailing, adaptor ligation and PCR amplification. Different adaptors were used for multiplexing samples in one lane. The data was sequenced on Illumina HiSeq 3000 for a single-read 50bp run. Data quality check was done on Illumina SAV. Demultiplexing was performed with Illumina Bcl2fastq2 v 2.17 program. The reads were mapped to the latest UCSC transcript set using Bowtie2 version 2.1.0[150] and the gene expression level was estimated using RSEM v1.2.15.[151] Gene and Isoform results are available in the RSEM output folder. Rsem_count.txt is a concatenation of the gene counts from the RSEM_output files. TMM (trimmed mean of M-values) was used to normalize the gene expression. Mapping statistics were average given rRNA depletion; between 42.94% and 51.08% of reads mapped to the reference. TMM (trimmed mean of M-values) were used to normalize the gene expression. Differentially expressed genes were identified using the

edgeR program.[152] Genes showing altered expression with $p < 0.05$ and more than 1.5 fold changes were considered differentially expressed. The files XXX_vs_YYY_atfc1.5p0.05_ZZZ_genes.txt were fed into Ingenuity Pathway Analysis (IPA).[153] IPA analysis files for Canonical pathways were compared between the three treatment groups vs control (15-HETE vs Control, EV vs Control, Tg6F vs Control). Significantly changing pathways were those with a -log(p-value) of 1.3 or higher, all others were discarded for comparisons. Pathways significantly increasing only in 15-HETE and EV but not Tg6F were compiled in a list as those being potentially relevant to PH onset and listed in Table 2.

RNA-seq files for these samples have been uploaded to PubMed under the BioProject ID: PRJNA757196. https://www.ncbi.nlm.nih.gov/bioproject/PRJNA757196

Gene Set Enrichment Analysis (GSEA) and Search Tool for the Retrieval of Interacting Genes/Proteins (STRING)

Genes with a fold change above 1.5 were considered up-regulated and genes with a fold change below -1.5 were considered down-regulated. All up- or down-regulated genes were used for gene sets enrichment analysis using GSEA software on all mouse gene ontology (GO) sets. STRING online software was used to analyze known associations of the 168 genes up-regulated by the 15-HETE and EV diets but not by chow and Tg6F diets and gene ontology GO analysis for Biological Processes from the STRING analysis was used to narrow down the GSEA networks by highlighting those with the most genes from clusters identified by STRING .[101,102] The top 40 gene sets with 5+ genes from STRING clusters were input into Cytoscape (version 3.8.0), an

open source software platform for visualizing complex networks, to create an enrichment map.[154] Gene sets were connected to GO Biological Processes by cross-referencing individual genes present in both.

Real-Time PCR

Total RNA from lungs was isolated with Trizol extraction method and reverse transcribed with poly dT primers using the Omniscript reverse transcription kit (Qiagen, Cat#205113). Real-time PCR was performed on polyA+ cDNA with specific primers (Table 4) using iTaq Universal SYBR® (BioRad, Cat#1725121).

Total RNA from the intestine was isolated with miRvana kit while RNA from the cells was isolated using RNeasy kit (Qiagen#74004) and reverse transcribed using the BioRad iScript Reverse Transcription Supermix (Cat#1708841). Real-time PCR was performed on polyA+cDNA with specific primers (Table 4) using iQ™ SYBR® Green Supermix (BioRad, Cat#1708882).

PH Assessment

PH progression and development was monitored weekly by noninvasive 2-dimensional Doppler echocardiography using Vevo 2100 (Visualsonics) and at the end of the protocol, open-chest direct catheterization was performed to assess RV systolic pressure (RVSP) and left ventricular (LV) systolic pressure as previously described.[54] Fulton index was measured by dividing the weight of the RV by the sum of the LV and intraventricular septum.

Cell Culture

Primary cultures of black 6 mouse pulmonary arterial endothelial cells (PAEC) were purchased from ATCC. PAECs were used from passage 3 to 6 and each experiment was repeated at least 3 times. CD8 cells (ALLCELLS) were incubated with IFNα4, siRNA targeting IFI44 (Accell, A-051791-13-0050) or non-targeting control siRNA (Accell, D-001910-01-50). In some experiments, PAECs were incubated with or without 15-HETE (100 ng/ml) and 12 hours later CD8 cells were added. After 12 hours of contact between EC and CD8 cells, the cells were collected, fixed, and stained for cleaved caspase 3.

Healthy rat small intestine epithelial cells (IEC-6) were purchased from ATCC. IEC-6 were used from passage 5 to 7. IEC-6 were exposed to increased concentrations of 15-HETE (1, 5, and 10 μM, Figure S3), after 12 hours the supernatant was collected, and RNA was extracted using the RNeasy kit as described above in Real-Time PCR.

Results

RNA-seq Analysis of the Intestine Implicates Pro-Inflammatory and Immune Response Pathways Increasing in 15-HETE fed mice and Countered by Tg6F

Ingenuity Pathway Analysis (IPA) analysis conducted by the Translational Pathology Core Laboratory at UCLA revealed 43 Canonical Pathways were significantly changed in the 15-HETE and EV groups but not in Tg6F (Table 3). The top 15 pathways are graphed in **Figure 14**, showing that many of them pertain in inflammatory responses; atherosclerosis signaling, leukocyte extravasation signaling, agranulocyte signaling and diapedesis, and airway pathology in chronic obstructive pulmonary disease being a few of peak interest. Unfortunately, not all these pathways had z-scores to confirm whether these were increasing or decreasing, so I used other forms of

analyses to gain more insight into directionality and precise genes implicated in these immune pathways. RNA-seq of the intestine showed that 168 genes increased in the 15-HETE and EV groups and decreased in the Tg6F group compared with EV while Gene Set Enrichment Analysis had 685 gene sets increased in the 15-HETE and EV groups that were decreased in the Tg6F group (data not shown). STRING network analysis showed that 57 of the 168 genes were connected in five clusters, thus, we proceeded to focus on these 57 genes in further analysis to narrow down the 685 gene sets. Gene Ontology (GO) enrichment of these 57 genes similarly indicated many response systems being upregulated by these genes, including response to biotic stimulus, stress, external stimulus, as well as immune response, and defense response. Filtering out gene sets containing less than 5 genes from the gene networks identified by Search Tool for the Retrieval of Interacting Genes/Proteins (STRING) and focusing on the top 40 allowed us to see that they can be broken up into five groups; 1. Response to various stimuli, 2. Immune Response/Cytokine, 3. Cell Adhesion, 4. Chemotaxis, and 5. Vasculature/Angiogenesis (**Figure 15**). Most of the contributing genes to these five groups of gene sets came from three of the clusters seen in the STRING network analysis, one of which has many genes implicated in immune response (**Figure 16**).

Analysis of PAH patient lung, 15-HETE fed mouse lung, and 15-HETE fed intestine data identifies IFI44 as common increasing gene

RNA-seq analysis of the lungs of mice after three weeks of 15-HETE diet and the lungs of PAH patients conducted in Chapter 2[54] was combined with RNA-seq analysis of the

intestines of mice fed 15-HETE diet for three weeks and showed increased levels of IFI44 (**Figure 17**), a gene that was also identified in the GSEA/STRING network analysis (**Figure 16**). Measurement of gene expression via qPCR of mouse lungs, intestine, and human lungs and peripheral blood mononuclear cells (PBMCs) also show an increase of IFI44 in both mice and humans (**Figure 17A-17C**). As IFI44 is an interferon stimulated gene, qPCRs of the intestine and lungs of mice after one, two, and three weeks of 15-HETE diet show that IFNα4 increases in the intestine during the first week of 15-HETE diet, a finding also seen in IEC-6 cells treated with 15-HETE *in vitro*, and IFI44 levels increase in the intestine before it increases in the lungs (**Figures 18A, 18B, 19A, and 19B**). IFNβ and IFNγ were also measured via qPCR in the jejunum of 15-HETE fed mice and IEC-6 cells treated with 15-HETE for 12 hours however neither increased with 15-HETE treatments (**Supplemental Figure 6**). Staining of IFI44 in the lung and intestine confirm these increases (**Figure 19C**). Exposing cluster of differentiation 8 positive (CD8+) cells to the supernatant from IEC-6 cells also activates IFI44 in CD8+ cells (**Figure 20**).

Silencing IFI44 *in vivo* prevents induction of PH by 15-HETE diet

In order to test how imperative IFI44 is to the onset of PH in mice on 15-HETE diet, we knocked down (KD) IFI44 via intratracheal instillation of siRNA for IFI44 or scramble siRNA and fed mice chow fortified with 15-HETE for 3 weeks and found that pulmonary arterial acceleration time (PAAT) was higher and the RVSP was significantly lower than the mice on 15-HETE diet administer scramble siRNA, showing that IFI44 is an important player in the onset of PH in the dietary model (**Figure 21A-21C**).

Genes highly correlated with IFI44 expression, CXCL10 and TRAIL, increase in tissues of mice on 15-HETE diet and in cells exposed to 15-HETE and IFNα4

C-X-C motif ligand 10 (CXCL10) and Tumor necrosis factor (TNF)-Related Apoptosis Inducing Ligand (TRAIL) were highly correlated with IFI44 expression in peripheral blood mononuclear cells of PAH patients (**Figure 22**). RNA-seq analysis of the intestines and lungs of 15-HETE mice show that transcripts of CXCL10 are significantly increased in the lungs of mice fed 15-HETE diet while qPCR analysis shows that expression of TRAIL also significantly increases in the lungs of 15-HETE fed mice (**Figure 23A and 23B**). CD8+ cells exposed to IFNα4 for 8 hours had increased levels of IFI44, CXCL10, and TRAIL (**Figure 24A**).

Silencing IFI44 in CD8+ cells decreases induction of CXCL10 and TRAIL by IFNα4 and decreases cell apoptosis induced by 15-HETE and IFNα4 *in vitro*

CD8+ cells exposed to IFNα4 with and without siRNA against IFI44 showed that IFI44 KD decreased CXCL10 and TRAIL induction observed when cells are only treated with IFNα4 (**Figure 24B**). To determine whether alterations in the expression of IFI44, CXCL10, and TRAIL affected cell apoptosis, CD8+ cells were exposed to 15-HETE, IFNα4, siRNA against IFI44, and scramble siRNA before treating PAECs with them showed that knocking while 15-HETE and IFNα4 treatment alone or together increases expression cell apoptosis, silencing IFI44 decreases apoptosis (**Figure 25**).

Discussion

PH to this day remains a potentially fatal disease affecting people of all ages with no cure to date. While our new 15-HETE model of PH has already provided novel insights into how oxylipins of the LOX pathway contribute to PH, here, we have dug

deeper into the understanding of what is happening in an underappreciated and unlikely culprit in the onset of PH, the intestine via RNA-seq analysis. While attempting to match up gene expression changes from the lung data we previously published did not show any obvious links, data analysis from the intestine revealed that multiple immune responses were upregulated by the 15-HETE and EV diets, but not in the Tg6F diet. This is interesting as the immune response is involved with PAH and the intestine serves as the largest compartment of the immune system, complete with organized lymphoid tissues and large populations of innate and adaptive effector cells.[143] It also substantiates findings from previous work with apoA-I mimetic peptides, showing that by modulating oxylipins in the intestine, systemic immune responses are reduced.[35,89] With regards to the development of PH in our model, there is no significant difference in PAAT after one week of 15-HETE diet, a significant difference after 2 weeks and 3 weeks, with RVSP measurement confirmation of PH at week 3.[54] In that first week, it is possible that an immune response is initiated in the gut and as time goes on, moves towards through the vasculature to the lungs. Studies have sighted the connection between the gut and the lung as a way for intestinal inflammation and immune response to affect the lungs.[155–159] For example, an autoimmune arthritis mouse model showed that T helper 17 (Th17) cells were differentiated in the intestine, left the gut and migrated to peripheral lymphoid tissue, leading to differentiation of B cells and production of antibodies in the spleen that travel to their target joints and leading to the development of disease.[155] Multiple papers cite the maintenance of intestinal immune cell homeostasis as well as the gut lung axis implicate the microbiota and its products as keys to both.[143,155–160] Microbiota analysis in PAH patients has also noted distinct

changes compared to healthy control cohort.[50] Indeed, it is possible that the modulation of the microbiota is playing a role in the onset of PH in the dietary 15-HETE model and would be interesting to explore in future studies (see Chapter 5).

Furthermore, this expanded dataset allowed us to compare a much wider window of genes with data from the lungs of mice on the 15-HETE diet as well as PAH patients. Utilizing RNA-seq data from PAH patients and PH mice on the 15-HETE diet, we have identified one gene, the interferon stimulated gene, IFI44, as a common link between the three data sets. IFI44 is known for playing a role in host antiviral response, supporting virus replication mediated by IFN response, facilitating HIV suppression and latency, and restriction of respiratory syncytial virus.[147–149] IFI44 is correlated with immune infiltration in head and neck squamous cell carcinoma, with more infiltration from neutrophils, natural killer (NK) cells, type 1 macrophage, type 2 macrophage, Th1 and Th2 CD4+ T cells, CD8+ effector memory T cells, and plasmacytoid dendritic cells in the tumor microenvironment with high IFI44 expression compared with lower IFI44 expression.[146] However, there was previously no known role for IFI44 with regards to PH.

Examining two genes positively correlating with IFI44 expression in PAH patients, CXCL10 and TRAIL helped determine a pathway in which IFI44 leads to PH. Multiple studies have implicated CXCL10 with heart failure and hypertension.[161–165] CXCL10 is a pro-inflammatory cytokine expressed on monocytes, macrophages, keratinocytes, and vascular fibroblasts, endothelial cells, and smooth muscle cells that acts as a chemoattractant for monocytes, T cells, and smooth muscle cells.[161] Our collaborators are currently conducting exciting work on the role of CXCL10 in PH. They

recently reported significant increases in CXCL10 expression in the lungs of PAH patients that is higher in women than men and shown that treating human PAECs with recombinant CXCL10 significantly increases cell apoptosis at a conference.[166] TRAIL is a transmembrane protein of the death receptor ligand family that is expressed in a variety of human tissues, namely lung, spleen, and prostate, that is known to induce apoptosis in cancer cells without toxic side effects.[167–169] TRAIL has similarly been implicated in PAH as elevated levels of TRAIL has been found in the serum of PAH patients, immunoreactivity of TRAIL has been shown in pulmonary vascular lesions of idiopathic PAH patients, PAH in rodent models has been reversed by anti-TRAIL antibody, and TRAIL knockout is protective in the Sugen/hypoxia model of PH.[169] TRAIL is also noted to induce proliferation of pulmonary artery smooth muscle cells of PAH patients *in vitro* and stimulate angiogenic processes of vascular endothelial cells *in vitro* however, this occurs at low levels of TRAIL, whereas high levels of TRAIL induce caspase 3 mediated apoptosis of ECs.[169] Here we have shown that IFI44 modulates expression of CXCL10 and TRAIL, as KD of IFI44 prevented increases of both in CD8+ cells that were observed when CD8+ cells were treated with IFNα4 alone, showing that IFI44 drives expression CXCL10 and TRAIL. Furthermore, IFI44 KD decreased PAEC apoptosis by CD8+ cells, linking IFI44 to the findings described in our earlier publication reporting that 15-HETE diet induced PH via increased t cell-dependent endothelial cell apoptosis.[54]

IFI44 expression increases in the intestine before the lungs, adding to the hypothesis that an immune response that leads to PH begins in the intestine due to dietary exposure to 15-HETE. This was illustrated *in vitro* where supernatant from the

15-HETE treated IEC-6 cells increased IFI44 expression of CD8+ cells. Our previous work described in Chapter 2[54] reports that IEC-6 cells exposed to 15-HETE have increased levels of multiple HETEs and HODEs and here I have shown that 15-HETE treatment of IEC-6 cells increases expression of IFNα4, providing two possible signals that could leave the gut and induce inflammation in immune cells that could attack the lungs, leading to PH. Blocking IFI44 in the lungs of mice prevented the onset of PH *in vivo*, whether the same is true for blocking IFI44 or IFNα4 in the intestine has not been determined and would be important to investigate to fully determine their roles in the intestine to the onset of PH by 15-HETE. While Tg6F prevents induction of IFNα4 expression in the intestine, further work also needs to be done to elucidate how Tg6F is regulating expression of IFI44.

Conclusions

- 15-HETE diet changes intestinal gene expression of hundreds of genes many of which the apoA-I mimetic peptide, Tg6F, which prevents 15-HETE induction of PH, counteracts
- Many pathways increased by 15-HETE, are unaffected by EV tomato, and are prevented from increasing by Tg6F are implicated in 1. Response to various stimuli, 2. Immune Response/cytokine, 3. Cell adhesion, 4. Chemotaxis, 5. Vasculature/Angiogenesis
- Analysis of RNA-seq data from the intestine and lungs of 15-HETE fed mice and lungs of PAH patients found IFI44 increasing in all 3
- IFI44 increases in the intestine earlier in the 15-HETE diet protocol than in the lungs

- Intratracheal administration of siRNA against IFI44 prevented development of 15-HETE diet induced PH

Figures

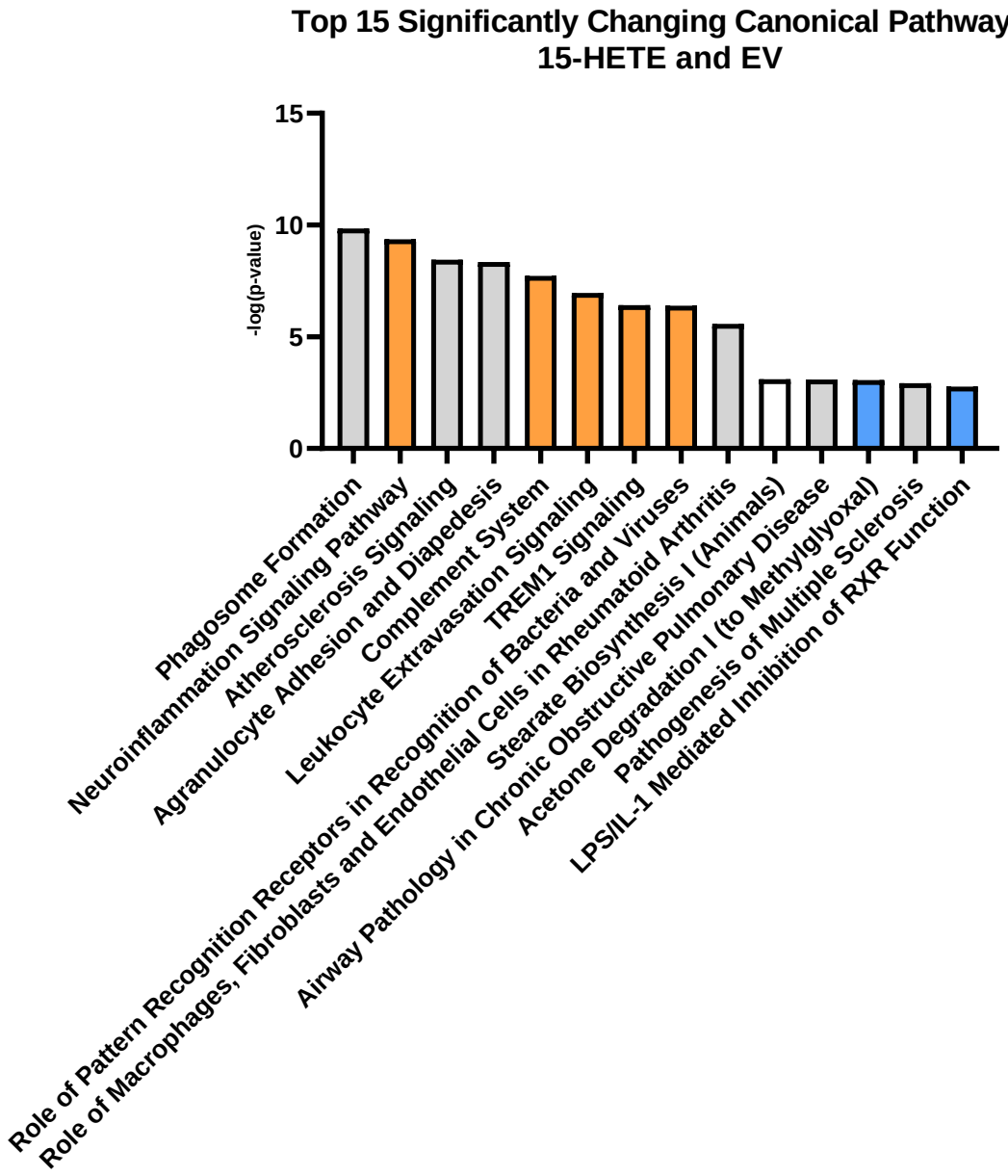

Figure 14: Top 15 Canonical Pathways significantly changing in 15-HETE and EV groups. IPA analysis of 15-HETE vs Control, EV vs Control, and Tg6F vs Control found 43 Canonical Pathways significantly changing in 15-HETE and EV groups, but not Tg6F (Table 2). The top 15 are graphed here, bars with no z-score in gray, positive in orange, negative in blue, and zero in white.

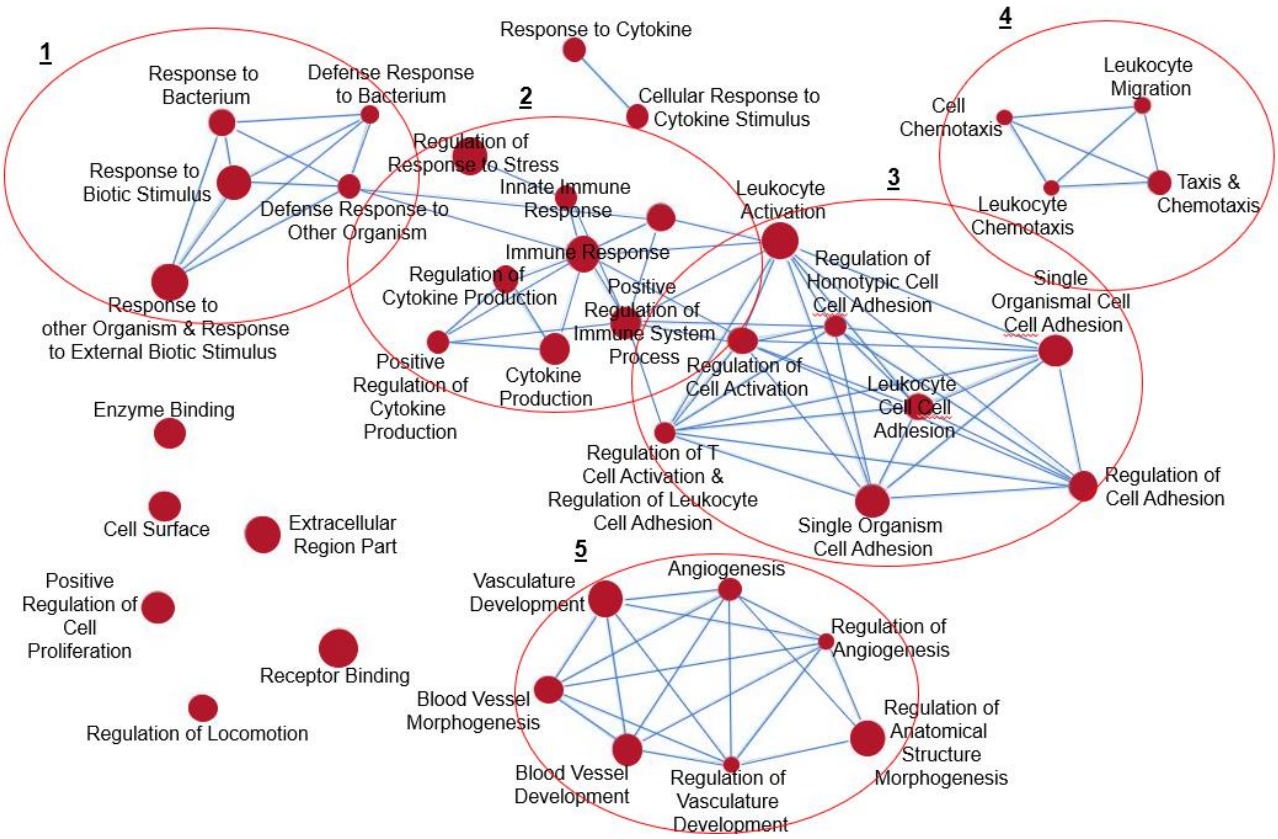

Figure 15: Top 40 gene sets containing 5 or more genes from STRING network analysis Can be broken up into five GO Biological Processes 1: response to various stimuli, 2. Immune Response/cytokine, 3. Cell adhesion, 4. Chemotaxis, 5. Vasculature/Angiogenesis

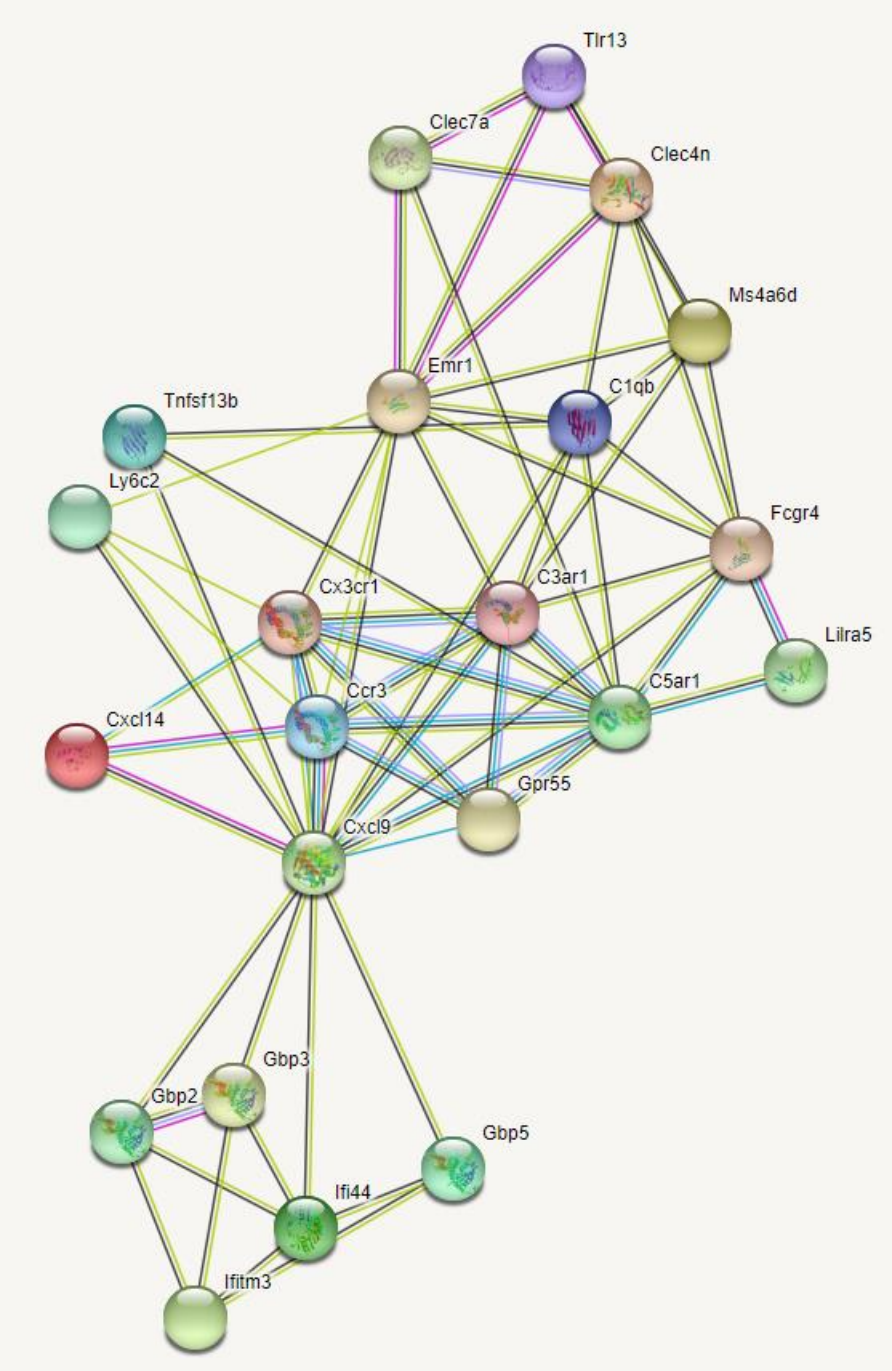

Figure 16: STRING network of genes pertaining to immune response gene sets from GSEA analysis.

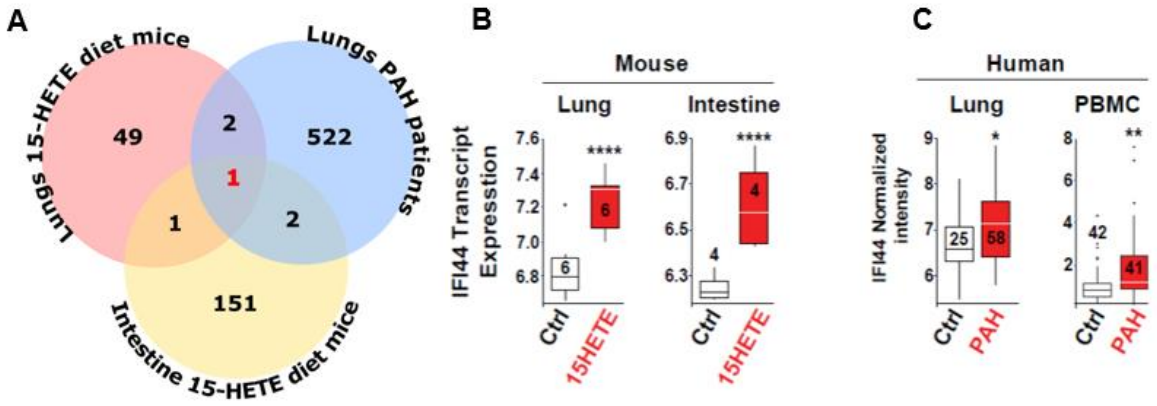

Figure 17: IFI44 identified to increase in PH human lungs, lungs of 15-HETE/PH mice, and intestines of 15-HETE/PH mice. A) Venn diagram of overlapping genes between the three data sets. B) Increased expression in mouse lungs and intestine as well as C) in the lungs and peripheral blood mononuclear cells of humans via microarray analysis.

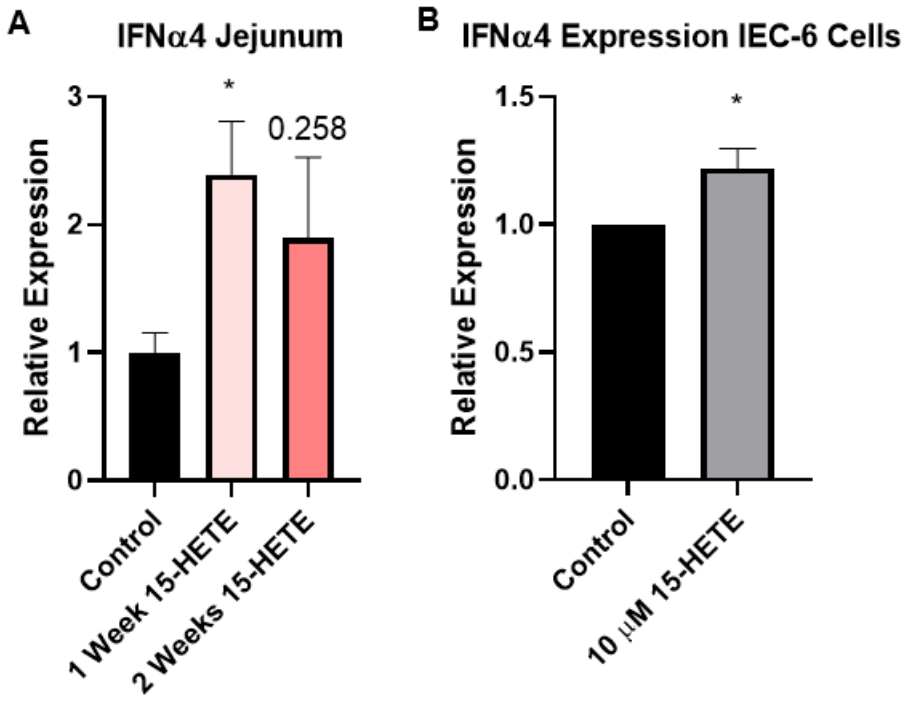

Figure 18: IFNα4 increases in the intestine after 15-HETE induction A) Time course analysis of intestines of mice on 15-HETE diet show IFNα4 increases in the intestine at week 1 (n=6 per group) and increases in B) IEC-6 cells treated with 15-HETE for 12 hours (n=3 experiments).

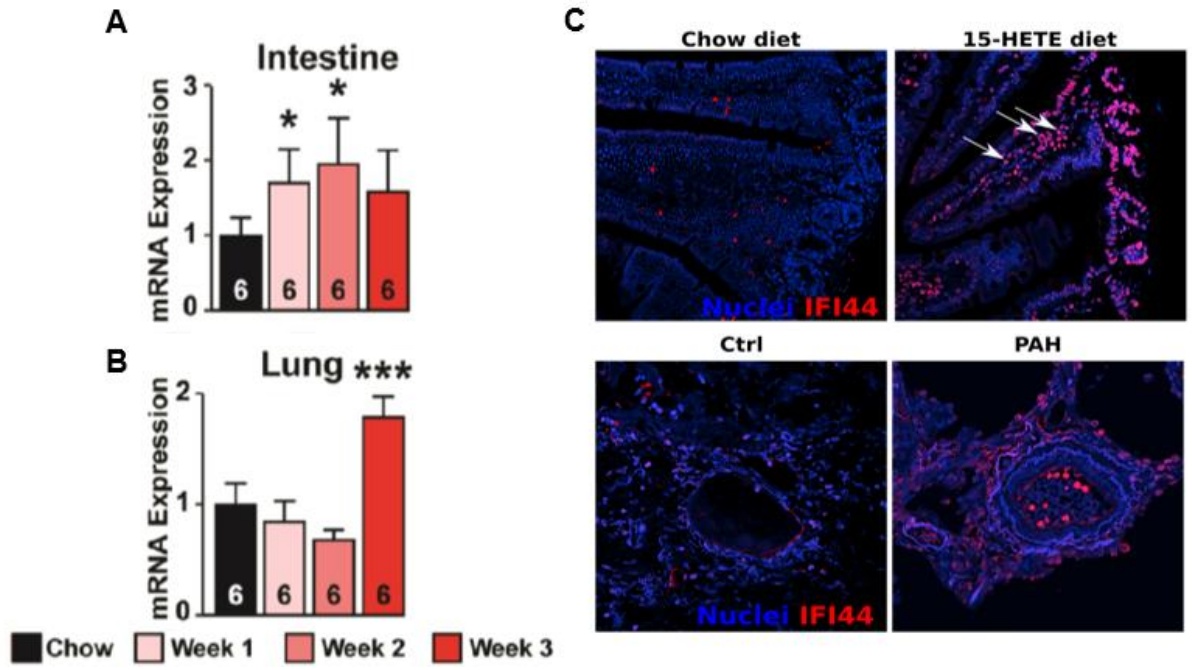

Figure 19: Time course analysis of lungs and intestines of mice on 15-HETE diet show IFI44 increases in the intestine before PH onset and increase of IFI44 in the lungs. qPCR analysis shows increase of IFI44 over three weeks in the A) intestine and B) lungs (n=6 per group). C) IHC staining shows increase of IFI44 in the intestine and lungs of 15-HETE fed mice at week 3.

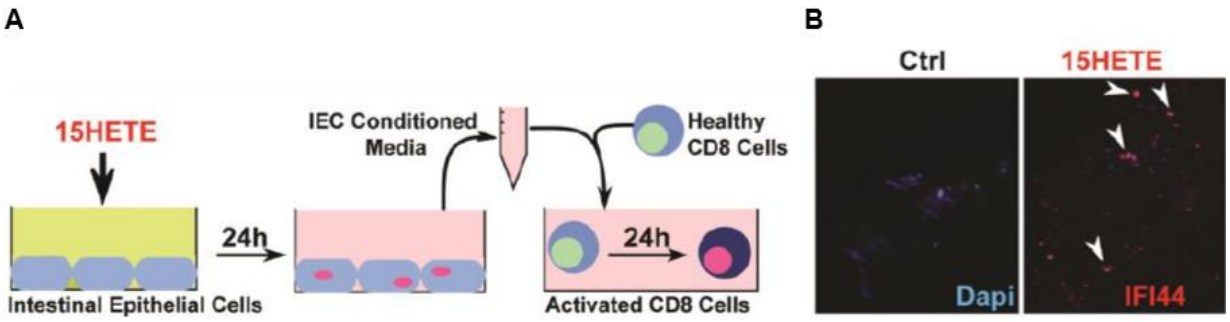

Figure 20: Cultured medium of IEC-6 cells treated with 15-HETE activates IFI44 in CD8 cells. A) Schematic of the experimental protocol. IEC-6 cells are cultured with or without 15-HETE for 24 hours and is then used to culture CD8 cells for 24 hours. B) Upregulation of IFI44 expression in CD8 cells after being cultured with cell conditioned media of IEC-6 cell treated with 15-HETE.

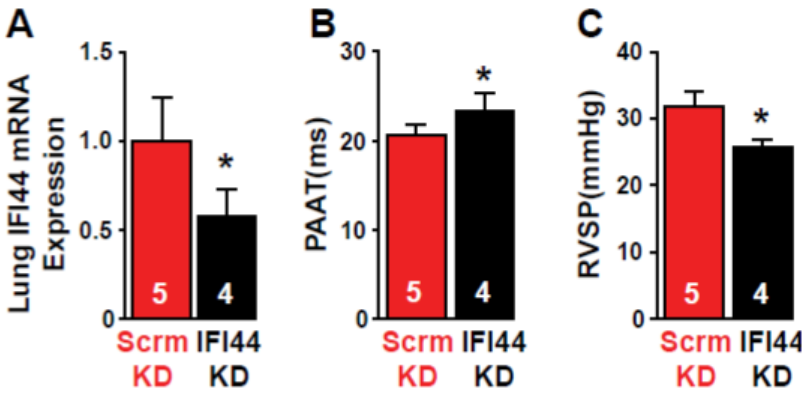

Figure 21: Knockdown of IFI44 in the lungs of 15-HETE fed mice prevents development of PH. A) qPCR expression showing decrease of IFI44 in the lungs of mice administered siRNA against IFI44 B) PAAT measurement showing increase in mice with siRNA against IFI44. C) RVSP showing decrease in mice with siRNA against IFI44 compared to mice administered scramble siRNA.

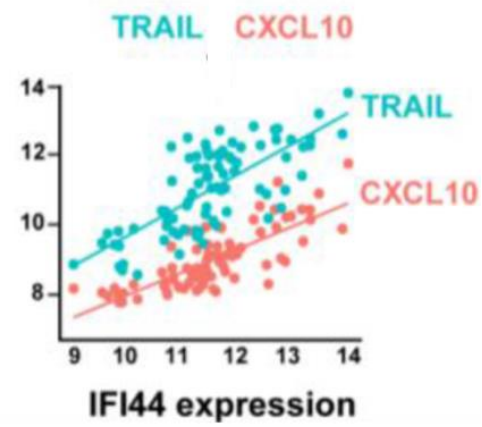

Figure 22: IFI44 expression is highly correlated with expression of TRAIL and CXCL10 in PBMCs of PAH patients.

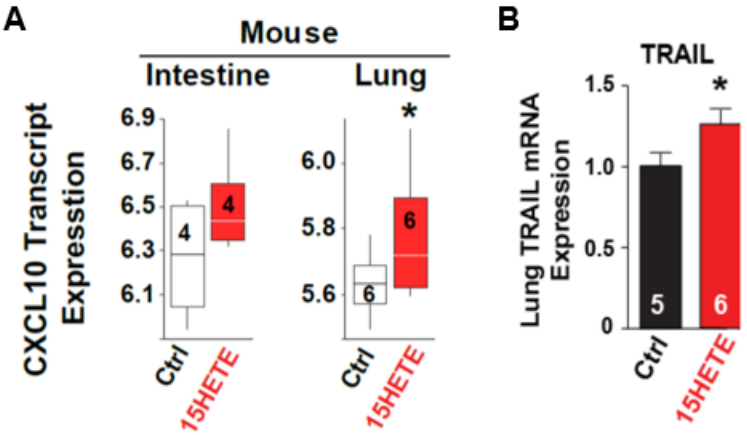

Figure 23: CXCL10 and TRAIL transcripts are upregulated in the tissues of mice fed 15-HETE diet. A) RNA-seq from 15-HETE diet mouse intestine and lung demonstrate a significant increase of CXCL10 in the lungs. B) TRAIL is up-regulated in the lungs of mice on 15-HETE diet with PH.

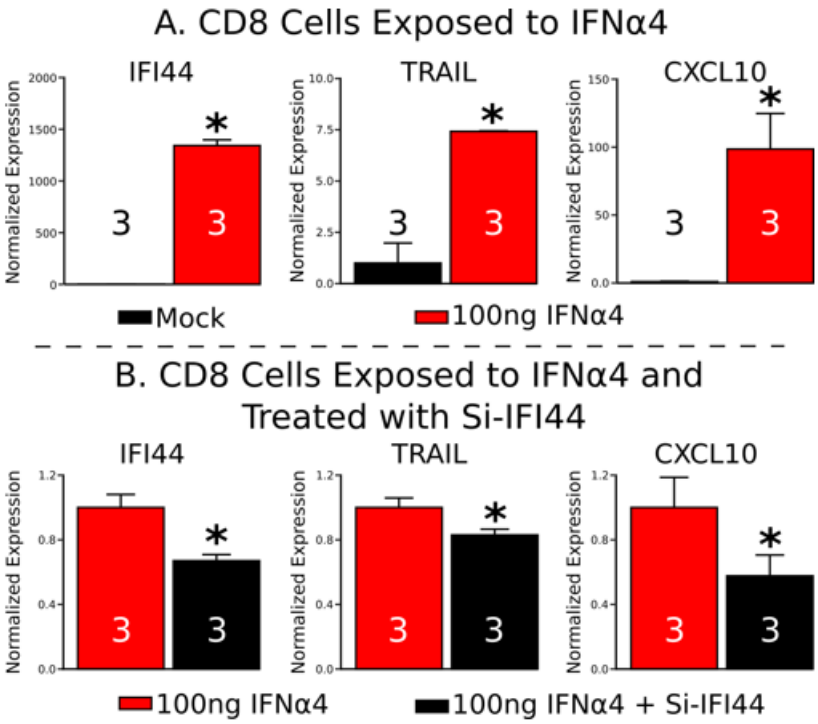

Figure 24: IFNα4 induces TRAIL, and CXCL10 expression in CD8 cells through IFI44 up-regulation. Immortalized mouse CD8 cells were exposed to 100ng of IFNα4 for 48h. A) IFNα4 treatment induces IFI44, TRAIL and CXCL10 expression. B) Silencing of IFI44 expression significantly decreases TRAIL and CXCL10 expression. (n=3 experiments)

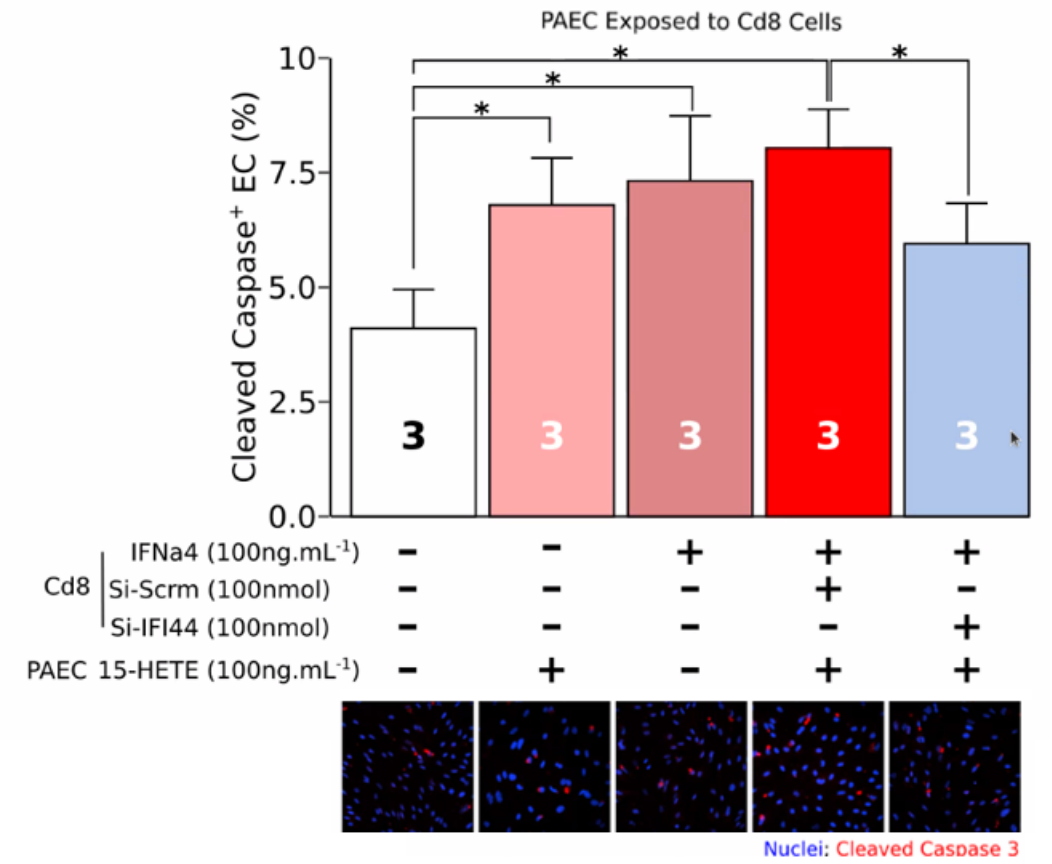

Figure 25: IFNα4 treatment of CD8 cells induces IFI44 expression and Silencing IFI44 in CD8 cells decreases endothelial cell apoptosis *in vitro*. A) qPCR analysis showing exposure of CD8 cells to IFNα4 increases IFI44 expression. B) PAEC cells exposed to CD8 cells exposed to IFNα4, scramble siRNA, siRNA against IFI44, with and without exposure to 15-HETE shows that siRNA administration of IFI44 decreases cell apoptosis (n= 3 experiments).

Table 3: All Canonical Pathways Significantly Changing in 15-HETE and EV Groups

Ingenuity Canonical Pathways	**-log(p-value)**	**z-score**
Phagosome Formation	9.84	n/a
Neuroinflammation Signaling Pathway	9.36	3.157
Atherosclerosis Signaling	8.44	n/a
Agranulocyte Adhesion and Diapedesis	8.34	n/a
Complement System	7.72	1.89
Leukocyte Extravasation Signaling	6.96	3.771
TREM1 Signaling	6.41	3.464
Role of Pattern Recognition Receptors in Recognition of Bacteria and Viruses	6.38	2.714

Role of Macrophages, Fibroblasts and Endothelial Cells in Rheumatoid Arthritis	5.57	n/a
Stearate Biosynthesis I (Animals)	3.09	0
Airway Pathology in Chronic Obstructive Pulmonary Disease	3.08	n/a
Acetone Degradation I (to Methylglyoxal)	3.06	-1.342
Pathogenesis of Multiple Sclerosis	2.91	n/a
LPS/IL-1 Mediated Inhibition of RXR Function	2.76	-0.816
Reelin Signaling in Neurons	2.63	n/a
Clathrin-mediated Endocytosis Signaling	2.6	n/a
HER-2 Signaling in Breast Cancer	2.57	n/a
Nicotine Degradation III	2.54	-1.633
Hepatic Fibrosis / Hepatic Stellate Cell Activation	2.52	n/a
Paxillin Signaling	2.48	n/a
Bupropion Degradation	2.47	-1
Retinol Biosynthesis	2.39	1.342
Role of Hypercytokinemia/hyperchemokinemia in the Pathogenesis of Influenza	2.35	n/a
IL-8 Signaling	2.23	2.887
Melatonin Degradation I	2.22	-1.633
Nicotine Degradation II	2.22	-1.633
Superpathway of Melatonin Degradation	2.06	-1.633
Coagulation System	1.94	0
MIF-mediated Glucocorticoid Regulation	1.94	2
Inhibition of Matrix Metalloproteases	1.78	-2
Estrogen Biosynthesis	1.7	-1
MIF Regulation of Innate Immunity	1.63	2
Eicosanoid Signaling	1.56	n/a
Colorectal Cancer Metastasis Signaling	1.53	2.714
Pancreatic Adenocarcinoma Signaling	1.48	1.342
MSP-RON Signaling Pathway	1.44	n/a
Acute Myeloid Leukemia Signaling	1.41	-0.447
HIF1α Signaling	1.41	n/a
Fatty Acid Activation	1.38	n/a
Mevalonate Pathway I	1.38	n/a
Glioma Invasiveness Signaling	1.36	1.342
Fatty Acid β-oxidation I	1.33	n/a
PPARα/RXRα Activation	1.32	0

Table 4: Primers

Gene	Species	Sense (Forward)	Antisense (Reverse)
IFNα4	Mouse	GCAGAAGTCTGGAGAGCCCTC	TGAGATGCAGTGTTCTGGTCC
IFI44	Mouse	TCACTTTTGTCTCCCTCACCC	AGTCCATTCCCAGTCCTTTCAG
CXCL10	Mouse	CCAAGTGCTGCCGTCATTTTC	GGCTCGCAGGGATGATTTCAA
IFNβ	Mouse	CCAGCTCCAAGAAAGGACGA	CGCCCTGTAGGTGAGGTTGAT
IFNγ	Mouse	AAAGAGATAATCTGGCTCTGC	GCTCTGAGACAATGAACGCT
TRAIL	Mouse	GCCAGCTCTGCTGTTTTGAG	CACCTGGTGGCACTAATGGT
GAPDH	Mouse	AGGTCGGTGTGAACGGATTTG	GGGGTCGTTGATGGCAACA
RPLP0	Mouse	CTCTCGCTTTCTGGAGGGTG	ACGCGCTTGTACCCATTGAT
IFNα4	Rat	TGATGGTTCTGGTGGTGATG	GAGTGTGAAGGCTCTCTTGTT
IFNγ	Rat	CACGCCGCGTCTTGGT	TCTAGGCTTTCAATGAGTGTGCC
IFI44	Rat	AGCCGTATGGAGACCTGG	TGAGTGATGCTGCCCTTG
PPIA	Rat	AGCATACAGGTCCTGGCATC	TTCACCTTCCCAAAGACCAC

Table 5: Antibodies

Protein	Company	Reference
IFI44	Abcam	ab236657
IFNα4	Invitrogen	PA5-97861

Supplemental Figures

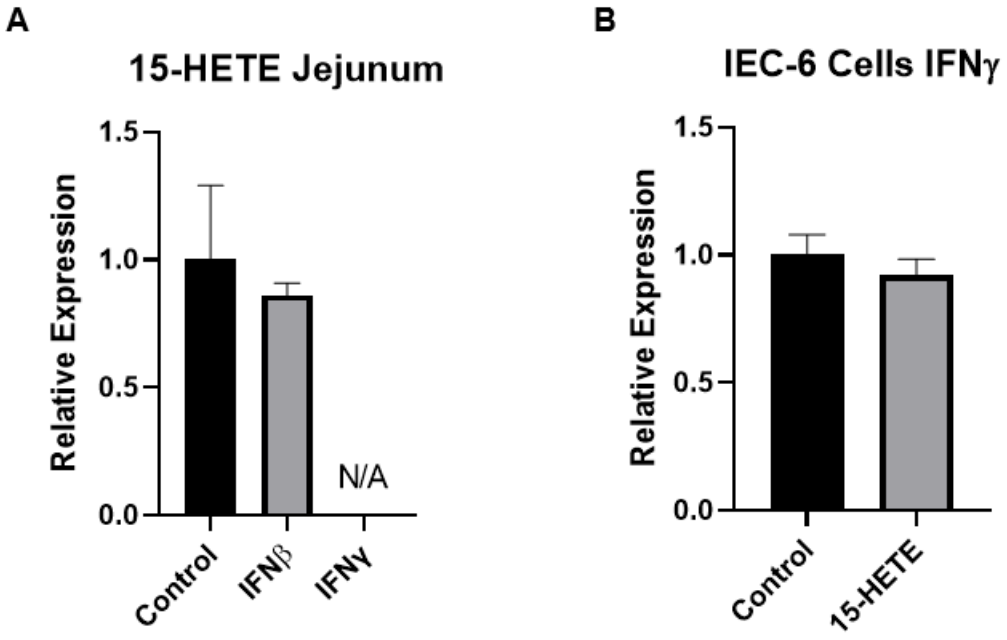

Supplemental Figure 6: qPCR analysis of A) the jejunum of mice fed 15-HETE diet did not have increases IFNβ while IFNγ was not detected, while in B) IEC-6 cells treated with 10μM 15-HETE for 12 hours did not have increases in IFNγ.

CHAPTER 5: 15-HETE, the Microbiota, Short Chain Fatty Acids, and Hypertension

Abbreviations

PAH	Pulmonary Arterial Hypertension
RV	Right Ventricle
PH	Pulmonary Hypertension
15-HETE	15-hydroxyeicosatetraenoic Acid
WT	Wild Type
ApoA-I	Apolipoprotein A-I
Ldlr	Low Density Lipoprotein Receptor
WD	Western Diet
RVSP	Right Ventricle Systolic Pressure
HETE	Hydroxyeicosatetraenoic Acid
HODE	Hydroxyoctadecadienoic Acid
MCT	Monocrotaline
CHP	Chronic Hypoxia
LA	Linoleic Acid
AA	Arachidonic Acid
PAAT	Pulmonary Arterial Acceleration Time
RVSP	Right Ventricle Systolic Pressure
PASMC	Pulmonary Arterial Smooth Muscle Cells
Tg6F	Transgenic Tomatoes Expressing the ApoA-I Mimetic Peptide 6F
SCFA	Short Chain Fatty Acid
LPS	Lipopolysaccharide
LTA	Lipoteichoic Acid
TLR	Toll-like Receptor
BMPR	Bone Morphogenic Protein Receptor Type 2
EV	Empty Vector Tomato
LV	Left Ventricle
IVS	Intraventricular Septum
FITC	Fluorescein Isothiocyanate–Dextran
IFNα4	Interferon Alpha 4
IFI44	Interferon Induced Protein 44
HFD	High Fat Diet

Abstract

Pulmonary arterial hypertension (PAH) is an incurable disease that targets the lungs causing increased mean arterial pressure and right ventricle (RV) hypertrophy leading to death in 50% of patients at 5 years. Our previous work established the connection between oxylipins and pulmonary hypertension (PH) and demonstrated that addition of a pro-inflammatory oxylipin; 15-hydroxyeicosatetraenoic acid (15-HETE) to chow diet for 21 days is sufficient to induce PH in wild type (WT) mice and that an apolipoprotein A-I (apoA-I) mimetic peptide, Tg6F prevents 15-HETE induced PH. Here we continue to utilize our PH model and Tg6F to delineate the molecular mechanisms leading to PH. Microbiota analysis of fecal samples from female mice on a 15-HETE diet showed significant dysbiosis, significantly decreasing the abundance of *Lachnospiraceae*, *Ruminococcaceae*, and *Anaerostipes*, all of which produce the anti-inflammatory short chain fatty acid (SCFA); butyrate, in 15-HETE fed mice. Moreover, together with our collaborators, our laboratory recently reported that low density lipoprotein deficient (*Ldlr-/-*) mice on a western diet (WD) develop PH that is prevented by apoA-I mimetic peptides. Interestingly, microbial analysis demonstrated that *Ldlr*$^{-/-}$ mice on WD also had reduced butyrate producing microbiota which were restored by Tg6F. SCFA measurements showed that the pellets of mice fed the Tg6F diet had elevated levels of acetate, propionate, isobutyrate, and butyrate. We hypothesized that reduction in butyrate producing microbiota, may, in part lead to 15-HETE induced PH and that increased SCFA levels could prevent 15-HETE induced PH. We supplemented WT male mice eating 15-HETE diet with 0.1 M sodium butyrate in their drinking water and found that right ventricle systolic pressure (RVSP) and vascular remodeling decreased

compared with those receiving non supplemented water. Microbiota analysis of mice fed 15-HETE with either Tg6F or sodium butyrate water had increased abundances of butyrate, propionate, and acetate producers, and qPCR analysis shows that Tg6F and butyrate prevent increases in the interferon stimulated gene, interferon stimulated protein 44 (IFI44), shown to be imperative to PH development in Chapter 4, suggesting that SCFAs and the microbiota play an important role, in part *via* the interferon response pathway, in the development of oxylipin mediated PH.

Introduction

PH is a chronic disease affecting the pulmonary vasculature characterized by vascular changes and structural remodeling leading to vasoconstriction of the pulmonary arteries, increased vasculature resistance, right ventricular failure, and in 50% of cases in 5 years' time, death. As discussed in Chapter 1.2, the role of lipids in PH has been studied for years and in recent years those of oxylipins, particularly hydroxyeicosatetraenoic acids (HETEs) and hydroxyoctadecadienoic acids (HODEs) has been investigated after being noted to increase in the lungs and plasma of human PAH patients and in those of multiple animal models of PH including monocrotaline (MCT) injection and chronic hypoxia (CHP).[6] As discussed in Chapter 1.3, utilizing apoA-I mimetic peptides has been successful in multiple disease models including atherosclerosis and cancer in part due to binding to oxylipins and decreasing the levels of HETEs and HODEs in the circulation.[32,35,65] In both MCT and CHP models of PH, apoA-I mimetic peptides were able to decrease levels of HETEs and HODEs while ameliorating PH, further connecting oxylipins to PH.[11]

The diet serves as a source of oxylipins as their precursors linoleic acid (LA) and arachidonic acid (AA) are present in western foods including vegetable oils, meats,

eggs, pizza, bread, and grains.[15,16] Further implicating the role of the diet, *Ldlr-/-* mice on WD have increased levels of HETEs and HODEs in the small intestine and liver.[69] Bringing this finding into the context of PH, Soban et al. showed that *Ldlr-/-* mice on WD for 12 weeks develop PH as evidenced by decreased pulmonary arterial acceleration time (PAAT), increased RVSP, increased RV hypertrophy, and decreased ejection fraction.[91] The use of the apoA-I mimetic peptide 4F prevented the development of PH in *Ldlr-/-* mice, making a case for the diet and possibly the intestine in PH.

HETEs and HODEs are pro-inflammatory lipids related to multiple factors that promote PH including fibrosis, vascular remodeling, pulmonary arterial smooth muscle cell (PASMC) proliferation and resistance to apoptosis, inflammation, vasoconstriction, and angiogenesis.[6] Our lab has demonstrated that oxylipins play a causal role in PH by establishing a model where supplementing the diet with 5 µg of 15-HETE per mouse per day for 21 days is sufficient to cause PH.[11,54] Once again, it has been previously shown that apoA-I mimetic peptides decrease HETEs and HODEs in MCT, CHP, and *Ldlr-/-* mice fed WD, while ameliorating and preventing PH, restoring RVSP.[11] This is also true in the 15-HETE model of PH, where transgenic tomatoes expressing the apoA-I mimetic peptide 6F (Tg6F) prevented and rescued mice from PH by modulating T cell-dependent endothelial apoptosis.[54]

Despite these exciting findings and results, there is still much to learn about how this mechanism leads to PH and how apoA-I mimetics prevent it. Previous work has shown that the dose of apoA-I mimetics and not the peak plasma levels determine efficacy and that feces levels of D-4F were similar regardless of administration, oral or subcutaneous, implicating the intestine as the site of action, however the mechanisms

behind its prevention of PH are still elusive.[170,171] The gut microbiome is known to play a role in metabolism and influence immune cell populations and in recent years has been recognized as a player in gastrointestinal, neurological, cardiovascular, and respiratory illnesses including, but not limited to, obesity, type 2 diabetes, behavioral disorders, and asthma.[44,155,156,160,172] It has also been cited as a key element in the gut lung axis, with changes in bacteria and their metabolites leading to changes in immune cells and metabolites that move to distal organs.[43,158,159] Similarly, Tg6F acts on the intestine to modulate distant targets, evidenced by its ability to reduce tumor burden in mouse models of metastatic lung cancer by changing the immune cell repertoire in the intestine.[65]

In human PAH patients, microbial dysbiosis is being studied and characterized to link changes in the gut to the cascade of changes in the lung resulting in PAH.[50] SU5416/hypoxic rats also had gut dysbiosis, with decreases in butyrate and acetate producing bacteria along with decreased acetate serum levels.[53] As both 15-HETE and Tg6F are administered orally in these mice, both come into direct contact with the gut microbiota. Dietary lipids are capable of modulating the microbiome profile via toxic effects and by acting as substrates for microbial metabolism, thus altering the levels of metabolites produced, resulting in different host phenotypes.[43]

Metabolites produced in the gut include SCFAs. Gram-positive anaerobic bacteria are capable of producing one in particular, butyrate, which has been established to be an anti-inflammatory agent.[46,48] Studies in recent years have found that supplementation with sodium butyrate can ameliorate high-fat diet-induced obesity in mice by modulating the gut microbiota and ameliorating gut microbiota dysbiosis in

Lupus-like mice.[173,174] When examining the microbiota of human PAH patients, butyrate-producing bacteria are more abundant in the reference cohort than in the patients, indicating that there may be a connection between the microbiota and PAH, with the SCFA butyrate serving as the link.[50] However, studies to determine whether SCFAs, including butyrate, can prevent the onset of, or improve, PH have not been conducted. Therefore, in this study I tested the effects of sodium butyrate supplementation on development and prevention of PH utilizing our dietary 15-HETE model.

Materials and Methods

Animals

Female *Ldlr-/-* mice aged 4.8 ± 0.1 months (n = 10 mice per group) were fed the four diets for two weeks and taxonomic composition at the phylum level was determined in the mucus as described in Microbiota analysis. Significance of differences across groups was determined by DESeq2 analysis as described in Statistical Analysis: WD vs. chow; WD vs. empty vector tomato (EV); WD vs. Tg6F; EV vs. Tg6F.

Male and female C57BL/6J mice (Jackson Laboratory) aged 8-12 weeks were fed Envigo/Harland Teklad diet (T.7013M.15 NIH-31 Modified 6% Mouse/Rat Diet) supplemented with 5μg 15(S)-HETE (Cayman Item number 34720) per mouse per day for 21 days to induce PH. Tg6F tomatoes were freeze-dried, powdered, and added to the diet at 2.2% by weight as previously described.[63,65] Sodium butyrate (Cayman) was added to the drinking water at 0.1M and made fresh daily.

PH Assessment

PH progression and development was monitored weekly by noninvasive 2-dimensional Doppler echocardiography using Vevo 2100 (Visualsonics) and at the end

of the protocol, open-chest direct catheterization was performed to assess RV systolic pressure (RVSP) and left ventricular (LV) systolic pressure as previously described.[54] Fulton index was measured by dividing the weight of the RV by the sum of the LV and intraventricular septum (RV/(LV+IVS)).

Microbiota Sampling

Mucosal scrapings of the *Ldlr-/-* mice were prepared by collecting a gelatinous layer on the luminal side of the enterocytes in the jejunum and preparing enterocytes from the same segment of jejunum. Mice were euthanized using isoflurane immediately prior to removing the small intestine. The small intestine was washed twice by flushing gently with ice cold 1X PBS. The duodenum was removed, and the following ~14 cm of jejunum was then carefully opened longitudinally and pinned at the edge of one side using a supportive Styrofoam base. Any residual luminal content was removed (if required) by another gentle wash with1X PBS. The gelatinous mucosal surface was washed with 2 mL of a solution containing 10mM Tris-HCl; pH 7.4 and 5mM CaCl2. The gelatinous mucosal surface was then scraped gently with a Fisherbrand disposable cell lifter (Fisher Scientific Catalog #08-100-240). The gelatinous material was transferred from the cell lifter into a 1.5 mL Eppendorf tube containing 500 µL of Triton Lysis Buffer (50 mM Tris pH 7.5, 100 mM NaCl, 5mM EDTA, 50 mM Na-orthovanadate, 1% Triton X-100, and a protease inhibitor tablet [Sigma-Aldrich and Catalogue #04693159001], and was centrifuged for 10 minutes at 13,000 rpm to remove debris. The supernatant was transferred to another tube and centrifuged again for 10 minutes at 13,000 rpm. This supernatant was transferred to a new tube, and protein content was determined using

Bradford reagent; absorbance was measured at 595 nm before storing the samples at -20°C.

Fecal samplings of the female C57BL/6J mice that were euthanized using isoflurane immediately prior to removing the small intestine were collected by scraping fecal contents out of the isolated intestine, flushing it with 1mL of DNase/RNase free water (Invitrogen™, 10977015), and collecting in a 1.5 mL tube, briefly vortexing the contents, centrifuging the tubes at 10,000 rpm for 10 minutes, and separating the supernatant from the fecal pellet.

Fecal samplings of the male C57BL/6J for microbiota analysis and SCFA measurements were obtained by collecting noninvasive samplings of fresh fecal pellets from each mouse on a weekly basis and storing them in -80°C until needed for analysis.

Microbiota Analysis

Microbiome analysis was conducted by the UCLA Microbiome Core. DNA extraction and sequencing of the 16S ribosomal RNA gene was performed for mouse fecal samples as previously described.[175] In brief, bacterial DNA was extracted using the ZymoBIOMICS DNA kit (cat#D4300) with bead beating. The V4 region of the 16S gene was amplified and barcoded using 515f/806r primers then 250x2 bp sequencing was performed on an Illumina Miseq system. Raw data were processed using DADA2 scripts in R platform and quality-filtered reads (~115002 average reads per sample) were used to identify amplicon sequence variants (ASV) by closed reference picking against the Silva database.[176]

The fastq files for the 15-HETE female fecal samples have been uploaded to PubMed under the BioProject ID: PRJNA757837 https://www.ncbi.nlm.nih.gov/bioproject/PRJNA757837

The fastq files for the *Ldlr*$^{-/-}$ mucosal scrapings have been uploaded to PubMed under the BioProject ID: PRJNA757839 https://www.ncbi.nlm.nih.gov/bioproject/PRJNA757839

The fastq files for the time course analysis of mice fed chow, 15-HETE, and 15-HETE+Tg6F diets have been uploaded to PubMed under the BioProject ID: PRJNA757467 https://www.ncbi.nlm.nih.gov/bioproject/PRJNA757467

Statistical Analyses

For the microbiome, alpha diversity metrics included Faith's phylogenetic diversity (Faith's PD) metric, Chao1, and Shannon index. The significance of differences in alpha diversity was calculated by T-tests and non-parametric Wilcoxon signed rank test. Beta diversity was calculated using square root Jensen-Shannon divergence and visualized by principal coordinates analysis. Association of microbial genera with knockout mice were evaluated using DESeq2 in R, which employs an empirical Bayesian approach to shrink dispersion and fit non-rarified count data to a negative binomial model [doi:10.1186/s13059-014-0550-8.]. P-values for differential abundance were converted to q-values to correct for multiple hypothesis testing (< 0.05 for significance).[177]

Histology and imaging

Lungs were embedded in OCT and flash frozen for histological analysis. OCT-embedded lungs were sectioned at 5μm. Vascular wall thickness was calculated from

H&E staining by determining the mean distance between the lamina elastica externa and lumen in two perpendicular directions of transversally cut vessels (<100µm). 10 randomly selected arteries were measured per animal in a minimum of 8 mice per group. Images were taken using an inverted microscope (Leica Dmi8).

Short Chain Fatty Acid Measurement

SCFAs were measured in non-invasively collected fecal pellets via gas chromatography by the Center for Human Nutrition according to a protocol described previously.[172]

Real-Time PCR

Total RNA from lungs was isolated with Trizol extraction method and reverse transcribed with poly dT primers using the Omniscript reverse transcription kit (Qiagen, Cat#205113). Real-time PCR was performed on polyA+ cDNA with specific primers (Table 6) using iTaq Universal SYBR® (BioRad, Cat#1725121).

Total RNA from the intestine was isolated with miRvana kit while RNA from the cells was isolated using RNeasy kit (Qiagen#74004) and reverse transcribed using the BioRad iScript Reverse Transcription Supermix (Cat#1708841). Real-time PCR was performed on polyA+cDNA with specific primers (Table 6) using iQ™ SYBR® Green Supermix (BioRad, Cat#1708882).

Barrier Permeability Analysis

Barrier permeability was assessed via measurement of fluorescein isothiocyanate conjugated dextran (FITC-dextran) (Sigma-Aldrich, FD4) in the serum of mice 4 hours after being gavaged with FITC-dextran at a dose of 44 mg/100g body weight as described previously.[178] FITC measurements were conducted on a weekly basis in C57BL/6 mice

eating chow and 15-HETE diets. Fluorescence was read using a BMG Labtech, FLUOstar Omega plate reader.

Results

Ldlr-/- mice fed WD and 15-HETE fed mice have decreased abundances of butyrate-producing bacteria which are restored in Ldlr-/- mice fed WD by Tg6F

Female *Ldlr-/-* mice fed WD for two weeks have decreased abundances of butyrate producing bacteria, *Lachnospiraceae* and *Ruminococcaceae*, compared to chow fed mice while *Ldlr-/-* mice fed WD and Tg6F had increased abundances of *Ruminococcaceae* and *Lachnospiraceae* (**Figure 26A and 26B**). Similarly, female WT mice fed 15-HETE diet for three weeks had decreased abundances of the butyrate-producing bacteria *Ruminoccocaceae*, *Lachnospiraceae*, and *Anerostipes* (**Figure 26C**).

Tg6F increases fecal pellet levels of SCFAs

To investigate how changes in the microbiota affected SCFA production levels, I measured SCFA in the fecal pellets of control, 15-HETE, and Tg6F fed mice. The results showed that Tg6F mice had higher levels SCFAs, specifically propionate, isobutyrate, and butyrate compared to control and 15-HETE fed mice (**Figure 27A and 27B**), implying that the effects of 15-HETE and Tg6F go beyond the production of butyrate.

Supplementation of drinking water with 0.1 M sodium butyrate prevents and rescues dietary 15-HETE induced PH

Mice fed 15-HETE diet and sodium butyrate in the drinking water at 0.1 M had significantly lower RVSPs than those only on the 15-HETE diet and did not develop PH,

similar to mice fed both 15-HETE diet with Tg6F (**Figure 28A and 28B**). This was true of mice who drank sodium butyrate through the entire 21-day protocol as well as in mice who received 15-HETE diet for 14 days before adding sodium butyrate in the final week of feeding, showing that it can both protect against and rescue mice from 15-HETE induced PH.

Addition of Tg6F or sodium butyrate to the 15-HETE diet increases the abundances of SCFA producing bacteria

Microbiota analysis of mice on chow, 15-HETE, Tg6F, or sodium butyrate supplemented diets for three weeks significantly altered microbiome compositions starting at week 1 that continued through weeks 2 and 3 (**Supplemental Figure 9**). At week 2, 15-HETE fed mice had significantly decreased abundances of *Acetatifactor* and *Lachnospiracea_A2*, both of which produce butyrate (**Figure 29A**). Analysis of the microbiomes at week 3 showed significant increases in multiple genera that produce SCFAs, *Ruminococcaceae_ucg-10*, *Ruminococcaceae_ucg-005*, and *Ruminococcaceae_nk4A214*, increased only in Tg6F fed mice while *Ruminococcaceae_ucg-014*, *Bacteroides*, and *Lachnoclostridium* increased between in both Tg6F and sodium butyrate fed mice (**Figure 29B**). These genera produce not only butyrate, but propionate and acetate as well, explaining the SCFA increases seen in Figure 27.[179]

The apoA-I mimetic peptide Tg6F prevents increases of IFNα4 and IFI44 in the intestines of 15-HETE mice

Investigating a potential mechanism for SCFAs in the prevention of 15-HETE induced PH, I conducted qPCR analysis that showed that interferon alpha 4 (IFNα4)

increases in the 15-HETE and empty vector tomato (EV) fed mice which is accompanied by increases in IFI44 expression in these same groups (trending in 15-HETE, p=0.055) and significantly in the EV group (**Figure 30A and 30B**).

Sodium butyrate supplementation decreases IFI44 expression in the intestine and the lungs

Exploring whether butyrate supplementation has similar effects on the intestine and lungs as Tg6F, qPCR analysis showed that IFNα4 is trending towards increase in the 15-HETE and sodium butyrate prevention groups, however, IFI44 expression is only significantly increased in the jejunum of mice fed 15-HETE diet but is not increased in the jejunum of mice on the Tg6F or either of the sodium butyrate treatment groups (**Figure 31A and 31B**). QPCR analysis in the lungs showed that IFI44 is trending towards significant increase in the lungs while Tg6F and sodium butyrate groups do not change significantly with respect to control and are to a lesser degree than 15-HETE (**Figure 32**).

Discussion

Utilizing our novel dietary model of PH in WT mice, we have found a connection between the microbiota and development of PH. Interestingly, the changes in microbiota of WT mice fed 15-HETE were similar to that of *Ldlr-/-* mice fed WD, which, like the WT mice on 15-HETE supplemented diet, develop hypertension that is prevented with the addition of apoA-I mimetic peptides.[54,91] In both experimental models of PH, abundance levels of *Lachnospiraceae*, *Ruminococcaceae*, and *Anaerostipes* are decreased by WD and 15-HETE diet and are restored in diets including Tg6F (**Figure 26**). These species of bacteria are known producers of the SCFA butyrate, which is a known to have anti-inflammatory properties.[46,47,180] Bacteria

have a history and reputation for causing illness typically by components of the cell wall, namely lipopolysaccharide (LPS), or endotoxin in the cell walls of gram negative bacteria, and lipoteichoic acid (LTA), which is specific to gram positive bacteria.[181] As mentioned earlier, SCFA producing bacteria are gram positive and therefore does not possess LPS.[46,48] LPS plays a role in causing systemic inflammation when gut permeability changes in response to factors such as weight gain, high fat diet, and increased exposure to fatty acids as it enters the circulation and activates immune responses via toll like receptors (TLRs).[43,46,87,156,173] Chronic administration of LPS has been reported to induce PH in bone morphogenic protein receptor type 2, $Bmpr2^{+/-}$, mice.[182] LTA acts similarly to LPS, having pro-inflammatory responses through activation of TLRs, reportedly leading to inflammatory diseases including colitis.[181,183] However, dietary 15-HETE does not change barrier permeability as we have determined via serum measurement of fluorescein isothiocyanate–dextran (FITC) 4 hours after gavaging mice with FITC once a week while on the 15-HETE diet (**Supplemental Figure 7**).

Measurements of fecal pellets of control, 15-HETE, and Tg6F fed mice show that Tg6F had significantly higher SCFA levels overall (**Figure 27**). This also included higher levels of acetate, propionate, isobutyrate, as well as butyrate. Acetate and propionate, like butyrate, are also anti-inflammatory agents, decreasing LPS-stimulated TNFα release from neutrophils, decreasing NF-κB reporter in human colon cells, and suppressed IL-6 protein release from organ cultures with similar efficacies as butyrate.[47] There are also many studies showing that supplementation with sodium butyrate has beneficial effects in other disease models. For example, butyrate prevented damage to

the liver in a rat model of sepsis, alleviated lung injury in a mouse model of sepsis, pretreatment with sodium butyrate reduced infarct size in a model of myocardial ischemia and reperfusion in rats, and improved mucosa lesions and attenuated the inflammatory profile of intestinal mucosa and lymph nodes in a model of dextran sulfate sodium-induced colitis.[46] WT mice on high fat diet (HFD) given 0.1 M sodium butyrate in their drinking water had reduced weight gain, inflammation and cytokine levels, and intestinal barrier integrity compared to those only on HFD.[173]

Sodium butyrate supplementation also altered the microbiota composition, making it resemble mice fed a low fat diet more than the HFD, increasing relative abundances of *Coprococcus*, *Lachnospiraceae*, *Ruminococcus*, *Bifidobacteriaceae*, and *Actinobacteria*, the first three being butyrate-producing bacteria.[173,184] Therefore, we sought to determine whether butyrate supplementation can prevent onset of PH. Three weeks of feeding mice 15-HETE supplemented diet and 0.1 M sodium butyrate in drinking water showed that butyrate prevented the development of PH (**Figure 28**). Equally as interesting, just one week of sodium butyrate supplementation following two weeks of just 15-HETE diet, when PAAT is significantly different from chow-fed mice, also led to improved RVSPs compared to the 15-HETE fed mice who drank normal water all three weeks.

These results show that improving both the composition of the microbiota to favor SCFA producers and direct supplementation with SCFAs to counteract the dysbiosis and SCFA decreases seen in PAH patients and Sugen/hypoxic rats can be potential approaches to PAH therapies.[42,53] Microbiota analysis of mice on chow, 15-HETE, Tg6F, and sodium butyrate diets showed that after 2 weeks of 15-HETE diet,

Acetatifactor and *Lachnospiraceae_A2* decrease in abundance while Tg6F and sodium butyrate treatments increased the abundances of SCFA producers at the end of the 3 week protocol (**Figure 29**). *Acetatifactor* is part of the *Lachnospiraceae* family and has been reported to produce acetate and butyrate.[185] While it is interesting to note that decreases in 15-HETE fed mice were not observed in the males at week 3 compared to the *Ldlr-/-* females on WD or the females on the 15-HETE diet, it is worth nothing that the fecal samples for the four groups of males were collected noninvasively, while the others were scraped mucosa samples or collected directly from the intestine, which is more of a direct representation of the small intestine, may represent a different niche, and probably contribute to the variability in results, especially in the two groups fed 15-HETE diet.[186] However, across all three groups, modulations in SCFA producers were still evident. Genera of *Ruminococcaceae* were shown to decrease in female *Ldlr-/-* mice on WD and female WT mice on the 15-HETE diet and here we see that Tg6F and sodium butyrate supplementation increases abundances of *Ruminococcaceae_ucg-10*, *Ruminococcaceae_ucg-005*, and *Ruminococcaceae_nk4A214*, which are butyrate producers, *Ruminococcaceae_ucg-10* and *Ruminococcaceae_nk4A214* having been noted to increase in normotensive patients when compared with hypertensive patients in a cross-sectional study.[187] *Lachnoclostridium*, while not changed in the *Ldlr-/-* or 15-HETE fed female mice, is another butyrate-producer.[179] Bacteroides also increase in both Tg6F and butyrate supplemented mice and is a preferred propionate producer that is also capable of producing acetate, likely contributing to the increased levels of both observed in the fecal pellets of Tg6F fed mice.[188]

Although SCFA supplementation has not been tested in the classic animal models of PH such as MCT, CHP, and Sugen/hypoxia, there are some studies noting that targeting the gut and SCFAs can help with hypertension. In male C57Bl/6 mice that received a slow release deoxycorticosterone acetate pellet to induce hypertension, both high fiber diets and acetate supplementation decreased gut dysbiosis, reduced systolic and diastolic blood pressure, cardiac fibrosis, and left ventricle hypertrophy.[189] Similarly, prebiotics, probiotics, and acetate supplementation were able to prevent hypertension in a rat model of obstructive sleep apnea.[190]

These results, in addition to the results seen here, are exciting as they show focusing on increasing the levels of SCFAs by direct supplementation and by decreasing gut dysbiosis to support SCFA producing bacteria, both of which can be achieved through available supplements, probiotics, and even moderate consumption of beer[191], can be effective preventative or therapeutic strategies against PAH.

Recent studies have discovered that butyrate's anti-inflammatory properties may, in part, be linked to its ability to modulate the expression of interferon stimulated genes (ISG) and reprogram the immune response of type I interferons (IFNs).[49] In Chapter 4 I discussed the importance of the ISG interferon induced protein 44 (IFI44) in the development of PH in 15-HETE fed mice and we investigated whether that is being modulated by SCFAs in the Tg6F and sodium butyrate treatment groups. Analysis of the intestines of mice on chow,15-HETE, Tg6F, and EV qPCR analysis shows that intestinal levels of interferon alpha 4 (IFNα4) are increased in 15-HETE and EV mice but not in the Control or Tg6F mice (**Figure 30A**). Similarly, IFI44 is trending towards significantly increasing in the 15-HETE group, is significantly increasing in the EV group,

but not in the control or Tg6F mice (**Figure 30B**). In the supplemental sodium butyrate experiments, this holds true in the intestine and lung where IFI44 is elevated by the 15-HETE diet but suppressed in by the Tg6F diet, where SCFA levels are elevated, and in the sodium butyrate supplemented groups, regardless of IFNα4 levels (**Figure 30 and 31**). Trending increases were observed the lungs of 15-HETE fed mice while lower and nonsignificant changes in IFI44 were observed in Tg6F and sodium butyrate supplemented mice (**Figure 32**). As stated in, Chapter 4, increases of IFI44 were observed not only in the lungs and intestines of 15-HETE fed mice, but also the lungs of PAH patients. Knocking down IFI44 in the lungs of mice using siRNA was able to prevent onset of PH by 15-HETE, which is being replicated here by increases in butyrate levels Tg6F and by sodium butyrate supplementation. I also noted in Chapter 4 that IFI44 expression increased in the intestine before the lungs, however, supplementation with sodium butyrate at the start of the 21-day protocol and only during the last seven days of the protocol resulted in lower RVSPs. As IFI44 levels are lower in the intestine and lungs in both sodium butyrate supplementation groups, this could mean that blocking the signaling at the intestine can quickly shut down signaling to the lung or that the excess sodium butyrate is entering the circulation and is acting on the lung directly. Further studies would be needed to determine this and SCFA analysis of the plasma for these groups would be needed as well.

Conclusions

- Microbiota analysis of female WT mice on the 15-HETE diet showed decreases in bacteria species that produce the SCFA, butyrate

- Similar decreases are seen in *Ldlr$^{-/-}$ mice*, who when fed WD for 12 weeks, also develop PH and can have PH prevented with the intervention of ApoA-I mimetic peptides
- Compared with mice on Control and 15-HETE diets, mice on the Tg6F diet had increased levels of SCFAs including propionate, isobutyrate, and butyrate
- Supplementation of drinking water with 0.1 M sodium butyrate prevented and rescued mice fed the 15-HETE diet from PH
- Microbiota composition changes as early as 1 week into the 15-HETE diet and by week three both Tg6F and butyrate mice had increases in SCFA producing bacteria
- Tg6F and supplemental Butyrate may modulate PH by decreasing IFI44 levels in the intestine and lungs of mice on 15-HETE diet (**Figure 33**)

Figures

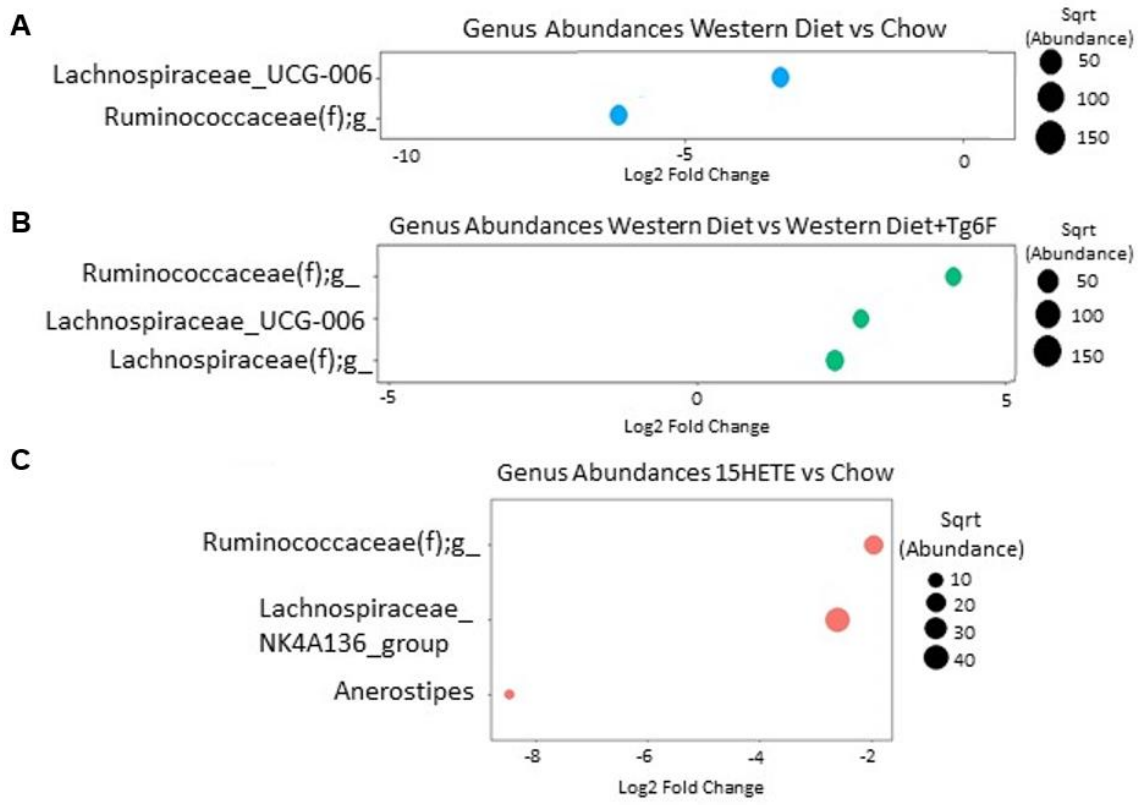

Figure 26: Decrease in abundance of butyrate-producing bacteria observed in two dietary models of PH in mice that is prevented by Tg6F A) *Ldlr-/-* KO mice on Western Diet and Wild type mice on 15-HETE diet have decreased abundances of butyrate producers that are protected by the B) ApoA-I mimetic peptide Tg6F (n=10 per group). Similarly, C) female mice on the 15-HETE diet have decreased abundances of butyrate producers (n=8 per group).

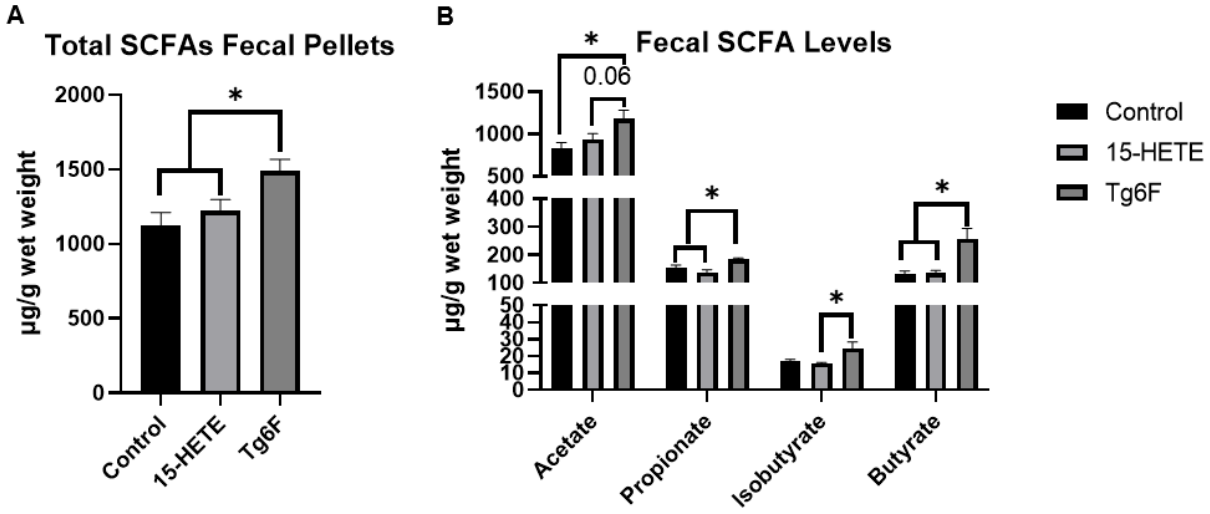

Figure 27: SCFA level changes in mouse fecal pellets from Control, 15-HETE and Tg6F diets A) total SCFA levels significantly increase in mice fed Tg6F diet (n=8 per group). B) SCFA analysis of individual SCFAs show that Acetate, Propionate, Isobutyrate, and Butyrate increase in mice on Tg6F diet.

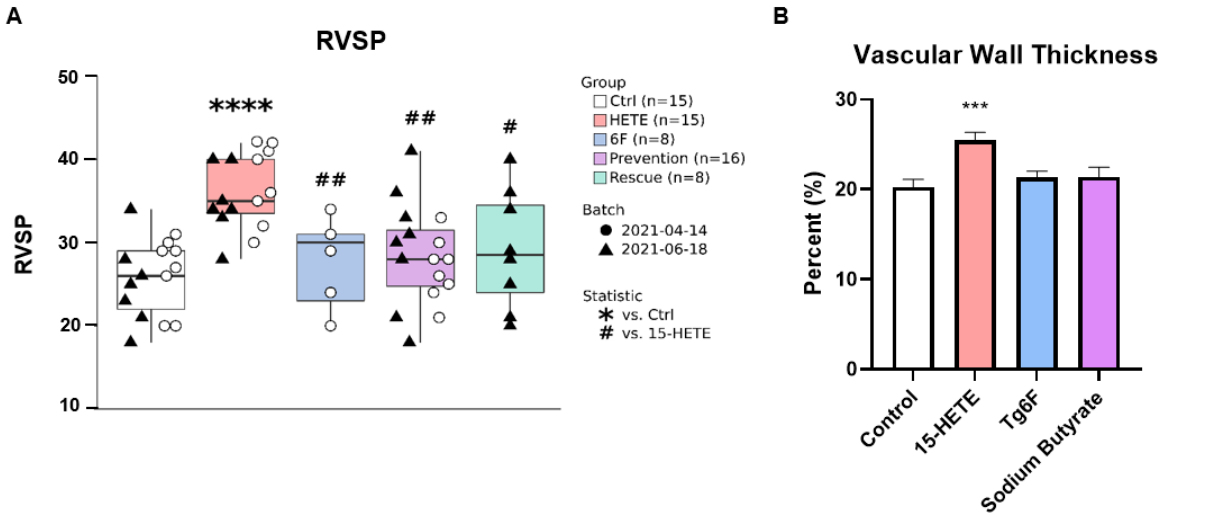

Figure 28: Mice on 15-HETE diet with Sodium Butyrate in their drinking water do not develop PH when concurrently administered with 15-HETE and when administered after 2 weeks of 15-HETE diet. A) RVSP measurements of mice on chow, 15-HETE, Tg6F, Sodium Butyrate Prevention, and Sodium Butyrate Rescue diets. B) Vascular remodeling measurements of mice on the 5 diets (n=8 animals).

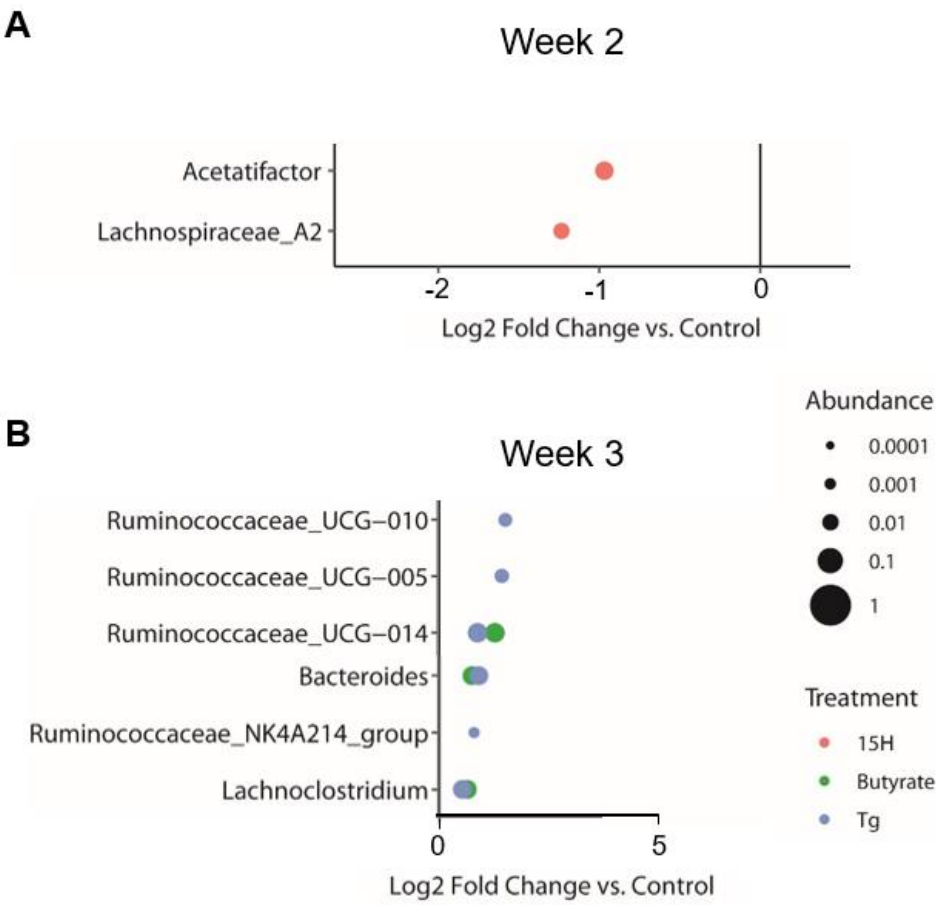

Figure 29: Abundances of SCFA-producers decreased by 15-HETE increased by Tg6F and Sodium Butyrate addition to 15-HETE diet. The treatment groups were compared to controls at weeks A) 2 and B) 3 (n=8 per group). Plot shows genera with q<0.05 in DESEQ2 models. Each dot represents one genus, with dot color indicating which of the three comparisons is shown and dot size representing genus abundance. Magnitude of difference is shown as the log2 of the fold change compared to controls.

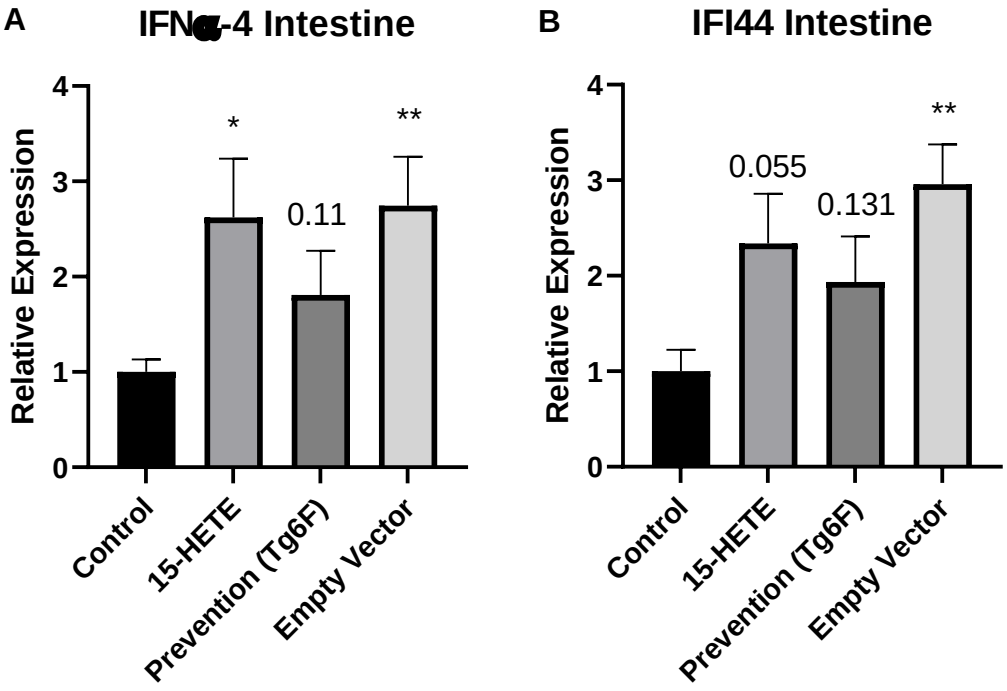

Figure 30: IFNα4 and IFI44 both increase in intestines of mice fed 15-HETE diet which is decreased by Tg6F. qPCR measurement of expression of IFNα4 and IFI44 in the intestines of 15-HETE fed mice (n=8 per group)

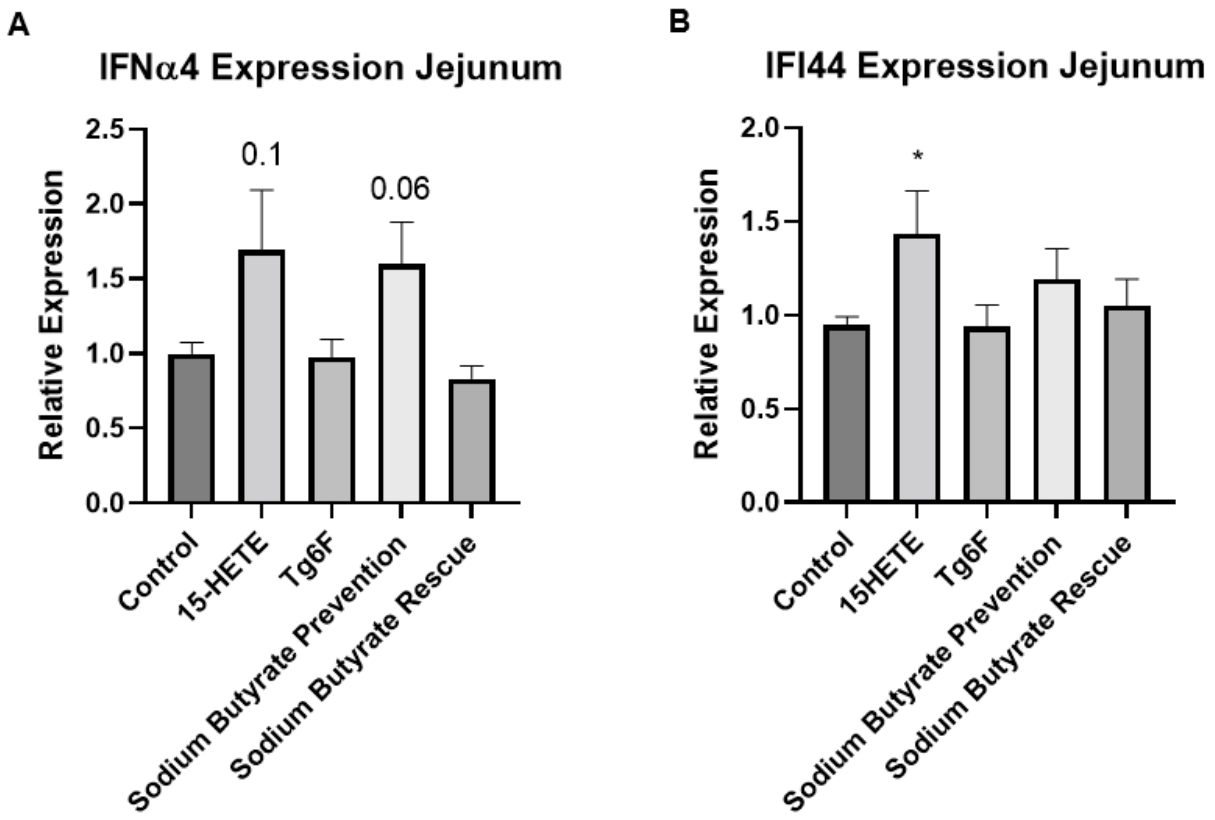

Figure 31: Sodium Butyrate does not consistently modulate levels of IFNα4 in the intestine but modulates IFI44 levels A) IFNα4 expression in the jejunum of mice on control, 15-HETE, Tg6F, Sodium Butyrate Prevention, and Sodium Butyrate Rescue diets (n=16 for all groups except Rescue n=8). B) IFI44 expression in the jejunum of mice on control, 15-HETE, Tg6F, Sodium Butyrate Prevention, and Sodium Butyrate Rescue diets.

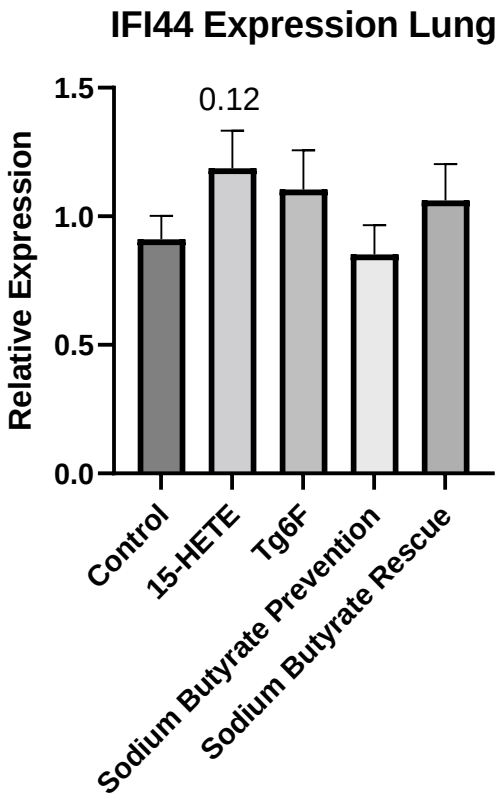

Figure 32: Sodium butyrate decreases IFI44 expression in the lungs. IFI44 expression in the lungs of mice on control, 15-HETE, Tg6F, Sodium Butyrate Prevention, and Sodium Butyrate Rescue diets.

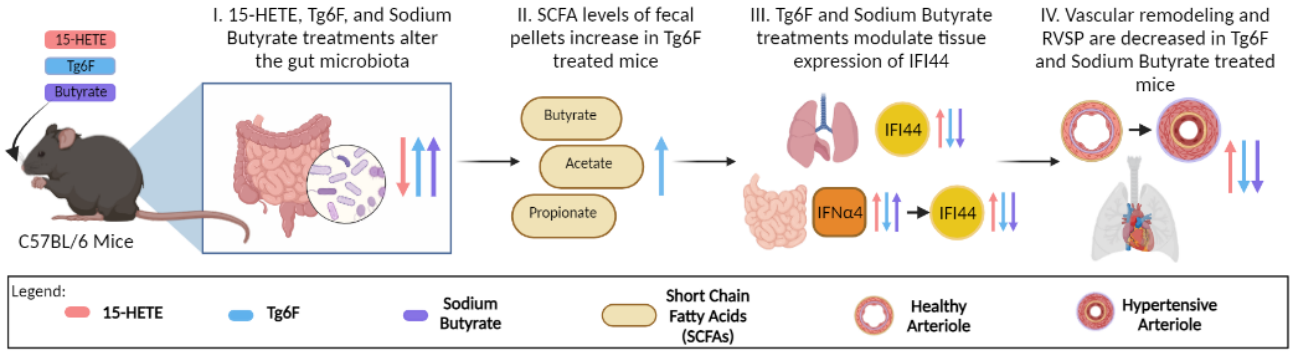

Figure made using BioRender

Figure 33: 15-Hydroxyeicosatetraenoic acid (15-HETE) diet (pink) decreases the abundance of butyrate producing bacteria in the gut, increases intestinal expression of IFNα4 and IFI44, lung expression of IFI44, resulting in vascular remodeling and increased right ventricle systolic pressure (RVSP). Tg6F treatment (blue) increases the

abundance of butyrate producing bacteria and fecal pellet levels of SCFA, which is representative of gut levels of SCFAs, while decreasing expression of IFNα4 and IFI44 in the intestine and lung. Similarly, supplementation of drinking water with 0.1M Sodium Butyrate (purple) increased abundances of SCFA producing bacteria and decreased IFI44 expression in the intestine and lungs, preventing vascular remodeling and increased RVSP.

Table 6: Primers

Gene	Species	Sense (Forward)	Antisense (Reverse)
IFNα4	Mouse	GCAGAAGTCTGGAGAGCCCTC	TGAGATGCAGTGTTCTGGTCC
IFI44	Mouse	TCACTTTTGTCTCCCTCACCC	AGTCCATTCCCAGTCCTTTCAG
GAPDH	Mouse	AGGTCGGTGTGAACGGATTTG	GGGGTCGTTGATGGCAACA
RPLP0	Mouse	CTCTCGCTTTCTGGAGGGTG	ACGCGCTTGTACCCATTGAT
IFNα4	Rat	TGATGGTTCTGGTGGTGATG	GAGTGTGAAGGCTCTCTTGTT
IFI44	Rat	AGCCGTATGGAGACCTGG	TGAGTGATGCTGCCCTTG
PPIA	Rat	AGCATACAGGTCCTGGCATC	TTCACCTTCCCAAAGACCAC

Supplemental Figures

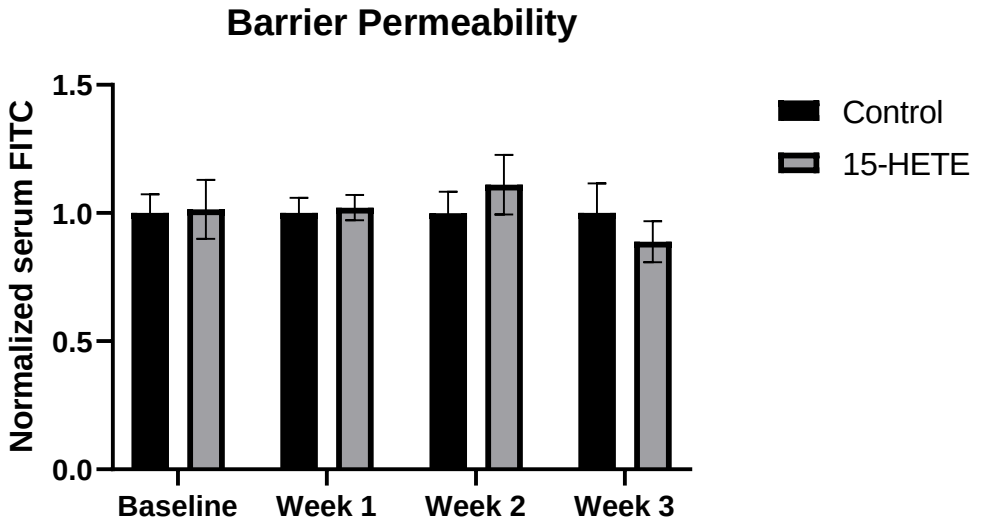

Supplemental Figure 7: On a weekly basis, mice fed chow and 15-HETE diets (n=8 per group) were gavaged with Fluorescein isothiocyanate–dextran (FITC) at 44 mg/100g body weight collecting serum via eye bleed and measuring fluorescence 4 hours later. No change in fluorescence was detected between the two groups.

A

DESeq2 Plot showing significant genus abundances in WD vs Chow (controlled for batch)

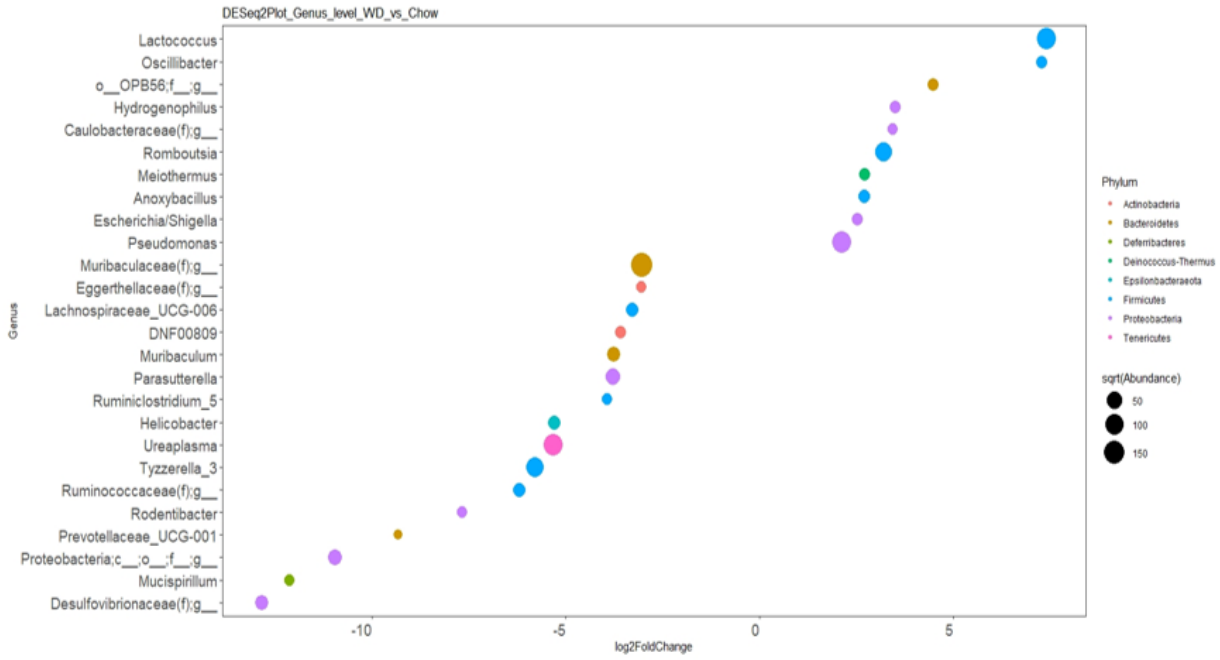

B

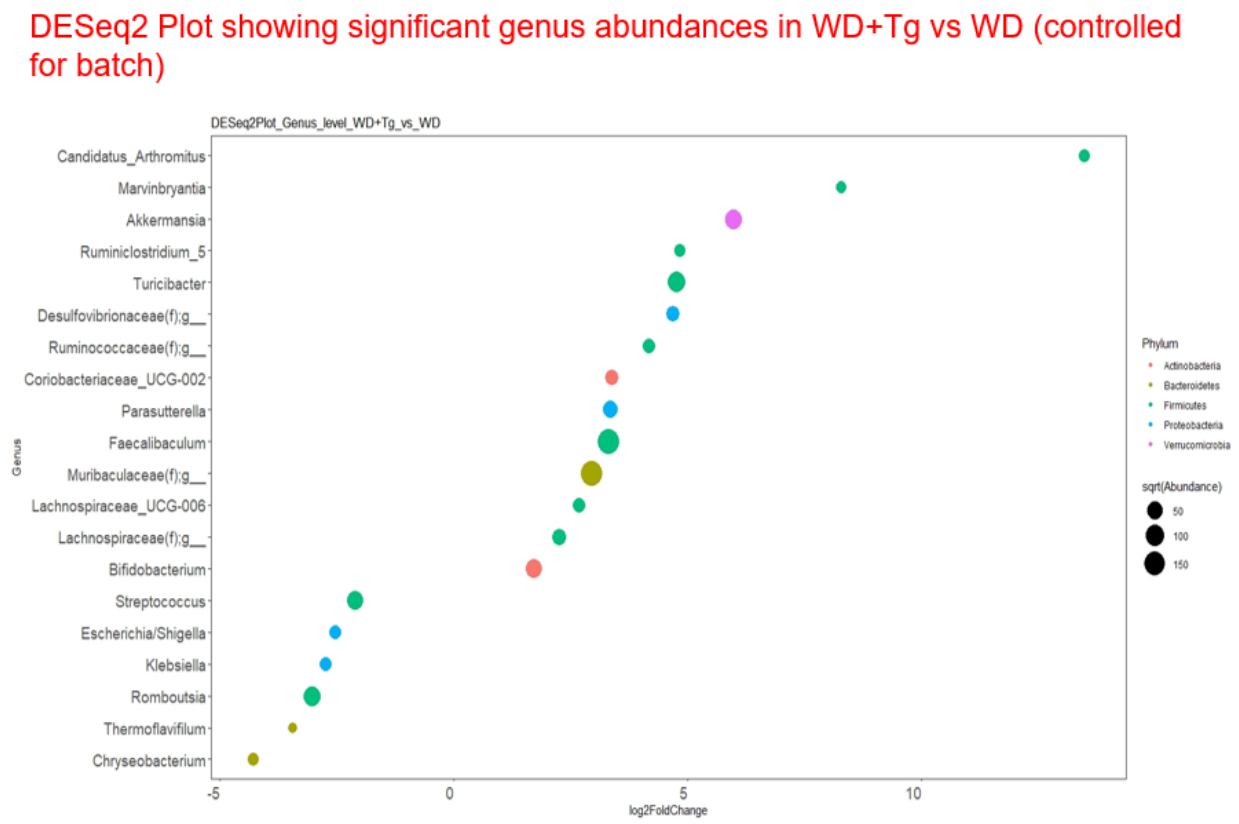

C

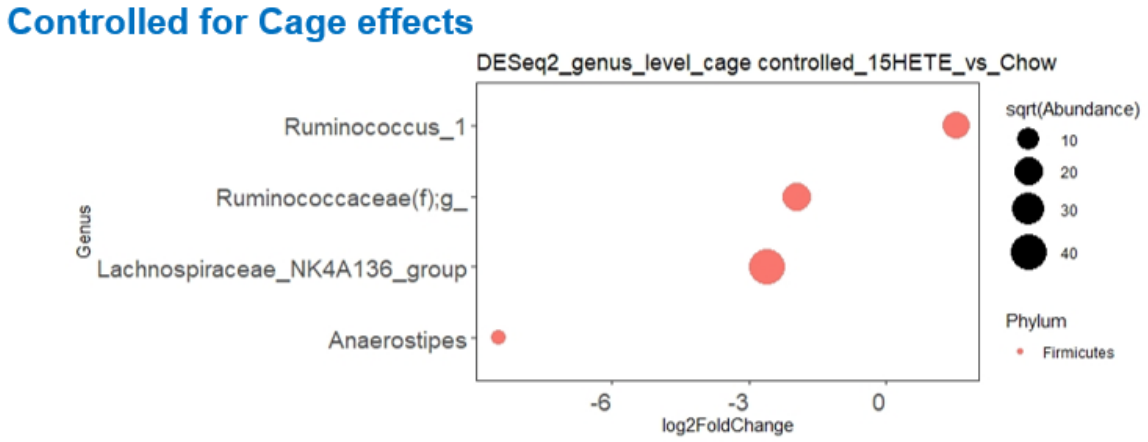

Supplemental Figure 8: Significant changing bacteria genera in A) Ldlr-/- mice on WD B) Ldlr-/- mice on WD+Tg6F, and C) mice on 15-HETE diet. Plot shows genera with q<0.05 in DESEQ2 models. Each dot represents one genus, with dot color indicating

which of the treatments is shown and dot size representing genus abundance. Magnitude of difference is shown as the log2 of the fold change compared to controls.

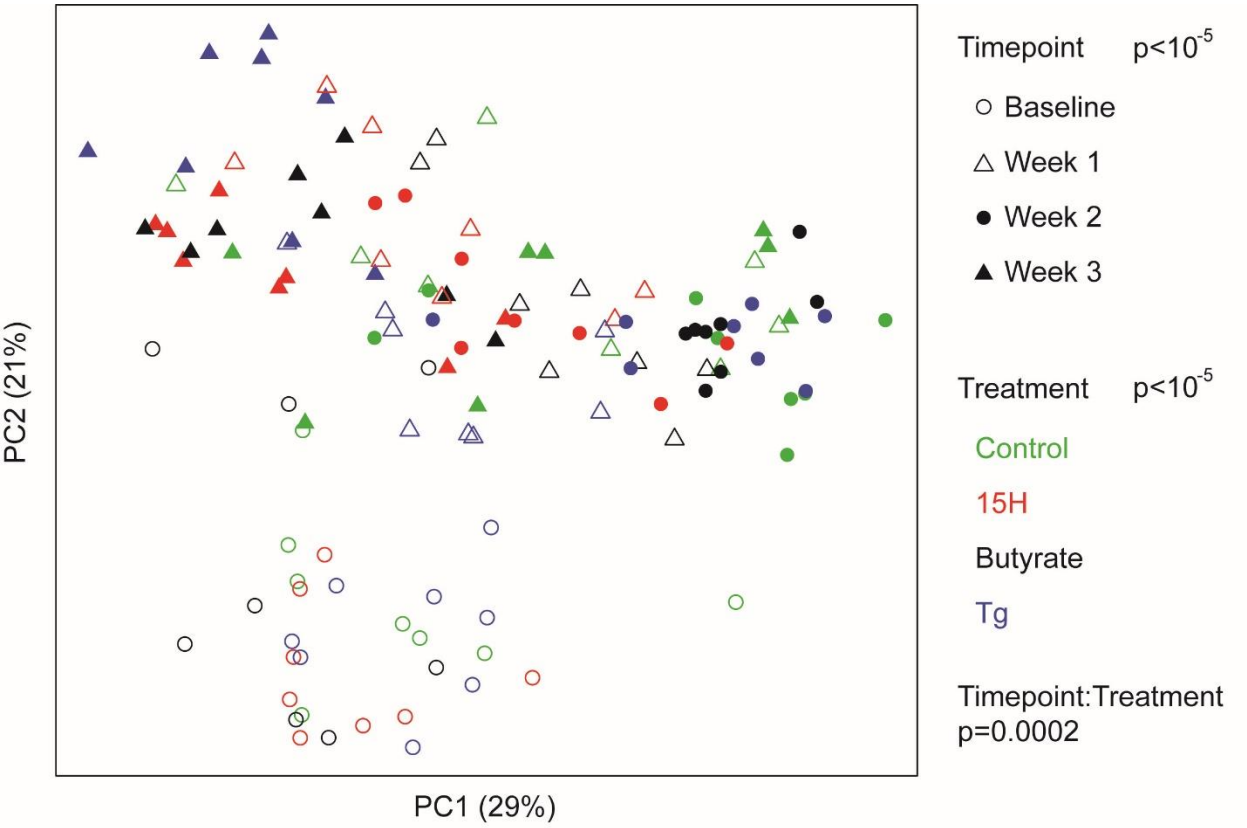

Supplemental Figure 9: Microbiome composition shifted markedly at week 1 for all four treatment groups, with subsequent changes at week 2 and week 3 that varied by treatment group. Beta diversity analysis was performed using Bray-Curtis dissimilarity and visualized by principal coordinates analysis. Each dot represents one sample, colored by treatment group and with shape representing time point. P-values calculated by PERMANOVA model with time point, treatment group, and their interaction as implemented in the Adonis function of the R package, vegan. Permutations were stratified by cage to account for cage effects.

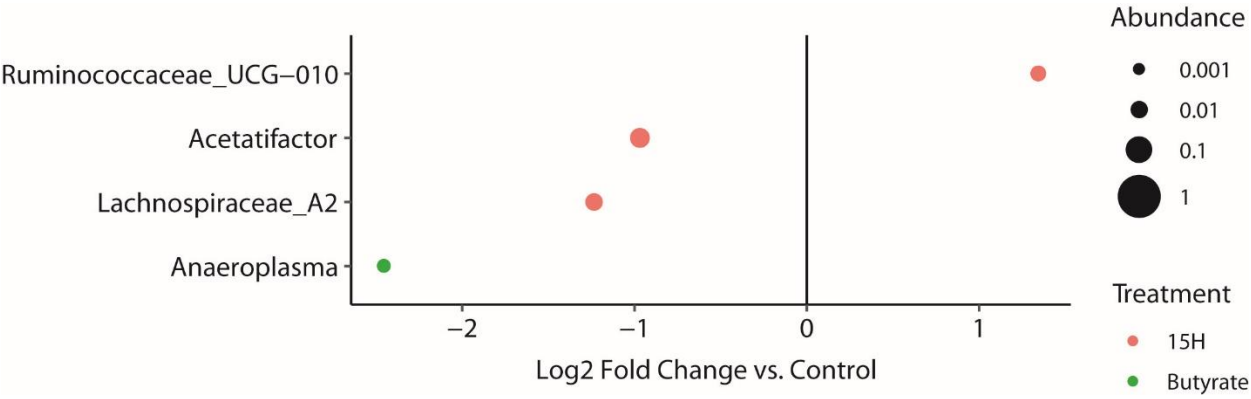

Supplemental Figure 10. Differential genera in the 15-HETE, Tg6F, and sodium butyrate groups after 2 weeks of treatments. The three treatment groups were compared to controls at week 2. Plot shows genera with q<0.05 in DESEQ2 models. Each dot represents one genus, with dot color indicating which of the three comparisons is shown and dot size representing genus abundance. Magnitude of difference is shown as the log2 of the fold change compared to controls.

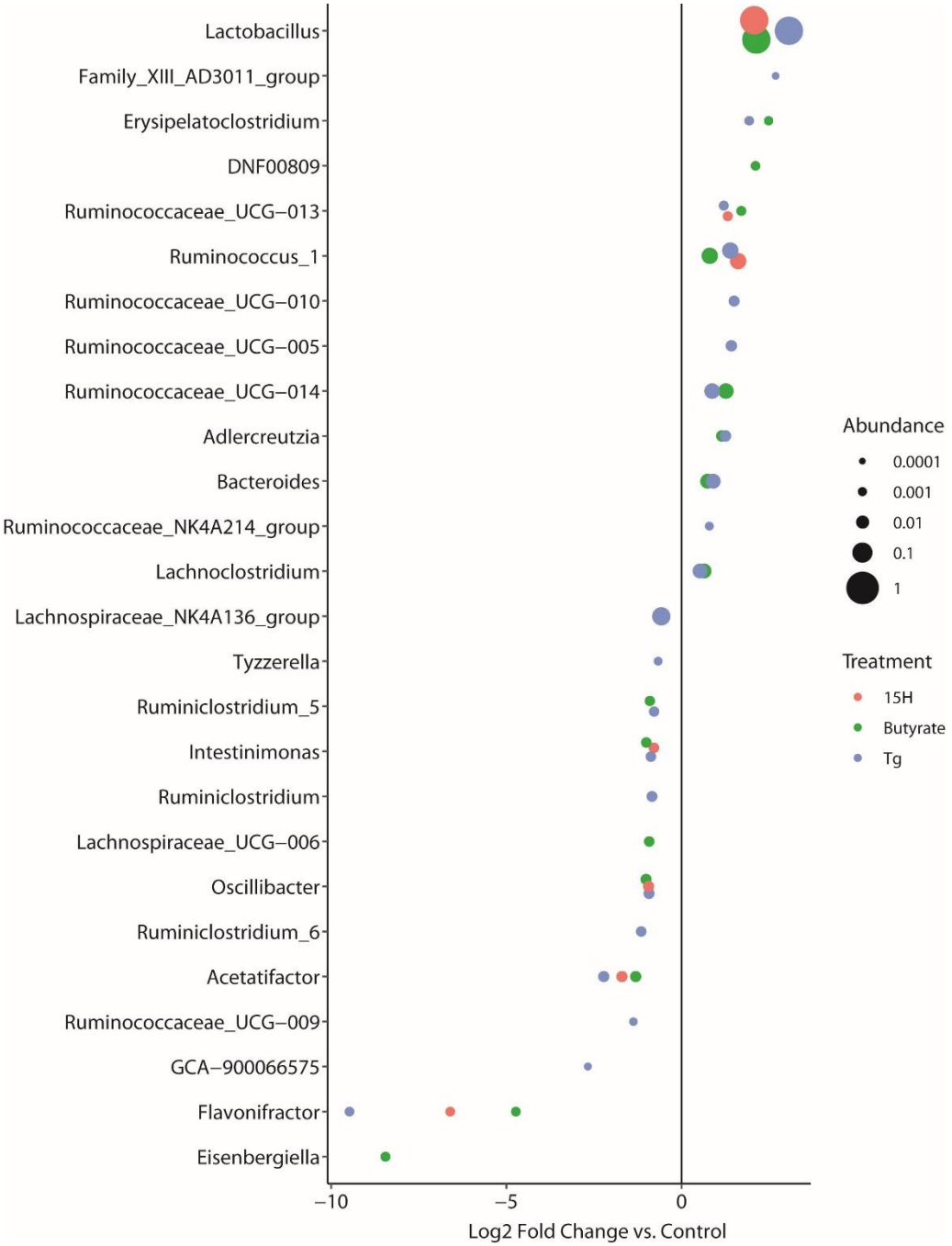

Supplemental Figure 11: Differential genera in the 15-HETE, Tg6F, and sodium butyrate groups. The three treatment groups were compared to controls at week 3. Plot

shows genera with q<0.05 in DESEQ2 models. Each dot represents one genus, with dot color indicating which of the three comparisons is shown and dot size representing genus abundance. Magnitude of difference is shown as the log2 of the fold change compared to controls.

Chapter 6: Conclusions and Future Directions

Abbreviations

PAH	Pulmonary Arterial Hypertension
RV	Right Ventricle
HETE	Hydroxyeicosatetraenoic Acid
HODE	Hydroxyoctadecadienoic Acid
PH	Pulmonary Hypertension
MCT	Monocrotaline
CHP	Chronic Hypoxia
ApoA-I	Apolipoprotein A-I
15-HETE	15-Hydroxyeicosatetraenoic Acid
Tg6F	Transgenic Tomatoes Expressing the ApoA-I Mimetic Peptide 6F
IEC-6	Intestinal Epithelial Cells
HDL	High Density Lipoprotein
TAG	Triacylglycerol
CE	Cholesterol Ester
HCER	Hexosylceramides
FFA	Free Fatty Acids
LA	Linoleic Acid
LOX	Lipoxygenase
EV	Empty Vector Tomato
IFI44	Interferon Induced Protein 44
CD8	Cluster of Differentiation 8
PAEC	Pulmonary Arterial Endothelial Cells
TRAIL	Tumor Necrosis Factor-Related Apoptosis-Inducing Ligand
CXCL10	C-X-C Motif Ligand 10
WT	Wild Type
SCFA	Short Chain Fatty Acid
CVD	Cardiovascular Disease
LDL	Low Density Lipoprotein
WD	Western Diet

Pulmonary arterial hypertension (PAH) is a multifactorial disease that is characterized by vascular remodeling that increases right ventricle (RV) pressure leading to hypertrophy and in some cases, death, with no cure to date.[3,6,9] Increased levels of the oxylipins hydroxyeicosatetraenoic acids (HETEs) and hydroxyoctadecadienoic acids

(HODEs) have been observed not only in PAH patients but in multiple animal models of pulmonary hypertension (PH) including monocrotaline injection (MCT) and chronic hypoxia (CHP).[11–13] Our lab in conjunction with our collaborators has not only shown that decreasing levels of HETEs and HODEs through the use of apolipoprotein A1 (apoA-I) mimetic peptides ameliorates PH in MCT and CHP mice, but also that dietary administration of 15-hydroxyeicosatetraenoic acid (15-HETE) at 5 μg per mouse per day for 21 days can lead to PH. As oxylipins are pro-inflammatory lipids, this led me to hypothesize that the 15-HETE/PH model acts by increasing inflammation, immune lipids, and the immune response, reduces the production of anti-inflammatory lipids, and that the transgenic tomato expression the apoA-I mimetic peptide 6F (Tg6F) prevents and reverses these effects.

In Chapter 2, we showed that 15-HETE plays a causal role in PH by inducing PAEC apoptosis through a CD8+-dependent mechanism and that the apoA-I mimetic peptide, Tg6F, prevents and rescues PH induced by 15-HETE. Due to the observation that treatment of intestinal epithelial cells (IEC-6) cells with 15-HETE led to increases in multiple HETEs and HODEs coupled with the fact that ~30% of the plasma high density lipoprotein (HDL) is synthesized the small intestine[94], and apoA-I mimetic peptides act on the small intestine to modulate levels of oxylipins[69], brought a potential role of the intestine in the onset of PH to our attention as something to investigate further. The therapeutic effects of Tg6F in this model are also unknown and further studies were necessary to clarify the therapeutic potential of apoA-I mimetic peptides for patients with various forms of PH.

Chapter 3 revealed a lot about the 15-HETE/PH model. First, it causes changes

in triacylglycerol (TAG), cholesterol ester (CE), hexosylceramides (HCER), and free fatty acids (FFA) and in linoleic acid (LA), the precursor of HETEs and HODEs in the plasma, explaining how HETEs and HODEs aside from 15-HETE increase in the plasma and tissues. Plasma cytokine levels and macrophage populations in the intestine increased in mice fed 15-HETE diet, further expanding on the immunomodulatory effects of this diet. Next, I found that the effects of the 15-HETE diet were not specific to 15-HETE, as 5-HETE and a combination of 5-12-and 15-HETE at a total dose of 5 μg/mouse/day can also cause PH in wild type mice. Finally, focusing on the role of lipoxygenase (LOX) enzymes, I found that 12/15 LOX KO mice administered a 5 LOX inhibitor do not develop PH when fed 15-HETE diet. Interestingly, intestine levels of HETEs and HODEs are significantly lowered in 12/15 LOX KO mice, once again bringing the role of the intestine into question. To further investigate the role of intestinal expression of 12/15 LOX to the development of PH in the 15-HETE model, we purchased and are breeding 12/15 LOX flox mice (B6.129S2-Alox15tm1Fun/J, Jackson Laboratories) to cross with Vil-Cre mice (B6.Cg-Tg[Vil1-cre]997Gum/J) to knock out intestine expression of 12/15 LOX. I would feed these mice 15-HETE fortified diet for three weeks and assess the development of PH. Gene analysis from these experiments would be incredibly powerful to combine with the RNA-seq results from the jejunum of mice on 15-HETE, Tg6F, and empty vector tomato (EV) diets as it would help isolate potential pathways more directly connected to intestinal 12/15 LOX activity.

Chapter 4 showed that 15-HETE/PH changes intestinal gene expression of hundreds of genes many of which the apoA-I mimetic peptide, Tg6F, which prevents 15-HETE induction of PH, counteracts while EV has no effect on the increases caused by

15-HETE. These genes are implicated in multiple pathways including response to various stimuli, immune response/cytokine, cell adhesion, chemotaxis, and vasculature/angiogenesis. Analysis of RNA-seq data from the intestine and lungs of 15-HETE fed mice and lungs of PAH patients found interferon induced protein 44 (IFI44) increasing across all three and qPCR analysis showed that it increases in the intestine one week into the 15-HETE/PH protocol, earlier than when it increases in the lungs. Intratracheal administration of siRNA against IFI44 prevented development of 15-HETE diet induced PH and siRNA treatment of CD8+ cells decreased pulmonary arterial endothelial cell (PAEC) apoptosis. We identified two genes positively correlated in human PAH data, tumor necrosis factor-related apoptosis-inducing ligand (TRAIL) and (CXCL10) and found that IFNα4 treatment of CD8+ cells increased expression of IFI44, TRAIL, and CXCL10, however, IFNα4 treatment combined with IFI44 siRNA prevented the increase in TRAIL and CXCL10, showing that IFI44 is what regulates these genes that are both known to be pro-inflammatory with apoptotic properties, accounting for the apoptosis that occurs when IFI44 is increased, and its decrease when IFI44 is knocked down.[161,162,169] As the supernatant of 15-HETE treated IEC-6 cells induced IFI44 expression in CD8+ cells, this suggests that the signals that lead to increased IFI44 expression start at the gut, however, whether this is due to the induction of IFNα4, IFI44, and whether blocking IFNα4 or IFI44 in the intestine can prevent endothelial cell apoptosis and the onset of PH requires further investigation.

Chapter 5 highlights the role of the intestine when it comes to the onset of PH by 15-HETE and one major way Tg6F prevents it. Microbiota analysis of female wild type (WT) mice on the 15-HETE diet showed decreases in bacteria species that produce the

short chain fatty acid (SCFA) butyrate which reflected those seen in *Ldlr-/- mice*, which when fed WD for 12 weeks, also develop PH that is prevented by the intervention of apoA-I mimetic peptides. Fecal pellet analysis of SCFAs found that mice fed chow and 15-HETE diets had lower levels of SCFAs including acetate, propionate, isobutyrate, and butyrate compared to those of mice on the Tg6F diet, implicating that other anti-inflammatory SCFAs may be instrumental to how Tg6F counteracts the pro-inflammatory effects of 15-HETE. I tested the potential therapeutic capacity of butyrate by supplementing drinking water with 0.1 M sodium butyrate and found that it prevented and rescued mice fed the 15-HETE diet from PH by preventing significant increases of IFI44 levels in the intestine and lungs of mice on the 15-HETE diet which was also accomplished by the Tg6F diet. At the same time, both Tg6F and sodium butyrate treatments prevented decreases in SCFA-producers that were seen in the 15-HETE group at week 2 and increased the abundances of multiple SCFA-producing bacteria by the end of the 3-week protocol. These exciting findings answered some major questions regarding the role of the intestine while bringing up several additional ones to investigate. The first being whether a mouse with the altered microbiota composition observed in 15-HETE fed mice is sufficient to cause PH. This could be accomplished via fecal microbiota transplant of 15-HETE fed mice to in germ free WT mice or, the reverse can be investigated by determining whether an impaired microbiota can cause PH, by administering probiotics of bacteria reduced in abundance by 15-HETE can prevent development of PH by the 15-HETE diet, especially the butyrate-producing species. Studies have shown that supplementation with commercially available products including omega-3, inulin fiber, prebiotics, and probiotics are beneficial to other

species, including SCFA-producing bacteria. For example, a two-arm dietary intervention assessing the effects of omega-3 and fiber supplementation on traditional cardiovascular disease (CVD) risk factors in 70 middle-aged healthy participants found that both interventions caused significant drops in blood pressure, cholesterol, proinflammatory cytokines, increases in butyric-acid production and butyrogenic bacteria.[180] In mice with acute colitis, one week of intervention with probiotics, lactitol (a prebiotic), synbiotics (probiotics and inulin), and probiotics + lactitol had significantly lower pathologic scores compared with the control group and also had increased *Lachnospiraceae* abundance.[192] In another dietary intervention study, supplementation with casein formula supplemented with *Lactobacillus rhamoss* GG accelerates tolerance acquisition in infants with cow's milk allergy and also increases fecal levels of butyrate levels as well as increase abundance in butyrate-producing bacteria.[184] Therefore, approaches to investigate whether increasing butyrate-producing bacteria would prevent the onset of PH in mice with imbalanced microbiota caused by 15-HETE or co-administered with 15-HETE to prevent the development of PH could be accomplished by these commercially available means. In Chapter 5 it was noted that multiple SCFAs were increased in the Tg6F fed mice, including acetate and propionate. It would be worth investigating whether these SCFAs have the same therapeutic capacity in hypertensive mice by administering them to mice in a similar fashion as sodium butyrate was administered to the mice in Chapter 5. Finally, to explore the extent to which supplemental butyrate and other SCFAs improve or prevent PH, determining whether butyrate has an effect in other animal models of PH would be worth exploring. Such models to investigate include hypoxic mice, MCT injected rats, and rodents subjected to

Sugen/hypoxia treatment are a few models that could be administered sodium butyrate or other SCFAs as Sugen/hypoxic rats have reported gut dysbiosis including decreases in butyrate and acetate-producing bacteria along with decreased serum levels of acetate.[53]

My dissertation work has explored the multiple ways dietary administration of oxylipins of the LOX pathway are causal to PH by focusing on the effects of one lipid, 15-HETE, to further understand how it exerts multiple inflammatory effects leading to the onset of PH and identifying pathways that can be targeted utilizing a therapeutic in multiple animal models of PH, Tg6F. The pro-inflammatory effects of 15-HETE are vast, it causes dyslipidemia, increases cytokine levels, the levels of multiple proinflammatory lipids in the intestine, plasma, and lungs, and T cell mediated apoptosis. Homing in on the effects of 15-HETE on the intestine, I discovered novel players in the onset of 15-HETE. First, RNA-seq analysis of the intestine, combined with that of the lungs of mice on the 15-HETE diet and lungs of PAH patients, identified IFI44 as the common increasing gene among all three datasets, and furthermore, when silencing IFI44 *in vivo*, it prevented the onset of PH by 15-HETE and *in vitro*, decreased apoptosis by CD8+ cells. Second, microbiota analysis of the intestines of mice on the 15-HETE diet noted that abundances of butyrate producing bacteria were decreased, similar to changes observed in low density lipoprotein deficient (*Ldlr-/-)* mice on Western diet (WD), who had these abundances increased when administered Tg6F. SCFA analysis further showed Tg6F increased fecal pellet levels of multiple SCFAs including acetate, propionate, and butyrate, compared to 15-HETE and chow fed mice. Following these results, we showed that both increasing the abundance of SCFA producing bacteria as well as direct

supplementation with the SCFA butyrate, can help prevent and ameliorate PH by decreasing expression of IFI44 in the intestine. In conclusion, these studies elucidated many ways 15-HETE causes PH while also identifying targets and potential therapeutics against PH that may one day help patients with PAH.

Appendices

Appendix A: All Lipid Changes in 15-HETE Plasma

Class	Sub Class	Chemical Name	HMDC	LIPID MAPS	P-Value	Fold Change
CE	-	CE(24:0)	HMDB10376		0.0690	-1.8251
CER	CER	CER(14:0)	HMDB11773	LMSP02010001		
CER	CER	CER(18:0)	HMDB04950	LMSP02010006		
DAG	ester	DAG(12:0/18:2)	-	LMGL02010337		
DAG	ester	DAG(14:0/16:0)	HMDB07095	LMGL02010378		
DAG	ester	DAG(14:0/16:1)	HMDB07012	LMGL02010379		
DAG	ester	DAG(14:0/18:1)	HMDB07015	LMGL02010384		
DAG	ester	DAG(14:1/18:1)	HMDB07044	LMGL02010408		
DAG	ester	DAG(15:0/18:1)	HMDB07073	LMGL02010432		
DAG	ester	DAG(16:0/16:0)	HMDB07098	LMGL02010009		1.1667
DAG	ester	DAG(16:0/16:1)	HMDB07099	LMGL02010010		
DAG	ester	DAG(16:0/18:2)	HMDB07103	LMGL02010027	0.0007	2.0932
DAG	ester	DAG(16:0/20:4)	HMDB07112	LMGL02010070		
DAG	ester	DAG(16:0/22:6)	HMDB07121	LMGL02010162		
DAG	ester	DAG(16:1/16:1)	HMDB07128	LMGL02010011		
DAG	ester	DAG(16:1/18:1)	HMDB07131	LMGL02010026		
DAG	ester	DAG(16:1/18:2)	HMDB07132	LMGL02010031		1.8938
DAG	ester	DAG(16:1/18:3)	HMDB07134	LMGL02010035		
DAG	ester	DAG(16:1/20:0)	HMDB07360	LMGL02010047		
DAG	ester	DAG(16:1/20:2)	HMDB07138	LMGL02010061		
DAG	ester	DAG(16:1/22:6)	HMDB07150	LMGL02010174		
DAG	ester	DAG(18:0/18:1)	HMDB07160	LMGL02010043		

DAG	ester	DAG(18:0/18:2)	HMDB07161	LMGL02010050		
DAG	ester	DAG(18:0/22:6)	HMDB07179	LMGL02010216		
DAG	ester	DAG(18:1/20:4)	HMDB07228	LMGL02010121	0.0934	1.4041
DAG	ester	DAG(18:1/22:6)	HMDB07237	LMGL02010225	0.1685	1.1584
DAG	ester	DAG(18:2/18:3)	HMDB07250	LMGL02010071		
DAG	ester	DAG(18:2/20:3)	HMDB07256	LMGL02010120		
DAG	ester	DAG(18:2/20:4)	HMDB07257	LMGL02010131	0.0002	1.7949
DAG	ester	DAG(18:2/22:6)	HMDB07266	LMGL02010234	0.1058	1.3048
DCER	DCER	DCER(16:0)	HMDB11760	LMSP02020001		
DCER	DCER	DCER(24:0)	HMDB11768	LMSP02020012		
DCER		total_class				
HCER	HCER	HCER(18:0)	HMDB04972	LMSP0501AA05		
HCER	HCER	HCER(20:0)	HMDB04973	LMSP0501AA06	0.0054	2.7118
HCER	HCER	HCER(20:1)	-			
HCER	HCER	HCER(22:1)	-		0.1593	1.5199
LCER	LCER	LCER(16:0)	HMDB06750	LMSP0501AB03		
LCER	LCER	LCER(22:0)	HMDB11594	LMSP0501AB06		
LCER		total_class				
LPC	ester	LPC(14:1)	HMDB10380	LMGP01050014		
LPE	ester	LPE(15:0)	HMDB11502	LMGP02050031		
LPE	ester	LPE(16:1)	HMDB11474	LMGP02050037	0.2647	-1.2267
LPE	ester	LPE(17:0)	-	LMGP02050030		-1.1251

LPE	ester	LPE(22:5)	HMDB11495	LMGP02050059	0.6091	1.2310
PC	Ester	PC(12:0/16:1)	-	LMGP01011319		
PC	Ester	PC(12:0/18:1)	-	LMGP01010440		
PC	Ester	PC(12:0/18:2)	-	LMGP01011323	0.1243	1.5318
PC	Ester	PC(12:0/18:3)	-	LMGP01011325		
PC	Ester	PC(12:0/20:1)	-	LMGP01011329		
PC	Ester	PC(12:0/20:3)	-	LMGP01011331		
PC	Ester	PC(12:0/20:4)	-	LMGP01011332		
PC	Ester	PC(14:0/14:0)	HMDB07866	LMGP01010477		
PC	Ester	PC(14:0/16:1)	HMDB07870	LMGP01010485		
PC	Ester	PC(14:0/18:3)	HMDB07876	LMGP01010497		
PC	Ester	PC(14:0/20:1)	HMDB07879	LMGP01011372		
PC	Ester	PC(14:0/20:2)	HMDB07880	LMGP01011373		
PC	Ester	PC(14:0/22:1)	HMDB07887	LMGP01012129		
PC	Ester	PC(14:0/22:4)	HMDB07889	LMGP01011378		
PC	Ester	PC(14:0/22:5)	HMDB07891	LMGP01012131		
PC	Ester	PC(14:0/22:6)	HMDB07892	LMGP01010512	0.1601	1.3463
PC	Ester	PC(15:0/14:1)	HMDB07933	LMGP01011411		
PC	Ester	PC(15:0/16:1)	HMDB07936	LMGP01010535		

PC	Ester	PC(15:0/20:3)	HMDB07948	LMGP01011423		
PC	Ester	PC(15:0/20:4)	HMDB07949	LMGP01011424	0.4224	1.2115
PC	Ester	PC(15:0/20:5)	HMDB07951	LMGP01011425		
PC	Ester	PC(15:0/22:6)	HMDB07958	LMGP01011430	0.4122	-1.2676
PC	Ester	PC(16:0/18:4)	HMDB07976	LMGP01010603		
PC	Ester	PC(16:0/22:1)	HMDB07986	LMGP01010638		
PC	Ester	PC(16:0/22:2)	HMDB07987	LMGP01011472		
PC	Ester	PC(17:0/14:1)	-	LMGP01010008		
PC	Ester	PC(17:0/16:1)	-	LMGP01011502		-1.5006
PC	Ester	PC(17:0/20:5)	-	LMGP01011515		
PC	Ester	PC(17:0/22:4)	-	LMGP01011520		
PC	Ester	PC(17:0/22:5)	-	LMGP01010719		
PC	Ester	PC(18:0/12:0)	-	LMGP01010736		
PC	Ester	PC(18:0/14:0)	HMDB08031	LMGP01010739		
PC	Ester	PC(18:0/22:1)	HMDB08052	LMGP01010811		
PC	Ester	PC(18:0/22:2)	HMDB08053	LMGP01011594		
PC	Ester	PC(18:1/14:1)	HMDB08098	LMGP01011597		
PC	Ester	PC(18:1/22:1)	HMDB08118	LMGP01012166		
PC	Ester	PC(18:1/22:2)	HMDB08119	LMGP01011612		

PC	Ester	PC(18:2/14:1)	HMDB08131	LMGP01011617		
PC	Ester	PC(18:2/20:5)	HMDB08149	LMGP01011634	0.6233	-1.1256
PC	Ester	PC(18:2/22:1)	HMDB08151	LMGP01012172		
PC	Ester	PC(18:2/22:4)	HMDB08153	LMGP01011639		
PC	Ester	PC(18:2/22:5)	HMDB08155		0.1140	-1.9333
PC	Ester	PC(20:0/16:1)	HMDB08266	LMGP01011790		
PC	Ester	PC(20:0/18:3)	HMDB08272	LMGP01011795		
PC	Ester	PC(20:0/20:2)	HMDB08276	LMGP01011021		
PC	Ester	PC(20:0/20:5)	HMDB08281	LMGP01011800		
PC	Ester	PC(20:0/22:5)	HMDB08287	LMGP01011027		
PC	Ester	PC(20:0/22:6)	HMDB08288	LMGP01011028		-1.6898
PE	ester	PE(14:0/18:1)	HMDB08828	LMGP02011247		
PE	ester	PE(14:0/18:2)	HMDB08829	LMGP02011246		
PE	ester	PE(14:0/20:1)	HMDB08834	LMGP02010415		
PE	ester	PE(14:0/20:4)	HMDB08838			
PE	ester	PE(14:0/22:4)	HMDB08844	LMGP02010421		
PE	ester	PE(14:0/22:6)	HMDB08847	LMGP02011239		
PE	ester	PE(15:0/20:4)	HMDB08904	LMGP02010467		
PE	ester	PE(16:0/14:0)	HMDB08920	LMGP02010297		
PE	ester	PE(16:0/16:0)	HMDB08923	LMGP02010037		1.3932

PE	ester	PE(16:0/16:1)	HMDB08924	LMGP02011228		
PE	ester	PE(16:0/18:3)	HMDB08930	LMGP02010041		
PE	ester	PE(16:0/20:1)	HMDB08933	LMGP02010312		
PE	ester	PE(16:0/20:2)	HMDB08934	LMGP02010510		
PE	ester	PE(16:0/20:5)	HMDB08939	LMGP02011221		
PE	ester	PE(16:0/22:4)	HMDB08943	LMGP02010116		2.0686
PE	ester	PE(16:0/22:5)	HMDB08945		0.4953	1.2692
PE	ester	PE(17:0/18:2)	-	LMGP02010546		
PE	ester	PE(17:0/20:4)	-	LMGP02010003		1.3018
PE	ester	PE(17:0/22:4)	-	LMGP02010560		
PE	ester	PE(17:0/22:6)	-	LMGP02011210		
PE	ester	PE(18:0/14:0)	HMDB08986	LMGP02011206		
PE	ester	PE(18:0/16:0)	HMDB08989	LMGP02011205	0.5542	-1.1317
PE	ester	PE(18:0/16:1)	HMDB08990	LMGP02011204		
PE	ester	PE(18:0/18:3)	HMDB08996	LMGP02010629	0.3871	1.9022
PE	ester	PE(18:0/20:1)	HMDB08999	LMGP02010141	0.7370	-1.0573
PE	ester	PE(18:0/20:5)	HMDB09005	LMGP02011201	0.6942	-1.1793
PE	ester	PE(18:0/22:4)	HMDB09009	LMGP02011200		1.1427
PE	ester	PE(18:1/14:1)	HMDB09053			
PE	ester	PE(18:1/16:1)	HMDB09056	LMGP02011198		

PE	ester	PE(18:1/20:1)	HMDB09065	LMGP02010126		
PE	ester	PE(18:1/20:2)	HMDB09066	LMGP02010647		
PE	ester	PE(18:1/20:5)	HMDB09071	LMGP02011195		-1.7432
PE	ester	PE(18:1/22:4)	HMDB09075	LMGP02010652		1.7536
PE	ester	PE(18:1/22:5)	HMDB09077		0.9772	-1.0187
PE	ester	PE(18:2/14:1)	HMDB09086	LMGP02010656		
PE	ester	PE(18:2/16:1)	HMDB09089	LMGP02010659		-1.2222
PE	ester	PE(18:2/18:2)	HMDB09093	LMGP02010111	0.1956	-1.5383
PE	ester	PE(18:2/20:1)	HMDB09098	LMGP02010670		
PE	ester	PE(18:2/20:2)	HMDB09099	LMGP02010671		
PE	ester	PE(18:2/20:3)	HMDB09101	LMGP02010672		
PE	ester	PE(18:2/20:4)	HMDB09102	LMGP02011192	0.0540	-1.5266
PE	ester	PE(18:2/20:5)	HMDB09104	LMGP02010673		
PE	ester	PE(18:2/22:6)	HMDB09111	LMGP02011191		-1.4658
PE	Ether	PE(O-16:0/16:0)	HMDB11158	LMGP02020103		
PE	Ether	PE(O-16:0/18:0)	HMDB11157	LMGP02020018		
PE	Ether	PE(O-16:0/18:3)	-	LMGP02020099		
PE	Ether	PE(O-16:0/20:1)	-	LMGP02020033		
PE	Ether	PE(O-16:0/20:3)	-			
PE	Ether	PE(O-16:0/20:5)	-			

PE	Ether	PE(O-16:0/22:2)	-	LMGP02020037		
PE	Ether	PE(O-18:0/16:0)	-	LMGP02020094	0.0748	1.5238
PE	Ether	PE(O-18:0/16:1)	-	LMGP02020093		1.8570
PE	Ether	PE(O-18:0/18:0)	-	LMGP02020011		1.4167
PE	Ether	PE(O-18:0/18:3)	-	LMGP02020050		1.4277
PE	Ether	PE(O-18:0/20:1)	-	LMGP02020054	0.0297	2.8663
PE	Ether	PE(O-18:0/20:2)	-	LMGP02020055		
PE	Ether	PE(O-18:0/20:5)	-	LMGP02020008	0.0660	-1.2038
PE	Plasmalogen	PE(P-14:0/18:0)	HMDB11434			
PE	Plasmalogen	PE(P-14:0/18:1)	-			
PE	Plasmalogen	PE(P-14:1/18:1)	-			
PE	Plasmalogen	PE(P-16:0/16:0)	-	LMGP02030013		
PE	Plasmalogen	PE(P-16:0/16:1)	HMDB11339	LMGP02030014		
PE	Plasmalogen	PE(P-16:0/18:0)	HMDB11340	LMGP02030018		
PE	Plasmalogen	PE(P-16:0/18:3)	HMDB11345	LMGP02030020		
PE	Plasmalogen	PE(P-16:0/20:1)	HMDB11348	LMGP02030025		2.1068
PE	Plasmalogen	PE(P-16:0/20:2)	HMDB11349	LMGP02030026		
PE	Plasmalogen	PE(P-16:0/20:5)	HMDB11354	LMGP02030028		-1.3128
PE	Plasmalogen	PE(P-16:1/18:1)	-			
PE	Plasmalogen	PE(P-18:0/16:0)	HMDB11371	LMGP02030040	0.9189	-1.0056

PE	Plasmalogen	PE(P-18:0/16:1)	HMDB11372	LMGP02030041		2.2667
PE	Plasmalogen	PE(P-18:0/18:0)	-	LMGP02030045		
PE	Plasmalogen	PE(P-18:0/18:3)	HMDB11378	LMGP02030048		1.5967
PE	Plasmalogen	PE(P-18:0/20:1)	HMDB11381	LMGP02030053		2.8803
PE	Plasmalogen	PE(P-18:0/20:5)	HMDB11387	LMGP02030056	0.2712	-1.3348
PE	Plasmalogen	PE(P-18:1/16:1)	HMDB11438			
PE	Plasmalogen	PE(P-18:1/18:3)	HMDB11444			
PE	Plasmalogen	PE(P-18:1/20:1)	HMDB11447			
PE	Plasmalogen	PE(P-18:1/20:2)	HMDB11448			
PE	Plasmalogen	PE(P-18:1/20:3)	HMDB11450			
PE	Plasmalogen	PE(P-18:1/20:5)	HMDB11420			
PE	Plasmalogen	PE(P-18:2/18:2)	HMDB09093		0.1957	-1.4259
PE	Plasmalogen	PE(P-18:2/20:4)	-		0.4636	-1.2491
PE	Plasmalogen	PE(P-18:2/22:6)	-		0.7628	-1.1012
TAG	ester	TAG36:0-FA12:0	HMDB00638	LMFA01010012		
TAG	ester	TAG38:0-FA12:0	HMDB00638	LMFA01010012		
TAG	ester	TAG40:0-FA12:0	HMDB00638	LMFA01010012		
TAG	ester	TAG40:0-FA14:0	HMDB00806	LMFA01010014		
TAG	ester	TAG40:0-FA16:0	HMDB00220	LMFA01010001		
TAG	ester	TAG42:0-FA12:0	HMDB00638	LMFA01010012		
TAG	ester	TAG42:0-FA14:0	HMDB00806	LMFA01010014		
TAG	ester	TAG42:0-FA16:0	HMDB00220	LMFA01010001		
TAG	ester	TAG42:1-FA12:0	HMDB00638	LMFA01010012		
TAG	ester	TAG42:1-FA14:0	HMDB00806	LMFA01010014		
TAG	ester	TAG42:1-FA16:0	HMDB00220	LMFA01010001		
TAG	ester	TAG42:1-FA16:1	HMDB03229	LMFA01030056		
TAG	ester	TAG42:1-FA18:1	HMDB00207	LMFA01030002		
TAG	ester	TAG44:0-FA12:0	HMDB00638	LMFA01010012		

TAG	ester	TAG44:0-FA14:0	HMDB00806	LMFA01010014		
TAG	ester	TAG44:0-FA16:0	HMDB00220	LMFA01010001		
TAG	ester	TAG44:0-FA18:0	HMDB00827	LMFA01010018		
TAG	ester	TAG44:1-FA12:0	HMDB00638	LMFA01010012		
TAG	ester	TAG44:1-FA14:0	HMDB00806	LMFA01010014		
TAG	ester	TAG44:1-FA14:1	HMDB02000	LMFA01030051		
TAG	ester	TAG44:1-FA16:0	HMDB00220	LMFA01010001		
TAG	ester	TAG44:1-FA16:1	HMDB03229	LMFA01030056		
TAG	ester	TAG44:1-FA18:1	HMDB00207	LMFA01030002		
TAG	ester	TAG44:2-FA14:0	HMDB00806	LMFA01010014		
TAG	ester	TAG44:2-FA16:0	HMDB00220	LMFA01010001		
TAG	ester	TAG44:2-FA16:1	HMDB03229	LMFA01030056		
TAG	ester	TAG44:2-FA18:1	HMDB00207	LMFA01030002		
TAG	ester	TAG44:2-FA18:2	HMDB00673	LMFA01030120		
TAG	ester	TAG45:0-FA14:0	HMDB00806	LMFA01010014		
TAG	ester	TAG45:0-FA15:0	HMDB00826	LMFA01010015		
TAG	ester	TAG45:0-FA16:0	HMDB00220	LMFA01010001		
TAG	ester	TAG45:1-FA15:0	HMDB00826	LMFA01010015		
TAG	ester	TAG45:1-FA16:0	HMDB00220	LMFA01010001		
TAG	ester	TAG45:1-FA18:1	HMDB00207	LMFA01030002		
TAG	ester	TAG46:0-FA12:0	HMDB00638	LMFA01010012		
TAG	ester	TAG46:0-FA18:0	HMDB00827	LMFA01010018		
TAG	ester	TAG46:1-FA12:0	HMDB00638	LMFA01010012		
TAG	ester	TAG46:1-FA14:0	HMDB00806	LMFA01010014	0.4368	1.1040
TAG	ester	TAG46:1-FA14:1	HMDB02000	LMFA01030051		
TAG	ester	TAG46:1-FA16:1	HMDB03229	LMFA01030056	0.5669	-1.1053
TAG	ester	TAG46:1-FA18:0	HMDB00827	LMFA01010018		
TAG	ester	TAG46:2-FA12:0	HMDB00638	LMFA01010012		
TAG	ester	TAG46:2-FA14:0	HMDB00806	LMFA01010014		
TAG	ester	TAG46:2-FA14:1	HMDB02000	LMFA01030051		

TAG	ester	TAG46:2-FA16:0	HMDB00220	LMFA01010001		1.9199
TAG	ester	TAG46:2-FA16:1	HMDB03229	LMFA01030056	0.9296	-1.0078
TAG	ester	TAG46:2-FA18:1	HMDB00207	LMFA01030002		
TAG	ester	TAG46:2-FA18:2	HMDB00673	LMFA01030120		
TAG	ester	TAG46:3-FA14:1	HMDB02000	LMFA01030051		
TAG	ester	TAG46:3-FA16:0	HMDB00220	LMFA01010001		
TAG	ester	TAG46:3-FA16:1	HMDB03229	LMFA01030056		
TAG	ester	TAG46:3-FA18:1	HMDB00207	LMFA01030002		
TAG	ester	TAG46:3-FA18:2	HMDB00673	LMFA01030120		
TAG	ester	TAG46:4-FA18:2	HMDB00673	LMFA01030120		
TAG	ester	TAG47:0-FA14:0	HMDB00806	LMFA01010014		
TAG	ester	TAG47:0-FA15:0	HMDB00826	LMFA01010015	0.2261	1.1654
TAG	ester	TAG47:0-FA17:0	HMDB02259	LMFA01010017		
TAG	ester	TAG47:1-FA14:0	HMDB00806	LMFA01010014		
TAG	ester	TAG47:1-FA15:0	HMDB00826	LMFA01010015		-1.0501
TAG	ester	TAG47:1-FA16:0	HMDB00220	LMFA01010001	0.2745	-1.2940
TAG	ester	TAG47:1-FA16:1	HMDB03229	LMFA01030056		
TAG	ester	TAG47:1-FA17:0	HMDB02259	LMFA01010017		
TAG	ester	TAG47:1-FA18:1	HMDB00207	LMFA01030002		
TAG	ester	TAG47:2-FA14:0	HMDB00806	LMFA01010014		
TAG	ester	TAG47:2-FA15:0	HMDB00826	LMFA01010015		
TAG	ester	TAG47:2-FA16:1	HMDB03229	LMFA01030056		
TAG	ester	TAG47:2-FA18:1	HMDB00207	LMFA01030002		
TAG	ester	TAG47:2-FA18:2	HMDB00673	LMFA01030120		
TAG	ester	TAG48:1-FA12:0	HMDB00638	LMFA01010012		
TAG	ester	TAG48:1-FA14:1	HMDB02000	LMFA01030051		
TAG	ester	TAG48:1-FA18:0	HMDB00827	LMFA01010018		
TAG	ester	TAG48:2-FA12:0	HMDB00638	LMFA01010012		
TAG	ester	TAG48:2-FA14:1	HMDB02000	LMFA01030051		
TAG	ester	TAG48:2-FA18:0	HMDB00827	LMFA01010018		

TAG	ester	TAG48:3-FA12:0	HMDB00638	LMFA01010012		1.9286
TAG	ester	TAG48:3-FA14:0	HMDB00806	LMFA01010014	0.0005	1.9164
TAG	ester	TAG48:3-FA14:1	HMDB02000	LMFA01030051	0.0570	4.7998
TAG	ester	TAG48:3-FA16:0	HMDB00220	LMFA01010001	0	3.9463
TAG	ester	TAG48:3-FA18:3	HMDB01388	LMFA01030152		
TAG	ester	TAG48:4-FA12:0	HMDB00638	LMFA01010012		
TAG	ester	TAG48:4-FA14:1	HMDB02000	LMFA01030051		
TAG	ester	TAG48:4-FA16:0	HMDB00220	LMFA01010001		
TAG	ester	TAG48:4-FA16:1	HMDB03229	LMFA01030056		
TAG	ester	TAG48:4-FA18:1	HMDB00207	LMFA01030002		
TAG	ester	TAG48:4-FA18:2	HMDB00673	LMFA01030120	0.0010	2.2973
TAG	ester	TAG48:4-FA18:3	HMDB01388	LMFA01030152		1.7138
TAG	ester	TAG48:5-FA18:2	HMDB00673	LMFA01030120		
TAG	ester	TAG48:5-FA18:3	HMDB01388	LMFA01030152		
TAG	ester	TAG49:0-FA17:0	HMDB02259	LMFA01010017	0.3320	1.1364
TAG	ester	TAG49:1-FA14:0	HMDB00806	LMFA01010014		
TAG	ester	TAG49:1-FA16:1	HMDB03229	LMFA01030056		1.0713
TAG	ester	TAG49:1-FA17:0	HMDB02259	LMFA01010017		
TAG	ester	TAG49:2-FA14:0	HMDB00806	LMFA01010014		
TAG	ester	TAG49:2-FA17:0	HMDB02259	LMFA01010017		
TAG	ester	TAG49:3-FA15:0	HMDB00826	LMFA01010015	0.0023	1.5435
TAG	ester	TAG49:3-FA16:0	HMDB00220	LMFA01010001	0.7959	-1.0432
TAG	ester	TAG49:3-FA16:1	HMDB03229	LMFA01030056	0.0255	1.2684
TAG	ester	TAG49:3-FA18:2	HMDB00673	LMFA01030120	0.0022	1.3792
TAG	ester	TAG49:3-FA18:3	HMDB01388	LMFA01030152		
TAG	ester	TAG50:0-FA14:0	HMDB00806	LMFA01010014		
TAG	ester	TAG50:2-FA14:1	HMDB02000	LMFA01030051		
TAG	ester	TAG50:3-FA14:1	HMDB02000	LMFA01030051		
TAG	ester	TAG50:3-FA18:0	HMDB00827	LMFA01010018		
TAG	ester	TAG50:4-FA14:0	HMDB00806	LMFA01010014	0.0086	1.4038

TAG	ester	TAG50:4-FA14:1	HMDB02000	LMFA01030051	0	3.7142
TAG	ester	TAG50:4-FA16:0	HMDB00220	LMFA01010001	0	2.9107
TAG	ester	TAG50:4-FA18:1	HMDB00207	LMFA01030002	0	2.3350
TAG	ester	TAG50:4-FA20:4	HMDB01043	LMFA01030001		
TAG	ester	TAG50:5-FA14:0	HMDB00806	LMFA01010014	0.0045	1.9490
TAG	ester	TAG50:5-FA16:0	HMDB00220	LMFA01010001		
TAG	ester	TAG50:5-FA16:1	HMDB03229	LMFA01030056	0.0003	2.8144
TAG	ester	TAG50:5-FA18:1	HMDB00207	LMFA01030002		
TAG	ester	TAG50:5-FA18:2	HMDB00673	LMFA01030120	0	2.5410
TAG	ester	TAG50:5-FA18:3	HMDB01388	LMFA01030152	0.0001	1.9680
TAG	ester	TAG50:5-FA20:4	HMDB01043	LMFA01030001		
TAG	ester	TAG50:5-FA20:5	HMDB01999	LMFA01030759		
TAG	ester	TAG50:6-FA20:4	HMDB01043	LMFA01030001		
TAG	ester	TAG51:3-FA16:1	HMDB03229	LMFA01030056	0.0271	1.2299
TAG	ester	TAG51:3-FA17:0	HMDB02259	LMFA01010017	0.2492	1.4866
TAG	ester	TAG51:3-FA18:3	HMDB01388	LMFA01030152		-1.1915
TAG	ester	TAG51:4-FA15:0	HMDB00826	LMFA01010015	0.1151	1.1059
TAG	ester	TAG51:4-FA16:1	HMDB03229	LMFA01030056	0.3192	1.1517
TAG	ester	TAG51:4-FA18:3	HMDB01388	LMFA01030152		-1.1275
TAG	ester	TAG51:4-FA20:4	HMDB01043	LMFA01030001		
TAG	ester	TAG51:5-FA18:2	HMDB00673	LMFA01030120	0.5729	-1.0351
TAG	ester	TAG51:5-FA18:3	HMDB01388	LMFA01030152	0.5199	1.1289
TAG	ester	TAG52:1-FA20:0	HMDB02212	LMFA01010020		1.4261
TAG	ester	TAG52:2-FA14:0	HMDB00806	LMFA01010014		
TAG	ester	TAG52:2-FA20:0	HMDB02212	LMFA01010020		
TAG	ester	TAG52:2-FA20:1	HMDB34296	LMFA01030085	0.0124	1.2597
TAG	ester	TAG52:2-FA20:2	HMDB05060	LMFA01030130		-1.0887
TAG	ester	TAG52:3-FA14:0	HMDB00806	LMFA01010014		
TAG	ester	TAG52:3-FA20:0	HMDB02212	LMFA01010020	0.0163	1.9204
TAG	ester	TAG52:3-FA20:1	HMDB34296	LMFA01030085	0.1999	1.3693

TAG	ester	TAG52:3-FA20:2	HMDB05060	LMFA01030130	0.0005	1.5775
TAG	ester	TAG52:3-FA22:1	HMDB02068	LMFA01030089		
TAG	ester	TAG52:4-FA14:0	HMDB00806	LMFA01010014		
TAG	ester	TAG52:4-FA18:0	HMDB00827	LMFA01010018	0.0068	1.5242
TAG	ester	TAG52:4-FA20:0	HMDB02212	LMFA01010020	0.0002	1.8774
TAG	ester	TAG52:4-FA20:2	HMDB05060	LMFA01030130		1.6937
TAG	ester	TAG52:4-FA22:1	HMDB02068	LMFA01030089		
TAG	ester	TAG52:5-FA14:0	HMDB00806	LMFA01010014		
TAG	ester	TAG52:5-FA20:3	HMDB02925	LMFA01030158		1.53
TAG	ester	TAG52:5-FA20:5	HMDB01999	LMFA01030759	0.0009	1.7611
TAG	ester	TAG52:5-FA22:5	HMDB06528	LMFA04000044	0.0023	2.3003
TAG	ester	TAG52:6-FA14:0	HMDB00806	LMFA01010014		1.9817
TAG	ester	TAG52:6-FA16:0	HMDB00220	LMFA01010001	0	3.3550
TAG	ester	TAG52:6-FA16:1	HMDB03229	LMFA01030056	0	2.1098
TAG	ester	TAG52:6-FA18:1	HMDB00207	LMFA01030002	0.0004	2.9732
TAG	ester	TAG52:6-FA18:2	HMDB00673	LMFA01030120	0	2.3674
TAG	ester	TAG52:6-FA18:3	HMDB01388	LMFA01030152	0	2.2306
TAG	ester	TAG52:6-FA20:4	HMDB01043	LMFA01030001	0	2.2640
TAG	ester	TAG52:6-FA20:5	HMDB01999	LMFA01030759	0.0001	2.1811
TAG	ester	TAG52:6-FA22:6	HMDB02183	LMFA01030185	0.0006	2.3774
TAG	ester	TAG52:7-FA18:1	HMDB00207	LMFA01030002		
TAG	ester	TAG52:7-FA20:5	HMDB01999	LMFA01030759	0	1.7091
TAG	ester	TAG52:7-FA22:6	HMDB02183	LMFA01030185		
TAG	ester	TAG52:8-FA16:1	HMDB03229	LMFA01030056		1.3093
TAG	ester	TAG52:8-FA18:2	HMDB00673	LMFA01030120	0.0436	1.4448
TAG	ester	TAG53:4-FA16:0	HMDB00220	LMFA01010001	0.0169	1.5720
TAG	ester	TAG53:4-FA17:0	HMDB02259	LMFA01010017	0.7724	1.0258
TAG	ester	TAG53:4-FA18:3	HMDB01388	LMFA01030152	0.0791	1.3534
TAG	ester	TAG53:4-FA20:4	HMDB01043	LMFA01030001		2.5316
TAG	ester	TAG53:5-FA20:4	HMDB01043	LMFA01030001		1.4714

TAG	ester	TAG53:6-FA20:4	HMDB01043	LMFA01030001	0.1028	1.6788
TAG	ester	TAG54:4-FA22:1	HMDB02068	LMFA01030089		1.8381
TAG	ester	TAG54:4-FA22:4	HMDB02226	LMFA01030178		
TAG	ester	TAG54:5-FA20:2	HMDB05060	LMFA01030130	0.0743	1.1680
TAG	ester	TAG54:5-FA20:5	HMDB01999	LMFA01030759	0.0002	1.5835
TAG	ester	TAG54:5-FA22:1	HMDB02068	LMFA01030089	0.0367	1.4618
TAG	ester	TAG54:5-FA22:4	HMDB02226	LMFA01030178		1.4352
TAG	ester	TAG54:5-FA22:5	HMDB06528	LMFA04000044	0.0046	2.0721
TAG	ester	TAG54:6-FA20:3	HMDB02925	LMFA01030158	0.0028	1.6237
TAG	ester	TAG54:6-FA22:5	HMDB06528	LMFA04000044	0	2.0510
TAG	ester	TAG54:7-FA16:1	HMDB03229	LMFA01030056	0.0001	1.9111
TAG	ester	TAG54:7-FA18:1	HMDB00207	LMFA01030002	0.0006	1.6228
TAG	ester	TAG54:7-FA20:4	HMDB01043	LMFA01030001	0	2.2124
TAG	ester	TAG54:7-FA22:5	HMDB06528	LMFA04000044	0.0051	1.6475
TAG	ester	TAG54:8-FA18:2	HMDB00673	LMFA01030120	0.0014	1.6558
TAG	ester	TAG54:8-FA18:3	HMDB01388	LMFA01030152	0	1.8416
TAG	ester	TAG54:8-FA20:4	HMDB01043	LMFA01030001	0.0569	3.1385
TAG	ester	TAG54:8-FA20:5	HMDB01999	LMFA01030759	0	1.7139
TAG	ester	TAG54:8-FA22:6	HMDB02183	LMFA01030185	0	1.2046
TAG	ester	TAG55:5-FA18:2	HMDB00673	LMFA01030120	0.6783	-1.0536
TAG	ester	TAG55:5-FA20:4	HMDB01043	LMFA01030001	0.0013	1.9590
TAG	ester	TAG55:7-FA22:6	HMDB02183	LMFA01030185	0.9559	-1.0044
TAG	ester	TAG56:3-FA16:0	HMDB00220	LMFA01010001	0.0222	-1.4668
TAG	ester	TAG56:4-FA16:0	HMDB00220	LMFA01010001		-1.1472
TAG	ester	TAG56:4-FA22:4	HMDB02226	LMFA01030178		
TAG	ester	TAG56:5-FA22:5	HMDB06528	LMFA04000044	0	1.5942
TAG	ester	TAG56:6-FA18:3	HMDB01388	LMFA01030152	0.1815	-1.0704
TAG	ester	TAG56:6-FA22:4	HMDB02226	LMFA01030178	0.0009	1.3027
TAG	ester	TAG56:7-FA16:1	HMDB03229	LMFA01030056	0.0704	1.1166
TAG	ester	TAG56:7-FA18:3	HMDB01388	LMFA01030152	0.0193	1.3776

TAG	ester	TAG56:7-FA22:4	HMDB02226	LMFA01030178	0.0803	1.2512
TAG	ester	TAG56:8-FA16:1	HMDB03229	LMFA01030056	0.9128	-1.0069
TAG	ester	TAG56:8-FA18:3	HMDB01388	LMFA01030152	0	1.9157
TAG	ester	TAG56:8-FA22:5	HMDB06528	LMFA04000044	0.0076	1.3645
TAG	ester	TAG56:9-FA18:3	HMDB01388	LMFA01030152	0	2.0939
TAG	ester	TAG56:9-FA20:4	HMDB01043	LMFA01030001	0	2.3220
TAG	ester	TAG56:9-FA20:5	HMDB01999	LMFA01030759	0.0040	1.2828
TAG	ester	TAG58:10-FA20:5	HMDB01999	LMFA01030759	0.0050	1.2009
TAG	ester	TAG58:10-FA22:5	HMDB06528	LMFA04000044	0.0170	1.2409
TAG	ester	TAG58:6-FA16:0	HMDB00220	LMFA01010001		-1.1079
TAG	ester	TAG58:6-FA18:0	HMDB00827	LMFA01010018	0.7668	1.1406
TAG	ester	TAG58:6-FA20:4	HMDB01043	LMFA01030001	0.3882	1.0926
TAG	ester	TAG58:7-FA16:0	HMDB00220	LMFA01010001	0.0689	-1.3064
TAG	ester	TAG58:7-FA18:2	HMDB00673	LMFA01030120	0.4431	-1.0718
TAG	ester	TAG58:7-FA20:4	HMDB01043	LMFA01030001	0.0585	1.2962
TAG	ester	TAG58:7-FA22:4	HMDB02226	LMFA01030178	0.2099	1.1734
TAG	ester	TAG58:8-FA20:3	HMDB02925	LMFA01030158	0.0399	1.2607
TAG	ester	TAG58:9-FA22:5	HMDB06528	LMFA04000044	0.6974	1.0242
TAG	ester	TAG60:10-FA22:5	HMDB06528	LMFA04000044	0.5653	1.0441
TAG	ester	TAG60:11-FA22:5	HMDB06528	LMFA04000044	0.3516	1.0574
TAG	ester	TAG60:11-FA22:6	HMDB02183	LMFA01030185	0.0376	-1.1551
CE	-	CE(16:1)	HMDB00658	LMST01020006	0	1.5493
CE	-	CE(17:0)	HMDB60059	LMST01020026	0.0450	1.19
CE	-	CE(18:0)	HMDB10368	LMST01020007	0.1749	1.0787
CE	-	CE(18:1)	HMDB00918	LMST01020003	0.1037	1.0362
CE	-	CE(18:3)	HMDB10370	LMST01020009	0.0001	1.4158
CE	-	CE(20:1)	HMDB05193	LMST01020011	0.0769	1.1607
CE	-	CE(20:3)	HMDB06736	LMST01020013	0.0018	1.2320
CE	-	CE(20:4)	HMDB06726	LMST01020014	0.0001	1.6263
DAG	ester	DAG(18:1/18:1)	HMDB07218	LMGL02010049	0.0502	1.3770

TAG	ester	TAG46:0-FA16:0	HMDB00220	LMFA01010001	0.1822	-1.1518
TAG	ester	TAG46:1-FA16:0	HMDB00220	LMFA01010001	0.0113	1.2683
TAG	ester	TAG47:0-FA16:0	HMDB00220	LMFA01010001	0.6033	-1.0352
TAG	ester	TAG48:0-FA14:0	HMDB00806	LMFA01010014		1.5946
TAG	ester	TAG48:0-FA16:0	HMDB00220	LMFA01010001	0	1.3905
TAG	ester	TAG48:0-FA18:0	HMDB00827	LMFA01010018		1.0307
TAG	ester	TAG48:1-FA14:0	HMDB00806	LMFA01010014	0.0014	1.6524
TAG	ester	TAG48:1-FA16:0	HMDB00220	LMFA01010001	0	2.3024
TAG	ester	TAG48:1-FA16:1	HMDB03229	LMFA01030056	0	2.0993
TAG	ester	TAG48:2-FA14:0	HMDB00806	LMFA01010014	0.0003	2.0681
TAG	ester	TAG48:2-FA16:0	HMDB00220	LMFA01010001	0	2.4097
TAG	ester	TAG48:2-FA16:1	HMDB03229	LMFA01030056	0.0002	2.1387
TAG	ester	TAG48:2-FA18:1	HMDB00207	LMFA01030002	0.0043	2.4021
TAG	ester	TAG48:2-FA18:2	HMDB00673	LMFA01030120	0.0004	1.7146
TAG	ester	TAG49:0-FA18:0	HMDB00827	LMFA01010018	0.8169	-1.0456
TAG	ester	TAG49:1-FA16:0	HMDB00220	LMFA01010001	0.0144	1.1765
TAG	ester	TAG49:1-FA18:1	HMDB00207	LMFA01030002	0.8818	1.0104
TAG	ester	TAG49:2-FA18:2	HMDB00673	LMFA01030120	0.4955	1.0375
TAG	ester	TAG50:0-FA16:0	HMDB00220	LMFA01010001	0.0018	1.3334
TAG	ester	TAG50:0-FA18:0	HMDB00827	LMFA01010018	0.5418	1.0688
TAG	ester	TAG50:1-FA14:0	HMDB00806	LMFA01010014	0.5121	1.1643
TAG	ester	TAG50:1-FA16:0	HMDB00220	LMFA01010001	0	2.0962
TAG	ester	TAG50:1-FA16:1	HMDB03229	LMFA01030056	0	2.2275
TAG	ester	TAG50:1-FA18:0	HMDB00827	LMFA01010018	0.0002	1.8360
TAG	ester	TAG50:1-FA18:1	HMDB00207	LMFA01030002	0	1.9859
TAG	ester	TAG50:2-FA16:0	HMDB00220	LMFA01010001	0	2.2378
TAG	ester	TAG50:2-FA18:0	HMDB00827	LMFA01010018	0.0086	1.3849
TAG	ester	TAG50:2-FA18:1	HMDB00207	LMFA01030002	0.0001	2.1167
TAG	ester	TAG50:2-FA18:2	HMDB00673	LMFA01030120	0	2.1238
TAG	ester	TAG50:3-FA14:0	HMDB00806	LMFA01010014	0	1.4094

TAG	ester	TAG50:3-FA16:0	HMDB00220	LMFA01010001	0	2.6258
TAG	ester	TAG50:3-FA16:1	HMDB03229	LMFA01030056	0	2.6951
TAG	ester	TAG50:3-FA18:1	HMDB00207	LMFA01030002	0	1.6469
TAG	ester	TAG50:3-FA18:2	HMDB00673	LMFA01030120	0	2.3953
TAG	ester	TAG50:3-FA18:3	HMDB01388	LMFA01030152	0	1.9724
TAG	ester	TAG51:1-FA15:0	HMDB00826	LMFA01010015	0.1438	-1.1160
TAG	ester	TAG51:1-FA16:0	HMDB00220	LMFA01010001	0.0114	1.2611
TAG	ester	TAG51:1-FA17:0	HMDB02259	LMFA01010017	0.0282	1.2604
TAG	ester	TAG51:1-FA18:1	HMDB00207	LMFA01030002	0.0439	1.2111
TAG	ester	TAG51:2-FA16:0	HMDB00220	LMFA01010001	0.0008	1.1935
TAG	ester	TAG51:2-FA17:0	HMDB02259	LMFA01010017	0.0041	1.3804
TAG	ester	TAG51:2-FA18:1	HMDB00207	LMFA01030002	0.0269	1.1185
TAG	ester	TAG51:2-FA18:2	HMDB00673	LMFA01030120	0.0073	1.1896
TAG	ester	TAG51:3-FA18:2	HMDB00673	LMFA01030120	0.0001	1.1964
TAG	ester	TAG52:0-FA16:0	HMDB00220	LMFA01010001	0.5222	1.0594
TAG	ester	TAG52:0-FA18:0	HMDB00827	LMFA01010018	0.8685	-1.0097
TAG	ester	TAG52:1-FA16:0	HMDB00220	LMFA01010001	0.0012	1.5527
TAG	ester	TAG52:1-FA18:0	HMDB00827	LMFA01010018	0.0002	1.4803
TAG	ester	TAG52:1-FA20:1	HMDB34296	LMFA01030085	0.0022	1.4764
TAG	ester	TAG52:2-FA16:0	HMDB00220	LMFA01010001	0.0001	1.6476
TAG	ester	TAG52:2-FA16:1	HMDB03229	LMFA01030056	0.0010	1.5790
TAG	ester	TAG52:2-FA18:0	HMDB00827	LMFA01010018	0	1.5811
TAG	ester	TAG52:2-FA18:1	HMDB00207	LMFA01030002	0.0001	1.6501
TAG	ester	TAG52:2-FA18:2	HMDB00673	LMFA01030120	0	1.7220
TAG	ester	TAG52:3-FA16:0	HMDB00220	LMFA01010001	0	1.8585
TAG	ester	TAG52:3-FA16:1	HMDB03229	LMFA01030056	0	1.4995
TAG	ester	TAG52:3-FA18:0	HMDB00827	LMFA01010018	0.0001	1.7777
TAG	ester	TAG52:3-FA18:1	HMDB00207	LMFA01030002	0	1.8097
TAG	ester	TAG52:3-FA18:2	HMDB00673	LMFA01030120	0	1.8607
TAG	ester	TAG52:3-FA18:3	HMDB01388	LMFA01030152	0	1.9434

TAG	ester	TAG52:4-FA16:0	HMDB00220	LMFA01010001	0	1.8831
TAG	ester	TAG52:4-FA16:1	HMDB03229	LMFA01030056	0	1.6238
TAG	ester	TAG52:4-FA18:1	HMDB00207	LMFA01030002	0	1.7904
TAG	ester	TAG52:4-FA18:2	HMDB00673	LMFA01030120	0	1.8564
TAG	ester	TAG52:4-FA18:3	HMDB01388	LMFA01030152	0	2.0427
TAG	ester	TAG52:5-FA16:0	HMDB00220	LMFA01010001	0	2.2426
TAG	ester	TAG52:5-FA16:1	HMDB03229	LMFA01030056	0	1.8668
TAG	ester	TAG52:5-FA18:1	HMDB00207	LMFA01030002	0	2.1052
TAG	ester	TAG52:5-FA18:2	HMDB00673	LMFA01030120	0	1.9317
TAG	ester	TAG52:5-FA18:3	HMDB01388	LMFA01030152	0	2.2679
TAG	ester	TAG52:7-FA16:0	HMDB00220	LMFA01010001	0.0003	1.6292
TAG	ester	TAG53:0-FA16:0	HMDB00220	LMFA01010001	0.0005	1.9670
TAG	ester	TAG53:1-FA16:0	HMDB00220	LMFA01010001	0.0014	1.3435
TAG	ester	TAG53:1-FA18:1	HMDB00207	LMFA01030002	0.0865	1.2004
TAG	ester	TAG53:2-FA16:0	HMDB00220	LMFA01010001	0.0050	1.3691
TAG	ester	TAG53:2-FA18:1	HMDB00207	LMFA01030002	0.0146	1.1721
TAG	ester	TAG53:2-FA18:2	HMDB00673	LMFA01030120	0.0005	1.1844
TAG	ester	TAG53:3-FA17:0	HMDB02259	LMFA01010017	0.0253	1.2126
TAG	ester	TAG54:0-FA16:0	HMDB00220	LMFA01010001	0.9096	-1.0150
TAG	ester	TAG54:0-FA18:0	HMDB00827	LMFA01010018	0.4385	-1.0901
TAG	ester	TAG54:1-FA16:0	HMDB00220	LMFA01010001	0.1593	1.1531
TAG	ester	TAG54:1-FA18:0	HMDB00827	LMFA01010018	0.0217	1.2030
TAG	ester	TAG54:1-FA18:1	HMDB00207	LMFA01030002	0.4447	1.0762
TAG	ester	TAG54:1-FA20:0	HMDB02212	LMFA01010020	0.2081	-1.1256
TAG	ester	TAG54:1-FA20:1	HMDB34296	LMFA01030085	0.0919	1.2757
TAG	ester	TAG54:2-FA18:0	HMDB00827	LMFA01010018	0.0156	1.2356
TAG	ester	TAG54:2-FA18:1	HMDB00207	LMFA01030002	0.0062	1.2895
TAG	ester	TAG54:2-FA18:2	HMDB00673	LMFA01030120	0.6696	1.0370
TAG	ester	TAG54:2-FA20:0	HMDB02212	LMFA01010020	0.8363	-1.0331
TAG	ester	TAG54:2-FA20:1	HMDB34296	LMFA01030085	0.7811	1.0153

TAG	ester	TAG54:2-FA20:2	HMDB05060	LMFA01030130		
TAG	ester	TAG54:3-FA16:0	HMDB00220	LMFA01010001	0.9218	1.0058
TAG	ester	TAG54:3-FA16:1	HMDB03229	LMFA01030056	0.4725	1.0820
TAG	ester	TAG54:3-FA18:0	HMDB00827	LMFA01010018	0.0122	1.2994
TAG	ester	TAG54:3-FA18:1	HMDB00207	LMFA01030002	0.0088	1.3392
TAG	ester	TAG54:3-FA18:2	HMDB00673	LMFA01030120	0.0192	1.1808
TAG	ester	TAG54:3-FA20:1	HMDB34296	LMFA01030085	0.4183	1.0586
TAG	ester	TAG54:3-FA20:2	HMDB05060	LMFA01030130	0.1289	-1.0934
TAG	ester	TAG54:3-FA20:3	HMDB02925	LMFA01030158	0.1983	1.1672
TAG	ester	TAG54:4-FA16:0	HMDB00220	LMFA01010001	0.0682	1.1191
TAG	ester	TAG54:4-FA16:1	HMDB03229	LMFA01030056	0.2125	1.1075
TAG	ester	TAG54:4-FA18:0	HMDB00827	LMFA01010018	0.0843	1.1276
TAG	ester	TAG54:4-FA18:1	HMDB00207	LMFA01030002	0.0019	1.4146
TAG	ester	TAG54:4-FA18:2	HMDB00673	LMFA01030120	0.0062	1.3244
TAG	ester	TAG54:4-FA18:3	HMDB01388	LMFA01030152	0.0531	1.1472
TAG	ester	TAG54:4-FA20:2	HMDB05060	LMFA01030130	0.6341	1.0353
TAG	ester	TAG54:4-FA20:4	HMDB01043	LMFA01030001	0.0016	2.3374
TAG	ester	TAG54:5-FA16:1	HMDB03229	LMFA01030056	0.0467	1.2984
TAG	ester	TAG54:5-FA18:0	HMDB00827	LMFA01010018	0.0008	1.3427
TAG	ester	TAG54:5-FA18:1	HMDB00207	LMFA01030002	0.0030	1.3623
TAG	ester	TAG54:5-FA18:2	HMDB00673	LMFA01030120	0.0049	1.3235
TAG	ester	TAG54:5-FA18:3	HMDB01388	LMFA01030152	0.0004	1.4572
TAG	ester	TAG54:5-FA20:3	HMDB02925	LMFA01030158	0.0002	1.5629
TAG	ester	TAG54:5-FA20:4	HMDB01043	LMFA01030001	0	2.0829
TAG	ester	TAG54:6-FA16:0	HMDB00220	LMFA01010001	0.0002	2.1537
TAG	ester	TAG54:6-FA18:1	HMDB00207	LMFA01030002	0.0008	1.5151
TAG	ester	TAG54:6-FA18:2	HMDB00673	LMFA01030120	0.0397	1.1267
TAG	ester	TAG54:6-FA18:3	HMDB01388	LMFA01030152	0	1.5347
TAG	ester	TAG54:6-FA20:4	HMDB01043	LMFA01030001	0.0003	2.2920
TAG	ester	TAG54:6-FA22:6	HMDB02183	LMFA01030185	0	2.3935

TAG	ester	TAG54:7-FA18:2	HMDB00673	LMFA01030120	0.0002	1.3573
TAG	ester	TAG54:7-FA22:6	HMDB02183	LMFA01030185	0.0002	1.7119
TAG	ester	TAG55:2-FA18:1	HMDB00207	LMFA01030002	0.0037	1.2713
TAG	ester	TAG55:3-FA18:1	HMDB00207	LMFA01030002	0.1562	1.1158
TAG	ester	TAG55:3-FA18:2	HMDB00673	LMFA01030120	0.0272	1.1851
TAG	ester	TAG56:1-FA18:1	HMDB00207	LMFA01030002	0.2067	-1.2459
TAG	ester	TAG56:10-FA18:2	HMDB00673	LMFA01030120	0.0221	1.2505
TAG	ester	TAG56:2-FA16:0	HMDB00220	LMFA01010001	0.2018	-1.1629
TAG	ester	TAG56:2-FA18:0	HMDB00827	LMFA01010018	0.6501	1.0273
TAG	ester	TAG56:2-FA20:0	HMDB02212	LMFA01010020	0.1132	-1.1990
TAG	ester	TAG56:2-FA20:1	HMDB34296	LMFA01030085	0.0018	1.5162
TAG	ester	TAG56:3-FA18:1	HMDB00207	LMFA01030002	0.0843	-1.1965
TAG	ester	TAG56:3-FA18:2	HMDB00673	LMFA01030120	0.0293	-1.2943
TAG	ester	TAG56:3-FA20:0	HMDB02212	LMFA01010020	0.0016	-1.5379
TAG	ester	TAG56:3-FA20:1	HMDB34296	LMFA01030085	0.5477	-1.0456
TAG	ester	TAG56:3-FA20:2	HMDB05060	LMFA01030130		1.1680
TAG	ester	TAG56:4-FA18:0	HMDB00827	LMFA01010018	0.0486	1.3309
TAG	ester	TAG56:4-FA18:1	HMDB00207	LMFA01030002	0.0768	-1.1672
TAG	ester	TAG56:4-FA18:2	HMDB00673	LMFA01030120	0.0273	-1.2395
TAG	ester	TAG56:4-FA20:1	HMDB34296	LMFA01030085	0.2413	-1.0970
TAG	ester	TAG56:4-FA20:2	HMDB05060	LMFA01030130	0.1873	-1.2845
TAG	ester	TAG56:4-FA20:3	HMDB02925	LMFA01030158	0.0052	1.2482
TAG	ester	TAG56:5-FA18:0	HMDB00827	LMFA01010018	0.0122	1.5360
TAG	ester	TAG56:5-FA18:1	HMDB00207	LMFA01030002	0.0428	1.1757
TAG	ester	TAG56:5-FA20:2	HMDB05060	LMFA01030130	0.0403	-1.2503
TAG	ester	TAG56:5-FA20:3	HMDB02925	LMFA01030158	0.0340	1.24
TAG	ester	TAG56:5-FA20:4	HMDB01043	LMFA01030001	0.0022	1.8703
TAG	ester	TAG56:6-FA16:0	HMDB00220	LMFA01010001	0.0031	1.4529
TAG	ester	TAG56:6-FA18:1	HMDB00207	LMFA01030002	0.0070	1.4675
TAG	ester	TAG56:6-FA18:2	HMDB00673	LMFA01030120	0.0122	1.2618

TAG	ester	TAG56:6-FA20:3	HMDB02925	LMFA01030158	0.0281	1.2810
TAG	ester	TAG56:6-FA22:5	HMDB06528	LMFA04000044	0.0051	1.4528
TAG	ester	TAG56:7-FA18:1	HMDB00207	LMFA01030002	0.0030	1.4183
TAG	ester	TAG56:7-FA18:2	HMDB00673	LMFA01030120	0.0041	1.4583
TAG	ester	TAG56:7-FA20:4	HMDB01043	LMFA01030001	0.0011	1.6473
TAG	ester	TAG56:7-FA22:5	HMDB06528	LMFA04000044	0.0016	1.4224
TAG	ester	TAG56:7-FA22:6	HMDB02183	LMFA01030185	0.1458	1.1110
TAG	ester	TAG56:8-FA18:2	HMDB00673	LMFA01030120	0.0091	1.3026
TAG	ester	TAG56:8-FA22:6	HMDB02183	LMFA01030185	0.0525	1.1547
TAG	ester	TAG57:2-FA18:1	HMDB00207	LMFA01030002	0.0614	-1.0945
TAG	ester	TAG58:10-FA18:2	HMDB00673	LMFA01030120	0.1522	-1.1056
TAG	ester	TAG58:3-FA18:1	HMDB00207	LMFA01030002	0.0008	-1.4098
TAG	ester	TAG58:6-FA18:1	HMDB00207	LMFA01030002	0.6548	-1.0396
TAG	ester	TAG58:7-FA22:5	HMDB06528	LMFA04000044	0.5643	1.0492
TAG	ester	TAG58:7-FA22:6	HMDB02183	LMFA01030185	0.7525	-1.0433
TAG	ester	TAG58:8-FA22:6	HMDB02183	LMFA01030185	0.0501	-1.1787
TAG	ester	TAG58:9-FA22:6	HMDB02183	LMFA01030185	0.0555	-1.1770
TAG		total_class			0.0004	1.5629
CE	-	CE(16:0)	HMDB00885	LMST01020005	0.0018	1.2372
HCER	HCER	HCER(24:1)	HMDB04975	LMSP0501AA08	0.0002	1.4442
TAG	ester	TAG48:1-FA18:1	HMDB00207	LMFA01030002	0.0002	1.6157
TAG	ester	TAG48:3-FA16:1	HMDB03229	LMFA01030056	0	2.1444
TAG	ester	TAG50:2-FA14:0	HMDB00806	LMFA01010014	0.0028	1.3574
TAG	ester	TAG50:2-FA16:1	HMDB03229	LMFA01030056	0	2.4460
TAG	ester	TAG50:4-FA16:1	HMDB03229	LMFA01030056	0.0002	2.5163
TAG	ester	TAG50:4-FA18:2	HMDB00673	LMFA01030120	0.0001	1.6762
TAG	ester	TAG51:0-FA16:0	HMDB00220	LMFA01010001	0.0031	1.6545
TAG	ester	TAG51:0-FA17:0	HMDB02259	LMFA01010017		
TAG	ester	TAG51:1-FA18:0	HMDB00827	LMFA01010018	0.8058	1.0969
TAG	ester	TAG51:2-FA16:1	HMDB03229	LMFA01030056	0.0080	1.4328

TAG	ester	TAG51:3-FA15:0	HMDB00826	LMFA01010015	0.0131	1.1356
TAG	ester	TAG52:0-FA20:0	HMDB02212	LMFA01010020		-1.2201
TAG	ester	TAG52:1-FA16:1	HMDB03229	LMFA01030056	0.2985	1.1395
TAG	ester	TAG52:1-FA18:1	HMDB00207	LMFA01030002	0.0002	1.6039
TAG	ester	TAG52:3-FA20:3	HMDB02925	LMFA01030158	0.0237	1.8398
TAG	ester	TAG53:1-FA17:0	HMDB02259	LMFA01010017	0.4093	1.1627
TAG	ester	TAG53:4-FA18:2	HMDB00673	LMFA01030120	0.4614	1.0328
TAG	ester	TAG54:2-FA16:0	HMDB00220	LMFA01010001	0.6987	-1.0291
TAG	ester	TAG54:3-FA18:3	HMDB01388	LMFA01030152		1.0359
TAG	ester	TAG54:4-FA20:3	HMDB02925	LMFA01030158	0.0061	1.3336
TAG	ester	TAG54:6-FA20:5	HMDB01999	LMFA01030759	0.0002	1.6422
TAG	ester	TAG54:7-FA20:5	HMDB01999	LMFA01030759	0.0001	1.7815
TAG	ester	TAG55:1-FA18:1	HMDB00207	LMFA01030002	0.0016	1.2338
TAG	ester	TAG55:4-FA18:1	HMDB00207	LMFA01030002	0.9406	1.0026
TAG	ester	TAG56:3-FA18:0	HMDB00827	LMFA01010018	0.5307	1.0441
TAG	ester	TAG56:5-FA20:1	HMDB34296	LMFA01030085	0.2247	-1.1237
TAG	ester	TAG56:5-FA22:4	HMDB02226	LMFA01030178	0.0734	1.2292
TAG	ester	TAG56:6-FA22:6	HMDB02183	LMFA01030185	0.0114	1.2639
TAG	ester	TAG56:7-FA20:5	HMDB01999	LMFA01030759	0.0121	1.2515
TAG	ester	TAG56:8-FA16:0	HMDB00220	LMFA01010001	0.0249	1.2021
TAG	ester	TAG56:8-FA18:1	HMDB00207	LMFA01030002	0.0091	1.2726
TAG	ester	TAG58:2-FA18:1	HMDB00207	LMFA01030002	0.4923	-1.2408
TAG	ester	TAG58:5-FA18:1	HMDB00207	LMFA01030002		-1.0570
TAG	ester	TAG58:6-FA22:5	HMDB06528	LMFA04000044	0.7116	1.0198
TAG	ester	TAG58:7-FA18:1	HMDB00207	LMFA01030002	0.6858	-1.0342
TAG	ester	TAG58:8-FA18:1	HMDB00207	LMFA01030002	0.1524	-1.1324
CE		total_class			0.0007	1.2682
LPE		total_class			0.6446	1.0535
TAG	ester	TAG46:0-FA14:0	HMDB00806	LMFA01010014	0.5621	-1.0689
TAG	ester	TAG49:2-FA16:0	HMDB00220	LMFA01010001	0.10	1.0668

TAG	ester	TAG51:0-FA18:0	HMDB00827	LMFA01010018	0.0395	1.3276
TAG	ester	TAG51:2-FA15:0	HMDB00826	LMFA01010015	0.1968	1.0420
TAG	ester	TAG54:5-FA16:0	HMDB00220	LMFA01010001	0.0002	1.6343
TAG	ester	TAG56:6-FA20:4	HMDB01043	LMFA01030001	0.0014	1.6555
TAG	ester	TAG56:7-FA18:0	HMDB00827	LMFA01010018	0.0456	1.2485
TAG	ester	TAG56:8-FA20:5	HMDB01999	LMFA01030759	0.0045	1.3303
TAG	ester	TAG58:10-FA22:6	HMDB02183	LMFA01030185	0.1689	-1.0739
TAG	ester	TAG58:6-FA22:4	HMDB02226	LMFA01030178	0.8307	-1.0359
LPE	ester	LPE(18:0)	HMDB11130	LMGP02050001	0.7837	-1.0536
TAG	ester	TAG49:0-FA16:0	HMDB00220	LMFA01010001	0.0534	1.2412
TAG	ester	TAG53:3-FA18:2	HMDB00673	LMFA01030120	0.0151	1.2108
TAG	ester	TAG54:4-FA20:1	HMDB34296	LMFA01030085	0.0655	1.1126
TAG	ester	TAG58:8-FA22:5	HMDB06528	LMFA04000044	0.7457	1.0186
CER	CER	CER(16:0)	HMDB04949	LMSP02010004	0.0296	1.6082
TAG	ester	TAG53:1-FA18:0	HMDB00827	LMFA01010018	0.3870	1.0784
TAG	ester	TAG57:3-FA18:2	HMDB00673	LMFA01030120	0.1839	-1.0810
CE	-	CE(14:1)	HMDB10367	LMST01020021		1.1026
TAG	ester	TAG55:4-FA18:2	HMDB00673	LMFA01030120	0.9377	1.0024
CE	-	CE(15:0)	HMDB60057	LMST01020027	0.6770	1.0361
TAG	ester	TAG46:1-FA18:1	HMDB00207	LMFA01030002		
TAG	ester	TAG50:4-FA18:3	HMDB01388	LMFA01030152	0	2.9447
TAG	ester	TAG52:4-FA20:4	HMDB01043	LMFA01030001	0.0001	2.4617
TAG	ester	TAG56:6-FA18:0	HMDB00827	LMFA01010018	0.0001	1.8559
TAG	ester	TAG56:7-FA16:0	HMDB00220	LMFA01010001	0.0086	1.3015
TAG	ester	TAG56:7-FA20:3	HMDB02925	LMFA01030158	0.0099	1.3443
TAG	ester	TAG58:10-FA20:4	HMDB01043	LMFA01030001	0.0006	1.5778
CE	-	CE(22:6)	HMDB06733	LMST01020019	0.0017	1.3173
TAG	ester	TAG56:6-FA20:2	HMDB05060	LMFA01030130	0.3189	-1.0725
TAG	ester	TAG58:8-FA18:2	HMDB00673	LMFA01030120	0.3507	-1.0692
TAG	ester	TAG53:2-FA17:0	HMDB02259	LMFA01010017	0.7182	1.0315

PE	Ether	PE(O-18:0/18:2)	-	LMGP02020048	0.0232	1.4423
TAG	ester	TAG55:1-FA16:0	HMDB00220	LMFA01010001	0.0088	1.2482
TAG	ester	TAG49:2-FA15:0	HMDB00826	LMFA01010015	0.0793	1.1215
HCER	HCER	HCER(24:0)	HMDB04978	LMSP0501AA09	0.0711	1.2204
CE	-	CE(24:1)	HMDB06728	LMST01020020	0.3022	1.1631
TAG	ester	TAG52:5-FA20:4	HMDB01043	LMFA01030001	0	3.0781
TAG	ester	TAG54:7-FA18:3	HMDB01388	LMFA01030152	0.0001	1.3796
TAG	ester	TAG56:5-FA18:2	HMDB00673	LMFA01030120	0.1831	-1.0982
TAG	ester	TAG58:7-FA18:0	HMDB00827	LMFA01010018	0.7838	-1.0369
PE	Plasmalogen	PE(P-18:0/18:2)	HMDB11376	LMGP02030046	0.0871	1.4883
CE	-	CE(22:1)	HMDB10372	LMST01020025	0.0409	1.3523
TAG	ester	TAG49:2-FA18:1	HMDB00207	LMFA01030002	0.9883	1.0119
TAG	ester	TAG58:9-FA18:2	HMDB00673	LMFA01030120	0.1976	-1.0860
TAG	ester	TAG56:9-FA22:6	HMDB02183	LMFA01030185	0.0593	1.1131
TAG	ester	TAG58:9-FA18:1	HMDB00207	LMFA01030002	0.0511	-1.1481
CE	-	CE(20:0)	HMDB06740	LMST01020010	0.5667	1.0822
HCER	HCER	HCER(16:0)	HMDB04971	LMSP0501AA03	0.0004	1.8107
PC	Ester	PC(16:0/18:3)	HMDB07975	LMGP01010601	0.0154	1.6654
TAG	ester	TAG56:4-FA20:4	HMDB01043	LMFA01030001	0.0181	1.9072
PC	Ester	PC(16:0/16:1)	HMDB07969	LMGP01010566	0.2270	1.2053
DAG		total_class			0.8815	1.0760
PC	Ester	PC(15:0/18:2)	HMDB07940	LMGP01010543	0.3628	-1.1109
TAG	ester	TAG51:4-FA18:2	HMDB00673	LMFA01030120	0.6873	1.0285
CE	-	CE(18:4)	-		0.9674	-1.0016
LPE	ester	LPE(16:0)	HMDB11503	LMGP02050002	0.1155	1.2466
TAG	ester	TAG49:1-FA15:0	HMDB00826	LMFA01010015	0.2075	1.1783

TAG	ester	TAG56:6-FA20:5	HMDB01999	LMFA01030759	0.0501	1.1761
TAG	ester	TAG55:2-FA18:2	HMDB00673	LMFA01030120	0.0281	1.2153
PE	Plasmalogen	PE(P-18:0/18:1)	HMDB11375	LMGP02030004	0.0057	1.5189
CE	-	CE(20:2)	-	LMST01020012	0.6409	1.0351
PC	Ester	PC(15:0/18:1)	HMDB07939	LMGP01011415	0.0741	-1.5984
TAG	ester	TAG55:5-FA18:1	HMDB00207	LMFA01030002	0.1030	1.1869
CER	CER	CER(24:0)	HMDB04956	LMSP02010012	0.5981	-1.0568
DAG	ester	DAG(20:0/20:0)	HMDB07368	LMGL02010117	0.8073	1.0272
PE	Ether	PE(O-18:0/18:1)	-		0.0006	2.1903
TAG	ester	TAG48:3-FA18:2	HMDB00673	LMFA01030120	0.0013	2.7822
PC	Ester	PC(18:0/16:1)	HMDB08035	LMGP01010744	0.9241	-1.0064
PC	Ester	PC(14:0/18:2)	HMDB07874	LMGP01010496	0.4655	1.0880
TAG	ester	TAG58:9-FA20:4	HMDB01043	LMFA01030001	0	1.5810
CE	-	CE(20:5)	HMDB06731	LMST01020015	0.0001	-1.5548
TAG	ester	TAG56:8-FA20:4	HMDB01043	LMFA01030001	0.0008	1.7572
DAG	ester	DAG(16:0/18:1)	HMDB07102	LMGL02010006	0.0060	1.5006
PC	Ester	PC(17:0/18:2)	-	LMGP01011505	0.7899	1.0254
HCER		total_class			0	1.6358
DAG	ester	DAG(18:1/18:2)	HMDB07219	LMGL02010056	0.0024	1.9839
CE	-	CE(22:5)	HMDB10375	LMST01020031	0.0011	1.1964
PE	Ether	PE(O-18:0/22:6)	-	LMGP02020104	0.0130	1.6521
TAG	ester	TAG52:4-FA20:3	HMDB02925	LMFA01030158	0.0002	1.9979
TAG	ester	TAG53:3-FA16:0	HMDB00220	LMFA01010001	0.0025	1.5297
PE	ester	PE(16:0/18:1)	HMDB08927	LMGP02010009	0.8643	-1.0605
TAG	ester	TAG58:8-FA20:4	HMDB01043	LMFA01030001	0.0108	1.3836
CE	-	CE(22:2)	HMDB06737	LMST01020017	0.0509	1.4118

PC	Ester	PC(16:0/16:0)	HMDB00564	LMGP01010564	0.8310	-1.0308
TAG	ester	TAG56:1-FA16:0	HMDB00220	LMFA01010001		1.1825
CE	-	CE(14:0)	HMDB06725	LMST01020004	0.0043	1.3366
PC	Ester	PC(18:2/16:1)	HMDB08134	LMGP01011620	0.9426	-1.0420
PC	Ester	PC(16:0/20:5)	HMDB07984	LMGP01010633	0.6854	-1.0421
LPE	ester	LPE(18:1)	HMDB11476	LMGP02050040	0.5330	-1.1633
PE	ester	PE(16:0/18:2)	HMDB08928	LMGP02010042	0.7879	1.0845
TAG	ester	TAG56:5-FA16:0	HMDB00220	LMFA01010001	0.0171	1.3571
CER		total_class			0.6245	1.0293
PE	ester	PE(18:0/18:2)	HMDB08994	LMGP02010044	0.96	1.0141
CE		CE(22:0)	HMDB06727	LMST01020016	0.9358	1.0001
TAG	ester	TAG49:2-FA16:1	HMDB03229	LMFA01030056	0.1548	-1.2267
PC	Ester	PC(18:2/18:2)	HMDB08138	LMGP01010937	0.0296	-1.3429
PE	Ether	PE(O-18:0/22:4)	-	LMGP02020060	0.0638	1.5533
PC	Ester	PC(16:0/14:0)	HMDB07965	LMGP01010560	0.7964	-1.0611
PC	Ester	PC(16:0/18:2)	HMDB07973	LMGP01010594	0.2009	1.1328
PE	Plasmalogen	PE(P-18:1/18:2)	HMDB11442		0.5810	-1.1313
PC	Ester	PC(18:0/20:0)	HMDB08043	LMGP01010781	0.8352	-1.1127
PE	ester	PE(18:0/18:1)	HMDB08993	LMGP02010036	0.5883	-1.0429
PC	Ester	PC(16:0/22:4)	HMDB07988	LMGP01010642	0.2096	1.2465
FFA	-	FFA(24:0)	HMDB02003	LMFA01010024	0.5281	-1.1683
PC	Ester	PC(18:2/20:3)	HMDB08146	LMGP01011633	0.0509	-1.9116

PE		total_class			0.5879	1.0769
CER	CER	CER(24:1)	HMDB04953	LMSP02010009	0.1421	1.1406
CE	-	CE(22:4)	HMDB06729	LMST01020018	0.0668	1.1553
PE	Plasmalogen	PE(P-18:1/18:1)	HMDB11441		0.7507	1.0842
PC	Ester	PC(17:0/18:1)	-	LMGP01010711	0.9501	-1.0136
DAG	ester	DAG(16:0/18:0)	HMDB07100	LMGL02010020	0.8084	-1.0596
LPE	ester	LPE(20:4)	HMDB11487	LMGP02050051	0.4847	1.2447
PC	Ester	PC(18:0/18:3)	HMDB08040	LMGP01011588	0.1601	1.2530
PE	ester	PE(18:1/18:2)	HMDB09060	LMGP02010048	0.5047	-1.1551
PC	Ester	PC(18:2/20:4)	HMDB08147	LMGP01010943	0.8863	-1.0281
TAG	ester	TAG54:6-FA16:1	HMDB03229	LMFA01030056	0.0001	1.8213
PC	Ester	PC(14:0/18:1)	HMDB07873	LMGP01010492	0.9195	-1.0338
PE	ester	PE(16:0/20:4)	HMDB08937	LMGP02010096	0.3517	1.2666
TAG	ester	TAG60:10-FA22:6	HMDB02183	LMFA01030185	0.0019	-1.3209
SM	sphingomyelin	SM(20:0)	HMDB12102	LMSP03010005	0.0018	1.5033
PC	Ester	PC(14:0/20:4)	HMDB07883	LMGP01010506	0.0067	1.7886
TAG	ester	TAG49:0-FA15:0	HMDB00826	LMFA01010015		
PE	ester	PE(18:1/18:1)	HMDB09059	LMGP02010052	0.0398	-1.3993
FFA	-	FFA(22:6)	HMDB02183	LMFA01030185	0.8623	1.1217
FFA	-	FFA(15:0)	HMDB00826	LMFA01010015	0.7677	-1.0792
PC	Ester	PC(18:2/18:3)	HMDB08141	LMGP01011626	0.3785	-1.1871
PC	Ester	PC(18:1/22:4)	HMDB08120	LMGP01011613		
FFA	-	FFA(20:4)	HMDB01043	LMFA01030001	0.2051	1.7741

LPE	ester	LPE(18:2)	HMDB11477	LMGP02050041	0.8022	-1.0284
PE	Ether	PE(O-18:0/20:3)	-	LMGP02020056	0.0051	1.4319
PE	Plasmalogen	PE(P-18:0/20:4)	HMDB11386		0.0084	1.6477
CER	CER	CER(22:0)	HMDB04952	LMSP02010008	0.7910	-1.0299
TAG	ester	TAG48:3-FA18:1	HMDB00207	LMFA01030002		1.9370
PC	Ester	PC(17:0/22:6)	-	LMGP01010720	0.4233	-1.1715
PE	Plasmalogen	PE(P-16:0/18:1)	HMDB11342		0.0427	1.33
PC	Ester	PC(18:2/22:6)	HMDB08156	LMGP01010947	0.1144	-1.6314
PC	Ester	PC(18:1/22:5)	HMDB08122		0.4763	-1.3395
PC	Ester	PC(18:2/20:2)	HMDB08145	LMGP01011632	0.0078	-2.2545
PE	ester	PE(18:1/20:4)	HMDB09069	LMGP02011196	0.9781	-1.0798
PC	Ester	PC(14:0/20:3)	HMDB07882	LMGP01011374		-1.8683
PC	Ester	PC(18:0/20:1)	HMDB08044	LMGP01010783		1.2618
PC	Ester	PC(20:0/18:1)	HMDB08269	LMGP01011010	0.0068	-2.1161
PC	Ester	PC(20:0/18:2)	HMDB08270	LMGP01011296	0.0163	-2.0056
LPE	ester	LPE(20:1)	HMDB11482	LMGP02050046	0.3452	-1.7375
PC	Ester	PC(18:1/20:1)	HMDB08110	LMGP01011607	0.1504	-1.8166
PE	ester	PE(18:0/20:4)	HMDB09003	LMGP02010118	0.2903	1.2458
PC	Ester	PC(18:0/18:2)	HMDB08039	LMGP01010768	0.7940	-1.0480
LPE	ester	LPE(20:0)	HMDB11511	LMGP02050012		-1.5485
LPC	ester	LPC(20:5)	HMDB10397	LMGP01050050	0.0252	-1.6828

PE	Plasmalogen	PE(P-18:0/22:6)	HMDB11394	LMGP02030005	0.0421	1.5219
FFA	-	FFA(20:3)	HMDB02925	LMFA01030158	0.1666	1.8945
PC	Ester	PC(16:0/18:0)	HMDB07970	LMGP01010573	0.1808	-1.1967
PC	Ester	PC(18:0/20:5)	HMDB08050	LMGP01010805	0.1346	-1.2514
PE	Plasmalogen	PE(P-16:0/18:2)	HMDB11343	LMGP02030094	0.0330	1.4793
PC	Ester	PC(18:1/20:5)	HMDB08116	LMGP01010907	0.2572	-1.2274
PC		total_class			0.9469	-1.1081
FFA	-	FFA(22:4)	HMDB02226	LMFA01030178	0.4642	1.3069
PE	Ether	PE(O-18:0/20:4)	-	LMGP02020092	0.0010	2.2643
TAG	ester	TAG60:12-FA22:6	HMDB02183	LMFA01030185	0.0052	-1.2093
PC	Ester	PC(18:1/16:1)	HMDB08101	LMGP01010887	0.4713	-1.21
HCER	HCER	HCER(22:0)	HMDB04974	LMSP0501AA07	0.0011	1.3860
PC	Ester	PC(16:0/12:0)	-	LMGP01010557	0.6148	-1.3753
PE	ester	PE(18:0/22:6)	HMDB09012	LMGP02010094	0.1260	1.5116
PC	Ester	PC(20:0/20:4)	HMDB08279	LMGP01011023	0.2444	-1.3469
PC	Ester	PC(16:0/18:1)	HMDB07972	LMGP01010005	0.8179	-1.0561
FFA	-	FFA(20:0)	HMDB02212	LMFA01010020	0.8314	1.0781
PC	Ester	PC(16:0/22:5)	HMDB07990	LMGP01010647	0.4365	1.1108
FFA	-	FFA(18:1)	HMDB00207	LMFA01030002	0.0072	3.4394
PE	ester	PE(16:0/22:6)	HMDB08946	LMGP02010095	0.5268	1.3030
SM		total_class			0.2145	1.0978
PC	Ester	PC(18:1/18:3)	HMDB08107	LMGP01010898	0.5301	1.11

SM	sphingomyelin	SM(24:1)	HMDB12107	LMSP03010007	0.3873	-1.0979
LPC	ester	LPC(16:1)	HMDB10383	LMGP01050022	0.3883	-1.2955
FFA	-	FFA(22:5)	HMDB06528	LMFA04000044	0.7131	1.1573
PC	Ester	PC(20:0/20:3)	HMDB08278	LMGP01011799		
PC	Ester	PC(18:1/18:2)	HMDB08105	LMGP01010895	0.3290	-1.1336
PE	Ether	PE(O-18:0/22:5)	-		0.0553	1.7266
PE	Ether	PE(O-16:0/18:1)	HMDB11157		0.0105	1.9174
FFA	-	FFA(22:1)	HMDB02068	LMFA01030089	0.0533	2.8707
LPC	ester	LPC(15:0)	HMDB10381	LMGP01050016	0.1036	-1.3646
PC	Ester	PC(18:1/20:4)	HMDB08114	LMGP01010905	0.0940	1.2988
LPC	ester	LPC(18:2)	-		0.6232	-1.0577
FFA		total_class			0.0153	2.0860
PC	Ester	PC(16:0/20:4)	HMDB07982	LMGP01010007	0.0058	1.8005
PC	Ester	PC(18:2/20:1)	HMDB08144	LMGP01011631	0.1131	-1.4863
LPC	ester	LPC(20:0)	HMDB10390	LMGP01050045	0.0151	-2.0214
PE	Plasmalogen	PE(P-18:0/22:5)	HMDB11393		0.1361	1.6044
FFA	-	FFA(14:0)	HMDB00806	LMFA01010014	0.3251	1.2722
PC	Ester	PC(20:0/14:1)	HMDB08263	LMGP01011787	0.7453	1.0369
LPC	ester	LPC(18:3)	HMDB10388	LMGP01050038	0.4059	1.0839
FFA	-	FFA(17:0)	HMDB02259	LMFA01010017	0.8932	1.0357
PC	Ester	PC(17:0/20:4)	-	LMGP01010003	0.2941	1.1753
LPE	ester	LPE(20:3)	HMDB11486	LMGP02050050	0.5933	-1.3047

PE	Plasmalogen	PE(P-16:0/22:6)	-	LMGP02030001	0.0241	1.44
PC	Ester	PC(16:0/20:2)	HMDB07979	LMGP01011469	0.0094	-1.8406
PE	Plasmalogen	PE(P-18:0/22:4)	HMDB11391	LMGP02030061	0.2568	1.4003
FFA	-	FFA(18:0)	HMDB00827	LMFA01010018	0.1985	1.6678
PC	Ester	PC(18:0/22:6)	HMDB08057	LMGP01010821	0.5266	1.0719
PE	ester	PE(18:1/22:6)	HMDB09078	LMGP02011264	0.9667	1.0379
PC	Ester	PC(18:0/18:1)	HMDB08038	LMGP01010761	0.3254	-1.1403
PC	Ester	PC(18:0/20:3)	HMDB08047	LMGP01010799	0.1157	-1.5862
PE	Ether	PE(O-16:0/20:4)	-	LMGP02020095	0.0058	1.9160
PC	Ester	PC(18:1/20:2)	HMDB08111	LMGP01011608	0.0306	-1.9880
PC	Ester	PC(18:1/18:1)	HMDB00593	LMGP01010890	0.3863	-1.2219
SM	sphingomyelin	SM(16:0)	HMDB10169	LMSP03010003	0.0088	1.2961
SM	sphingomyelin	SM(26:0)	HMDB11698	LMSP03010010	0.0699	1.4238
SM	sphingomyelin	SM(20:1)	-	LMSP03010059	0.0240	1.6423
PE	ester	PE(16:0/20:3)	HMDB08936	LMGP02011222	0.3302	-1.3611
LPE	ester	LPE(20:2)	HMDB11483	LMGP02050047	0.1438	-1.8889
LPE	ester	LPE(22:4)	HMDB11493	LMGP02050057		2.2135
SM	sphingomyelin	SM(14:0)	HMDB12097	LMSP03010028	0.0173	1.5232
PC	Ester	PC(18:0/22:5)	HMDB08056	LMGP01010818	0.6011	-1.1403
FFA	-	FFA(20:2)	HMDB05060	LMFA01030130	0.1177	1.8513

FFA	-	FFA(22:0)	HMDB00944	LMFA01010022	0.3563	1.3035
PE	Plasmalogen	PE(P-16:0/20:4)	HMDB11353		0.0024	1.6857
PC	Ester	PC(18:1/22:6)	HMDB08123	LMGP01010913	0.8198	-1.1009
LPC	ester	LPC(22:5)	HMDB10403	LMGP01050143	0.6976	-1.1565
PC	Ester	PC(16:0/20:3)	HMDB07981	LMGP01010627	0.1493	-1.4124
PE	ester	PE(18:0/20:3)	HMDB11382	LMGP02011202	0.0703	-1.4792
PE	Plasmalogen	PE(P-18:0/20:3)	HMDB11384	LMGP02030055	0.4398	1.1333
FFA	-	FFA(20:5)	HMDB01999	LMFA01030759	0.1812	1.9498
CER	CER	CER(20:0)	HMDB04951	LMSP02010007		
LPC	ester	LPC(18:0)	HMDB10384	LMGP01050026	0.0688	-1.3263
TAG	ester	TAG55:7-FA15:0	HMDB00826	LMFA01010015	0.9763	1.0031
PC	Ester	PC(16:0/22:6)	HMDB07991	LMGP01012137	0.0708	1.34
FFA	-	FFA(12:0)	HMDB00638	LMFA01010012	0.5280	-1.2501
CER	CER	CER(22:1)	HMDB11775			
FFA	-	FFA(20:1)	HMDB34296	LMFA01030085	0.3181	1.3465
FFA	-	FFA(18:3)	HMDB01388	LMFA01030152	0.0201	2.7736
SM	sphingomyelin	SM(26:1)	-	LMSP03010009	0.6098	1.2307
LPC	ester	LPC(18:1)	-	LMGP01050082	0.2350	-1.3692
LPC		total_class			0.2765	-1.1742
LPC	ester	LPC(20:4)	HMDB10395	LMGP01050121	0.1079	1.3791
PE	ester	PE(18:0/22:5)	HMDB09011		0.2184	1.3584
LPC	ester	LPC(14:0)	HMDB10379	LMGP01050012	0.4032	-1.2372
PC	Ester	PC(16:0/20:1)	HMDB07978	LMGP01011468	0.2678	-1.3024

PC	Ester	PC(18:0/20:4)	HMDB08048	LMGP01010802	0.0211	1.5845
PE	Ether	PE(O-16:0/18:2)	-	LMGP02020098	0.0278	1.5574
PE	Plasmalogen	PE(P-18:1/22:4)	HMDB11424			
PC	Ester	PC(18:0/22:4)	HMDB08054	LMGP01010813	0.9240	1.0066
PE	Plasmalogen	PE(P-18:1/22:6)	HMDB11460	LMGP02030006	0.4338	1.1327
FFA	-	FFA(24:1)	HMDB02368	LMFA01030092	0.8657	1.0686
PE	Plasmalogen	PE(P-18:1/20:4)	HMDB11451		0.0655	1.3006
SM	sphingomyelin	SM(24:0)	HMDB11697	LMSP03010008	0.0897	-1.1549
PE	Plasmalogen	PE(P-18:1/22:5)	HMDB11459		0.1022	1.2246
PE	ester	PE(18:1/20:3)	HMDB09068	LMGP02010648	0.1445	-1.7266
PE	Plasmalogen	PE(P-16:0/20:3)	HMDB11351		0.0384	1.3533
LPC	ester	LPC(20:2)	HMDB10392	LMGP01050132	0.0105	-2.8886
LPC	ester	LPC(17:0)	-	LMGP01050024	0.0374	-1.3932
LPC	ester	LPC(22:4)	HMDB10401	LMGP01050124		1.8362
FFA	-	FFA(16:0)	HMDB00220	LMFA01010001	0.3630	1.3708
LPC	ester	LPC(22:6)	HMDB10404	LMGP01050056	0.6930	1.0573
PE	Ether	PE(O-16:0/22:6)	-	LMGP02020020	0.0211	1.7354
LPC	ester	LPC(20:3)	HMDB10394	LMGP01050133	0.10	-1.7941
SM	sphingomyelin	SM(22:1)	HMDB12104	LMSP03010072	0.5796	-1.1196
FFA	-	FFA(18:4)	HMDB06547	LMFA01030355	0.0551	2.5266
PE	Ether	PE(O-16:0/22:5)	-	LMGP02020007	0.1220	1.7631
LPC	ester	LPC(16:0)	HMDB10382	LMGP01050018	0.2397	-1.1827

PC	Ester	PC(18:0/18:0)	HMDB08036	LMGP01010006	0.2644	-1.1480
LPE	ester	LPE(22:6)	HMDB11496	LMGP02050060	0.1907	1.6375
SM	sphingomyelin	SM(18:1)	HMDB12101	LMSP03010029	0.0008	1.7417
SM	sphingomyelin	SM(18:0)	HMDB01348	LMSP03010001	0.0001	1.7874
LPC	ester	LPC(20:1)	HMDB10391	LMGP01050131	0.0511	-2.1016
PE	ester	PE(18:0/18:0)	HMDB08991	LMGP02010097	0.0185	1.4544
FFA	-	FFA(22:2)	HMDB61714	LMFA01030405	0.1883	1.9635
FFA	-	FFA(14:1)	HMDB02000	LMFA01030051	0.1459	1.38
PC	Ester	PC(18:1/20:3)	HMDB08113	LMGP01011609	0.0737	-1.7140
PE	Plasmalogen	PE(P-16:0/22:5)	HMDB11360		0.2588	1.3445
SM	sphingomyelin	SM(22:0)	HMDB12103	LMSP03010006	0.2438	-1.1421
PC	Ester	PC(18:0/20:2)	HMDB08045	LMGP01010788	0.0418	-1.8109
PE	Ether	PE(O-16:0/22:4)	-	LMGP02020006		2.0248
PE	Plasmalogen	PE(P-18:1/16:0)	HMDB11437		0.6078	1.0832
PE	Plasmalogen	PE(P-16:0/22:4)	HMDB11358	LMGP02030033	0.0591	1.4431
CE	-	CE(18:2)	HMDB00610	LMST01020008	0.0002	1.0881
FFA	-	FFA(18:2)	HMDB00673	LMFA01030120	0.0079	3.6808
PE	ester	PE(18:0/20:2)	HMDB09000	LMGP02010124		1.5080
PC	Ester	PC(17:0/20:3)	-	LMGP01011514	0.0232	-1.3636
FFA	-	FFA(16:1)	HMDB03229	LMFA01030056	0.0024	2.7714

Bibliography

1. JJ, R. *et al.* The WHO classification of pulmonary hypertension: A case-based imaging compendium. *Pulm. Circ.* **2**, 107–121 (2012).
2. G, S. *et al.* Updated clinical classification of pulmonary hypertension. *J. Am. Coll. Cardiol.* **54**, (2009).
3. SA, M., HS, M. & A, V. Pulmonary Hypertension: A Brief Guide for Clinicians. *Mayo Clin. Proc.* **95**, 1978–1988 (2020).
4. Shults, N. V *et al.* Ultrastructural Changes of the Right Ventricular Myocytes in. *J. Am. Heart Assoc.* 16–18 (2019). doi:10.1161/JAHA.118.011227
5. Maarman, G., Lecour, S., Thienemann, F., Sliwa, K. & Butrous, G. A Comprehensive Review: The Evolution of Animal Models in Pulmonary Hypertension Research; Are We there Yet? *Pulm. Circ.* **3**, 739–756 (2014).
6. Sharma, S. *et al.* Role of Oxidized Lipids in Pulmonary Arterial Hypertension. *Pulm. Circ.* **6**, 261–273 (2016).
7. T Lau, E. M., Giannoulatou, E., Celermajer, D. S. & Humbert, M. Epidemiology and treatment of pulmonary arterial hypertension. *Nat. Publ. Gr.* **14**, (2017).
8. JS, C. *et al.* Balloon atrial septostomy in pulmonary arterial hypertension: effect on survival and associated outcomes. *J. Heart Lung Transplant.* **34**, 376–380 (2015).
9. KR, S., B, M., N, G., WJ, M. & IF, M. Animal models of pulmonary arterial hypertension: the hope for etiological discovery and pharmacological cure. *Am. J. Physiol. Lung Cell. Mol. Physiol.* **297**, (2009).
10. Zhao, L. Chronic hypoxia-induced pulmonary hypertension in rat: The best animal model for studying pulmonary vasoconstriction and vascular medial hypertrophy. *Drug Discov. Today Dis. Model.* **7**, 83–88 (2010).
11. Sharma, S. *et al.* Apolipoprotein A-I mimetic peptide 4f rescues pulmonary hypertension by inducing MicroRNA-193-3p. *Circulation* **130**, 776–785 (2014).
12. Warburton, R. R. *et al.* Plasma 12- and 15-Hydroxyeicosanoids are Predictors of Survival in Pulmonary Arterial Hypertension. *Pulm. Circ.* **6**, 224–233 (2016).
13. R, B. *et al.* Oxidative stress in severe pulmonary hypertension. *Am. J. Respir. Crit. Care Med.* **169**, 764–769 (2004).
14. Saini, R. K. & Keum, Y. S. Omega-3 and omega-6 polyunsaturated fatty acids: Dietary sources, metabolism, and significance — A review. *Life Sci.* **203**, 255–267 (2018).
15. Whelan, J. & Fritsche, K. Linoleic Acid. *Adv. Nutr.* **4**, 311 (2013).
16. Powell, W. S. & Rokach, J. Biosynthesis, biological effects, and receptors of hydroxyeicosatetraenoic acids (HETEs) and oxoeicosatetraenoic acids (oxo-ETEs) derived from arachidonic acid. *Biochim. Biophys. Acta* **1851**, 340 (2015).
17. Martin, S. A., Brash, A. R. & Murphy, R. C. The discovery and early structural studies of arachidonic acid. *J. Lipid Res.* **57**, 1126–1132 (2016).
18. Vangaveti, V., Baune, B. T. & Kennedy, R. L. Hydroxyoctadecadienoic acids: novel regulators of macrophage differentiation and atherogenesis. *Ther. Adv. Endocrinol. Metab.* **1**, 51 (2010).
19. Imaizumi, S. *et al.* L-4F Differentially Alters Plasma Levels of Oxidized Fatty Acids Resulting in more Anti-Inflammatory HDL in Mice. *Drug Metab. Lett.* **4**, 139 (2010).

20. Harats, D. *et al.* Overexpression of 15-Lipoxygenase in Vascular Endothelium Accelerates Early Atherosclerosis in LDL Receptor–Deficient Mice. *Arterioscler. Thromb. Vasc. Biol.* **20**, 2100–2105 (2000).
21. IR, P., NS, H., RR, W. & BL, F. Role of 12-lipoxygenase in hypoxia-induced rat pulmonary artery smooth muscle cell proliferation. *Am. J. Physiol. Lung Cell. Mol. Physiol.* **290**, (2006).
22. C, M. *et al.* Key role of 15-lipoxygenase/15-hydroxyeicosatetraenoic acid in pulmonary vascular remodeling and vascular angiogenesis associated with hypoxic pulmonary hypertension. *Hypertens. (Dallas, Tex. 1979)* **58**, 679–688 (2011).
23. Yu, X. *et al.* Modulation of pulmonary vascular remodeling in hypoxia: Role of 15-LOX-2/15-HETE-MAPKs pathway. *Cell. Physiol. Biochem.* **35**, 2079–2097 (2015).
24. L, Z. *et al.* 15-LO/15-HETE mediated vascular adventitia fibrosis via p38 MAPK-dependent TGF-β. *J. Cell. Physiol.* **229**, 245–257 (2014).
25. T, H. *et al.* Low HDL cholesterol is associated with the risk of stroke in elderly diabetic individuals: changes in the risk for atherosclerotic diseases at various ages. *Diabetes Care* **32**, 1221–1223 (2009).
26. SM, T., MS, S., PP, T. & WE, B. HDL hypothesis: where do we stand now? *Curr. Atheroscler. Rep.* **16**, (2014).
27. Bartlett, J. *et al.* Is Isolated Low HDL-C a CVD Risk Factor?: New Insights from the Framingham Offspring Study. *Circ. Cardiovasc. Qual. Outcomes* **9**, 206 (2016).
28. EM, G., DM, F., AV, B., X, Y. & SJ, L. High-density Lipoproteins and Apolipoprotein A-I: Potential New Players in the Prevention and Treatment of Lung Disease. *Front. Pharmacol.* **7**, (2016).
29. Assmann, G. & Antonio M. Gotto, J. HDL Cholesterol and Protective Factors in Atherosclerosis. *Circulation* **109**, (2004).
30. Reddy, S. T., Navab, M., Anantharamaiah, G. M. & Fogelman, A. M. Apolipoprotein A-I Mimetics. *Curr. Opin. Lipidol.* **25**, 304–308 (2014).
31. Georgila, K., Vyrla, D. & Drakos, E. Apolipoprotein A-I (ApoA-I), Immunity, Inflammation and Cancer. *Cancers (Basel).* **11**, (2019).
32. Lenten, B. J. Van *et al.* Anti-inflammatory apoA-I-mimetic peptides bind oxidized lipids with much higher affinity than human apoA-I. *J. Lipid Res.* **49**, 2302 (2008).
33. SC, D., A, C., JC, E.-G., AM, F. & ST, R. Apolipoprotein mimetics in cancer. *Semin. Cancer Biol.* **73**, 158–168 (2021).
34. Morgantini, C. *et al.* Anti-inflammatory and Antioxidant Properties of HDLs Are Impaired in Type 2 Diabetes. *Diabetes* **60**, 2617 (2011).
35. Morgantini, C. *et al.* Apolipoprotein A-I Mimetic Peptides Prevent Atherosclerosis Development and Reduce Plaque Inflammation in a Murine Model of Diabetes. *Diabetes* **59**, 3223–3228 (2010).
36. Kelesidis Theodoros, Madhav Sharma, Petcherski Anton, Christelle Hugo, O'Connor Ellen, Eleni Ritou, Shirihai Orian S, R. S. T. The ApoA-I mimetic peptide 4F attenuates in vitro replication of SARS-CoV-2, associated apoptosis, oxidative stress and inflammation in epithelial cells. *Virulence* (Accepted as of July, 2021).
37. Flores, S. C. *et al.* Oxidative Stress in Severe Pulmonary Hypertension. *Am. J. Respir. Crit. Care Med.* **169**, 764–769 (2004).

38. Fallah, F. Recent Strategies in Treatment of Pulmonary Arterial Hypertension, A Review. *Glob. J. Health Sci.* **7**, 307–322 (2015).
39. Naruhn, S. *et al.* 15-Hydroxyeicosatetraenoic Acid Is a Preferential Peroxisome Proliferator-Activated Receptor / Agonist. *Mol. Pharmacol.* **77**, 171–184 (2009).
40. Yokomizo, T., Kato, K., Hagiya, H., Izumi, T. & Shimizu, T. Hydroxyeicosanoids Bind to and Activate the Low Affinity Leukotriene B 4 Receptor, BLT2. *J. Biol. Chem.* **276**, 12454–12459 (2002).
41. Thursby, E. & Juge, N. Introduction to the human gut microbiota. *Biochem. J.* **474**, 1823 (2017).
42. Yang, T. *et al.* Gut Dysbiosis is Linked to Hypertension. *Hypertension* **65**, 1331–1340 (2015).
43. Schoeler, M. & Caesar, R. Dietary lipids, gut microbiota and lipid metabolism. *Rev. Endocr. Metab. Disord.* **20**, 461–472 (2019).
44. Durack, J. & Lynch, S. V. The gut microbiome: Relationships with disease and opportunities for therapy. *J. Exp. Med.* **216**, 20–40 (2019).
45. RC, S. *et al.* The TMAO-Producing Enzyme Flavin-Containing Monooxygenase 3 Regulates Obesity and the Beiging of White Adipose Tissue. *Cell Rep.* **19**, 2451–2461 (2017).
46. Vinolo, M. A. R., Rodrigues, H. G., Nachbar, R. T. & Curi, R. Regulation of inflammation by short chain fatty acids. *Nutrients* **3**, 858–876 (2011).
47. Tedelind, S., Westberg, F., Kjerrulf, M. & Vidal, A. Anti-inflammatory properties of the short-chain fatty acids acetate and propionate: A study with relevance to inflammatory bowel disease. *World J. Gastroenterol.* **13**, 2826–2832 (2007).
48. Canani, R. B. *et al.* Potential beneficial effects of butyrate in intestinal and extraintestinal diseases. *World J. Gastroenterol.* **17**, 1519–1528 (2011).
49. Chemudupati, M. *et al.* Butyrate Reprograms Expression of Specific Interferon-Stimulated Genes. *J. Virol.* **94**, (2020).
50. Kim, S. *et al.* Altered gut microbiome profile in patients with pulmonary arterial hypertension. *Hypertension* 1063–1071 (2020). doi:10.1161/HYPERTENSIONAHA.119.14294
51. Wang, L. *et al.* Sodium butyrate suppresses angiotensin II-induced hypertension by inhibition of renal (pro)renin receptor and intrarenal renin-Angiotensin system. *J. Hypertens.* **35**, 1899–1908 (2017).
52. Jose, P. A. & Raj, D. Gut microbiota in hypertension. *Curr Opin Nephrol Hypertens* **24**, 405–409
53. Callejo, M. *et al.* Pulmonary Arterial Hypertension Affects the Rat Gut Microbiome. *Sci. Rep.* **8**, (2018).
54. Ruffenach, G. *et al.* Oral 15-Hydroxyeicosatetraenoic Acid Induces Pulmonary Hypertension in Mice by Triggering T Cell-Dependent Endothelial Cell Apoptosis. *Hypertension* 985–996 (2020). doi:10.1161/HYPERTENSIONAHA.120.14697
55. M, V., G, R., J, M. & S, B. Adaptation and remodelling of the pulmonary circulation in pulmonary hypertension. *Can. J. Cardiol.* **31**, 407–415 (2015).
56. G, R. *et al.* Role for Runt-related Transcription Factor 2 in Proliferative and Calcified Vascular Lesions in Pulmonary Arterial Hypertension. *Am. J. Respir. Crit. Care Med.* **194**, 1273–1285 (2016).
57. N, A. *et al.* Histological analysis of vasculopathy associated with pulmonary

hypertension in combined pulmonary fibrosis and emphysema: comparison with idiopathic pulmonary fibrosis or emphysema alone. *Histopathology* **70**, 896–905 (2017).
58. F, P. *et al.* Downregulation of MicroRNA-126 Contributes to the Failing Right Ventricle in Pulmonary Arterial Hypertension. *Circulation* **132**, 932–943 (2015).
59. P, H., M, H. & U, D. Formation of 15-HETE as a major hydroxyeicosatetraenoic acid in the atherosclerotic vessel wall. *Biochim. Biophys. Acta* **834**, 272–274 (1985).
60. DJ, R. *et al.* Proinflammatory high-density lipoprotein results from oxidized lipid mediators in the pathogenesis of both idiopathic and associated types of pulmonary arterial hypertension. *Pulm. Circ.* **5**, 640–648 (2015).
61. R, S. *et al.* Hypoxia promotes rabbit pulmonary artery smooth muscle cells proliferation through a 15-LOX-2 product 15(S)-hydroxyeicosatetraenoic acid. *Prostaglandins. Leukot. Essent. Fatty Acids* **86**, 85–90 (2012).
62. L, Z. *et al.* Platelet-derived growth factor (PDGF) induces pulmonary vascular remodeling through 15-LO/15-HETE pathway under hypoxic condition. *Cell. Signal.* **24**, 1931–1939 (2012).
63. Chattopadhyay, A. *et al.* A novel approach to oral apoA-I mimetic therapy. *J. Lipid Res.* **54**, 995–1010 (2013).
64. P, M. *et al.* Transgenic tomatoes expressing the 6F peptide and ezetimibe prevent diet-induced increases of IFN-β and cholesterol 25-hydroxylase in jejunum. *J. Lipid Res.* **58**, 1636–1647 (2017).
65. Chattopadhyay, A. *et al.* Treating the Intestine with Oral ApoA-I Mimetic Tg6F Reduces Tumor Burden in Mouse Models of Metastatic Lung Cancer. *Sci. Rep.* **8**, 1–12 (2018).
66. Meriwether, D. *et al.* ApoA-I mimetic therapies inhibit IBD in COX-2 dependent mouse models. Manuscript in review (2019).
67. L, T.-S. *et al.* Inhibition of the VEGF receptor 2 combined with chronic hypoxia causes cell death-dependent pulmonary endothelial cell proliferation and severe pulmonary hypertension. *FASEB J.* **15**, 427–438 (2001).
68. S, S. *et al.* Initial apoptosis is followed by increased proliferation of apoptosis-resistant endothelial cells. *FASEB J.* **19**, 1178–1180 (2005).
69. Navab, M. *et al.* D-4F-mediated reduction in metabolites of arachidonic and linoleic acids in the small intestine is associated with decreased inflammation in low-density lipoprotein receptor-null mice. *J. Lipid Res.* **53**, 437–445 (2012).
70. BJ, V. L. *et al.* Multiple indications for anti-inflammatory apolipoprotein mimetic peptides. *Curr. Opin. Investig. Drugs* **9**, 1157–1162 (2008).
71. M, H., P, H. & K, R. Identification of 15-hydroxy-5,8,11,13-eicosatetraenoic acid (15-HETE) as a major metabolite of arachidonic acid in human lung. *Acta Physiol. Scand.* **110**, 219–221 (1980).
72. T, S. *et al.* Positive feedback-loop of telomerase reverse transcriptase and 15-lipoxygenase-2 promotes pulmonary hypertension. *PLoS One* **8**, (2013).
73. A, A.-H. *et al.* Increased eicosanoid levels in the Sugen/chronic hypoxia model of severe pulmonary hypertension. *PLoS One* **10**, (2015).
74. AC, O. *et al.* Chemokine signaling axis between endothelial and myeloid cells regulates development of pulmonary hypertension associated with pulmonary

fibrosis and hypoxia. *Am. J. Physiol. Lung Cell. Mol. Physiol.* **317**, L434–L444 (2019).
75. Y, L. *et al.* 15-HETE suppresses K(+) channel activity and inhibits apoptosis in pulmonary artery smooth muscle cells. *Apoptosis* **14**, 42–51 (2009).
76. 倩李 *et al.* Kv3.4 通道参与 15-羟二十碳四烯酸诱导的大鼠肺动脉收缩 Kv3.4 channel is involved in rat pulmonary vasoconstriction induced by 15-hydroxyeicosatetraenoic acid. *生理学报 Acta Physiol. Sin.* **58**, 77–82 (2006).
77. X, C. *et al.* Hypoxia suppresses KV1.5 channel expression through endogenous 15-HETE in rat pulmonary artery. *Prostaglandins Other Lipid Mediat.* **88**, 42–50 (2009).
78. MR, N. & NF, V. The Roles of Immunity in the Prevention and Evolution of Pulmonary Arterial Hypertension. *Am. J. Respir. Crit. Care Med.* **195**, 1292–1299 (2017).
79. E, D. *et al.* Pulmonary arterial remodeling induced by a Th2 immune response. *J. Exp. Med.* **205**, 361–372 (2008).
80. R, S. *et al.* Immune and inflammatory cell involvement in the pathology of idiopathic pulmonary arterial hypertension. *Am. J. Respir. Crit. Care Med.* **186**, 897–908 (2012).
81. R, T. *et al.* Dominant Role for Regulatory T Cells in Protecting Females Against Pulmonary Hypertension. *Circ. Res.* **122**, 1689–1702 (2018).
82. JD, S. Apolipoprotein A-I and its mimetics for the treatment of atherosclerosis. *Curr. Opin. Investig. Drugs* **11**, 989–996 (2010).
83. K, W. *et al.* Endothelial apoptosis in pulmonary hypertension is controlled by a microRNA/programmed cell death 4/caspase-3 axis. *Hypertens. (Dallas, Tex. 1979)* **64**, 185–194 (2014).
84. Z, C., SM, H. & AV, G. Identification of the immunoproteasome as a novel regulator of skeletal muscle differentiation. *Mol. Cell. Biol.* **34**, 96–109 (2014).
85. GA, H., M, A., J, N., J, D. & RA, D. Plasma levels of high-density lipoprotein cholesterol and outcomes in pulmonary arterial hypertension. *Am. J. Respir. Crit. Care Med.* **182**, 661–668 (2010).
86. B, S. & JW, H. HDL, lipid peroxidation, and atherosclerosis. *J. Lipid Res.* **50**, 599–601 (2009).
87. L, D. *et al.* The apolipoprotein A-I mimetic peptide 4F prevents defects in vascular function in endotoxemic rats. *J. Lipid Res.* **51**, 2695–2705 (2010).
88. Meriwether, D. *et al.* Transintestinal transport of the anti-inflammatory drug 4F and the modulation of transintestinal cholesterol efflux. *J. Lipid Res.* **57**, 1175–1193 (2016).
89. Navab, M. *et al.* High-density lipoprotein and 4F peptide reduce systemic inflammation by modulating intestinal and lipid metabolism: novel hypotheses and review of literature. *Atheriosclerosis, Thromb. Vasc. Biol.* **32**, 2553–2560 (2012).
90. Chattopadhyay, A. *et al.* Efficacy of tomato concentrates in mouse models of dyslipidemia and cancer. *Pharmacol. Res. Perspect.* **3**, 1–13 (2015).
91. Umar, S. *et al.* Involvement of Low-Density Lipoprotein Receptor in the Pathogenesis of Pulmonary Hypertension. *J. Am. Heart Assoc.* **9**, (2020).
92. LL, B. *et al.* Cholesterol-Independent Suppression of Lymphocyte Activation,

Autoimmunity, and Glomerulonephritis by Apolipoprotein A-I in Normocholesterolemic Lupus-Prone Mice. *J. Immunol.* **195**, 4685–4698 (2015).
93. M, N., GM, A., ST, R., BJ, V. L. & AM, F. Apo A-1 mimetic peptides as atheroprotective agents in murine models. *Curr. Drug Targets* **9**, 204–209 (2008).
94. LR, B. *et al.* Intestinal ABCA1 directly contributes to HDL biogenesis in vivo. *J. Clin. Invest.* **116**, 1052–1062 (2006).
95. Rabinovitch, M. Molecular Pathogenesis of Pulmonary Arterial Hypertension. *J. Clin. Invest.* **122**, 4306–4313 (2012).
96. G, H. *et al.* An antiproliferative BMP-2/PPARgamma/apoE axis in human and murine SMCs and its role in pulmonary hypertension. *J. Clin. Invest.* **118**, 1846–1857 (2008).
97. G, H. *et al.* Pulmonary arterial hypertension is linked to insulin resistance and reversed by peroxisome proliferator-activated receptor-gamma activation. *Circulation* **115**, 1275–1284 (2007).
98. L, L. *et al.* LRH-1 mediates anti-inflammatory and antifungal phenotype of IL-13-activated macrophages through the PPARγ ligand synthesis. *Nat. Commun.* **6**, (2015).
99. CJ, R. *et al.* Genetic determinants of risk in pulmonary arterial hypertension: international genome-wide association studies and meta-analysis. *Lancet. Respir. Med.* **7**, 227–238 (2019).
100. A, L. *et al.* The Molecular Signatures Database (MSigDB) hallmark gene set collection. *Cell Syst.* **1**, 417–425 (2015).
101. D, S. *et al.* The STRING database in 2017: quality-controlled protein-protein association networks, made broadly accessible. *Nucleic Acids Res.* **45**, D362–D368 (2017).
102. D, S. *et al.* STRING v11: protein-protein association networks with increased coverage, supporting functional discovery in genome-wide experimental datasets. *Nucleic Acids Res.* **47**, D607–D613 (2019).
103. Jonas, K., Magoń, W., Podolec, P. & Kopeć, G. Triglyceride-to-High-Density Lipoprotein Cholesterol Ratio and Systemic Inflammation in Patients with Idiopathic Pulmonary Arterial Hypertension. *Med. Sci. Monit.* **25**, 746 (2019).
104. Talati, M. & Hemnes, A. Fatty acid metabolism in pulmonary arterial hypertension: role in right ventricular dysfunction and hypertrophy. *Pulm. Circ.* **5**, 269 (2015).
105. Hemnes, A. R. *et al.* Fatty Acid Metabolic Defects and Right Ventricular Lipotoxicity in Human Pulmonary Arterial Hypertension. *Circulation* **133**, 1936–1944 (2016).
106. Groth, A. *et al.* Inflammatory cytokines in pulmonary hypertension. *Respir. Res.* **15**, 47 (2014).
107. Soon, E. *et al.* Elevated Levels of Inflammatory Cytokines Predict Survival in Idiopathic and Familial Pulmonary Arterial Hypertension. *Circulation* **122**, 920–927 (2010).
108. Nakaoka, Y., Inagaki, T. & Shirai, M. Inflammatory Cytokines in the Pathogenesis of Pulmonary Arterial Hypertension. *Mol. Mech. Congenit. Hear. Dis. Pulm. Hypertens.* 157–161 (2020). doi:10.1007/978-981-15-1185-1_20
109. Kim, K. & Choi, J.-H. Involvement of immune responses in pulmonary arterial hypertension; lessons from rodent models. *Lab. Anim. Res.* **35**, (2019).

110. Voelkel, N. F. *et al.* Inhibition of 5-Lipoxygenase – activating Protein (FLAP) Reduces Pulmonary Vascular Reactivity and Pulmonary Hypertension in Hypoxic Rats. *J. Clin. Invest.* **97**, 2491–2498 (1996).
111. Cyrus, T. *et al.* Disruption of the 12/15-lipoxygenase gene diminishes atherosclerosis in apo E–deficient mice. *J. Clin. Invest.* **103**, 1597 (1999).
112. Rossaint, J., Nadler, J. L., Ley, K. & Zarbock, A. Eliminating or blocking 12/15-lipoxygenase reduces neutrophil recruitment in mouse models of acute lung injury. *Crit. Care 2012 165* **16**, 1–15 (2012).
113. Izquierdo-Garcia, J. L. *et al.* Metabolic Reprogramming in the Heart and Lung in a Murine Model of Pulmonary Arterial Hypertension. *Front. Cardiovasc. Med.* **0**, 110 (2018).
114. Bujak, R. *et al.* New Biochemical Insights into the Mechanisms of Pulmonary Arterial Hypertension in Humans. *PLoS One* **11**, e0160505 (2016).
115. Hemnes, A. R. *et al.* Evidence for right ventricular lipotoxicity in heritable pulmonary arterial hypertension. *Am. J. Respir. Crit. Care Med.* **189**, 325–334 (2014).
116. A, C. *et al.* Hexosylceramides as intrathecal markers of worsening disability in multiple sclerosis. *Mult. Scler.* **21**, 1271–1279 (2015).
117. Dowds, C. M., Kornell, S.-C., Blumberg, R. S. & Zessig, S. Lipid antigens in immunity. *Biol. Chem.* **395**, 61–81 (2015).
118. Adar, T., Shteingart, S., Ben Ya'acov, A., Bar-Gil Shitrit, A. & Goldin, E. From airway inflammation to inflammatory bowel disease: Eotaxin-1, a key regulator of intestinal inflammation. *Clin. Immunol.* **153**, 199–208 (2014).
119. Martins, A., Han, J. & Kim, S. O. The Multifaceted Effects of Granulocyte Colony-Stimulating Factor in Immunomodulation and Potential Roles in Intestinal Immune Homeostasis. *IUBMB Life* **62**, 611 (2010).
120. LIU, J.-F., DU, Z.-D., CHEN, Z., HAN, Z.-C. & HE, Z.-X. Granulocyte colony-stimulating factor attenuates monocrotaline-induced pulmonary hypertension by upregulating endothelial progenitor cells via the nitric oxide system. *Exp. Ther. Med.* **6**, 1402 (2013).
121. Jiang, H.-M. *et al.* Role for Granulocyte Colony Stimulating Factor in Angiotensin II–Induced Neutrophil Recruitment and Cardiac Fibrosis in Mice. *Am. J. Hypertens.* **26**, 1224–1233 (2013).
122. Guo, L. *et al.* Role of interleukin-15 in cardiovascular diseases. *J. Cell. Mol. Med.* **24**, 7094 (2020).
123. Guo, Y. *et al.* Interleukin-15 Enables Septic Shock by Maintaining Natural Killer Cell Integrity and Function. *J. Immunol.* **198**, 1320 (2017).
124. Jabri, B. & Abadie, V. IL-15 functions as a danger signal to regulate tissue-resident T cells and tissue destruction. *Nat. Rev. Immunol.* **15**, 771 (2015).
125. T, I. *et al.* Increased plasma monocyte chemoattractant protein-1 level in idiopathic pulmonary arterial hypertension. *Respirology* **11**, 158–163 (2006).
126. KIMURA, H. *et al.* Plasma Monocyte Chemoattractant Protein-1 and Pulmonary Vascular Resistance in Chronic Thromboembolic Pulmonary Hypertension. *https://doi.org/10.1164/ajrccm.164.2.2006154* **164**, 319–324 (2012).
127. Ikeda, Y. *et al.* Anti-monocyte chemoattractant protein-1 gene therapy attenuates pulmonary hypertension in rats. *https://doi.org/10.1152/ajpheart.00919.2001* **283**,

2021–2028 (2002).
128. Bain, C. C. & Schridde, A. Origin, Differentiation, and Function of Intestinal Macrophages. *Front. Immunol.* **9**, 2733 (2018).
129. Caprara, G., Allavena, P. & Erreni, M. Intestinal Macrophages at the Crossroad between Diet, Inflammation, and Cancer. *Int. J. Mol. Sci.* **21**, 1–31 (2020).
130. Ruder, B. & Becker, C. At the Forefront of the Mucosal Barrier: The Role of Macrophages in the Intestine. *Cells* **9**, (2020).
131. Sugimoto, M. A., Sousa, L. P., Pinho, V., Perretti, M. & Teixeira, M. M. Resolution of Inflammation: What Controls Its Onset? *Front. Immunol.* **0**, 160 (2016).
132. Greenlee-Wacker, M. C. Clearance of apoptotic neutrophils and resolution of inflammation. *Immunol. Rev.* **273**, 357 (2016).
133. Bratton, D. L. & Henson, P. M. Neutrophil Clearance: when the party's over, cleanup begins. *Trends Immunol.* **32**, 350 (2011).
134. YA, Y. *et al.* Nonclassical Monocytes Sense Hypoxia, Regulate Pulmonary Vascular Remodeling, and Promote Pulmonary Hypertension. *J. Immunol.* **204**, 1474–1485 (2020).
135. Wenzel, P. Monocytes as immune targets in arterial hypertension. *Br. J. Pharmacol.* **176**, 1966 (2019).
136. Voelkel, N. F. *et al.* Inhibition of 5-lipoxygenase-activating protein (FLAP) reduces pulmonary vascular reactivity and pulmonary hypertension in hypoxic rats. *J. Clin. Invest.* **97**, 2491 (1996).
137. Montford, J. R. *et al.* Inhibition of 5-Lipoxygenase Decreases Renal Fibrosis and Progression of Chronic Kidney Disease. *Am. J. Physiol. Physiol.* 732–742 (2019). doi:10.1152/ajprenal.00262.2018
138. Singh, N. K. & Rao, G. N. Emerging role of 12/15-Lipoxygenase (ALOX15) in human pathologies. *Prog. Lipid Res.* **73**, 28 (2019).
139. Kriska, T. *et al.* Mice lacking macrophage 12/15-lipoxygenase are resistant to experimental hypertension. *Am. J. Physiol. - Hear. Circ. Physiol.* **302**, H2428 (2012).
140. Cho, K. *et al.* Blockade of Airway Inflammation and Hyperresponsiveness by Inhibition of BLT2 , a Low-Affinity Leukotriene B 4 Receptor. *Am. J. Respir. Cell Mol. Biol.* **42**, 294–303 (2010).
141. Austin, E. D. *et al.* T lymphocyte subset abnormalities in the blood and lung in pulmonary arterial hypertension. *Respir. Med.* **104**, 454–462 (2010).
142. D, M. *et al.* Apolipoprotein A-I mimetics mitigate intestinal inflammation in COX2-dependent inflammatory bowel disease model. *J. Clin. Invest.* **129**, 3670–3685 (2019).
143. Mowat, A. M. & Agace, W. W. Regional specialization within the intestinal immune system. *Nat. Rev. Immunol. 2014 1410* **14**, 667–685 (2014).
144. Kitamura', A., Takahashi', K., Okajima', A. & Kitamura', N. *Induction of the human gene for p44, a hepatitis-C-associated microtubular aggregate protein, by interferon-orlp*. *Eur. J. Biochem* **224**, (1994).
145. Hwang, Y. *et al.* Genetic predisposition of responsiveness to therapy for chronic hepatitis C. *http://dx.doi.org/10.2217/14622416.7.5.697* **7**, 697–709 (2006).
146. Pan, H. *et al.* Interferon-Induced Protein 44 Correlated With Immune Infiltration Serves as a Potential Prognostic Indicator in Head and Neck Squamous Cell

Carcinoma. *Front. Oncol.* **10**, (2020).
147. Busse, D. C. *et al.* Interferon-Induced Protein 44 and Interferon-Induced Protein 44-Like Restrict Replication of Respiratory Syncytial Virus. *J. Virol.* **94**, (2020).
148. Power, D. *et al.* IFI44 suppresses HIV-1 LTR promoter activity and facilitates its latency. *Virology* **481**, 142 (2015).
149. DeDiego, M. L., Nogales, A., Martinez-Sobrido, L. & Topham, D. J. Interferon-Induced Protein 44 Interacts with Cellular FK506-Binding Protein 5, Negatively Regulates Host Antiviral Responses, and Supports Virus Replication. *MBio* **10**, (2019).
150. B, L. & SL, S. Fast gapped-read alignment with Bowtie 2. *Nat. Methods* **9**, 357–359 (2012).
151. B, L. & CN, D. RSEM: accurate transcript quantification from RNA-Seq data with or without a reference genome. *BMC Bioinformatics* **12**, (2011).
152. MD, R., DJ, M. & GK, S. edgeR: a Bioconductor package for differential expression analysis of digital gene expression data. *Bioinformatics* **26**, 139–140 (2010).
153. A, K., J, G., J, P. & S, T. Causal analysis approaches in Ingenuity Pathway Analysis. *Bioinformatics* **30**, 523–530 (2014).
154. Reimand, J. *et al.* Pathway enrichment analysis and visualization of omics data using g:Profiler, GSEA, Cytoscape and EnrichmentMap. *Nat. Protoc. 2019 142* **14**, 482–517 (2019).
155. Wu, H.-J. & Wu, E. The role of gut microbiota in immune homeostasis and autoimmunity. *Gut Microbes* **3**, 4 (2012).
156. Hill, D. A. & Artis, D. Intestinal Bacteria and the Regulation of Immune Cell Homeostasis. *Annu. Rev. Immunol.* **28**, 623 (2010).
157. Zhou, B. *et al.* Intestinal Flora and Disease Mutually Shape the Regional Immune System in the Intestinal Tract. *Front. Immunol.* **0**, 575 (2020).
158. Anand, S. & Mande, S. S. Diet, Microbiota and Gut-Lung Connection. *Front. Microbiol.* **9**, 2147 (2018).
159. Enaud, R. *et al.* The Gut-Lung Axis in Health and Respiratory Diseases: A Place for Inter-Organ and Inter-Kingdom Crosstalks. *Front. Cell. Infect. Microbiol.* **0**, 9 (2020).
160. Santaolalla, R., Fukata, M. & Abreu, M. T. Innate immunity in the small intestine. *Curr. Opin. Gastroenterol.* **27**, 125 (2011).
161. TP, M. *et al.* Role of inflammatory chemokines in hypertension. *Pharmacol. Ther.* **223**, (2021).
162. H, M., A, J., D, N. & G, M. The role of chemokines in hypertension. *Adv. Clin. Exp. Med.* **23**, 319–325 (2014).
163. A, A. *et al.* High serum levels of CXC (CXCL10) and CC (CCL2) chemokines in untreated essential hypertension. *Int. J. Immunopathol. Pharmacol.* **25**, 387–395 (2012).
164. R, A. *et al.* CXCL10 Is a Circulating Inflammatory Marker in Patients with Advanced Heart Failure: a Pilot Study. *J. Cardiovasc. Transl. Res.* **9**, 302–314 (2016).
165. R, A., Z, M., GW, B. & FA, Z. The CXCL10/CXCR3 Axis and Cardiac Inflammation: Implications for Immunotherapy to Treat Infectious and

Noninfectious Diseases of the Heart. *J. Immunol. Res.* **2016**, (2016).
166. Cunningham, C. M. *et al.* Abstract MP172: Y-chromosome Gene, Uty, Confers Male Protection Against Pulmonary Hypertension by Mediating Pro-inflammatory Chemokine Effects. *Circ. Res.* **127**, (2020).
167. D, K., N, S., RJ, W.-S., MS, Y. & J, C. Muscle-derived TRAIL negatively regulates myogenic differentiation. *Exp. Cell Res.* **394**, (2020).
168. U, S., O, V., D, W. & H, W. TRAIL: a multifunctional cytokine. *Front. Biosci.* **12**, 3813–3824 (2007).
169. AT, B., HM, M. & A, L. Divergent Roles for TRAIL in Lung Diseases. *Front. Med.* **5**, (2018).
170. Navab, M. *et al.* Intestine may be a major site of action for the apoA-I mimetic peptide 4F whether administered subcutaneously or orally. *J. Lipid Res.* **52**, 1200–1210 (2011).
171. Navab, M. *et al.* Transgenic 6F tomatoes act on the small intestine to prevent systemic infl ammation and dyslipidemia caused by Western diet and intestinally derived lysophosphatidic acid. *J. Lipid Res.* **54**, 3403–3418 (2013).
172. G, Z., M, N. & JA, J. Rapid determination of short-chain fatty acids in colonic contents and faeces of humans and rats by acidified water-extraction and direct-injection gas chromatography. *Biomed. Chromatogr.* **20**, 674–682 (2006).
173. W, F., H, X., X, C., K, C. & W, L. Supplementation with Sodium Butyrate Modulates the Composition of the Gut Microbiota and Ameliorates High-Fat Diet-Induced Obesity in Mice. *J. Nutr.* **149**, 747–754 (2019).
174. H, H. *et al.* Sodium Butyrate Ameliorates Gut Microbiota Dysbiosis in Lupus-Like Mice. *Front. Nutr.* **7**, (2020).
175. Jacobs, J. P. *et al.* Microbial, metabolomic, and immunologic dynamics in a relapsing genetic mouse model of colitis induced by T-synthase deficiency. *Gut Microbes* **8**, 1–16 (2017).
176. Callahan, B. J. *et al.* DADA2: High-resolution sample inference from Illumina amplicon data. *Nat. Methods* **13**, 581–583 (2016).
177. Storey, J. D. & Tibshirani, R. Statistical significance for genomewide studies. *Proc. Natl. Acad. Sci.* **100**, 9440–9445 (2003).
178. Gupta, J. & Nebreda, A. Analysis of Intestinal Permeability in Mice. *BIO-PROTOCOL* **4**, (2014).
179. Gutiérrez, N. & Garrido, D. Species Deletions from Microbiome Consortia Reveal Key Metabolic Interactions between Gut Microbes. *mSystems* **4**, (2019).
180. A, V. *et al.* Dietary Interventions Reduce Traditional and Novel Cardiovascular Risk Markers by Altering the Gut Microbiome and Their Metabolites. *Front. Cardiovasc. Med.* **8**, (2021).
181. Szentirmai, É., Massie, A. R. & Kapás, L. Lipoteichoic acid, a cell wall component of Gram-positive bacteria, induces sleep and fever and suppresses feeding. *Brain. Behav. Immun.* **92**, 184–192 (2021).
182. T, T., A, K., Y, C. & EK, W. Can intestinal microbiota and circulating microbial products contribute to pulmonary arterial hypertension? *Am. J. Physiol. Heart Circ. Physiol.* **317**, H1093–H1101 (2019).
183. M, Z. *et al.* Induction of intestinal pro-inflammatory immune responses by lipoteichoic acid. *J. Inflamm. (Lond).* **9**, (2012).

184. R, B. C. *et al.* Lactobacillus rhamnosus GG-supplemented formula expands butyrate-producing bacterial strains in food allergic infants. *ISME J.* **10**, 742–750 (2016).
185. N, P. *et al.* Acetatifactor muris gen. nov., sp. nov., a novel bacterium isolated from the intestine of an obese mouse. *Arch. Microbiol.* **194**, 901–907 (2012).
186. Tang, Q. *et al.* Current Sampling Methods for Gut Microbiota: A Call for More Precise Devices. *Front. Cell. Infect. Microbiol.* **10**, 151 (2020).
187. Calderón-Pérez, L. *et al.* Gut metagenomic and short chain fatty acids signature in hypertension: a cross-sectional study. *Sci. Rep.* **10**, (2020).
188. Rios-Covian, D., Salazar, N., Gueimonde, M. & de los Reyes-Gavilan, C. G. Shaping the Metabolism of Intestinal Bacteroides Population through Diet to Improve Human Health. *Front. Microbiol.* **0**, 376 (2017).
189. FZ, M. *et al.* High-Fiber Diet and Acetate Supplementation Change the Gut Microbiota and Prevent the Development of Hypertension and Heart Failure in Hypertensive Mice. *Circulation* **135**, 964–977 (2017).
190. BP, G. *et al.* Prebiotics, Probiotics, and Acetate Supplementation Prevent Hypertension in a Model of Obstructive Sleep Apnea. *Hypertens. (Dallas, Tex. 1979)* **72**, 1141–1150 (2018).
191. González-Zancada, N. *et al.* Association of Moderate Beer Consumption with the Gut Microbiota and SCFA of Healthy Adults. *Molecules* **25**, (2020).
192. YN, W. *et al.* Effects of probiotics and prebiotics on intestinal microbiota in mice with acute colitis based on 16S rRNA gene sequencing. *Chin. Med. J. (Engl).* **132**, 1833–1842 (2019).